Alfredo Raúl Carella

Spectral Finite Element Methods for solving Fractional Differential Equations with applications in Anomalous Transport

Thesis for the degree of Philosophiae Doctor

Trondheim, September 2012

Norwegian University of Science and Technology
Faculty of Engineering Science and Technology
Department of Energy and Process Engineering

NTNU – Trondheim
Norwegian University of
Science and Technology

NTNU
Norwegian University of Science and Technology

Thesis for the degree of Philosophiae Doctor

Faculty of Engineering Science and Technology
Department of Energy and Process Engineering

ISBN 978-82-471-3783-3 (printed ver.)
ISBN 978-82-471-3784-0 (electronic ver.)
ISSN 1503-8181

Doctoral theses at NTNU, 2012:239

Printed by NTNU-trykk

A mi familia:
José, Ana, Luis, Adolfo, Virginia
y todos los que ofrecen
más que lo que sobra
a quien le falta

Abstract

Quantifying species transport rates is a main concern in chemical and petrochemical industries. In particular, the design and operation of many large-scale industrial chemical processes is as much dependent on diffusion as it is on reaction rates. However, the existing diffusion models sometimes fail to predict experimentally observed behaviors and their accuracy is usually insufficient for process optimization purposes.

Fractional diffusion models offer multiple possibilities for generalizing Fick's law in a consistent manner in order to account for history dependence and nonlocal effects. These models have not been extensively applied to the study of real systems, mainly due to their computational cost and mathematical complexity.

A least squares spectral formulation was developed for solving fractional differential equations. The proposed method was proven particularly well-suited for dealing with the numerical difficulties inherent to fractional differential operators. The practical implementation was explained in detail in order to enhance reproducibility, and directions were specified for extending it to multiple dimensions and arbitrarily shaped domains.

A numerical framework based on the least-squares spectral element method was developed for studying and comparing anomalous diffusion models in pellets. This simulation tool is capable of solving arbitrary integro-differential equations and can be effortlessly adapted to various problems in any number of dimensions.

Simulations of the flow around a cylindrical particle were achieved by extending the functionality of the developed framework. A test case was analyzed by coupling the boundary condition yielded by the fluid model with two families of anomalous diffusion models: hyperbolic diffusion and fractional diffusion. Qualitative guidelines for determining the suitability of diffusion models can be formulated by complementing experimental data with the results obtained from this approach.

Preface

This thesis was submitted to the Norwegian University of Science and Technology in partial fulfillment of the requirements for obtaining the degree of Philosophiae Doctor (Dr Ing). The work was carried out at the Department of Energy and Process Engineering, Faculty of Engineering Science and Technology, in the period May 2009 - May 2012, under the supervision of Prof. Carlos A. Dorao and Dr. Jana P. Jakobsen. The funding was provided by the PAFFrx project (*Particle Fluid Flow with Chemical Reaction – Multi level models for design and optimization of fluidized bed processes, NFR 186933/I30*) of the Norwegian Research Council.

Acknowledgments

I would like to thank a lot of people who helped me throughout the last three years. As a matter of fact, I owe my gratitude to so many that I doubt I will be able to remember all of them. If I am up to the challenge, many will be present here. However, the essential ones will join me along the rest of my life.

The members of my family are the first in the latter group, particularly (and not extensively) my parents José and Ana, brothers Luis and Adolfo, sisters in law Úrsula and Cecilia, nieces and nephew Agustina, Delfina and Benicio, and my grandmother Tita. They have been an endless source of love, concern, support and strength throughout the last (27) years.

Virginia has been the one closest to me during this time as both my caring friend and inspiring muse, and eventually my wife. We keep teaching each other to see the world in a different and hopefully better way.

I had the good fortune of meeting a lot of nice guys in Trondheim, and I also got to know some incredibly awesome people with golden hearts like Juan Pablo & Ingeborg, Ismael, Alejandro & Ingrid, Alfredo, Julio, Rafael, Ida, Vegard & Kristin, María & Alexis, José Luis & Sara, Pablo & Kristin, Federico & Tatiana. They keep offering me their unconditional help every single time, without having to ask for it.

Some other people, even from thousands of kilometers away, have been responsible for a significant part of my daily smiles. Thank you Chango, Marcos, Pepe, Mati, Seba, Aero, Pela, Javi, Suja, Elbi, Osqui, Esteban, Juan, Diego, Martín, Víctor & Olga, Nico, Víctor, Elisa.

Thanks also Ezequiel, Fabio, Luis, Bahram & Tarlan, Alex, Lucho & Ada, Jenny, Andrea, Jorge, María, Nicolás & Ayelén, Gürsu & Türkan, Gonzalo & Juliana, Juan & Jessica, Sara, Nicla, Peder, Eli & Stein, the French and Italian gangs.

Last but not least, thanks to my advisors Prof. Carlos Dorao and Dr. Jana Jakobsen for giving me the opportunity to have this experience.

Alfredo R. Carella
Oslo, August 2012

Material produced in this work

A list of the additional material produced during this thesis is presented in this section. It is divided into two categories: peer-reviewed publications and other materials.

Peer-reviewed publications

This category includes articles that were accepted after a review process. A distinction is made between papers in journals and in conference proceedings as follows.

Papers in journals

In chronological order according to submission date, these articles are:

- Carella, A.R. and Dorao, C.A. (2010) *Solution of a Cattaneo-Maxwell diffusion model using a Spectral element least-squares method.* Journal of Natural Gas Science and Engineering **2**, pp. 253-258.
  doi:10.1016/j.jngse.2010.08.001.

- Carella, A.R. and Dorao, C.A. (2011) *Least-Squares Spectral Method for the solution of a fractional advection-dispersion equation.* Journal of Computational Physics. Accepted for publication. Manuscript number JCOMP-D-11-00463R1.
  dx.doi.org/10.1016/j.jcp.2012.04.050.

- Carella, A.R. and Dorao, C.A. (2012) *Modeling of fractional diffusion on a catalytic particle under different flow conditions.* Defect and Diffusion Forum **323-325**(121), pp. 121-126.
  dx.doi.org/10.4028/www.scientific.net/DDF.323-325.121

- Carella, A.R. and Dorao, C.A. (2012) *N-dimensional Least Squares Spectral Method formulation for the general Fractional Diffusion Equation.* Journal of Computational Physics - Under review.

Papers in conference proceedings

Also in chronological order of submission date, the following articles were published in conference proceedings.

- Carella, A.R., Dorao, C.A. (2011) *Migration of Species into a Particle Under Different Flow Conditions*. In Kuzmin, A. (Ed.): Computational Fluid Dynamics 2010, Proceedings of the Sixth International Conference on Computational Fluid Dynamics, ICCFD6, St. Petersburg, Russia, on July 12-16 2010. Springer-Verlag, Berlin Heidelberg. ISBN: 978-3-642-17883-2, pp. 869-871. dx.doi.org/10.1007/978-3-642-17884-9_112

Other material

This second category includes scientific works presented at international conferences and workshops *without* an exhaustive review process. In other words, the following articles were accepted for presentation based on a reviewed abstract, and were not published. They are split into oral and poster presentations.

Oral presentations

- Carella, A.R. and Dorao, C.A. - *"On the solution of the Cattaneo-Maxwell model for anomalous diffusion inside a catalytic particle"*, 1st Trondheim Gas Technology Conference, October 21-22, 2009, Trondheim, Norway.

- Carella, A.R. and Dorao, C.A. - *"Simulation of gas flow around a particle using a Cattaneo diffusion model"*, 6th Conference on Diffusion in Solids and Liquids (DSL 2010). July 5-7, 2010. Paris, France

- Carella, A.R. and Dorao, C.A. - *"Fractional diffusion modeling inside a catalytic particle in a gas flow"*, 4th International Conference on Advanced Computational Engineering and Experimenting (ACE-X 2010). July 8-9, 2010. Paris, France

- Carella, A.R. and Dorao, C.A. - *"Applications and modeling issues of anomalous transport"*, LNG seminar for PhDs and PostDocs. August 7, 2010. Trondheim, Norway

- Carella, A.R. and Dorao, C.A. - *"Modeling of fractional diffusion into a catalytic particle under different flow conditions"*, 8th International Conference on Diffusion in Materials. July 3-8, 2011. Dijon, France

Poster presentations

- Johannessen, B., Carella, A.R. and Dorao, C.A. - *"Micro and macro scale simulation of anomalous transport"*. 1st Trondheim Gas Technology Conference, October 21-22, 2009. Trondheim, Norway

- Carella, A.R. and Dorao, C.A. - *"Fractional derivative model for species diffusion into a particle"*. 6th International Conference on Computational Fluid Mechanics, July 13, 2010. St. Petersburg, Russia

Contents

Abstract i

Preface iii

Acknowledgments v

Material produced in this work vii

Contents xi

List of Figures xv

List of Tables xix

I Introduction 1

1 Background and motivation 3
1.1 Introduction . . . 3
1.1.1 Development strategies for natural gas . . . 6
1.1.2 Gas separation and conditioning. . . . 8
1.1.3 Conditioned gas processing . . . 9
1.1.4 Petrochemical commodities from natural gas . . . 11
1.2 Context & Objective . . . 12
1.3 Scope . . . 13
1.4 Thesis outline . . . 14

2 Anomalous transport models 17
2.1 What is anomalous transport? . . . 17
2.1.1 Infinite propagation velocity paradox . . . 18
2.1.2 Experimentally observed anomalous transport . . . 18
2.2 When should anomalous models be used . . . 20
2.2.1 Applicability of Fick's law . . . 22
2.2.2 Transport modeling according to level of detail . . . 22
2.3 Continuous Time Random Walks . . . 24

2.3.1 Long tail distributions . . . 24
2.3.2 Pseudo-Random PDF generation . . . 25
2.3.3 Linking CTRW and fractional diffusion . . . 26
2.4 Fractional diffusion models . . . 29
2.4.1 Fractional derivatives . . . 29
2.4.2 Fractional diffusion models . . . 32
2.5 Chapter summary . . . 34

II Numerical tools 35

3 The Least Squares Spectral Element Method 37
3.1 Overview of LSSEM features . . . 37
3.1.1 Why finite elements? . . . 38
3.1.2 Why least squares? . . . 38
3.1.3 Why spectral? . . . 38
3.2 Formulation . . . 39
3.2.1 Main concept . . . 39
3.2.2 Introduction of norms and search spaces . . . 40
3.3 Discretization . . . 41
3.3.1 Function interpolation . . . 41
3.3.2 Quadrature . . . 44
3.3.3 Construction of differential operators . . . 46
3.3.4 Subdivision into elements . . . 47
3.4 Chapter summary . . . 47

4 Numerical implementation 49
4.1 Fractional derivatives . . . 49
4.1.1 The fractional derivative operator . . . 50
4.1.2 Numerical approaches . . . 51
4.1.3 Implementation in a spectral framework . . . 53
4.1.4 Non-linear mapping technique . . . 54
4.2 Multi-dimensional tools . . . 57
4.2.1 Extension of nodal basis . . . 57
4.2.2 Extension of differential operators . . . 58
4.2.3 Homography mapping technique . . . 58
4.2.4 Bivariate blending function interpolation . . . 60
4.3 Chapter summary . . . 63

III Simulations and application to problems 65

5 Cattaneo-Maxwell diffusion model 67
5.1 Introduction . . . 67

5.2 The hyperbolic mass diffusion equation . . . 69
5.3 Numerical Solution . . . 70
5.3.1 Time-space formulation . . . 72
5.4 Numerical examples . . . 72
5.4.1 Analysis of Cattaneo-Maxwell model . . . 73
5.4.2 Convergence study . . . 75
5.5 Chapter conclusions . . . 76

6 Fractional diffusion models **77**
6.1 Introduction . . . 77
6.1.1 Fractional derivative applications . . . 78
6.1.2 Numerical issues . . . 78
6.2 Physical models . . . 79
6.2.1 Time fractional diffusion equation (2D+Time) . . . 79
6.2.2 General fractional diffusion equation . . . 80
6.2.3 General fractional diffusion equation with delay . . . 81
6.3 Numerical solution . . . 81
6.4 Numerical verification . . . 83
6.4.1 Quadrature validation . . . 83
6.4.2 Validation of fractional derivative operators . . . 85
6.4.3 Fractional advection-dispersion equation . . . 85
6.4.4 Time fractional diffusion equation (1D+Time) . . . 87
6.4.5 Time fractional diffusion equation (2D+Time) . . . 88
6.4.6 General fractional diffusion equation . . . 90
6.4.7 Convergence study of the numerical scheme . . . 92
6.5 Chapter conclusions . . . 95

7 Coupling convection and diffusion **97**
7.1 Introduction . . . 97
7.1.1 The problem scenario . . . 98
7.2 The physical models . . . 98
7.2.1 The fluid model . . . 99
7.2.2 The solid diffusion models . . . 100
7.3 Numerical flow solution . . . 101
7.3.1 Species convection and diffusion . . . 105
7.4 Diffusion in the particle . . . 106
7.4.1 Anomalous diffusion in coupled phenomena . . . 108
7.5 Chapter conclusions . . . 113

IV Final remarks **115**

8 Conclusions **117**
8.1 Revisiting the objectives . . . 117

8.2 Contributions in this work 118
8.2.1 Contribution to knowledge 119
8.2.2 Application scope 120
8.3 Future work 121

References **123**

Appendix **141**

A Publications **143**
A.1 Carella, A.R. and Dorao, C.A. (2010) *Solution of a Cattaneo-Maxwell diffusion model using a Spectral element least-squares method.* Journal of Natural Gas Science and Engineering **2**, pp. 253-258. doi:10.1016/j.jngse.2010.08.001. 147
A.2 Carella, A.R., Dorao, C.A. (2011) *Migration of Species into a Particle Under Different Flow Conditions.* In Kuzmin, A. (Ed.): Computational Fluid Dynamics 2010, Proceedings of the Sixth International Conference on Computational Fluid Dynamics, ICCFD6, St. Petersburg, Russia, on July 12-16 2010. Springer-Verlag, Berlin Heidelberg. ISBN: 978-3-642-17883-2, pp. 869-871. dx.doi.org/10.1007/978-3-642-17884-9_112. 155
A.3 Carella, A.R. and Dorao, C.A. (2011) *Least-Squares Spectral Method for the solution of a fractional advection-dispersion equation.* Journal of Computational Physics. Accepted for publication. Manuscript number JCOMP-D-11-00463R1. dx.doi.org/10.1016/j.jcp.2012.04.050. 161
A.4 Carella, A.R. and Dorao, C.A. (2012) *Modeling of fractional diffusion on a catalytic particle under different flow conditions.* Defect and Diffusion Forum **323-325**(121), pp. 121-126. dx.doi.org/10.4028/www.scientific.net/DDF.323-325.121. . . 185
A.5 Carella, A.R. and Dorao, C.A. (2012) *N-dimensional Least Squares Spectral Method formulation for the general Fractional Diffusion Equation.* Journal of Computational Physics - Under review. . . . 195

List of Figures

1.1 Main development options and products from natural gas 5
1.2 Division of costs in the Gas-to-Liquids value chain 7

2.1 Global classification of anomalous transport models according to scale 23
2.2 Conditions for the formation of Gaussian diffusive packets 24
2.3 Jumping probability distribution for a random walk model 27
2.4 Diffusion of a concentration pulse by Fick and random walk models 27
(a) Test sample with 10^3 walkers 27
(b) Test sample with 10^4 walkers 27
(c) Test sample with 10^5 walkers 27
(d) Test sample with 10^6 walkers 27
2.5 Jumping probability distribution for non-Markovian random walk . 29
2.6 Time fractional diffusion of a pulse vs. non-Markovian random walk 30
(a) RW vs Fick's diffusion 30
(b) CTRW vs fractional diffusion: $\beta = 3/4$ 30
(c) CTRW vs fractional diffusion: $\beta = 1/2$ 30
(d) CTRW vs fractional diffusion: $\beta = 2/5$ 30

3.1 Example of an expansion in (a) a modal basis and (b) a nodal basis 42

4.1 Integration domains for computing the fractional derivative operator 53
4.2 Example of point redistribution according to the mapping $\mathcal{F}_{1,3}(\xi)$. 55
4.3 Plots of the reference domain mapped by $\mathcal{F}_{m,n}(\xi)$ 56
4.4 Convention for node enumeration in 2D and 3D grids 57
4.5 Homography mapping example of a pentagon 59
4.6 Concept illustration of the bivariate blending function interpolation 60
4.7 Mapping reference geometries into deformed elements 61
(a) Mapping a reference square into a deformed 2D element . . . 61
(b) Mapping a reference cube into a deformed 3D element 61
4.8 Extension of the simulation domain to 3 space dimensions 62

5.1 Lagrange polynomials of order $0 \leq O_e \leq 5$ for a reference domain . 71
5.2 Solving schemes for Cattaneo-Maxwell model 72
(a) Full-domain approach 72
(b) Time-slab approach 72

5.3 Physical interpretation of the 1-D numerical problem 73
5.4 Propagation of a concentration pulse 74
(a) Full solution for $\sqrt{k_p/\tau} = \infty$ 74
(b) Profile snapshots for $\sqrt{k_p/\tau} = \infty$ 74
(c) Full solution for $\sqrt{k_p/\tau} = \sqrt{10}$ 74
(d) Profile snapshots for $\sqrt{k_p/\tau} = \sqrt{10}$ 74
(e) Full solution for $\sqrt{k_p/\tau} = \sqrt{5}$ 74
(f) Profile snapshots for $\sqrt{k_p/\tau} = \sqrt{5}$ 74
5.5 Convergence plots for Cattaneo-Maxwell model 75
(a) Res vs. N_e Full-domain 75
(b) Res vs. N_e Time-slabs 75
(c) Res vs. O_x Full-domain 75
(d) Res vs. O_x Time-slabs 75
5.6 Precision vs. cost for full-domain and time-slab approaches 76

6.1 Plot of the temporal solution $E_\beta\left(-\frac{1}{2}\pi^2 t^\beta\right)$ in the interval $t \in [0, 1]$. 80
6.2 Convergence plots for numerical integration: $g(\xi)$ with $\gamma_1(\xi) = e^{p\xi}$. 82
6.3 Convergence plots for numerical integration: $g(\xi)$ with $\gamma_2(\xi) = \xi^p$. 84
6.4 Convergence plots for fractional derivative operator 86
6.5 Analytical value and polynomial approximation: ${}_aD_b^\beta\gamma(\xi)$ 86
6.6 Numerical solutions to the fractional advection-dispersion equation 87
6.7 Convergence plots for the fractional advection-dispersion equation . 88
6.8 Numerical solutions to time fractional diffusion equation (1D+time) 89
6.9 Convergence plots for the time fractional diffusion equation (1D+time) 89
6.10 Snapshots for time fractional diffusion equation (2D+time) $\beta = 0.3$ 90
6.11 Snapshots for time fractional diffusion equation (2D+time) $\beta = 0.9$ 91
6.12 Numerical solutions to the general fractional diffusion equation . . . 92
6.13 Solutions to the general fractional diffusion equation with delay . . 93
6.14 Convergence indicators for the time fractional diffusion equation . . 94

7.1 Simplified scheme of a packed bed reactor 98
7.2 Sketch of the simulation domain: flow around a particle 99
7.3 Plot of the mesh for the fluid problem 103
(a) Spatial discretization with 12 elements 103
(b) Spatial discretization with 108 elements 103
7.4 Vortex shedding by a circular cylinder at $Re = 200$ at $t = 150$ . . . 104
(a) Pressure contours 104
(b) Streamlines 104
(c) Velocity component in the x direction 104
7.5 Convergence test for the fluid problem 105
(a) 12 elements 105
(b) 108 elements 105
7.6 Velocity field around a circular cylinder at $Re = 1$ 106

7.7 Species concentration field for fluid region at different times 106
(a) $t = 1$s 106
(b) $t = 2$s 106
(c) $t = 3$s 106
7.8 Time evolution of the concentration on the particle boundary 107
7.9 Species concentration at short times (Cattaneo-Maxwell model) . . 109
(a) Time-space solution, $\sqrt{k_p/\tau} = \sqrt{\infty}$ 109
(b) Solution snapshots, $\sqrt{k_p/\tau} = \sqrt{\infty}$ 109
(c) Time-space solution, $\sqrt{k_p/\tau} = \sqrt{5}$ 109
(d) Solution snapshots, $\sqrt{k_p/\tau} = \sqrt{5}$ 109
(e) Time-space solution, $\sqrt{k_p/\tau} = \sqrt{2}$ 109
(f) Solution snapshots, $\sqrt{k_p/\tau} = \sqrt{2}$ 109
7.10 Species concentration at short times (Fractional diffusion model) . . 110
(a) Time-space solution, $\beta = 1$ 110
(b) Solution snapshots, $\beta = 1$ 110
(c) Time-space solution, $\beta = 0.6$ 110
(d) Solution snapshots, $\beta = 0.6$ 110
(e) Time-space solution, $\beta = 0.2$ 110
(f) Solution snapshots, $\beta = 0.2$ 110
7.11 Species concentration at long times (Cattaneo-Maxwell model) . . . 111
(a) Time-space solution, $\sqrt{k_p/\tau} = \sqrt{\infty}$ 111
(b) Solution snapshots, $\sqrt{k_p/\tau} = \sqrt{\infty}$ 111
(c) Time-space solution, $\sqrt{k_p/\tau} = \sqrt{5}$ 111
(d) Solution snapshots, $\sqrt{k_p/\tau} = \sqrt{5}$ 111
(e) Time-space solution, $\sqrt{k_p/\tau} = \sqrt{2}$ 111
(f) Solution snapshots, $\sqrt{k_p/\tau} = \sqrt{2}$ 111
7.12 Species concentration at long times (Fractional diffusion model) . . 112
(a) Time-space solution, $\beta = 1$ 112
(b) Solution snapshots, $\beta = 1$ 112
(c) Time-space solution, $\beta = 0.6$ 112
(d) Solution snapshots, $\beta = 0.6$ 112
(e) Time-space solution, $\beta = 0.2$ 112
(f) Solution snapshots, $\beta = 0.2$ 112

List of Tables

1.1 Main factors intervening in a natural gas development project . . . 4
1.2 Examples of catalytic processes in fixed bed reactors 6
1.3 Typical composition ranges of natural gas 8
1.4 Main reactions involved in syngas production from natural gas . . . 10

2.1 Summary of anomalous diffusion models reported in literature . . . 21

Part I

Introduction

Chapter 1

Background and motivation

A common approach in the design of high complexity engineering systems consists in dividing them into smaller parts whose behavior can be assessed in a simpler way. Each of the simple components is then analyzed in greater detail. The pitfall of this apparently simple and systematic formulation is that it can lead to losing sight of *'the big picture'* if applied in an uncritical manner. This chapter intends to be a review of the different processes related to natural gas processing that are highly dependent on heat and mass transfer phenomena.

Although mass transfer plays a major role throughout the processing of natural gas and has a strong impact in its economical aspects, the tools used for describing species transport still rely on the often inaccurate Fickian diffusion models. The theoretical basis and applicability of these models have been intensively investigated during the last decades, and new models have been developed as an alternative. However, only a limited amount of work has been carried out in order to quantify the influence of diffusion models on practical cases. This will be the central aspect of this thesis.

The objective of this introduction is to present a general overview of the current technical-economical context of natural gas, but not a rigorous treatment of it. This will serve the purpose of giving the reader a better grasp of the importance and ubiquity of transport phenomena occurring in chemical reactors. Audiences looking for a more comprehensive review are referred to textbooks such as [David and Michel, 2008].

1.1 Introduction

About 20% of all the world's primary energy requirements are covered today by natural gas [Odumugbo, 2010]. In this context it may be difficult to understand why the gas associated to oil reserves used to be flared only a few decades ago [Ishishone, 2004]. The reasons for this have historically been associated to the considerable energy consumption and capital investment required for conditioning and transporting the gas [Kaldany, 2006]. These processes are not easy to design,

and the methods that are technologically simple and reliable have not always been economically convenient [Gusev et al., 2000]. However, the main causes of gas flaring have in general been related to contract clauses, governance policies and market availability.

The factors determining the economics of a gas project can be grouped into two main categories, namely "soft" and "hard" (see Table 1.1). Hard factors are related to technical issues and are not likely to change radically in the short term. Soft factors are the ones that depend essentially on economical policies.

Hard factors	**Soft factors**
• Distance to significant gas markets	• Institutional, legal and regulatory framework for gas and associated gas
• Availability and reliability of gas supply	• Effectiveness of fiscal terms (gas price, tax structure, etc)
• Gas infrastructure constraints	• Development of domestic markets for gas and sub-products
• Risks of gas re-injection in oil reservoir	• Funding constraints due to the large required initial investment

Table 1.1: Main factors in a natural gas development project [World Bank, 2009]

As the worldwide environmental concern increases rapidly, the public and political pressure on eliminating gas flaring is changing the operating policies of many oil companies [Kaldany, 2006; Labeyrie and Rocher, 2010; Ishishone, 2004; Edino et al., 2010; Stanley, 2009]. This is important enough to stop the further advance of several oil developments until efficient means for gas disposal are available [Fitzgerald and Taylor, 2001]. A bold statement is made in [Economides and Wood, 2009], saying

> *"Natural gas is the only hydrocarbon source of energy that could easily and at manageable cost lead to a further reductions in global carbon intensity through reduction in carbon dioxide emissions."*

In addition, natural gas is in the process of becoming a highly desirable commodity due to the generation of new technologies which transform it into different products [Hall, 2005]. Under this context the market value increases and gas production becomes of interest. A diagram with the most adopted commercialization options for natural gas is presented in Fig. 1.1. As a complement, examples of important fixed bed catalytic processes with one fluid phase are included in Table 1.2. These processes constitute a large portion of the application field for the tools developed in this thesis.

The rest of Section 1.1 will provide a short overview of the natural gas value chain where the **fundamental role and omnipresence of diffusion processes** will be highlighted. This is mainly illustrative and may be skipped by the readers whose primary interest lies in the technical aspects of this work.

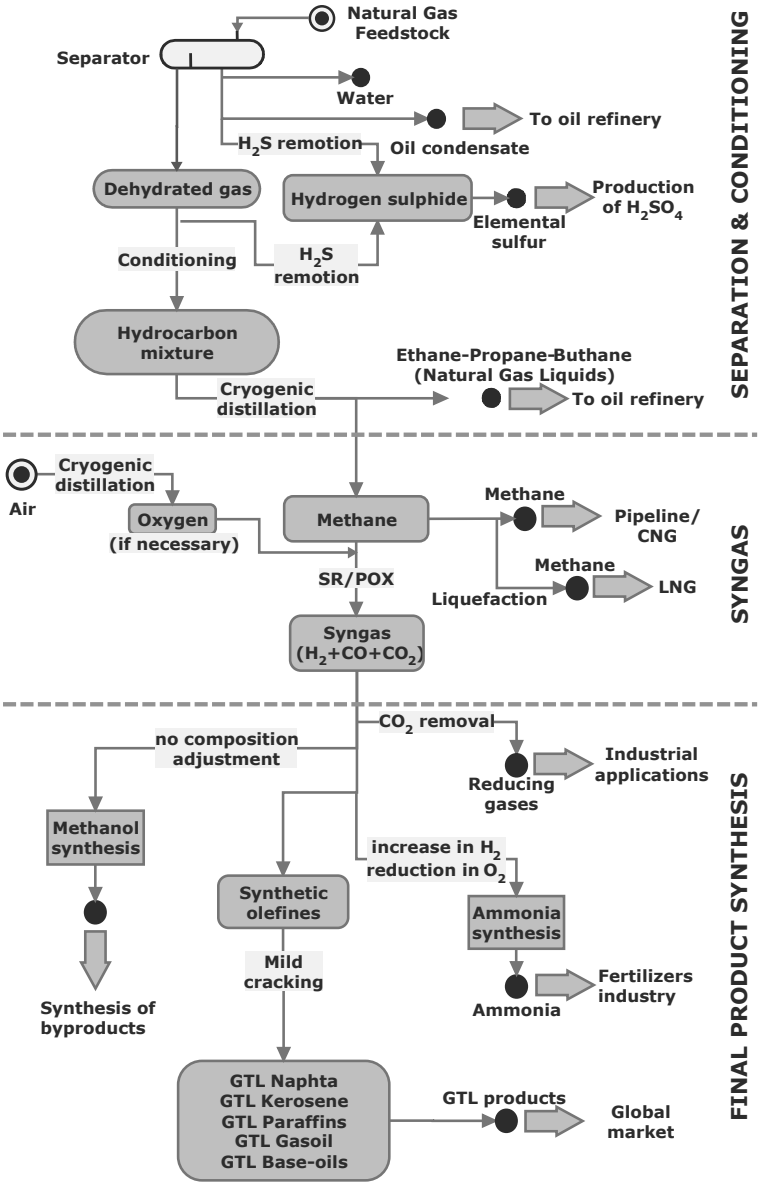

Figure 1.1: Main development options and products from natural gas

Basic Chemical Industry	Petrochemical Industry	Petroleum Refining
Primary steam reforming	Ethylene oxide	Catalytic reforming
Secondary steam reforming	Ethylene dichloride	Isomerization
Carbon monoxide conversion	Vinylacetate	Polymerization
Carbon monoxide methanation	Butadiene	Hydrodesulfurization
Ammonia synthesis	Maleic anhydride	Hydrocracking
Sulfuric acid synthesis	Phtalic anhydride	
Methanol synthesis	Cyclohexane	
Oxo synthesis	Styrene	
	Hydrodealkylation	

Table 1.2: Examples of catalytic processes in fixed bed reactors [Jakobsen, 2008]

1.1.1 Development strategies for natural gas

Gas field development can be accomplished in many ways, each strategy being suitable for a given set of conditions. Natural gas can be either re-injected (in the case of associate gas), commercialized directly as gas or LNG or further processed into more valuable products and commercialized as methanol, synfuels, etc.

Gas re-injection

Re-injection is a valuable technique for enhancing oil recovery in mature fields where production has begun to decline. The re-injected gas increases the reservoir pressure thus incrementing the amount of gas dissolved in the oil. The oil viscosity is therefore reduced and the production level is stimulated. In addition, a high percentage of the natural gas is recovered after having pumped the crude out. Re-injection is also a feasible alternative for CO_2 disposal [Sam and Holloway, 1997]. The efficiency of re-injection depends on *gas diffusion rates in porous media*.

Direct commercialization

Pipeline distribution, CNG and LNG technologies consist basically of sending the CH_4 component of the gas to its final destination. This technologies perform *only the necessary preprocessing to deliver the product safely*, but even taking that into account, the conditioning and transport are significantly expensive. Roughly less than half of the price of natural gas corresponds to the commodity (the gas itself). The rest corresponds to transmission and distribution costs [EIA, 2012].

Gas delivery is in itself a matter of study, and the convenience of a given transport technology is strongly dependent on the distance and the gas volume. A very interesting analysis is presented in [Durr et al., 2005]. Depending on the reserve-market distance, shipping accounts for 10 to 30% of the delivered value of LNG (this cost is below 10% for oil). The reason for this is the higher cost of

LNG tankers, which is mainly associated to their expensive cryogenic insulation. These currently cost more than double the price of a crude oil tanker capable of transporting 4 to 5 times as much energy. An approximate division of costs up to 2003 is given in Fig. 1.2 [EIA, 2003].

Gas To Products

Gas To Products is the common name given to the chain of processes involved in the production of *non-gaseous* long-chain hydrocarbons from gaseous short-chain hydrocarbons. The concept comprises both Gas To Liquid (GTL) technology, which yields liquid fuels from gas, and further processing which generates other petrochemical commodities. Most of the required processes involve diffusion in porous media and are listed in Table 1.2.

Gas To Products conversion requires further processing and a more expensive infrastructure, but makes the transport cheaper and allows to obtain products with higher added value. However, its main drawback lies in the required intermediate *syngas* production (see Section 1.1.3) which demands high capital investments. Syngas production comprises half the total capital cost of a GTL plant, and as a result GTL is competitive against oil production only in scenarios where the gas has low opportunity value and is not readily transported [Wilhelm et al., 2001]. GTL has potential, particularly in high oil price markets, but according to [Economides and Wood, 2009] much technological process and efficiency developments required before it becomes widely exploited.

Figure 1.2: Division of costs in GTL value chain. *Production*: gas production, from the reservoir to the LNG plant $(15-20\%)$; *Plant*: LNG plant, gas treating, liquefaction, LPG and condensate recovery $(30-45\%)$; *Shipping*: transport to final destination $(10-30\%)$; *Receiving*: unloading, storage, re-gasification and distribution $(15-25\%)$

1.1.2 Gas separation and conditioning.

The natural gas extracted from the well is a multi-phase, multi-component mixture. The composition of the mixture depends usually on many variables, but fields are generally classified in dry (mainly gas) and wet (high content of condensible hydrocarbons) [Beychok, 1975]. The simple hydrocarbons found in natural gas are mainly saturated compounds (principally methane, ethane, propane and butane), which means they contain the maximum allowable hydrogen content according to the formula C_nH_{2n+2}.

Name	**Formula**	**Volume %**
Methane	CH_4	$> 85\%$
Ethane	C_2H_6	$3 - 8\%$
Propane	C_3H_8	$1 - 2\%$
Butane	C_4H_{10}	$< 1\%$
Pentane	C_5H_{12}	$< 1\%$
Carbon dioxide	CO_2	$1 - 2\%$
Hydrogen sulfide	H_2S	$0 - 5\%$
Nitrogen	N_2	$1 - 5\%$
Helium	He	$< 0.5\%$
Rare gases	Ar, H_2, He	traces

Table 1.3: Typical composition ranges of natural gas (vol %)

In addition to these hydrocarbon components, the mixture contains rock fragments, water vapor, hydrogen sulphide (H_2S), carbon dioxide (CO_2), helium (He), Nitrogen (N), and other compounds. Typical compositions of natural gas are summarized in Table 1.3 [Mokhatab et al., 2006]. Prior to being sold, processed or even transported, natural gas requires a series of separation and conditioning processes. Conditioned gas can be either sold directly as a commodity or further processed into more valuable products.

The *separation and conditioning* stage consists in the four basic sub-processes described below. The reader looking for further detail is referred to [Guo and Ghalambor, 2005].

1. **Separation of gas from free liquids and entrained solids**
   At the extraction stage, scrubbers and heaters are installed as close as possible to the wellhead. The scrubbers remove most of the large-particle impurities. The heaters prevent the formation of hydrates, which tends to occur if the temperature drops below a certain threshold. The formation of hydrates can also be prevented by enriching the mixture with additives.

2. **Remotion of condensible and recoverable hydrocarbon vapors**
   Due to the high pressures occurring in the well, the gas is partially dissolved

into an oil phase consisting of long hydrocarbon chains. In some cases the mass transfer process driving to separation may occur spontaneously due to the decrease in solubility caused by the pressure reduction. When further separation is needed, it is often accomplished by distillation.

3. **Remotion of condensible water vapor (dehydration)**
   The gas dewatering and separation is usually done using the density difference as a driving force. Mechanical systems that make use of gravity and inertia are the usual choice for this step. Oil condensate and gas are separated and the first is sent to an oil refinery. If necessary, an additional separation stage eliminates most of the associated water [Dupuy, 2010].

4. **Remotion of other undesirable compounds, such as H_2S or CO_2**
   The sulfur content of natural gas ranges from virtually zero to approximately 30% H_2S. Pipeline gas is often specified at below 4 ppmv (parts per million on a volume basis), and even 1 ppmv [Maddox and Morgan, 2008]. Hydrogen sulphide is removed in order to reduce corrosion (and health risk in many cases) and then transformed into elemental sulfur. Most of the elemental sulfur used in industry goes into the production of sulfuric acid [Nehb and Vydra, 2000]. The most economically convenient method for gas sweetening is highly dependent on the acid gas (CO_2 and H_2S) content [Maddox and Morgan, 1986]. Solid bed adsorbents are recommended for mixtures with low acid content, while amines and membrane processes are recommended for moderate to high acid gas percentages [Bottoms, 1930]. Both sweetening methods are highly dependent on diffusion rates which lack a consistent quantitative theory behind them.

1.1.3 Conditioned gas processing

As mentioned above, natural gas is a relatively inexpensive feedstock that can be used in the production of a great number of hydrocarbons of higher value. The main products obtained from Gas To Products conversion are methanol, ammonia and synthetic crude oil (GTL) derivatives such as naphtha, kerosene, paraffins, diesel-oil and base-oil) among others. These liquid products can be transported in a cheaper way by using existing pipelines or tankers [Rajnauth et al., 2008]

GTL production

GTL technology is strategically important as it is capable of producing *more homogeneous products with less pollutants*. FT diesel can in general replace regular diesel fuel. In addition, having a high cetane number and no sulfur or nitrogen, it allows to endeavor the design of more efficient diesel engines with lower acid emissions [van Vliet et al., 2009]. This is highly desirable since environmentally friendly fuels are being increasingly demanded in Europe [Abrell, 2010].

GTL technologies are usually divided in two main categories: *direct conversion* and *indirect conversion* methods. On the one hand, the *indirect conversion* processes are based on the production of syngas as an intermediate step. The syngas is then used as a primary resource from which liquid fuels are produced via Fischer-Tropsch synthesis or via methanol. On the other hand, *direct conversion* processes save the cost of syngas production, but involve reactions with high activation energies and are more difficult to control. Both direct and indirect conversion methods involve catalytically enhanced reactions in which species transport plays an important role.

Syngas production

Syngas is the name given to a mixture of H_2, CO and CO_2 in variable proportions. It is produced by inducing a reforming reaction between methane (or carbon) and steam at elevated temperatures. Typical process conditions are around $1000°C$ and 3 *bar* [Lee and Han, 2009]. Conceptually, syngas can be produced from any carbon-based compound. In practice, the predominant feedstock of interest is low-value (e.g. stranded) natural gas.

Among the multiple applications of syngas the most important are:

- **Ammonia synthesis:** requires maximum H_2 production and removal of oxygen-bearing compounds.
- **Oxo-synthesis:** also known as hydroformylation, requires adjustment and CO_2 removal to give a 1:1 $H_2 : CO$ mixture. Produces aldehydes and some byproducts as alcohols, acetals and esters.
- **Reduction of oxides:** requires CO_2 removal, and the mix of CO and H_2 can be used to reduce oxides of base metals into ores.

Partial Oxidation Reforming	$CH_4 + CO_2 \rightarrow 2CO + 2H_2$	Exothermic
Steam Reforming	$CH_4 + H_2O \rightarrow CO + 3H_2$ $CO + H_2O \rightarrow CO_2 + H_2$	Endothermic

Table 1.4: Main reactions involved in syngas production from natural gas

The main technologies for syngas production from natural gas are based on the implementation of the chemical reactions depicted in Table 1.4. The choice of the process in made according to the size of the production, but also according to its final destination, which determines the desired characteristics of the product. The most important technologies for converting natural gas into syngas are, among others, Partial Oxidation *(POX)*, Steam Methane Reforming *(SMR)*, Autothermal Reforming *(ATR)* and two-step reforming.

These technologies for the production of GTL are compared in [Wilhelm et al., 2001]. It is concluded that SMR, two-step reforming and ATR processes are preferred for small, medium-sized and large scale productions respectively. The main process characteristics can be summarized as follows:

- **SMR** Yields a higher H_2/CO rate, which is the main reason behind the competitiveness of this process in hydrogen-intensive applications (e.g. ammonia synthesis, hydrogen production).
- **POX** Yields a lower H_2/CO rate, but the associated generation of CO_2 (usually undesirable as a byproduct) is also lower.
- **ATR** Consists in a combination of POX and catalytic SMR in the same reactor, taking advantage of the exothermic nature of POX in order to partially sustain the endothermic SMR reaction.

An additional advantage of the ATR process is that the final H_2/CO rate of the produced syngas can be adjusted to a specific value (a relation of 2 is required in feedstock for producing GTL liquids). The two-step reforming process is described in [Go et al., 2009].

1.1.4 Petrochemical commodities from natural gas

The countless final products obtained from natural gas are used in extremely diverse fields and applications that cover medicine, agriculture, energy production and many others. Four of the most important ones are mentioned below: all of them are produced by catalytic processes in which diffusion is a key element.

Sulfuric acid Sulfuric acid is normally manufactured at about twice the amount of any other chemical and is a leading economic indicator of the strength of many industrialized nations [Chenier, 2002, Chapter 2]. It is mainly used in production of fertilizers, but also in diverse applications such as dyes, explosives, metal cleaning, leather tanning, rayon and cellulose manufacturing and organic sulfonation processes for the production of detergents [E.S.A.A., 2000].

Ammonia It is the second largest synthetic chemical product worldwide. More than 90% of the world consumption is manufactured from nitrogen and hydrogen in a catalytic process originally developed by Haber and Bosch using a promoted iron catalyst discovered by Alwin Mittasch [Appl, 2000]. The catalytic synthesis of ammonia laid the foundations for subsequent high-pressure processes like methanol synthesis, oxo-synthesis, Fischer-Tropsch Process, coal liquefaction, and Reppe reactions. Its use as a fertilizer is so widespread that nitrate and ammonium are now the main pollutants in many areas, causing damage by acidification and base cation depletion in forests and freshwaters[1] [Schindler and Hecky, 2009].

[1] This is a compelling reason for controlling agricultural and industrial sources of nitrogen.

Hydrogen Steam Methane Reforming (SMR) accounts for about 95 percent of the hydrogen used today in the United States. The rest is generated by partial oxidation, which consists in burning methane in air. Both steam reforming and partial oxidation produce a synthesis gas, which is reacted with water to produce more hydrogen [U.S. Energy, 2008].

Methanol It is generated from a syngas mixture with no composition adjustment required for the process. Methanol finds application as a laboratory solvent and also as fuel for internal combustion engines or fuel cells, but mainly ($> 70\%$) as feedstock to produce other chemical compounds such as plastics, explosives, paints (from formaldehyde), gasoline additives (MTBE) and other compounds [Uhde Engineering, 2003].

1.2 Context & Objective

The current research was performed in the framework of the PAFFrx project (*Particle Fluid Flow with Chemical Reaction – Multi level models for design and optimization of fluidized bed processes*), sponsored by the Norwegian Research Council. The research objective of the PAFFrx project is to utilize knowledge and experience on CFD particle-fluid flow modeling and single-particle phenomena in order to improve predictions of the fluidized bed unit performance and generate knowledge contributing to optimal unit design and operation.

In this context, the ultimate goal is building a rigorous model of the whole system, coupling Computational Fluid Dynamics (CFD) analysis with physical models for mass and heat transfer and chemical reaction within each of the particles within the reactor. However, such a model would implicate an unmanageable numerical complexity and probably a restricted applicability. Therefore it is preferred to study the cross-effects on smaller systems with the aim of obtaining a simpler model based on well-understood underlying phenomena and a reduced number of meaningful parameters.

There is a lack of agreement between different diffusion theories, and therefore the most convenient validation method for the anomalous transport models seems to be comparing simulations against available experimental data. This will provide stronger arguments for determining whether a model is applicable or not. Hence, developing a suitable numerical framework prior to testing the new models is mandatory.

The objective of this Ph.D. project is generating tools for modeling transport phenomena occurring in a catalytic pellets inside a packed bed reactor. This requires developing a numerical framework capable of testing and comparing different diffusion models inside a particle and implementing their coupling with the diffusion of species in a fluid outside the particle. The goals for this project can then be summarized as:

1. **Developing an appropriate numerical technique for solving fractional differential equations.**
   Fractional differential models offer multiple possibilities for generalizing the scope covered by Fick's law in a consistent manner. However, their numerical implementation is challenging. The main concerns in this regard are their high computational requirements and mathematical complexity.

2. **Implementing models for anomalous diffusion in a particle.**
   Tools capable of reproducing and comparing different anomalous mass transport models are to be implemented. Three dimensional simulations may be required, but a two dimensional analysis is expected to suffice in accounting for the complete physics of the problem in many cases.

3. **Coupling solid diffusion and fluid flow.**
   The diffusion of species inside the particle is strongly coupled with the boundary conditions generated by the fluid flow around it. Therefore, modeling the flow is necessary in order to obtain accurate boundary conditions. A further step is coupling solid and fluid transport and studying their combined effect.

4. **Identifying criteria for choosing a proper diffusion model.**
   A benchmark should be formulated that helps determining whether anomalous effects should be considered given a particular case. As anomalous transport models are computationally expensive, their use is advantageous only when a significant difference in the obtained predictions is expected.

1.3 Scope

This work is aimed to building a platform from which contributions to a better understanding of diffusion physics can be made. At this early project stage, the scope of the present thesis is confined to developing and testing numerical tools.

Even though an exhaustive examination of the theoretical models was left as a secondary goal, a respectable amount of time was committed to generating a review of different anomalous transport models and finding a consistent structure between them.

The implemented models were restricted to a single particle where diffusion of a single chemical species was simulated. When considering flow around the particle, the fluid was assumed Newtonian and incompressible. Chemical reactions and heat transfer were not addressed in any case.

Simulations are based on least squares spectral element methods (LSSEM). The approach to the numerical formulation is made from a practical point of view, and the mathematical theory behind it is only addressed through references to other authors. Some of the mesh generation and operator mapping algorithms, however, are either a contribution by the author or tools that are regularly used in fields not related to modeling of transport phenomena.

1.4 Thesis outline

This thesis is divided into four parts: Part I consists in an introductory review meant to guide the reader through the topic of anomalous transport and its scope of application; Part II presents the essential numerical tools and concepts used throughout this thesis; Part III contains the code validation and results of the numerical simulations; Part IV features the main conclusions and suggestions for further work. An appendix presenting a collection of self-contained papers published at journals and conference proceedings is included.

Introduction

Chapter 1: Background and motivation. This chapter provides a general background on natural gas aimed for a layman reader, in order to provide a glimpse of its whole value chain and show the ubiquity of chemical processes where anomalous diffusion is relevant.

Chapter 2: Anomalous transport models. This chapter constitutes a short review of the most relevant theoretical and empirical refutations of Fick's law. A characterization of the models according to scale is proposed, and the connection and consistency between *fractional diffusion* and *continuous time random walk* is verified.

Numerical tools

Chapter 3: The Least Squares Spectral Element Method. This chapter consists in an introduction to the numerical technique used for the simulations throughout this thesis: the Least Squares Spectral Element Method. The concepts are presented from a practical point of view, aiming to make this chapter as self-contained as possible with the minimum necessary complexity.

Chapter 4: Numerical implementation. This chapter describes the numerical implementation details required to reproduce the calculations included in this thesis. The main points are the fractional derivative operator and geometrical mappings in spectral formulations.

Simulations and application to problems

Chapter 5: Cattaneo-Maxwell diffusion model. This chapter introduces a time-space implementation of the Cattaneo-Maxwell model, the simplest hyperbolic generalization of Fick's law that accounts for a finite information propagation velocity. This velocity affects the shape of the transient concentration profiles.

Chapter 6: Fractional diffusion models. This chapter presents a least squares spectral implementation of the five most common fractional diffusion models. The main numerical difficulties are discussed, and examples of calculated solutions are displayed in order to validate the current implementation.

Chapter 7: Coupling convection and diffusion. This chapter presents a framework for simulating species flow around a solid particle, coupled with anomalous diffusion inside the particle. The models presented in Chapters 5 and 6 are tested here as alternatives for describing diffusion in the solid.

Final remarks

Chapter 8: Conclusions. This chapter gives a brief overview of the main conclusions of this work and discusses possibilities for further research.

Publications

Article 1. Carella, A.R. and Dorao, C.A. (2010) *Solution of a Cattaneo-Maxwell diffusion model using a Spectral element least-squares method.* Journal of Natural Gas Science and Engineering 2, pp. 253-258. doi:10.1016/j.jngse.2010.08.001.
A Least Squares Spectral Element framework was implemented in order to solve the evolution of the concentration profile predicted by Cattaneo-Maxwell's law inside a catalytic pellet. Fick's and Cattaneo-Maxwell's models were compared, being the obtained predictions significantly different for time scales similar to the relaxation time but converging asymptotically for larger time scales. Time-marching and full-domain numerical approaches were compared. The convenience of the time-marching approach was verified as it yields the same accuracy with less computational cost.

Article 2. Carella, A.R., Dorao, C.A. (2011) *Migration of Species into a Particle Under Different Flow Conditions.* In Kuzmin, A. (Ed.): Computational Fluid Dynamics 2010, Proceedings of the Sixth International Conference on Computational Fluid Dynamics, ICCFD6, St. Petersburg, Russia, on July 12-16 2010. Springer-Verlag, Berlin Heidelberg. ISBN: 978-3-642-17883-2, pp. 869-871.
dx.doi.org/10.1007/978-3-642-17884-9_112
Fractional derivatives constitute a wider generalization of Fickian models that allows describing sub-diffusive and super-diffusive processes. Here the solution of an anomalous transport model based on fractional derivatives is discussed. The Least Squares Spectral Method is used along with Gauss-Jacobi quadrature in order to improve the numerical convergence.

Article 3. Carella, A.R. and Dorao, C.A. (2011) *Least-Squares Spectral Method for the solution of a fractional advection-dispersion equation.* Journal of Computational Physics. Accepted for publication. Manuscript number JCOMP-D-11-00463R1.
dx.doi.org/10.1016/j.jcp.2012.04.050.
This article describes a Least Squares Spectral Method for solving advection-dispersion equations using Caputo or Riemann-Liouville fractional derivatives. The implementation of a Gauss-Lobatto-Jacobi quadrature in order to approximate the singularities arising from the fractional derivative definition is explained in detail. Exponential convergence rate of the operator is verified when increasing the order of the approximation. Comparisons with finite difference schemes are included, showing that a significant decrease in required storage space is achieved by using a spectral time discretization as the resolution requirements in the time coordinate are reduced.

Article 4. Carella, A.R. and Dorao, C.A. (2012) *Modeling of fractional diffusion on a catalytic particle under different flow conditions.* Defect and Diffusion Forum 323-325(121), pp. 121-126.
dx.doi.org/10.4028/www.scientific.net/DDF.323-325.121
The problem of predicting the flow of species into a particle is of large importance in the design of catalytic particles. A numerical framework using the Least Squares Spectral Element Method is implemented in order to analyze the species transport into a particle immersed in a flow. The qualitative change in the concentration profiles in the transition from Fickian to fractional diffusion inside the particle is investigated. A sample case corresponding to a flow between two parallel plates and around a cylinder is displayed.

Article 5. Carella, A.R. and Dorao, C.A. (2012) *N-dimensional Least Squares Spectral Method formulation for the general Fractional Diffusion Equation.* Journal of Computational Physics - Under review.
This article presents an extension of the Least Squares Spectral Method capable of solving partial fractional differential equations for any number of dimensions. For adapting this method to various geometries and concentrating the interpolating nodes at given zones, two domain mapping techniques called homography and isoparametric method are presented. The linear homography method is simple and automatable, but is restricted to polygonal (linear) mappings, while the isoparametric technique can be used for non-linear mappings. Numerical solutions to three sample problems are presented and discussed. The strengths and weaknesses of the current implementation are analyzed through a convergence study.

Chapter 2

Anomalous transport models

Questions have arisen about the validity of Fick's diffusion model since the beginning of the systematization of diffusion study. On the one hand, many pieces of experimental evidence collected during the last years show diffusive phenomena that are not properly described by this model. On the other hand, strong theoretical arguments deter from considering Fick's law as a definitive model for diffusion.

This chapter provides a short review of the most actual and relevant diffusion models and the main ideas behind them. Section 2.1 defines the concept of anomalous transport and presents an overview of application cases. Section 2.2 divides the transport models into categories according to the level of detail considered in them. Section 2.3 presents the main features of the *Continuous Time Random Walk* (CTRW) model, a consistent generalization of the classical random walk model. Section 2.4 introduces *Fractional diffusion models*, an extension of Fick's law to fractional derivative exponents. The main ideas contained in this chapter are briefly summarized in Section 2.5.

2.1 What is anomalous transport?

Due to its mathematical simplicity and acceptable accuracy for describing certain diffusive processes, Fick's law has been accepted as the universal 'standard' diffusive law [Visscher, 1984a;b; Herwig and Beckert, 2000]. Fickian transport models obey certain well-defined characteristic rules such as dispersing linearly with time[1] and yielding constitutive laws that result in parabolic systems. Any alternative diffusion law not complying with these characteristics is then labeled as '*anomalous transport*'.

Fick's law is object of controversy based on both theoretical and empirical arguments. The main theoretical objection against Fick's law is the so-called

[1] Given the solution $f(x,t)$ to a transport problem, a linear dispersion means that the second moment of the x coordinate increases linearly with time, according to $\langle x^2 \rangle \propto t$.

infinite propagation velocity paradox, which will be discussed in Section 2.1.1. In addition, many pieces of experimental work (discussed in Section 2.1.2) have been published which contribute to discredit Fick's law as the universal diffusion model. An overwhelming amount of evidence suggests that *'anomalous diffusion is the rule in concentration-dependent diffusion processes'* [Küntz and Lavallée, 2001; 2004].

2.1.1 Infinite propagation velocity paradox

Infinite propagation velocity paradox is one of the mathematical consequences of using Fick's law as a constitutive law, by which disturbance propagation at an infinite speed is predicted. This means that a perturbation arising at any point of the domain is instantly detected everywhere (see Example 2.1), which disagrees with Einstein's theory of relativity. This paradox is inherent to linear parabolic models, and has been extensively discussed in several articles, e.g. [Liu, 1979; Gómez-Díaz, 2006].

Example 2.1: Fickian propagation of a concentration pulse

Let us analyze the fundamental problem of Fickian diffusion: a concentration pulse in an infinite medium. The mathematical form of the system (Eq. (2.1)*) consists of a second order differential equation and an initial condition.*

$$\begin{cases} \dfrac{\partial C(x,t)}{\partial t} = D\dfrac{\partial^2 C(x,t)}{\partial x^2} & -\infty < x < \infty, \quad t > 0 \\ C(x,0) = \delta(x) \end{cases} \tag{2.1}$$

The analytical solution for this case can be found in many textbooks e.g. [Incropera and DeWitt, 2002], and has the form

$$C(x,t) = \frac{1}{\sqrt{4\pi D t}} \exp\left(-\frac{x^2}{4Dt}\right) \tag{2.2}$$

which implies $C(x,t) > 0$ for every $t > 0$. In other words, the information propagates instantly to the whole domain.

2.1.2 Experimentally observed anomalous transport

Since most of (if not all) the known heat and mass transport processes fall into the anomalous transport category [Küntz and Lavallée, 2004], attempting to do an extensive review would be too ambitious. Even when a considerable effort is being done in order to elucidate the global picture, the best modeling approach for

each case is still a matter of discussion. Illustrating this point, the performance of five anomalous diffusion models is evaluated in [Gao et al., 2009] by comparing them with the same experimental setup. None of the models is found satisfactory by the authors.

A selection of relevant cases is introduced here in order to set the background for the present work. The considered articles are grouped into categories, and a summary is presented in Table 2.1. Further general reviews with examples of anomalous transport in many fields can be found in [Klafter and Sokolov, 2005; Sokolov and Klafter, 2005].

Model 1 ***Hyperbolic diffusion.*** Diffusion models are usually developed from a steady-state perspective. Starting from Einstein's mechanistic definition of molecular diffusion and replacing the mean quasi-static values by a full transient model, it is shown in [Landau and Lifshitz, 1959] that a hyperbolic description is valid.[2] However, this correction would only be noticeable for processes with extremely small characteristic times or in certain cases of composite materials. Under this conditions the validity of classical mechanics is, at least, arguable. A nonlinear alternative with vanishing diffusion coefficients for certain concentration values is proposed in [Kath, 1984]. It is described in [Klages et al., 2008, Chapter 3.9] how coupled memory random walks yield a hyperbolic diffusion model.

Model 2 ***Hyperbolic heat transfer.*** An exhaustive chronology of ideas about heat waves is presented in [Joseph and Preziosi, 1989]. No significant pieces of knowledge about the history dependence of the internal energy appear to be published prior to this date. The consistency of this model is severely questioned in [Bright, 2009].

Model 3 ***Non-linear parabolic diffusion.*** A model is proposed in [Islam, 2004], obtaining consistent results, in which the diffusive flux is proportional to the chemical potential gradient instead of the concentration. As boldly stated in this work, *"Fick's law loses to some extent its credibility as the flux is proportional to the gradient of some parameter (concentration) and at the same time the proportionality constant is also a function of the same parameter"*.

Model 4 ***Generalized Ohm's law.*** A relaxation equation for the electrical conduction current density is proposed in [Cuevas et al., 1999]. This generalized Ohm's law takes into account the inertial effects of electrons, and its predictions coincide with Drude's model for metals. However, experimental verification would require working with lengths of around 10^{-7}m and

[2]The arguments in [Landau and Lifshitz, 1959] assume that a classical mechanics description is applicable. This assumption is only valid for scales above the continuum limit.

frequencies of around 10^{14}Hz. This is expected to be relevant to the description of the magnetic field in plasma drift waves, where the inertia of electrons is expected to be significant.

Model 5 ***Mixed random walk models.*** The percentage of existing oil that can be extracted from a reservoir depends on the rate of migration of species into the porous soil [Jahn et al., 2008]. The system considered in [Tørå et al., 2009] is extremely heterogeneous and a 'pseudo-homogenization' modeling technique is presented. The microscopic diffusive properties are explored using random walkers and then related to electrical conductivity by using Einstein's relation. The associated problem of upscaling from microscopic to macroscopic lengths is addressed in [Hilfer, 1996].

Model 6 ***Time-dependent random walk.*** Continuous Time Random Walks with a Mittag-Leffler waiting time law lead to the space-time fractional diffusion equation [Mainardi et al., 2000; Gorenflo et al., 2001].A process not complying with the central limit theorem plays a key role in the analysis by [Scher and Montroll, 1975]. Long-tail time distributions can be obtained from random activation energies in an Arrhenius-law model [Bendler et al., 2007].

Model 7 ***Fractional derivative models.*** The fractional advection-dispersion equation is regarded as a model capable of coping with the heterogeneity of geological media by including non-local effects [Casper et al., 2012; Zhang et al., 2007]. Large ranges of solute displacement (superdiffusion) can be described with space-fractional models while long waiting times (subdiffusion) are generated by time-fractional models. Space-vs-time nonlocality is discussed in [Zhang et al., 2009].

2.2 When should anomalous models be used

The long list of arguments questioning Fick's law, including the ones summarized at Section 2.1, should plant a seed of doubt about using this model for analyzing diffusive phenomena. Nevertheless, Fick's law is still used in many applications, mainly because of practical reasons among which we can count the following:

- Parabolic equations are well known and mathematically simple.
- The predicted results are useful as estimative values in some applications (Gómez et al., 2010).
- Testing new models requires accurate dynamic diffusion measurements, which involve large difficulties and uncertainties (Leipertz and Fröba, 2005).

Attempted approach	**Motivation**	**Field**	**Overview**	**References**
Hyperbolic diffusion	Infinite propagation velocity paradox	Macroscopic diffusion in fluids and composites	**Model 1**	[4; 68; 99; 110]
Hyperbolic heat transfer	Infinite propagation velocity paradox	Heat conduction in various materials	**Model 2**	[37; 181]
Non-linear parabolic diffusion	Thermodynamical consistency	General theory for species diffusion	**Model 3**	[89; 105]
Generalized Ohm's law	Significant corrections for high frequencies	Electronic conduction in metals	**Model 4**	[37]
Mixed random walk	Oil reservoir optimization	Multiphase diffusion in geological media	**Model 5**	[13; 82; 181]
Time-dependent random walk	Development of photocopying machines	Photocurrent and vacancy diffusion in materials	**Model 6**	[10; 102; 167]
Fractional derivatives	Memory and space non-locality	Species migration in heterogeneous media	**Model 7**	[13; 27; 197; 198]

Table 2.1: Summary of the most relevant anomalous diffusion models reported in literature

However, some applications require an accurate description for heat or mass diffusion at short times. Some emblematic cases in addition to the list provided in Section 2.1.2 are presented in (Lane et al., 1947; Vick and Ozisik, 1983; Stöcker, 2005). The purpose of this section is providing estimative guidelines that can help to determine under which conditions anomalous transport models should be used.

2.2.1 Applicability of Fick's law

Fick's law can be derived with reasonable ease from a random walk model, see for example (Berg, 1993, Chapter 2). However, its theoretical range of validity is restricted to the following assumptions:

- no lateral interactions (mutual perturbations) exist between the particles,
- the behavior of the walkers is independent of the medium,
- the medium is isotropic and therefore no preferential interactions exist,
- the number of steps is "statistically significant" (non-valid at short times).

These strong assumptions are only fulfilled in a very limited number of cases, such as diffusion in very dilute solutions after a given onset time. Systems like multicomponent mixtures, mixtures of two gases in porous media or mixtures with cations generally do not satisfy the mentioned assumptions. An introductory level discussion of these topics can be found in (Wesselingh and Krishna, 1990).

The random walk model assumptions can be relaxed by considering the possibility of having a probability distribution (instead of a single value) of step lengths and waiting times. Fick's law is recovered by choosing probability distribution functions that decay fast enough. Arbitrary probability distribution functions result in *Continuous Time Random Walk* models, as presented in Section 2.3.

2.2.2 Transport modeling according to level of detail

The first broad characterization of diffusion models can be done according to the level of detail each model accounts for. This is accomplished as a compromise between the required precision and the affordable modeling complexity in the description of the physical phenomenon.

The anomalous transport models can be categorized in three basic levels, as depicted in Fig. 2.1 (Balescu, 2005; 2007). In order to achieve a consistent description, each level must be a suitable approximation of the more fundamental ones. This consistency is a challenging subject since the interrelation of these levels is not a closed matter.

Geometric characterizations of correlated microstructures and the problem of upscaling from microscopic to macroscopic length scales are introduced in (Hilfer, 1996). The topic is further considered in (Berkowitz et al., 2006), where the

fact that *species migration experiences a high sensitivity to inhomogeneities at all scales* is reasserted. This has motivated the development of macro-scale models that account for such inhomogeneity.

At one end we find *statistical mechanics*, a combination of the basic laws of microscopic dynamics with the laws of large numbers (Dorfman, 1999). Statistical mechanical models can account for the behavior of the high number of particles, but the analysis of real cases results unfeasible since the number of degrees of freedom becomes unmanageable.

Moving up in scale, *V-Langevin equation* and *CTRW* are regarded as semi-deterministic treatments. They provide a compromise between the complex statistical mechanical formulation and the macro-scale diffusive models. Each of the multiple considered particles is characterized by its instantaneous position $x(t)$ and obeys an equation of motion having the same shape as the Newtonian equation. The velocity of each particle, however, is considered to be a (stochastically) fluctuating quantity, following an external field. Some attempts to link different modeling scales have been done recently (Meerschaert et al., 2010).

The macro-scale generalization of these descriptions are *fractional diffusion models*. These account for inhomogeneities in the diffusive medium by considering variable step length and waiting time, and also include non-local effects. Analog to the case of RW and Fick's law, CTRW models lead to fractional diffusion under the conditions described in Section 2.3.3. The scope of this thesis is restricted to macro-scale anomalous transport, represented in the upper block of Fig. 2.1.

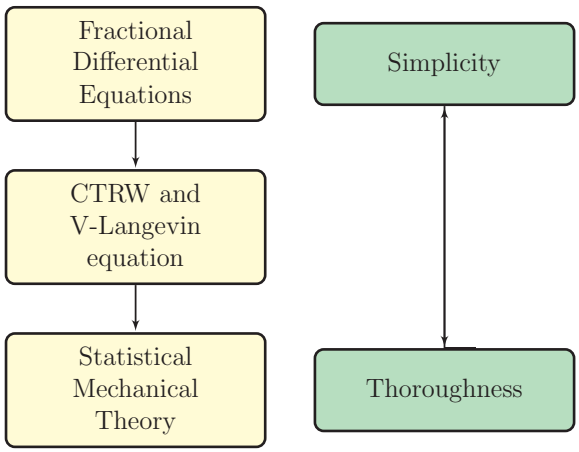

Figure 2.1: Global classification of anomalous transport models according to scale

2.3 Continuous Time Random Walks

The concept of Continuous Time Random Walk (CTRW) incorporates time and space non-local effects to the classical random walk (Montroll and Weiss, 1965). In this approach, a set of walkers performs jumps of lengths Δx_i at times t_i. The jumps Δx_i and waiting times $\Delta t_i = t_i - t_{i-1}$ are drawn from different probability density functions (PDF) $\psi_x(x)$ and $\psi_t(t)$, respectively. Therefore, the probability $P(x,t)$ of finding a walker at position x and time t is given by

$$P(x,t) = \delta(x) \int_t^\infty \psi_t(t')dt' + \int_0^t \psi_t(t-t') \left[\int_{-\infty}^{\infty} \psi_x(x-x')P(x',t')dx' \right] dt', \quad (2.3)$$

where the first term accounts for the accumulation of walkers up to time t and the second term accounts for the particles arriving to the position x at time t.

Since the laws of Brownian motion result from the Central Limit Theorem (CLT), the usual form of the theorem fails when anomalous diffusion is present (Bouchaud and Georges, 1990). This can be due to the existence of either long range time correlations or jump/wait PDFs with diverging first or second moment.

For any CTRW defined by a jump PDF $\psi_x(x)$ having at least finite first and second moments, and a waiting time PDF $\psi_t(t)$ having at least a finite first moment, the density profile $P(x,t)$ tends to a Gaussian packet for long times and large distances, as depicted in Fig. 2.2 (Balescu, 2005).

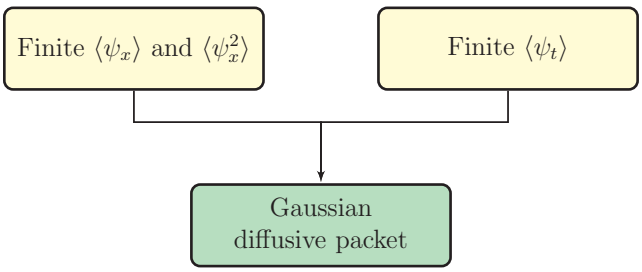

Figure 2.2: Conditions for the formation of Gaussian diffusive packets

An explicit relation can be found between the waiting time in a semi-Markovian random walk process and the memory kernel of Eq. (2.3) so that they describe an equivalent process (Kenkre et al., 1973). Both the fractional time diffusion equation (see Section 2.3.3) and Cattaneo's equation (see Chapter 5) can be derived from choosing the PDF kernels properly in the generalized master equation.

2.3.1 Long tail distributions

Gaussian distributions represent the limit distributions of independent identically distributed (*iid*) random variables with finite variance $\langle x^2 \rangle$. As an analogy, Lévy

flights represent the limit distributions of *iid* random variables with *infinite* variance $\langle x^2 \rangle \to \infty$. Lévy flights are also referred to as *long tail distributions*.

Long tail distributions have been used as a tentative approach to describe numerous processes. Examples are turbulence (Dubrulle and Laval, 1998), plasma physics (Chechkin et al., 2002; Krommes, 2002; Jha et al., 2003), animal migration (Reynolds and Frye, 2007; Ramos-Fernndez et al., 2004) and disease spreading (Bossak and Welford, 2010) among others (Metzler and Klafter, 2000; 2004; Shlesinger et al., 1999). Nevertheless, Lévy flights are under ongoing research since their thermodynamical consistency and proper formulation are still a matter of discussion.

Long tail distributions can be obtained either from random processes such as the *Saint Petersburg paradox* (Rieger and Wang, 2006, Section 1.3) and the model of *activated hopping* (Bendler et al., 2007) or through a deterministic approach, as illustrated in (Klages et al., 2008, Chapter 3).

2.3.2 Pseudo-Random PDF generation

In order to be able to test CTRW tendencies for different walking models, a non-uniform PDF (i.e. a random function with a non-uniform occurence probability) is required. The easiest way to generate such a function is by transforming a uniform PDF and mapping it into the target probability distribution $\psi(\xi)$. The procedure is explained next and proven in textbooks such as (Devroye, 1986, Chapter 1).

1. The cumulative distribution function $\Psi(\xi)$ is calculated as

$$\Psi(\xi) = \int_{-\infty}^{\xi} \psi(\xi')d\xi' \tag{2.4}$$

2. A random number s_U is drawn from a uniform PDF between 0 and 1

$$s_U = rand_{[0,1]} \tag{2.5}$$

3. A random sample s_{NU} from $\psi(\xi)$ is calculated as

$$s_{NU} = \Psi^{-1}(s_U) \tag{2.6}$$

The power law distribution $\psi(\xi) = C\xi^{-\beta}$ is particularly interesting when applied to CTRW processes since it gradually leads to different diffusion behaviors depending on the value of the exponent. In the cases with $\beta \leq 1$ the distribution does not have a finite integral and it is therefore necessary to truncate its infinite tail in order to obtain an approximation. The procedure for obtaining a truncated power law PDF $\psi_N(\xi)$ is illustrated in Example 2.2.

Example 2.2: Generation of a power law distributed PDF

The truncated power law PDF is defined as

$$\psi_N(\xi) = \begin{cases} \frac{1-\beta}{\xi_1^{1-\beta}-\xi_0^{1-\beta}}\xi^{-\beta} & \xi_0 < \xi < \xi_1 \\ 0 & otherwise \end{cases}$$

and so the cummulative distribution function $\Psi_N(\xi)$ *from Eq.* (2.4) *is*

$$\Psi_N(\xi) = \begin{cases} 0 & \xi \leq \xi_0 \\ \frac{\xi^{1-\beta}-\xi_0^{1-\beta}}{\xi_1^{1-\beta}-\xi_0^{1-\beta}} & \xi_0 < \xi < \xi_1 \\ 1 & \xi \geq \xi_1 \end{cases}$$

A sample from a power law distributed PDF is obtained from Eq. (2.6) *as*

$$s_{NU} = \Psi_N^{-1}(s_U) = \left[\left(\xi_1^{1-\beta} - \xi_0^{1-\beta}\right) s_U + \xi_0^{1-\beta}\right]^{\frac{1}{1-\beta}}$$

2.3.3 Linking CTRW and fractional diffusion

Continuous time random walk constitutes a flexible and attractive model for observing phenomena at a micro-scale. On one hand it has the capability of providing a detailed description of the physical behavior of particles. On the other hand, effects such as space non-locality and memory (time non-locality) can also be included in the description.

As mentioned in Section 2.2.2, the complexity grows exponentially as the number of particles is increased if interactions between particles are considered. In addition, as for any stochastic model, a large number of samples is required in order to assure repeatability. Therefore it becomes desirable to complement this model with its macro-scale counterpart in order to both simplify the treatment and reduce computational cost.

Random walk and Fick's law

It is commonly accepted that the predictions from a standard RW model are equivalent to Fick's law when continuum hypotheses are used (Berg, 1993). The propagation of a concentration pulse (see Example 2.1) can be represented by a random walk model where each particle faces an homogeneously distributed jumping probability distribution at each time step ($t_n = n\Delta t$), as depicted in Fig. 2.3. Calculations from a random walk model with parameters $\Delta x = 0.01$ and $\Delta t = 0.04$ are presented together with its Fick's law counterpart in Fig. 2.4. The

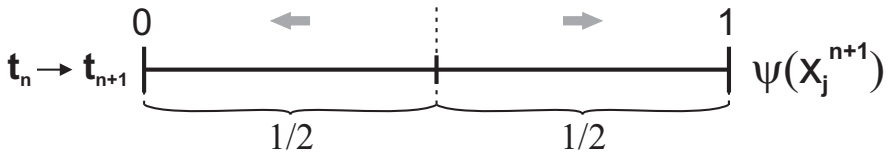

Figure 2.3: Jumping probability distribution for a random walk model

equivalence between models is given by

$$D = \frac{(\Delta x)^2}{2\Delta t}, \tag{2.7}$$

where D is the diffusion coefficient, Δx is the step length and Δt is the waiting time between steps. Note in Fig. 2.4 that the equivalence between models becomes clearer as the number of walkers increases.

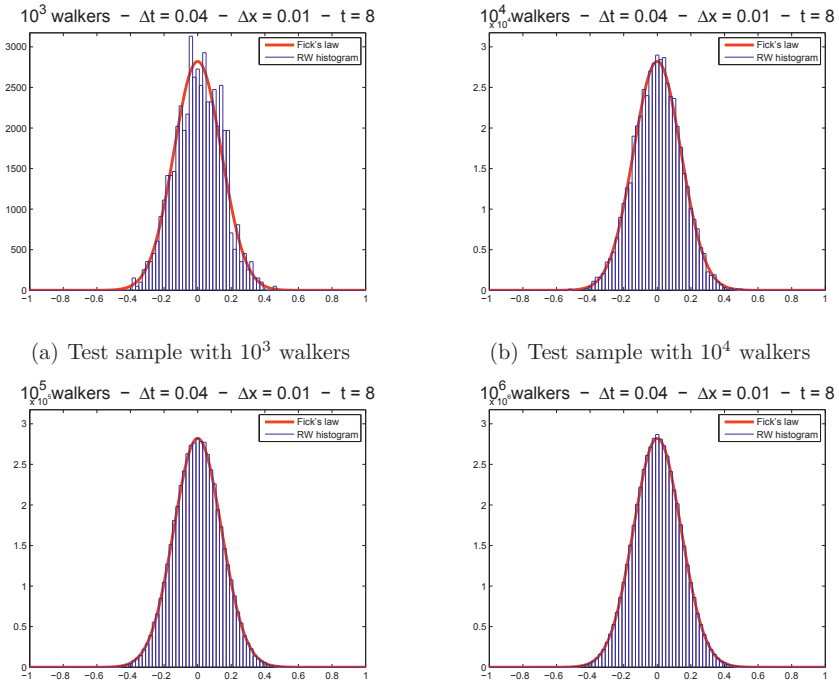

(a) Test sample with 10^3 walkers

(b) Test sample with 10^4 walkers

(c) Test sample with 10^5 walkers

(d) Test sample with 10^6 walkers

Figure 2.4: Diffusion of a concentration pulse by Fick and random walk models

Continuous time random walk and time fractional diffusion

A link between fractional diffusion and anomalous transport is provided by the theory of random walks (Klages et al., 2008, Chapter 6.1). In the continuum limit, the CTRW model leads to the fractional diffusion equation. Here the fractional order of the derivatives depends on the decay exponents of the jumping length and waiting time probability functions.

If a Markovian approach is taken (i.e. memory effects are neglected) Eq. (2.3), called the master equation, leads to the diffusion equation. When memory and long jumps are included through decaying probability density functions, the continuum limit leads to the fractional diffusion equation (Lynch et al., 2003). Due to its non-local nature, fractional diffusion models provide a non-bijective relationship between concentration gradient and flux (Paradisi et al., 2001). This means that the flux and the concentration gradient cannot be unambiguously determined from each other's local value since they depend on the previous history.

A relation analogous to the one described above between Fick's law and random walk can be found between continuous time random walk and Eq. (2.19), which will be presented in next section. Proof of the equivalence between the time fractional diffusion equation and a CTRW considering memory effects is given in (Gorenflo et al., 2002). In order to achieve this equivalence, the jumping probability distribution at each time step t_n includes terms that account for the possibility of staying at the same place or returning to previous positions, as depicted in Fig. 2.5.

During the first time instant the particles can either jump left, stay at the same position or jump right with probabilities μ, $(1-2\mu)$ and μ respectively. At subsequent times, a probability of returning to a previous position is added to the PDF. The constants in the sketch are defined as

$$\begin{cases} c_i = (-1)^{i+1}\binom{\beta}{i} = \left|\binom{\beta}{i}\right| & i \geq 1 \\ b_n = \sum_{i=0}^{n} (-1)^i \binom{\beta}{i} & n \geq 0 \\ \mu = \dfrac{\tau^\beta}{h^2} & 0 < \beta \leq 1 \end{cases} \tag{2.8}$$

where μ is the time-space renormalization constant, β is the time fractional derivative exponent, τ is the time step and h is the spatial step. The probability for a particle to return to a given old position vanishes as time advances, in agreement with Eq. (2.19). CTRW simulations reproducing the procedure in (Gorenflo et al., 2002) are presented in Fig. 2.6 superimposed with the analytical solution for Eq. (2.19).

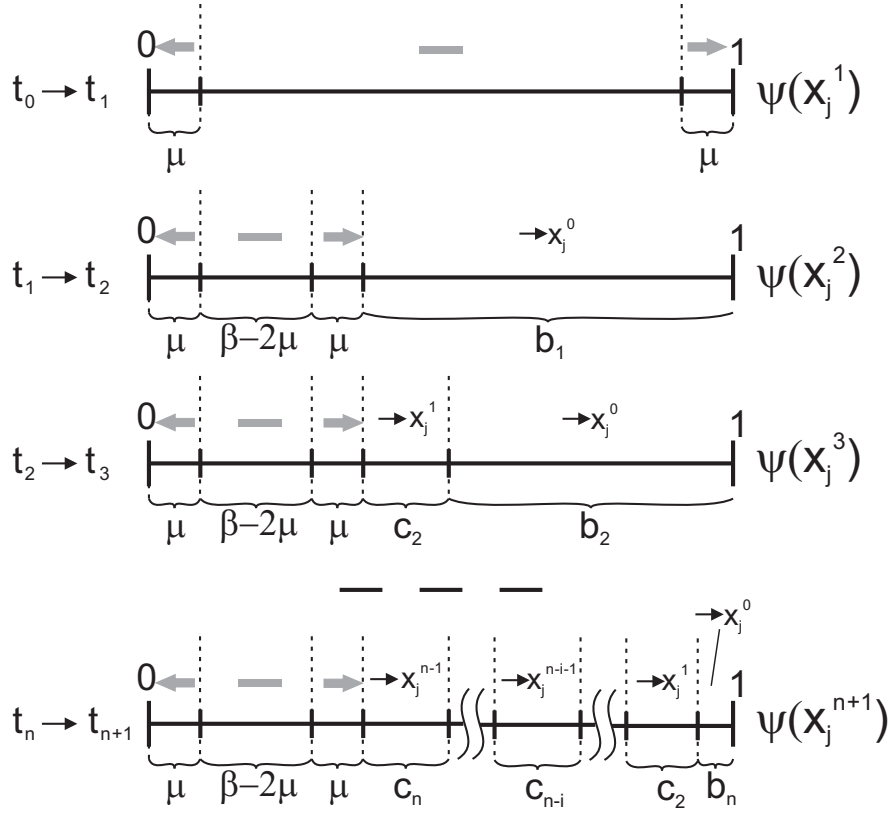

Figure 2.5: Jumping probability distribution for CTRW model with memory

2.4 Fractional diffusion models

This section presents the most common fractional diffusion models mentioned in Sections 2.1 to 2.3. Prior to discussing fractional diffusion, the fractional derivative operator must be properly introduced.

2.4.1 Fractional derivatives

Fractional derivatives are non-local operators that extend the notion of derivative from positive integers to any real exponent. The usual notation to refer to fractional derivatives is the same as the notation used for integer-order derivatives. That is, the expression

$$D^{\beta} f(t) = \frac{d^{\beta} f(t)}{dt^{\beta}}, \quad \beta \in \mathbb{R} \tag{2.9}$$

is used, where β can adopt any real value and $\beta < 0$ are fractional integrals.

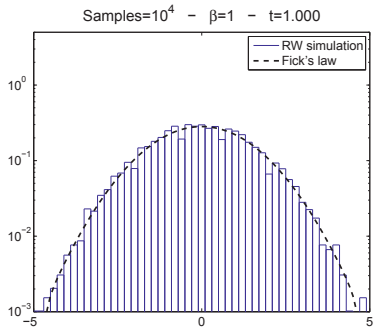

(a) RW vs Fick's diffusion

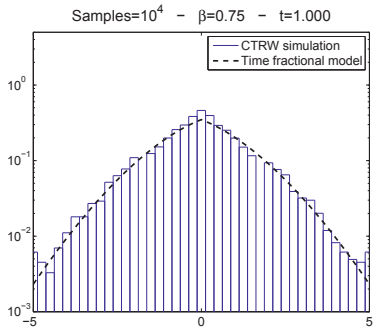

(b) CTRW vs fractional diffusion: $\beta = 3/4$

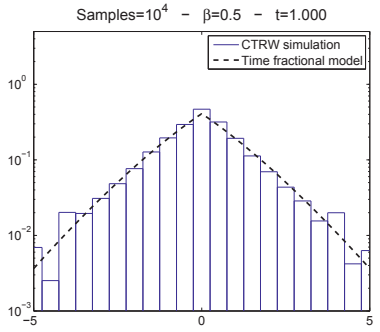

(c) CTRW vs fractional diffusion: $\beta = 1/2$

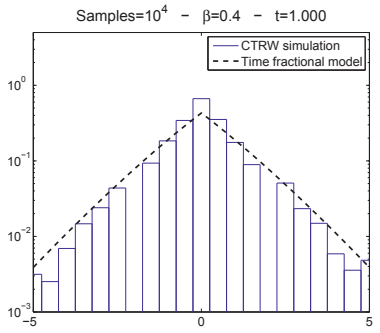

(d) CTRW vs fractional diffusion: $\beta = 2/5$

Figure 2.6: Fractional diffusion of a pulse by Eq. (2.19) vs. CTRW in Fig. 2.3

The extension from integer to fractional derivatives is not unique. The two main approaches for this generalization are *iterated integration* and *iterated differentiation* (Podlubny, 1999).

Iterated integration approach

Fractional derivatives can be approached as an inductive generalization through iterated definite integrals. This is extensively explained in (Kleinz and Osler, 2000), and yields the definition

$$RL: \ {}_0D_t^{\beta} f(t) = \frac{1}{\Gamma(n-\beta)} \frac{d^n}{dt^n} \int_0^t \frac{f(\xi)\, d\xi}{(t-\xi)^{\beta+1-n}}, \qquad n-1 < \beta \leq n \tag{2.10a}$$

by Riemann-Liouville (Klages et al., 2008), where n is the smallest integer that is greater than or equal to β and 0 is the lower integration limit. This is known as the left hand definition (LHD) of the fractional derivative (Podlubny, 1999).

An alternative definition, usually referred to as the right hand definition (RHD) and attributed to (Caputo, 1967), is

$$Ca: \ {}_0D_t^{\beta} f(t) = \frac{1}{\Gamma(n-\beta)} \int_0^t \frac{f^{(n)}(\xi)\, d\xi}{(t-\xi)^{\beta+1-n}}, \qquad n-1 < \beta \leq n \tag{2.10b}$$

with the same restrictions on β and n. The fact of inverting the order between the integration and the differentiation has consequences on the modeling implementation and the interpretation of results (Loverro, 2004). The two definitions are linked as presented in Eq. (2.11). A further comparison can be found in (Li and Deng, 2007).

$${}_0D_t^{\beta} f(t)_{\text{ RL}} = \frac{f(0)}{\Gamma(1-\beta)\, t^{\beta}} + \ {}_0D_t^{\beta} f(t)_{\text{ Ca}} \tag{2.11}$$

Note that the definitions in Eqs. (2.10a) and (2.10b) yield special cases when integer values of β are considered

$$\begin{cases} {}_0D_t^{\beta} u(\mathbf{x},t) = \dfrac{\partial^{\beta} u(\mathbf{x},t)}{\partial t^{\beta}} & \text{if } \beta \in \mathbb{Z} > 0 \\ {}_0D_t^{\beta} u(\mathbf{x},t) = \underbrace{\int_0^t \cdots \int_0^{t_{n_1}}}_{\text{n-fold integral}} u(\mathbf{x},t_n) dt_n \cdots dt_1 & \text{if } \beta \in \mathbb{Z} < 0 \end{cases} \tag{2.12}$$

The left hand definition in Eq. (2.10a) integrates the function $f(t)$ before differentiating it, and only requires $f(t)$ to be causal ($f(t) = 0$ for $t \leq 0$). However, a significant drawback in using this definition in the formulation of physical problems is the requirement of fractional initial conditions in order to solve the resulting fractional differential equations. The physical meaning of these fractional initial conditions is not completely clear (Rutman, 1995; Podlubny, 2002). Aditionally, according to this definition, the fractional derivative of a constant C is not zero but is calculated as $D^{\beta} C = \frac{Ct^{-\beta}}{\Gamma(1-\beta)}$. The latter is not necessarily a drawback, since it suitably describes phenomena related with aging processes (Jumarie, 2009).

On the other hand, if the right hand definition (Eq. (2.10b)) is used, then the requirements for $f(t)$ are more demanding. It is then required that the function and all its derivatives are zero at the left boundary of the integration interval, namely $f(0) = f^{(1)}(0) = f^{(2)}(0) = ... = f^{(n)}(0) = 0$ in order to ensure the convergence of the right hand side of equation Eq. (2.10b). However, this definition makes the fractional derivative of a constant zero, as for the integer exponent case. It also allows integer order initial conditions (with immediate physical interpretation) to be used in the solution of fractional differential equations.

Iterated differentiation approach

Another approach to fractional derivatives is through succesive differentiation. In this case, the generalization of Eq. (2.9) yields the definition

$$ {}_0D_t^{\beta} f(t) = \lim_{n\to 0} \left(\frac{1}{h}\right)^{\beta} \sum_{r=0}^{\frac{t-a}{h}} (-1)^r \binom{\beta}{r} f(t-rh) \tag{2.13} $$

It has been proven that if $f(t)$ is $(n-1)$ times continuously differentiable and $f^{(n)}(t)$ is integrable in $[0,T]$ formulations in Eqs. (2.10) and (2.13) exist and are equivalent (Podlubny, 1999).

Right derivatives

Equation (2.10) defines the fractional derivative ${}_0D_t^{\beta} f(t)$ using the information of the function in the interval $[0,t]$ and can thus be interpreted as a function of time before the current instant. However, the fractional derivative can also be defined as a function of time after the current instant as ${}_tD_{\infty}^{\beta} f(t)$ by performing the integral in the interval $[t,\infty)$.

If the variable t represents time for the process f, physical causality gives meaning only to the left definition, since it is an operation performed on the past states of the process $f(t)$. Although right derivative presents some similarities with a conjugate operator and remains of interest for mathematical theories, we will only be concerned with left derivatives in this thesis.

2.4.2 Fractional diffusion models

Mass transfer is governed by a transport equation in combination with a given constitutive equation. Equation (2.14) represents a one-dimensional transport equation without source terms. Here the variables $C(x,t)$ and $J(x,t)$ represent species concentration and species flux respectively.

$$ \frac{\partial C(x,t)}{\partial t} + \frac{\partial J(x,t)}{\partial x} = 0 \tag{2.14} $$

The traditional constitutive equation used to model diffusion is Fick's first law (Eq. (2.15)) which is appropriate only in a very limited number of cases (Küntz and Lavallée, 2004; Klafter and Sokolov, 2005). Diffusive flux is then modeled as

$$ J(x,t) = -\mu(x) \frac{\partial C(x,t)}{\partial x}, \tag{2.15} $$

where $\mu(x)$ is the diffusion coefficient. Using Eq. (2.15) as a constitutive law is appropriate only if the mean free path of the modeled dispersion process is short

enough. If, on the contrary, the mean free path is too long, the species flux can be modeled by equation Eq. (2.16), which represents a ballistic propagation process.

$$J\left(x,t\right) = C\left(x,t\right) \tag{2.16}$$

For moderately long mean free paths, Eq. (2.17) has been proposed as a constitutive law in order to account for an intermediate scenario in which neither Eq. (2.15) nor Eq. (2.16) are suitable approximations. Diffusive flux is then expressed as

$$J\left(x,t\right) = -\mu(x)\Bigg(\left(1-q\right)\ {}_0D_x^{\beta}C\left(x,t\right) + q\ {}_xD_1^{\beta}C\left(x,t\right)\Bigg), \qquad 0 \leq \beta \leq 1, \tag{2.17}$$

where q is the relative contribution of the right derivative to the total derivative ($0 \leq q \leq 1$). The cases $q = 0$, $q = 1$ and $q = 0.5$ are called *left derivative*, *right derivative* and *Riesz derivative* respectively. The operator ${}_aD_b^{\beta}$ denotes either the Riemann-Liouville or the Caputo fractional derivative from Eq. (2.10).

Equation (2.17), denominated the fractional advection-dispersion constitutive equation, has been proposed in (Chaves, 1998; Schumer et al., 2001) as a generalization of integer order derivatives to describe diffusion processes in which Lévy flights occur. More on the interpretation of this equation can be found in (Fix and Roop, 2004; Meerschaert et al., 1999). Note that if $\beta = 1$, then Eq. (2.17) reduces to Eq. (2.15).

The formulation of a wide range of problems is achieved by combining Eq. (2.14) and Eq. (2.17) and adding Dirichlet boundary condition as shown in Eq. (2.18)

$$\begin{cases} \dfrac{\partial C}{\partial t} = \mu(x)\left[\left(1-q\right)\ {}_0D_x^{1+\beta}C + q\ {}_xD_1^{1+\beta}C\right] & in\ \ \Omega = [0,1]\times[0,1] \\ C(0,t) = C_0 \\ C(1,t) = C_1 \\ C(x,0) = C_{IC}(x) \end{cases} \tag{2.18}$$

Further generalizations of this model are presented in (Luchko, 2009; Hanert, 2011). In order to model superdiffusive systems, the fractional derivative is moved to the time domain as presented in Eq. (2.19)

$$\begin{cases} \left(1-q\right)\ {}_0D_t^{\beta}C + q\ {}_tD_1^{\beta}C = \mu(x)\dfrac{\partial^2 C}{\partial x^2}, & in\ \ \Omega = [0,1]\times[0,1] \\ C(0,t) = C_0 \\ C(1,t) = C_1 \\ C(x,0) = C_{IC}(x) \end{cases} \tag{2.19}$$

Equation (2.19) is usually referred to as the *time fractional diffusion equation*. The time fractional derivative can be directly correlated with the effect of memory in diffusion phenomena, as explained in Section 2.3.3. Numerical solutions to these and other fractional diffusion models are presented in Chapter 6.

2.5 Chapter summary

Fick's law is extensively used for modeling diffusion phenomena, mainly due to its mathematical simplicity. However, the strong assumptions necessary for the derivation of this model restrict its range of validity to a limited amount of simple cases. A short review of the most important pieces of evidence refuting the general application of Fick's law was presented, together with a wide scope of alternative diffusion models grouped under the common name *'anomalous transport'*.

The anomalous transport models can be categorized according to their scale, in a compromise between simplicity and thoroughness. In any case, each level must be a suitable approximation of the most fundamental ones in order to achieve a consistent description. The mutually coherent Random Walk and Fick's law can be generalized to *Continuous Time Random Walk* and *Fractional Diffusion* respectively by relaxing some of the model assumptions. An introduction to these models was provided in this chapter, and their coherence was verified by reproducing numerical experiments from previous work.

Part II

Numerical tools

Chapter 3

The Least Squares Spectral Element Method

The Least Squares Spectral Element Method (LSSEM) is a relatively novel numerical technique which combines a formulation based on the *minimization of a residual norm* with a *finite element* approximation using *spectral* (high-order) base functions. The composition resulting from these three factors is a very robust numerical technique which yields good results for simulations in a broad range of problems.

This chapter presents the basic characteristics of the Least Squares Spectral Element Method. Section 3.1 gives an overview over the main features of the numerical method as a combination of different techniques. Section 3.2 explains briefly the principles behind the least squares formulation. Section 3.4 summarizes the key topics presented in this chapter.

3.1 Overview of LSSEM features

A least-squares numerical formulation yields always a symmetric positive-definite (SPD) system of algebraic equations which performs remarkably in combination with iterative solvers. The spectral scheme renders exponential convergence and the division in elements provides the flexibility to adapt to arbitrary geometries. This combination, known as the Least Squares Spectral Element Method, is specially suited for simulations in fluid dynamics and other equation systems with non-selfadjoint operators.

The main characteristics of the method are summarized and shortly described in each of the following subsections. The reader looking for a more detailed review is referred to specialized publications such as (Jiang, 1998; Gerritsma and De Maerschalck, 2010).

3.1.1 Why finite elements?

Generality The inconvenience of having a single polynomial approximating the solution over the whole domain, as in the case of spectral methods, becomes evident when rapid transients or any kind of non-smoothness are experienced. The best solution here consists in subdividing the domain in multiple elements, using local low-order representations in each of them and then connecting the elements in order to obtain the full solution. Solving many small problems instead of a single large problem is also a natural approach to parallel processing (Jiang, 1998). A similar situation occurs when the domain shape is complex. The division in multiple elements yields higher geometrical flexibility with simpler mappings.

3.1.2 Why least squares?

Cost-free a-posteriori error estimator As mentioned above, least squares methods are based on the minimization of a residual norm. If the smoothness requirements of the problem are satisfied, the residual minimization is equivalent to the error minimization (see Section 3.2.1). This is very convenient considering that a-posteriori error estimations involve extra computational cost for any other numerical method.

Advantages for iterative solvers The algebraic equation systems generated by the Least Squares methods are always Symmetric and Positive Definite (SPD), even for non-selfadjoint first order operators. This allows using efficient iterative solving algorithms such as the conjugate gradient method for every problem.

Strong or weak boundary conditions The boundary conditions to the problem can be included either in a strong or a weak form, which is often emphasized as an advantage of this method over others (Jiang, 1998; Gerritsma and De Maerschalck, 2010). If the strong form is used, the discrete search space is restricted to functions that fit the boundary conditions. Then the boundary is removed from the set of problem unknowns.

On the other hand, if weak boundary conditions are used, the boundary is included in the set of problem unknowns. In this case full compliance with boundary conditions is achieved at the limit case ($h \to 0$) when the element size goes to zero (Kayser-Herold and Matthies, 2005). This possibility allows for a greater degree of flexibility.

3.1.3 Why spectral?

Rapid convergence for smooth problems The LSSEM shares the characteristic rapid convergence of the spectral methods as the approximation order N is increased (p-refinement), provided the solution is smooth enough. The error

decreases faster than any algebraic power of N provided the solution is smooth enough, as formally stated in (Canuto et al., 2006). This is superior to the algebraic convergence rate obtained when increasing the number of elements (h-refinement). A successful combination of these (hp-refinement), is achieved by performing a p-refinement in the smooth regions and a h-refinement in the regions of low regularity.

3.2 Formulation

We will begin with the description of the least squares spectral numerical formulation by considering an arbitrary set of partial differential equations (PDEs) and boundary conditions (BCs):

$$\mathcal{L}\mathbf{u} = \mathbf{g} \quad \text{in} \quad \Omega \tag{3.1a}$$

$$\mathcal{B}\mathbf{u} = \mathbf{g}_\Gamma \quad \text{on} \quad \Gamma \subseteq \partial\Omega \tag{3.1b}$$

where $\mathcal{L}$ is an arbitrary linear operator and $\mathcal{B}$ is a linear boundary condition operator, $\mathbf{u}$ is the unknown vector, $\mathbf{g}$ and $\mathbf{g}_\Gamma$ are the source terms and Γ is a fraction of the boundary $\partial\Omega$ of the domain Ω.

3.2.1 Main concept

A norm-equivalent functional $\mathcal{J}(\mathbf{u})$ can be defined from the sum of residuals of Eq. (3.1) as:

$$\mathcal{J}(\mathbf{u}) \equiv \frac{1}{2}\left(\|\mathcal{L}\mathbf{u} - \mathbf{g}\|^2 + \|\mathcal{B}\mathbf{u} - \mathbf{g}_\Gamma\|^2\right) \tag{3.2}$$

The Least-Squares formulation seeks to minimize the functional $\mathcal{J}(\mathbf{u})$. If the operators $\mathcal{L}$ and $\mathcal{B}$ are *linear* and Eq. (3.2) is *well-posed*, this is equivalent to solve the system defined by Eq. (3.1). This is further clarified in (Proot and Gerritsma, 2002). In this context, an operator is well-posed if and only if it is bounded below, as explained in (Jiang, 1998). In this case, there is a finite proportionality constant between the solution error norm and the residual value. In other words, there is a norm equivalence between error and residual. Note that the suitability of the chosen norm depends on the operators $\mathcal{L}$ and $\mathcal{B}$.

A necessary condition for the function $\mathbf{u}$ to be a minimizer of the functional $\mathcal{J}(\mathbf{u})$ is that its first order variation vanishes at $\mathbf{u}$. This can be expressed as:

$$\lim_{\epsilon \to 0} \frac{d\mathcal{J}(\mathbf{u} + \epsilon\mathbf{v})}{d\epsilon} = 0 \quad \forall \mathbf{v} \in \Omega \tag{3.3}$$

where ϵ is a scalar and $\mathbf{v}$ represents an arbitrary perturbation function over the domain Ω.

3.2.2 Introduction of norms and search spaces

The norm $\|\bullet\|$ used for the definition of the functional $\mathcal{J}(\mathbf{u})$ in Eq. (3.2) is chosen to be the L^2 norm based on practicality considerations. This norm, defined over the domain Ω as

$$\|\bullet\|_{L^2(\Omega)} = \int_\Omega \bullet \bullet \, d\Omega, \tag{3.4}$$

is a particular case of the L^2 internal product, which is defined as

$$\langle \mathbf{v}, \mathbf{w} \rangle_{L^2(\Omega)} = \int_\Omega \mathbf{v}\, \mathbf{w} \;\; d\Omega. \tag{3.5}$$

If we introduce the definition of the L^2 norm in Eq. (3.2), the evaluation of Eq. (3.3) using the linearity of operators $\mathcal{L}$ and $\mathcal{B}$ yields

$$\int_\Omega \left[(\mathcal{L}\mathbf{u} - \mathbf{g})\, \mathcal{L}\mathbf{v} \right] d\Omega + \int_\Gamma \left[(\mathcal{B}\mathbf{u} - \mathbf{g}_\Gamma)\, \mathcal{B}\mathbf{v} \right] d\Gamma = 0 \;\; \forall \mathbf{v} \tag{3.6}$$

An additional requirement must be introduced at this point. In order to be able to evaluate Eq. (3.6), the solution $\mathbf{u}$ and the test functions $\mathbf{v}$ must be square integrable over the domain Ω. That is

$$\mathbf{u}, \mathbf{v} \in L^2(\Omega); \quad L^2(\Omega) = \{\mathbf{w} | \int_\Omega \mathbf{w}^2 d\Omega < \infty\}. \tag{3.7}$$

From now on, the numerical set $X(\Omega) \in L^2(\Omega)$ from which $\mathbf{u}$ and $\mathbf{v}$ are drawn will be addressed as the *search space*. The final variational formulation can thus be stated as:

Find $\mathbf{u} \in X(\Omega)$ *such that:*

$$\mathbf{B}(\mathbf{u}, \mathbf{v}) = \mathbf{F}(\mathbf{v}) \;\; \forall \mathbf{v} \in X(\Omega) \tag{3.8}$$

Here the operator $\mathbf{B} : X(\Omega) \times X(\Omega) \to \mathbb{R}$ is a symmetric, continuous bilinear form and the operator $\mathbf{F} : X(\Omega) \to \mathbb{R}$ is a continuous linear form. These are defined respectively as:

$$\mathbf{B}(\mathbf{u}, \mathbf{v}) = \int_\Omega \mathcal{L}\mathbf{u}\mathcal{L}\mathbf{v} d\Omega + \int_\Gamma \mathcal{B}\mathbf{u}\mathcal{B}\mathbf{v} d\Gamma \tag{3.9a}$$

$$\mathbf{F}(\mathbf{v}) = \int_\Omega \mathbf{g}\mathcal{L}\mathbf{v} d\Omega + \int_\Gamma \mathbf{g}_\Gamma \mathcal{B}\mathbf{v} d\Gamma \tag{3.9b}$$

Example 3.1: A simple Least-Squares problem

Let us analyze a simple first order problem where Eq. (3.1) *takes the form*

$$\frac{\partial \mathbf{u}(x)}{\partial x} = \mathbf{g}(x) \quad in\ \Omega = [0,1] \tag{3.10a}$$

$$\mathbf{u}(x)|_{x=0} = u_0 \tag{3.10b}$$

The functional $\mathcal{J}(\mathbf{u})$ *from Eq.* (3.2) *can be expressed as*

$$\mathcal{J}(\mathbf{u}) = \frac{1}{2}\left\{ \int_0^1 \left[\frac{\partial \mathbf{u}(x)}{\partial x} - \mathbf{g}(x)\right]^2 dx + \left[\mathbf{u}(0) - u_0\right]^2 \right\} \tag{3.11}$$

and the weak form as defined in Eqs. (3.8) *and* (3.9) *is then:*

Find $\mathbf{u}(x) \in X([0,1])$ such that:

$$\mathbf{B}\left\langle \mathbf{u}, \mathbf{v} \right\rangle = \mathbf{F}\left\langle \mathbf{v} \right\rangle \quad \forall \mathbf{v} \in X\left([0,1]\right) \tag{3.12}$$

where

$$\mathbf{B}\left\langle \mathbf{u}, \mathbf{v} \right\rangle = \int_0^1 \left[\frac{\partial \mathbf{u}(x)}{\partial x}\frac{\partial \mathbf{v}(x)}{\partial x}\right] dx + \left[\mathbf{u}(0)\mathbf{v}(0)\right] \tag{3.13a}$$

$$\mathbf{F}\left\langle \mathbf{v} \right\rangle = \int_0^1 \left[\mathbf{g}(x)\frac{\partial \mathbf{v}(x)}{\partial x}\right] dx + \left[u_0\mathbf{v}(0)\right] \tag{3.13b}$$

3.3 Discretization

The discretization of the problem consists in transforming it into a set of algebraic equations that can be solved either analytically or, more generally, by iterative methods. The three main parts in the discretization of a PDE problem are: **function interpolation**, **quadrature** and **construction of differential operators**. This section describes each of these parts. References to subdivision into elements are provided.

3.3.1 Function interpolation

The discrete representation of a given function $\mathbf{u}(\xi)$ in the reference domain $\bar{\Omega} = [-1,1] \in \mathbb{R}$ is carried out by projecting it on a given basis. Spectral methods approximate functions using polynomial interpolants. In the most general case, an approximation of order N is obtained as a linear combination of $(N+1)$

interpolating polynomials $l_i(\xi)$ each multiplied by a corresponding coefficient a_i as

$$\mathbf{u}(\xi) \approx \sum_{i=0}^{N} a_i l_i(\xi). \tag{3.14}$$

The minimum attainable interpolation error depends on the regularity of the function $\mathbf{u}(\xi)$. It can be proven that if $\mathbf{u}(\xi)$ is analytic the error decreases exponentially as the approximation order is increased (Jiang, 1998). This behavior of the error on interpolation and quadrature (see Section 3.3.2) is characteristic of spectral methods.

In general, $l_i(\xi)$ can be arbitrary basis functions. The two most usual approaches to function approximation are modal and nodal expansions. The coefficients a_i in a modal expansion determine the amplitude of the mode i (e.g. Fourier, Hermite or Chebyshev expansions). In a nodal expansions the coefficients a_i correspond to the function values at the interpolation nodes ξ_i. Both concepts are illustrated in Fig. 3.1.

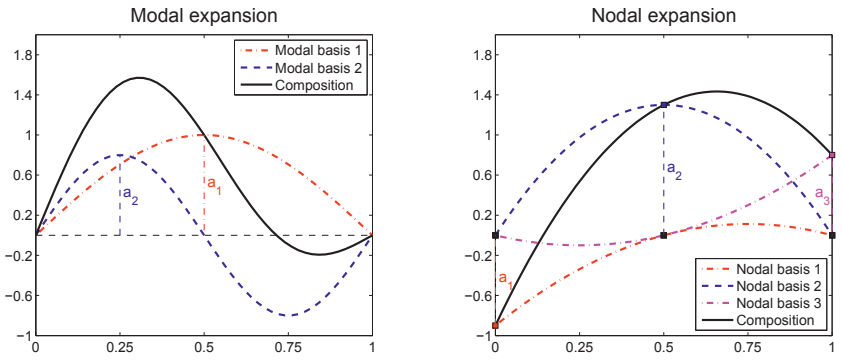

Figure 3.1: Example of an expansion in (a) a modal basis and (b) a nodal basis

Nodal interpolation

If the chosen interpolants constitute a *nodal basis* of order N, the set $I^N$of $(N+1)$ interpolants is defined such as the value of each interpolant $l_i(\xi)$ is unity at one of the interpolation nodes ξ_i and zero at the rest of them. This can be expressed as

$$I^N = \{l_i(\xi) \,|\, l_i(\xi) \in \mathbb{P}_N \;\wedge\; l_i(\xi_j) = \delta_{i,j}\} \quad i,j = 0,1,...,N \tag{3.15}$$

where $\mathbb{P}_N$ is the set containing the polynomials up to degree N.

The polynomials $l_i(\xi)$ can be expressed in its most intuitive form as

$$l_i(\xi) = \prod_{\substack{0 \le j \le N \\ j \neq i}} \frac{\xi - \xi_j}{\xi_i - \xi_j}, \tag{3.16}$$

where it is evident that $l_i(\xi_j) = \delta_{i,j}$. However, a more compact notation is convenient further on since it will also simplify the required calculations. Let us define an auxiliary polynomial $P_{N+1}(\xi)$ with roots at the $(N+1)$ interpolation nodes. Then the polynomials $l_i(\xi)$ can be written as

$$l_i(\xi) = \frac{P_{N+1}(\xi)}{(\xi - \xi_i)\,\dfrac{dP_{N+1}(\xi_i)}{d\xi}}. \tag{3.17}$$

Note that Eq. (3.17) is general for any choice of interpolation points ξ_i.

By joining Eqs. (3.14) and (3.15), it can be observed that the a_i coefficients multiplying each polynomial correspond to the value of the approximated function at the interpolation points ξ_i. So Eq. (3.14) becomes

$$\mathbf{u}(\xi) \approx \sum_{i=0}^{N} a_i l_i(\xi) = \sum_{i=0}^{N} \mathbf{u}(\xi_i)\, l_i(\xi). \tag{3.18}$$

This is very convenient when we deal with differential equations. Given these coefficients, the derivative of the approximation is only function of the derivatives of the interpolants, and can be calculated as

$$\frac{d\mathbf{u}(\xi)}{d\xi} \approx \frac{d}{d\xi}\left(\sum_{i=0}^{N} \mathbf{u}(\xi_i)\, l_i(\xi)\right) = \sum_{i=0}^{N} \mathbf{u}(\xi_i)\, \frac{dl_i(\xi)}{d\xi}. \tag{3.19}$$

Note that the last simplification in Eq. (3.19) is only valid when a *nodal interpolation* is used. Equation (3.19) is relevant for the analysis described in Section 3.3.3.

Gauss-Legendre interpolants

Nothing has been said up to this point about the location of the interpolation nodes ξ_i, which remain unspecified. The choice of these points determines the stability of the approximation and the conditioning of the system (De Maerschalck, 2003). A convenient, stable and efficient nodal interpolation basis for smooth functions is the set of Gauss-Legendre (GL) polynomials.

GL The interpolation points $(\xi_0, ..., \xi_N)$ for the Gauss-Legendre (GL) basis correspond to the roots of the Legendre polynomial of order $(N+1)$ denoted $L_{N+1}(\xi)$. The set of interpolants is obtained by defining $P_{N+1}(\xi)$ in Eq. (3.17) as

$$P_{N+1}(\xi) = L_{N+1}(\xi). \tag{3.20}$$

The Legendre polynomials are solutions to the Legendre differential equation (Deville et al., 2002, Appendix B). The Legendre polynomial $L_{N+1}(\xi)$ of order $(N+1)$

and its first derivative can be calculated by using the simple recurrence formulas from Eq. (3.21), which depend on the polynomials $L_{N-1}(\xi)$ and $L_N(\xi)$.

$$\begin{aligned} L_0(\xi) &= 0 \\ L_1(\xi) &= \xi \\ &\cdots \\ L_{N+1}(\xi) &= \frac{(2N+1)\,\xi L_N(\xi) - N L_{N-1}(\xi)}{N+1} \\ \frac{dL_{N+1}(\xi)}{d\xi} &= \frac{(N+1)\xi L_{N+1}(\xi) - (N+1) L_N(\xi)}{\xi^2 - 1} \end{aligned} \tag{3.21}$$

The derivative at the end points is calculated as

$$\frac{dL_{N+1}(\xi)}{d\xi} = \begin{cases} (-1)^{N+1}\dfrac{(N+1)(N+2)}{2} & \text{if } \xi = -1 \\ \dfrac{(N+1)(N+2)}{2} & \text{if } \xi = 1 \end{cases} \tag{3.22}$$

The roots of the $L_N(\xi)$ polynomials (and therefore the GL quadrature points) are found by solving the eigenvalue problem described in (Press et al., 1993).

GLL In the case of multi-domain problems and when the imposition of boundary conditions is required, it is convenient to include the extremes of the interval in the set of interpolation points $(\xi_0, ..., \xi_N)$. The interpolation points corresponding to the Gauss-Lobatto-Legendre (GLL) basis can be found by defining the polynomial $P_{N+1}(\xi)$ from Eq. (3.17) as

$$P_{N+1}(\xi) = (\xi - 1)(\xi + 1)\frac{dL_N(\xi)}{d\xi}. \tag{3.23}$$

Since it is computationally expensive to calculate the roots of Eq. (3.23) directly, they are computed iteratively by using the Newton-Raphson algorithm. The set of starting values or *iteration seeds* used for the approximation is the set of corresponding GL points. It can be proven that this iteration always converges to the GLL points (Press et al., 1993, Section 4.5).

3.3.2 Quadrature

As analytical integrals are rarely available for the functions of our interest, particularly for Eq. (3.9), it is necessary to approximate integrals by a quadrature. In the most general approach a quadrature approximates the integral of the product $f(\xi)\,W(\xi)$, where $f(\xi)$ is the *integrand function* and $W(\xi)$ is called the *integration weight*. The approximation is constructed as the sum of the values of the integrand

function $f(\xi)$ evaluated at the *quadrature points* ξ_α multiplied by coefficients w_α which are called *quadrature weights*:

$$\int_\Omega f(\xi) W(\xi) d\xi \approx \sum_{\alpha=0}^{N} w_\alpha f(\xi_\alpha). \tag{3.24}$$

Note that the choice of the quadrature points ξ_α and weights w_α depends on the integration weight $W(\xi)$. The accuracy of the approximation depends on the choice of quadrature points and weights and on the regularity of the function $f(\xi)$.

Gauss-Legendre quadrature

Gauss-Legendre and Gauss-Lobatto-Legendre quadrature rules include an integration weight equal to unity, which means $W(\xi) = 1$. The quadrature points ξ_α corresponding to the GL and GLL quadrature rules are the same as the GL and GLL interpolation points, respectively. The quadrature weight w_α corresponding to each quadrature point is calculated as

$$w_\alpha = \frac{2}{N(N+1)\left[L_N(\xi_\alpha)\right]} \quad \alpha = 0, 1, ..., N \tag{3.25}$$

The expression in Eq. (3.24) is exact if $f(\xi)$ is a polynomial of order up to $(2N+1)$ for GL and $(2N-1)$ for GLL quadrature. Otherwise the accuracy in the representation depends on the smoothness of the function $f(\xi)$. It can be proven that if $f(\xi)$ is analytical the approximation error decreases exponentially as N increases (Jiang, 1998).

Let us now focus on the particular case when the function $f(\xi)$ is a polynomial interpolation of a given function $g(\xi)$ on a GLL basis, as expressed in Eq. (3.26), and the integration weight is equal to unity over the whole integration domain Ω.

$$f(\xi) \approx \sum_{j=0}^{N} g(\xi_j) l_j(\xi). \tag{3.26}$$

In this case, the expression for the quadrature approximation results

$$\int_\Omega f(\xi) d\Omega \approx \int_\Omega \sum_{j=0}^{N} g(\xi_j) l_j(\xi) d\xi = \sum_{\alpha=0}^{N} \sum_{j=0}^{N} g(\xi_j) l_j(\xi_\alpha) w_\alpha \tag{3.27}$$

but due to the interpolation property it is simplified in a very convenient way as

$$\sum_{\alpha=0}^{N} \sum_{j=0}^{N} g(\xi_j) l_j(\xi_\alpha) w_\alpha = \sum_{\alpha=0}^{N} \sum_{j=0}^{N} g(\xi_j) \delta_{\alpha j} w_\alpha = \sum_{\alpha=0}^{N} g(\xi_\alpha) w_\alpha \tag{3.28}$$

Note that all the estimation error is introduced in the interpolation. As the function approximation is a polynomial of order N, the quadrature error for this case is zero and the integration yields an exact value.

Gauss-Jacobi quadrature

It was already mentioned in this section that the accuracy of GL quadrature depends on the regularity of the integrated function, and it is therefore very inaccurate for integrating functions with singularities. Gauss-Jacobi (GJ) quadrature can effectively deal with singularities located at the extremes of the integration domain. A textbook example for this case is the integration of a function $g(\xi)$ of the form

$$g(\xi) = \frac{f(\xi)}{(1-\xi)^{\beta_R}(1+\xi)^{\beta_L}} \qquad 0 \leq \beta_R, \beta_L < 1 \tag{3.29}$$

over the reference domain $[-1, 1]$.

This integrand has two singularities at $(\xi = -1)$ and $(\xi = 1)$. Therefore, the integration using GL quadrature yields highly inaccurate results. GLL quadrature is not even possible since the integrand would need to be evaluated at the singularity. A GL quadrature approximation would look like

$$\int_{-1}^{1} g(\xi)d\xi = \int_{-1}^{1} \frac{f(\xi)d\xi}{(1-\xi)^{\beta_R}(1+\xi)^{\beta_L}} \approx \sum_{\alpha=0}^{N} \omega_\alpha^{GL} \frac{f(\xi_\alpha)}{(1-\xi_\alpha)^{\beta_R}(1+\xi_\alpha)^{\beta_L}} \tag{3.30}$$

becoming increasingly inaccurate as $\xi_\alpha \to (-1)$ or $\xi_\alpha \to 1$.

In order to calculate the integral of the function $g(\xi)$ from Eq. (3.29) with singularities of order $\beta_R < 1$ and $\beta_L < 1$ at either (or both) of the extremes of the integration domain, the singularity must be transfered from the function $g\,(\xi)$ to the quadrature weights. This is achieved by constructing the non-singular function $p(\xi) = (\xi - 1)^{\beta_R}(\xi + 1)^{\beta_L} g(\xi)$ and then approximating the integral by Gauss-Lobatto-Jacobi quadrature. The weight function W^{GLJ} for this quadrature is

$$W^{GLJ}(\xi) = \frac{1}{(1-\xi)^{\beta_R}(1+\xi)^{\beta_L}} \qquad \beta_R, \beta_L < 1. \tag{3.31}$$

In this way the quadrature approximation results

$$\int_{-1}^{1} g(\xi)d\xi = \int_{-1}^{1} \frac{f(\xi)d\xi}{(1-\xi)^{\beta_R}(1+\xi)^{\beta_L}} = \int_{-1}^{1} W^{GLJ}(\xi) f(\xi) d\xi \approx \sum_{\alpha=0}^{N} \omega_\alpha^{GLJ} f(\xi_\alpha) \tag{3.32}$$

Note that if $p(\xi)$ is a polynomial of order up to $(2N + 1)$ the integration is exact (i.e. there is no quadrature error). Furthermore, GLL quadrature rule is recovered by setting $\beta_R = \beta_L = 0$. This procedure is useful for the evaluation of fractional derivative operators as described in Section 4.1.

3.3.3 Construction of differential operators

Recalling the result from Section 3.3.1, the derivative of a given solution $\mathbf{u}\,(\xi)$ is interpolated as the expression shown in Eq. (3.19), which depends only on the basis polynomials $l_i\,(\xi)$.

As the integrals required for the weak form require only the evaluation of the integrands at the quadrature points (intentionally coincident with the interpolation points ξ_i), the evaluation of the derivatives for the solution is only required at these points. The derivative at the quadrature points is given by

$$\frac{d\mathbf{u}\left(\xi\right)}{d\xi}|_{\xi=\xi_i} \approx \sum_{j=0}^{N} \mathbf{u}\left(\xi_\mathbf{i}\right) d_{ij}, \tag{3.33}$$

where d_{ij} is the differentiation matrix whose components are defined as

$$d_{ij} = \frac{dl_j\left(\xi\right)}{d\xi}|_{\xi=\xi_i}. \tag{3.34}$$

3.3.4 Subdivision into elements

The main idea behind subdivision into elements consists in splitting the domain Ω from Section 3.2 into N_e non-overlapping open sub-domains Ω^i such as

$$\Omega = \bigcup_{i=1}^{Ne}, \quad \Omega^i \cap \Omega^j = \emptyset, \quad i \neq j. \tag{3.35}$$

This topic will not be further addressed here since it has been extensively discussed in references such as (Gerritsma and De Maerschalck, 2010; Jiang, 1998; Proot and Gerritsma, 2002; Zhao and Liu, 2006). The reader is referred to the aforementioned sources for an extensive treatment of this subject.

3.4 Chapter summary

This chapter aimed to yield a transparent, reader friendly introduction to the least squares formulation and the spectral discretization from a practical point of view. The LSSEM is a numerical technique that combines the features of **finite element methods** and **spectral methods** using a **least squares formulation** in an attempt to capitalize on a combination of their best characteristics.

The subdivision into elements gives geometric flexibility, an improved performance for non-smooth functions and a natural approach to parallel processing. Using a least squares formulation is convenient for using iterative solvers and provides an estimator for the quality of the numerical solution. Finally, a spectral representation requires less points in order to achieve the same accuracy as a first order approximation. The introduced concepts are required for a thorough understanding of Chapters 5 to 7.

Chapter 4

Numerical implementation

Numerical methods are often written in a highly abstract language. This convention makes it possible to achieve greater generality at the price of increasing the complexity in their formulation. As a result the practical aspects are not always explicit and straightforwardly understood. This chapter describes some implementation details that will facilitate the reproduction of the calculations presented in this thesis.

Section 4.1 provides a brief introduction to the fractional derivative operator from a numerical point of view where the singularity problem is addressed. The steps for implementation in a spectral framework are detailed together with an example for mapping into nonlinearly deformed domains. Section 4.2 explains how to extend the method to multiple dimensions. Guidelines for an automatable linear mapping algorithm are included. Section 4.3 presents a brief summary of the topics discussed in this chapter.

4.1 Fractional derivatives

The fractional derivative operator has already been introduced in Section 2.4 from a modeling point of view. This section will focus on the numerical aspects of the operator. Explaining the idea of fractional derivatives is easier when starting from the derivative of a given function $f(x)$, defined as

$$\frac{df(x)}{dx} = \lim_{\Delta x \to 0} \frac{f(x + \Delta x) - f(x)}{\Delta x}. \tag{4.1}$$

Second order integer derivatives are defined as

$$\frac{d^2 f(x)}{dx^2} = f^{(2)}(x) = \frac{d}{dx}\left(\frac{df(x)}{dx}\right) \tag{4.2}$$

Extending this approach, higher order derivatives are immediately defined as

$$\frac{d^{\beta}f(x)}{dx^{\beta}} = f^{(\beta)}(x) = \underbrace{\frac{d}{dx}...\frac{df(x)}{dx}}_{\beta\ times} \tag{4.3}$$

In this definition the exponent β is required to be an integer which indicates the number of times the derivative operation is performed. We will refer to the operators in Eqs. (4.1) to (4.3) as *integer derivative* in contrast with the *fractional derivative operator* defined in Eq. (2.10).

4.1.1 The fractional derivative operator

The fractional derivative operator is a generalization of the integer derivative operator that allows to introduce any real value of β. Two main definitions are used in practice: *Riemann-Liouville* and *Caputo* derivative (Podlubny, 1999). These are presented in Eq. (2.10a) and Eq. (2.10b) respectively

$${}_0D_x^{\beta}f(x) = \frac{d}{dx^n}\left[\frac{1}{\Gamma(n-\beta)}\int_0^x \frac{f(\xi_1)d\xi_1}{(x-\xi_1)^{\beta+1-n}}\right] \tag{2.10a}$$

$${}_0D_x^{\beta}\mathbf{f}(x) = \frac{1}{\Gamma\left(n-\beta\right)}\int_0^x \frac{\mathbf{f^{(n)}}\left(\xi_\mathbf{1}\right)d\xi_1}{\left(x-\xi_1\right)^{\beta+1-n}}, \tag{2.10b}$$

where $\Gamma(x)$ represents the Gamma function which generalizes the factorial, β is the derivative order which can adopt any real value and n is the lowest integer that satisfies $\beta < n$. Equations (2.10a) and (2.10b) yield special cases when integer values of β are considered:

$$\begin{cases} {}_0D_x^{\beta}f(x) = \dfrac{\partial^{\beta}f(x)}{\partial x^{\beta}} & \text{if } \beta \in \mathbb{Z} > 0 \\ {}_0D_x^{\beta}f(x) = \underbrace{\displaystyle\int_0^x \cdots \int_0^{x_{n_1}}}_{\text{n-fold integral}} f(x_n)dx_n \cdots dx_1 & \text{if } \beta \in \mathbb{Z} < 0 \end{cases} \tag{4.5}$$

The evaluation of the fractional derivative operator includes differentiation and integration, but the order in which these are performed depends on which definition is used. This originates differences in significant aspects.

The Riemann-Liouville definition is less restrictive regarding the range of validity of the operator since it presents lower smoothness requirements. However, the solution of fractional order differential equations requires fractional initial conditions whose physical meaning is not completely clear. In addition, the fractional derivative of a non-zero constant is zero only for Eq. (2.10b). These aspects are discussed widely in (Loverro, 2004).

4.1.2 Numerical approaches

Different approaches have been used for calculating fractional derivatives during the last years and the common concern of integration over singularities has arisen in most of them. The quadrature problem for the fractional derivative operator has been addressed by (Sugiura and Hasegawa, 2009; Jiang and Lin, 2010; Pálfalvi, 2010). Comparisons of different solution methods for problems with Dirichlet homogeneous conditions are presented in (Yang et al., 2010; Diethelm et al., 2006; Lin and Xu, 2007).

The singular integral

Equation (2.10) shows that both Riemann-Liouville and Caputo definitions require approximating the integral of the auxiliary variable ξ_1 over the variable interval $[0 < \xi_1 < x]$, which cannot be done directly by quadrature. As a singularity in the integrand is present at $\xi_1 = x$, the integrand cannot be evaluated at that point and an evaluation at the vicinity of that point would be highly inaccurate.

The Yuan-Agrawal method for calculating the time Caputo fractional derivative of a function ${}_0D_t^\beta f(t)$ is proposed in (Yuan and Agrawal, 2002). This method consists in solving an initial value problem in order to find an intermediate function $\Phi(w,t)$ where w is an auxiliary variable. This function is then integrated in w over the interval $[0,\infty)$ in order to calculate the fractional derivative. This method requires solving a stiff first order equation for each quadrature point where $\Phi(w,t)$ is evaluated (Diethelm, 2009). Also several quadrature points are required for each operator evaluation, and thus the method becomes computationally expensive. In addition, the intermediate function $\Phi(w,t)$ has a singularity at $w = 0$ and consequently the results of using Gauss-Laguerre quadrature yield a very slow convergence as discussed in (Lu and Hanyga, 2005).

A modification to this method is presented in (Diethelm, 2009). It consists in splitting the integration interval for the function $\Phi(w,t)$ in two domains $[0,c)$ and $[c,\infty)$ and then integrating the first part using Gauss-Jacobi quadrature. This notoriously improves the accuracy of the method, but requires solving a stiff differential equation for each quadrature point. A further modification consists in using Gauss-Jacobi quadrature (Birk and Song, 2010).

J-R. Li presents a fast-time-stepping method for evaluating fractional derivatives (Li, 2010). A Gauss-Legendre quadrature is used in the smooth region of the operator integrand, obtaining good results. However, the model is restricted to what they call the region of analyticity, namely a region which is at least Δt away from the singularity. In other words, the time history is only considered from $t \geq \Delta t$.

Finite element approximations to fractional differential equations have been achieved by J. P. Roop in (Roop, 2006; 2008). A Least Squares Finite Element approach is presented by Fix and Roop in (Fix and Roop, 2004), where existence and uniqueness of the least squares approximation is proven and the singularity

problem is avoided by applying the operator only to example functions that cancel it with zeros. This first order technique does not take advantage of the storage efficiency of the spectral methods, and is still limited to functions that go to zero at the domain borders.

The order of the singularity in Eq. (2.10) must always be lower than unity since $(\beta + 1 - n) < 1$. Therefore, the singular integral can be elegantly treated by using the Gauss-Lobatto-Jacobi quadrature technique[1] presented in Section 3.3.2, as described in (Li and Xu, 2009; 2010; Carella and Dorao, 2012). This is in turn compatible with solvers using the Least Squares Spectral Element Method presented in Chapter 3. The main characteristic of this method consists in combining spectral convergence with the ability of treating the fractional derivative operator effectively and the possibility of imposing boundary conditions in a weak form (Jiang, 1998).

Memory requirement issue

One of the most important problems arising when combining finite difference methods and time fractional derivatives is the large amount of memory and storage space required. Since the current solution depends on all its previous values, the size of the problem becomes unmanageable for $t \gg 1$. This is currently discouraging the employment of fractional derivative models combined with finite difference frameworks for diffusion problems, especially in more than one dimension.

An interesting idea for tackling this issue is implementing the short-memory principle explained in (Podlubny, 1999; Deng, 2007). This consists in approximating the full-domain integral in $[0, \xi]$ by the partial integral in $[\xi - \Delta\xi, \xi]$, where ξ is the coordinate in which the fractional derivative operator is applied. This approach capitalizes on the fact that the contribution of the function values to the temporal integral decays as we move away from the singularity region, which would in principle reduce the required storage space and calculation time at the expense of some precision. The short-memory principle has been tested in (Lu and Hanyga, 2005; Deng, 2007; Brunner et al., 2010), where it has been found to be ineffective for this type of discretization as its implementation has devastating effects in the accuracy of the solution. Moreover, a very high density of points is required close to the last solution in order to cope with the arising numerical singularity.

The calculations in this thesis are carried out by using a spectral (high order) method. Using a high order approximation reduces drastically the degrees of freedom in a numerical problem, and consequently the storage requirements become significantly lower.

[1] Theoretical considerations and implementation details of the GLJ quadrature approximation are discussed in (Canuto et al., 2006) and (Press et al., 1993) respectively.

Multi-dimensional applications

As the calculation of fractional derivative operators is intrinsically complex and numerically expensive, the work on multi-dimensional applications is scarce. Finite difference schemes have often been used to calculate 1-dimensional and 2-dimensional fractional derivatives as in (Brunner et al., 2010; Langlands and Henry, 2005; Lin and Xu, 2007; Meerschaert et al., 2006; Tadjeran et al., 2006; Tadjeran and Meerschaert, 2007; Yuste, 2006; Zhang and Sun, 2011). Two dimensional fractional differentiation has been applied to signal processing in (Chang, 2009). However, these articles consist in finite difference schemes based on a Grünwald-Letnikov approach, which is defined as a limiting case for fractional order backward differentiation. As this formulation is not convenient for analytical manipulation, Caputo and Riemann-Liouville forms are preferred (Podlubny, 1999).

4.1.3 Implementation in a spectral framework

Using the Gauss-Lobatto-Jacobi quadrature to approximate the singular integrals in Eq. (2.10), the fractional derivative operator can be expanded in a Gauss-Lobatto-Legendre interpolant basis as

$$RL: \ {}_0D_x^{\beta} f(x) \approx \frac{1}{\Gamma(n-\beta)} \sum_{k=0}^{N} \phi_k^{(n)}(x_i) \left(\sum_{j=0}^{N} \Big(\sum_{\alpha=0}^{M} \omega_\alpha^k \phi_j(\xi_\alpha^k) \Big) f(x_j) \right) \tag{4.6a}$$

$$Ca: \ {}_0D_x^{\beta} f(x) \approx \frac{1}{\Gamma(n-\beta)} \sum_{j=0}^{N} \Big(\sum_{\alpha=0}^{M} \omega_\alpha^k \phi_j^{(n)}(\xi_\alpha^k) \Big) f(x_j). \tag{4.6b}$$

where $\phi_k(x)$ represents the k-th GLL Lagrangian interpolant of order N, ξ_α^k are the GLJ interpolant coordinates corresponding to the interval $[0 \leq \xi \leq x_j]$ and ω_α^k are their corresponding GLJ quadrature weights.

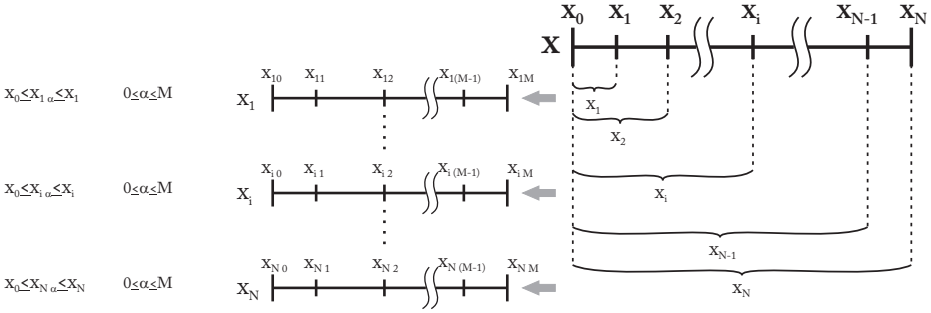

Figure 4.1: Integration domains for computing the fractional derivative operator

For the sake of clarity, a scheme of the domain is included in Fig. 4.1. The thick line marked as $\mathbf{x}$ represents the domain for the x variable, where x_0 and x_N are the

domain boundaries and each x_i is one of the GLL quadrature points of order N. The fractional derivative at $x = x_0$ is trivially zero. For calculating the fractional derivative at the rest of the x_i points, N partially overlapping sub-domains $[x_0, x_i]$ are constructed ($1 \leq i \leq N$) and GLJ quadrature points of order M are generated on each of these sub-domains.

Equations (4.6a) and (4.6b) can be written in matrix form as

$$RL: \ {}_0D_x^\beta f(x) \approx \bar{\mathbf{D}}^n \cdot \ {}_{RL}\bar{\mathbf{In}} \cdot \mathbf{f} \tag{4.7a}$$

$$Ca: \ {}_0D_x^\beta f(x) \approx \ {}_{Ca}\bar{\mathbf{In}} \cdot \mathbf{f} \tag{4.7b}$$

where $\mathbf{f}$ denotes the function $f(x)$ evaluated at the GLL interpolation points x_j. The operators $\bar{\mathbf{D}}$, ${}_{RL}\bar{\mathbf{In}}$ and ${}_{Ca}\bar{\mathbf{In}}$ are defined as

$$\bar{\mathbf{D}}_{[ik]} = \left.\frac{d\phi_k(x)}{dx}\right|_{x_i}$$

$${}_{RL}\bar{\mathbf{In}}_{[kj]} = \frac{1}{\Gamma(n-\beta)} \sum_{\alpha=0}^{M} \omega_\alpha^k \phi_j(\xi_\alpha^k)$$

$${}_{Ca}\bar{\mathbf{In}}_{[kj]} = \frac{1}{\Gamma(n-\beta)} \sum_{\alpha=0}^{M} \omega_\alpha^k \phi_j^{(n)}(\xi_\alpha^k)$$

and the nodal interpolation property by which

$$\left(\bar{\mathbf{D}}^n\right)_{[ik]} = \phi_k^{(n)}(x_i) = \left.\frac{d^n\phi_k(x)}{dx^n}\right|_{x_i} = \overbrace{\left(\bar{\mathbf{D}} \cdot \bar{\mathbf{D}} \cdots \bar{\mathbf{D}}\right)}^{(n\ times)}_{[ik]} \tag{4.8}$$

has been used. Note that the operator construction method is general for any choice of the derivative exponent β.

A crucial fact that should be highlighted is that the fractional derivative operators presented in Eq. (4.7) must be calculated only once, as long as the domain shape is preserved. The application of the operator to any vector is then achieved through a matrix-vector multiplication.

4.1.4 Non-linear mapping technique

Using more complex meshes such as a geometric time grid for fractional time diffusion problems has been proposed in order to increase the mesh resolution at time instants when the diffusive flux is higher (Brunner et al., 2010). The homography technique described in Section 4.2.3 makes it possible to stretch, rotate and deform linearly a given reference domain. More sophisticated shapes that cannot be constructed as polygons require using a non-linear mapping. The procedure for computing the fractional derivative operators when the interpolating nodes are nonlinearly distributed along the spectral domain is explained next.

The polynomial mappings $\mathcal{F}_{m,n}(\xi)$ defined next are chosen for demonstration

$$\mathcal{F}_{m,n}(\xi) = \frac{(\xi+n)^m - n^m}{(1+n)^m - n^m}, \tag{4.9}$$

and it is considered through the rest of this section that $\eta(\xi) = \mathcal{F}_{m,n}(\xi)$.

The parameters m and n define the shape of the mapped domain. Higher values of the exponent m cause a more compact concentration towards lower values of the ξ coordinate. The concept of the mapping is depicted in Fig. 4.2.

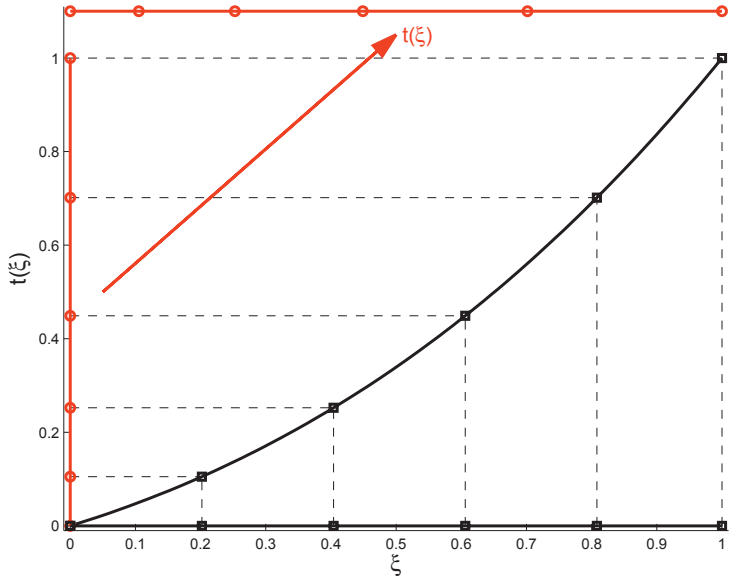

Figure 4.2: Example of point redistribution according to the mapping $\mathcal{F}_{1,3}(\xi)$: the lower horizontal (black) axis is mapped into the upper horizontal (red) axis

The introduction of the mapping $\mathcal{F}_{m,n}(\xi)$ from Eq. (4.9) transforms the definition Eq. (2.10) into its more general version presented in Eq. (4.10). Observe that the operators must be modified when solving the fractional differential equation in a deformed domain in order to keep addressing the same problem.

$$\begin{aligned} {}_0D_x^\beta f(x(\xi)) &= \frac{1}{\Gamma(1-\beta)} \int_{\mathcal{F}_{m,n}^{-1}(0)}^{\mathcal{F}_{m,n}^{-1}(x)} \left(\frac{\partial f(\eta(\xi))}{\partial \xi} \frac{\partial \xi}{\partial \eta} \right) \left(\frac{\partial \eta}{\partial \xi} \frac{d\xi}{(x-\eta(\xi))^\beta} \right) = \\ &= \frac{1}{\Gamma(1-\beta)} \int_{\mathcal{F}_{m,n}^{-1}(0)}^{\mathcal{F}_{m,n}^{-1}(x)} \frac{\partial f(\eta(\xi))}{\partial \xi} \frac{d\xi}{(x-\eta(\xi))^\beta} \end{aligned} \tag{4.10}$$

Every mapping in Eq. (4.9) for arbitrary values of m and n produces when substituted in Eq. (4.10) an operator of the shape

$$ {}_0D_x^{\beta} f\left(x(\xi)\right) = \frac{1}{\Gamma(1-\beta)} \int_{\xi_0}^{\xi_1} \frac{\partial f(\eta(\xi))}{\partial \xi} \frac{d\xi}{[P(\xi)]^{\beta}} \tag{4.11} $$

where the integral coordinate, the polynomial $P(\xi)$ and the integration limits are defined as

$$ \begin{aligned} \xi_0 &= \mathcal{F}_{m,n}^{-1}(0) \qquad & \eta(\xi) &= \mathcal{F}_{m,n}(\xi) \\ \xi_1 &= \mathcal{F}_{m,n}^{-1}(t) \qquad & P(\xi) &= \frac{(\xi_1+n)^m - (\xi+n)^m}{(1+n)^m - n^m} \end{aligned} \tag{4.12} $$

One of the roots of the polynomial $P(\xi)$ is always ξ_1, which allows approximating the integral by Gauss-Lobatto-Jacobi quadrature described in Section 3.3.2. For integer values of m, the polynomial $P(\xi)$ can be expanded in a finite number of terms, which makes its evaluation computationally cheaper. The cases analyzed in this work correspond to the four simplest cases of this mapping, namely

$$ \begin{aligned} \mathcal{F}_{1,1}(\xi) &= \xi & &\rightarrow P(\xi) = (\xi_1 - \xi) \\ \mathcal{F}_{2,1}(\xi) &= \frac{(\xi+1)^2 - 1}{3} & &\rightarrow P(\xi) = (\xi_1 - \xi)(\xi + \xi_1 + 2)/3 \\ \mathcal{F}_{3,1}(\xi) &= \frac{(\xi+1)^3 - 1}{7} & &\rightarrow P(\xi) = (\xi_1 - \xi)(\xi_1^2 + \xi\xi_1 + 3\xi_1 + \xi^2 + 3\xi + 3)/7 \\ \mathcal{F}_{4,1}(\xi) &= \frac{(\xi+1)^4 - 1}{15} & &\rightarrow P(\xi) = (\xi_1 - \xi)(\xi_1+1)^2(\xi+1)^2(\xi_1 + \xi + 2)/15 \end{aligned} \tag{4.13} $$

The mappings from Eq. (4.13) are depicted in Fig. 4.3.

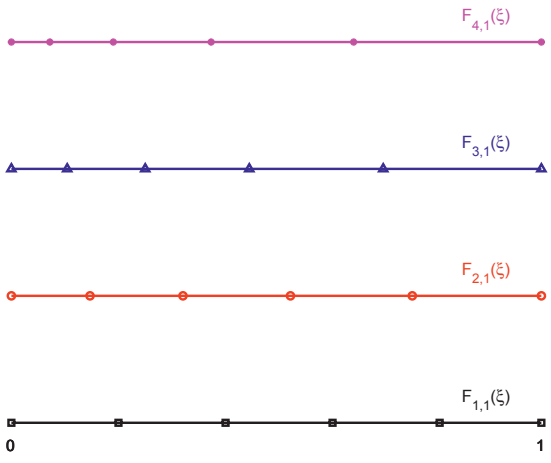

Figure 4.3: Plots of the reference domain mapped by $\mathcal{F}_{m,n}(\xi)$

4.2 Multi-dimensional tools

This section provides the basis for extending the Least-Squares Spectral Method to partial differential equations in multiple dimensions. The technique summarized in Sections 4.2.1 and 4.2.2 is more thoroughly explained in books such as (Jiang, 1998).

4.2.1 Extension of nodal basis

The nodal basis of Gauss-Lobatto-Legendre polynomials (Canuto et al., 2006) in which the solution is expanded can be straightforwardly extended to multiple dimensions. $\mathcal{D}$-dimensional basis functions are generated as the tensor product of $\mathcal{D}$ one-dimensional basis functions as

$$\Phi(x_1, \ldots, x_{\mathcal{D}}) = \prod_{i=1}^{\mathcal{D}} \phi_i(x_i) = \Phi(\mathbf{x}), \tag{4.14}$$

where $\mathbf{x}$ denotes the coordinates vector $(x_1, \ldots, x_{\mathcal{D}})$. The recommended and most standard node enumeration for the extended basis is generated by advancing the coordinate indices in the order they are given, as depicted in Fig. 4.4. If this convention is followed, the $\mathcal{D}$-dimensional basis $\Phi(\mathbf{x})$ can be easily computed as the tensorial product of the $\mathcal{D}$ one-dimensional bases $\phi_i(x_i)$.

$$\Phi(\mathbf{x}) = \phi_{\mathcal{D}}(x_{\mathcal{D}}) \otimes \cdots \otimes \phi_1(x_1) \tag{4.15}$$

Note the rapid increase in the number of basis functions $\Phi_j(\mathbf{x})$ as the number of dimensions grows. The resulting number of basis functions is equal to $N_1 \times \cdots \times N_{\mathcal{D}}$.

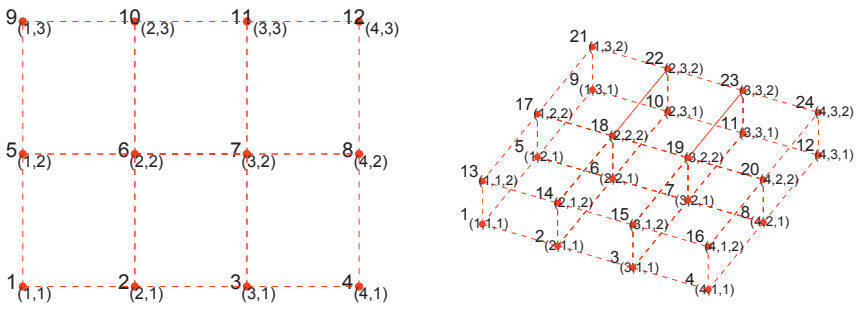

Figure 4.4: Convention for node enumeration in $\mathcal{D}$-dimensional tensor product basis for (a) 2D and (b) 3D grids

4.2.2 Extension of differential operators

Both derivative and fractional derivative evaluations are achieved in 1D by pre-multiplying the data vector $\mathbf{f}(\xi)$ by a derivative matrix $\mathbf{D}_\beta$ as

$$[\mathbf{D}_\beta]_{jk} = \frac{d^\beta \phi_j(\xi_k)}{d\xi^\beta} \quad \mathbf{f}_k = f(\xi_k) \quad \mathbf{D}_\beta \mathbf{f}(\xi) = \frac{d^\beta f(\xi_k)}{d\xi^\beta} \tag{4.16}$$

where β can take any real value. The procedure for computing the matrix $\mathbf{D}_\beta$ for a 1-D basis is explained in detail in Section 4.1.3. The extension of the matrix $\mathbf{D}_\beta$ to multiple dimensions is achieved through a procedure analog to the one explained in Section 4.2.1 for the extension of the nodal basis. This reduces in practice to

$$\begin{aligned}
{}^{\mathcal{D}}_{x_1}\mathbf{D}_\beta &= \underbrace{\mathbb{I} \otimes \cdots \otimes \mathbb{I}}_{\mathcal{D}\text{-1 times}} \otimes_{x_1} \mathbf{D}_\beta \\
&\cdots \\
{}^{\mathcal{D}}_{x_i}\mathbf{D}_\beta &= \underbrace{\mathbb{I} \otimes \cdots \otimes \mathbb{I}}_{\mathcal{D}\text{-i times}} \otimes_{x_i} \mathbf{D}_\beta \underbrace{\mathbb{I} \otimes \cdots \otimes \mathbb{I}}_{\text{i-1 times}} \\
&\cdots \\
{}^{\mathcal{D}}_{x_\mathcal{D}}\mathbf{D}_\beta &= {}_{x_\mathcal{D}}\mathbf{D}_\beta \otimes \underbrace{\mathbb{I} \otimes \cdots \otimes \mathbb{I}}_{\mathcal{D}\text{-1 times}}
\end{aligned} \tag{4.17}$$

where ${}_{x_i}\mathbf{D}_\beta$ is the 1-dimensional fractional derivative matrix of order β in the coordinate x_i and ${}^{\mathcal{D}}_{x_i}\mathbf{D}_\beta$ represents its $\mathcal{D}$-dimensional counterpart.

4.2.3 Homography mapping technique

The application of the method to non-orthogonal domains requires defining a mapping for the transformation from the regular reference domains into arbitrary shapes. This section demonstrates the application of a simple and automatable method whose applicability is restricted to polygonal (linear) mappings. To the author's knowledge, this technique has not been used in the context of finite element methods.

A two-dimensional arbitrarily shaped domain Ω is here thought as the image of a reference element $\hat{\Omega}$ through a bijective mapping $\mathcal{F}$. If the mapping function and its inverse are known for the domain, the process of changing the problem geometry is straightforward. This is always the case for polygonal domains. The method for finding a mapping from an arbitrary polygon $\Omega_\mathcal{S}$ of $\mathcal{S}$ sides to a regular reference polygon $\hat{\Omega}_\mathcal{S}$ with the same number of sides is presented next as described in (Criminisi et al., 1999).

The linear mapping between the domains $\Omega_\mathcal{S}$ and $\hat{\Omega}_\mathcal{S}$ is achieved through a matrix-vector product of the form

$$x_\Omega = H x_{\hat{\Omega}} \tag{4.18}$$

where $H \in \mathcal{R}^{3\times3}$ is called the homography matrix

$$H = \begin{pmatrix} h_{11} & h_{12} & h_{13} \\ h_{21} & h_{22} & h_{23} \\ h_{31} & h_{32} & h_{33} \end{pmatrix} \tag{4.19}$$

whose coefficients are calculated by the minimization of the residual $|Ah|$, with

$$A = \begin{pmatrix} x_1 & y_1 & 1 & 0 & 0 & 0 & -x_1u_1 & -y_1u_1 & -u_1 \\ 0 & 0 & 0 & x_1 & y_1 & 1 & -x_1v_1 & -y_1v_1 & -v_1 \\ \dots & \dots & \dots & \dots & \dots & \dots & \dots & \dots & \dots \\ x_i & y_i & 1 & 0 & 0 & 0 & -x_iu_i & -y_iu_i & -u_i \\ 0 & 0 & 0 & x_i & y_i & 1 & -x_iv_i & -y_iv_i & -v_i \\ \dots & \dots & \dots & \dots & \dots & \dots & \dots & \dots & \dots \\ x_\mathcal{S} & y_\mathcal{S} & 1 & 0 & 0 & 0 & -x_\mathcal{S}u_\mathcal{S} & -y_\mathcal{S}u_\mathcal{S} & -u_\mathcal{S} \\ 0 & 0 & 0 & x_\mathcal{S} & y_\mathcal{S} & 1 & -x_\mathcal{S}v_\mathcal{S} & -y_\mathcal{S}v_\mathcal{S} & -v_\mathcal{S} \end{pmatrix} \tag{4.20}$$

where (x_i, y_i) is a vertex of the original polygon, (u_i, v_i) is the corresponding transformed vertex and the vector h is defined as

$$h = (h_{11}, h_{12}, h_{13}, h_{21}, h_{22}, h_{23}, h_{31}, h_{32}, h_{33})^T. \tag{4.21}$$

Since the number of linearly independent rows of A is lower or equal to 8, a number of extra constraints must be added in order to obtain H.

By means of this algorithm, a reference domain $\hat{\Omega}_\mathcal{S}$ can be easily mapped into an arbitrary polygon of $\mathcal{S}$ sides. The inverse mapping can be obtained by exchanging the order of (x_i, y_i) and (X_i, Y_i), or alternatively by inverting the matrix $H_\mathcal{S}$. An example of a pentagon mapping is presented in Fig. 4.5.

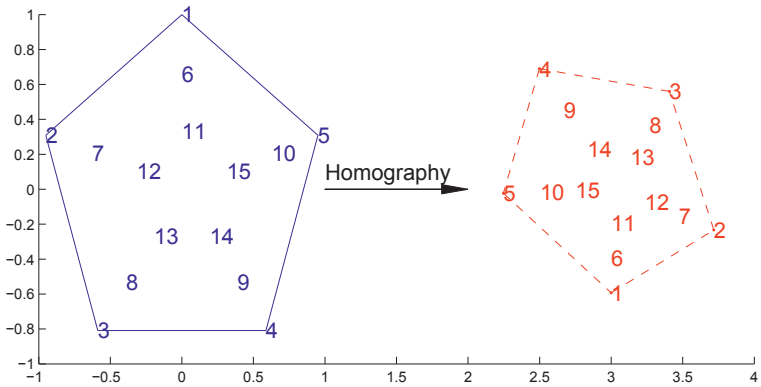

Figure 4.5: Homography mapping of a regular reference pentagon $\hat{\Omega}_5$ into an arbitrary pentagon

It is relevant to note that there is no similar closed solution form for non-linear transformations. The recommended approach for non-linear mappings is using a non-linear mapping technique as described next in Section 4.2.4.

The homography technique is a simple, systematic and fully automatable algorithm with low computational requirements. However, it is restricted to linear transformations only. This means that, for example, the reference square in 2D $[-1,1]^2$ can only be mapped into geometries delimited by four straight lines. In order to map more complex smooth-edged geometries, a non-linear mapping technique must be used.

4.2.4 Bivariate blending function interpolation

The technique called *bivariate 'blending function' interpolation*, as presented in (Gordon and Hall, 1973), is a tool for constructing invertible mappings $\mathcal{F}$ of the unit square $\hat{\Omega}_2 = [-1,1]^2$ onto $\mathbb{R}^2$ (or the unit cube $\hat{\Omega}_3 = [-1,1]^3$ onto $\mathbb{R}^3$). It is used for constructing the deformed meshes in Chapter 7.

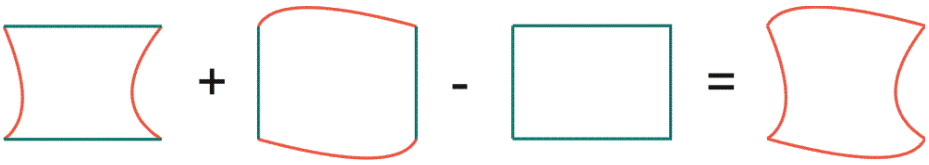

Figure 4.6: Concept illustration of the bivariate blending function interpolation

This procedure is capable of defining generalized curvilinear coordinate systems on *closed, bounded and simply connected domains* $\mathbb{R}^2$ (or $\mathbb{R}^3$). The set of mesh points can be obtained directly by mapping the mesh points in $\mathbb{R}^2$ (or $\mathbb{R}^3$) into the curvilinear system through the mapping $\mathcal{F}$.

Even when the explicit forms of the mapping $\mathcal{F}$ and its inverse $\mathcal{F}^{-1}$ are often difficult to find, only the mapping functions for the edges need to be mapped, namely

$$\begin{array}{lll} \partial\Omega_{x_0} & := \mathcal{F}(-1,\eta) & -1 \le \eta \le 1 \\ \partial\Omega_{x_1} & := \mathcal{F}(1,\eta) & \\ \partial\Omega_{y_0} & := \mathcal{F}(\xi,-1) & -1 \le \xi \le 1 \\ \partial\Omega_{y_1} & := \mathcal{F}(\xi,1) & \end{array} \tag{4.22}$$

As an intermediate step, the partial mappings $\mathcal{F}_x(\xi,\eta)$, $\mathcal{F}_y(\xi,\eta)$ and $\mathcal{F}_{xy}(\xi,\eta)$ are defined as

$$\begin{array}{rcllll} \mathcal{F}_x(\xi,\eta) & = & s_0(\xi)\mathcal{F}(-1,\eta) & + & s_1(\xi)\mathcal{F}(1,\eta) & \\ \mathcal{F}_y(\xi,\eta) & = & s_0(\eta)\mathcal{F}(\xi,-1) & + & s_1(\eta)\mathcal{F}(\xi,1) & \\ \mathcal{F}_{xy}(\xi,\eta) & = & s_0(\xi)s_0(\eta)\mathcal{F}(-1,-1) & + & s_0(\xi)s_1(\eta)\mathcal{F}(-1,1) & \\ & + & s_1(\xi)s_0(\eta)\mathcal{F}(1,-1) & + & s_1(\xi)s_1(\eta)\mathcal{F}(1,1) & \end{array} \tag{4.23}$$

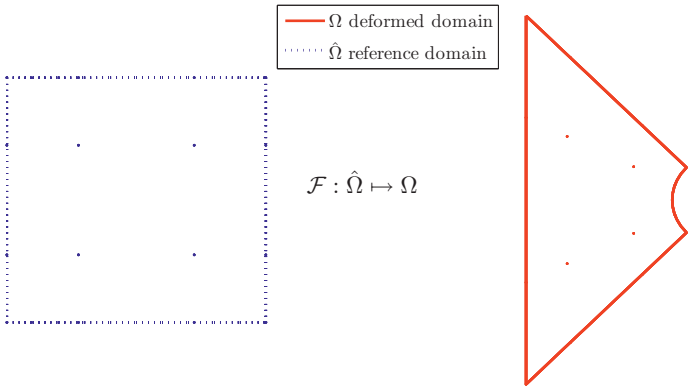

(a) Mapping a reference square into a deformed 2D element

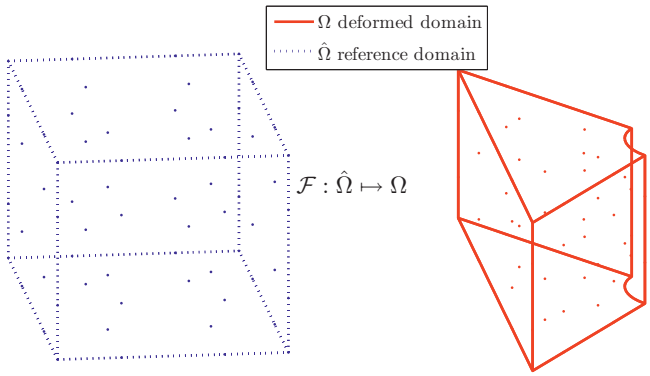

(b) Mapping a reference cube into a deformed 3D element

Figure 4.7: Mapping reference geometries into deformed elements

where $s_0(r)$ and $s_1(r)$, denominated *shape functions*, are *monotonically varying* functions of $r \in [-1, 1]$ which satisfy

$$\begin{cases} s_0(-1) = 1 \\ s_0(1) = 0 \\ s_0(r) + s_1(r) = 1 \qquad -1 \leq r \leq 1 \end{cases} \tag{4.24}$$

The simplest case corresponds to linear shape functions, defined as

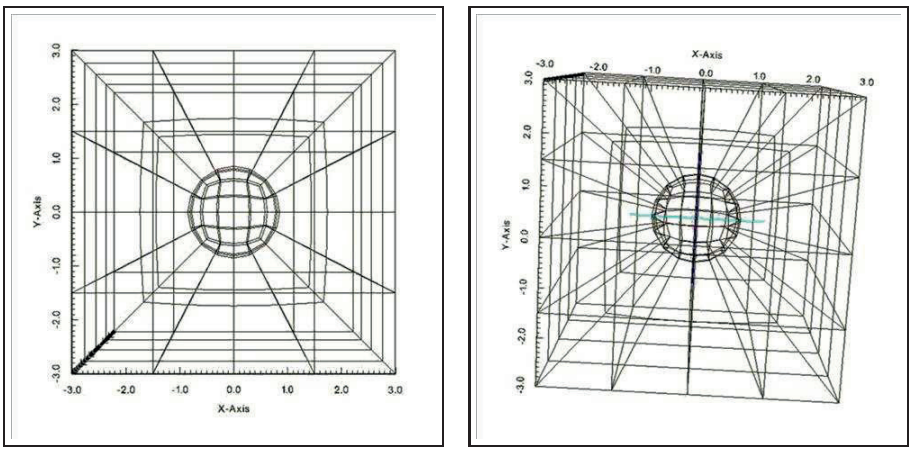

Figure 4.8: Extension of the simulation domain to 3 space dimensions

$$\begin{aligned} s_0(r) &= \frac{1-r}{2} \\ s_1(r) &= \frac{1+r}{2} \end{aligned} \tag{4.25}$$

$\mathcal{F}$ is then defined using the auxiliary definitions in Eq. (4.23) as

$$\mathcal{F}_{2D}(\xi,\eta) = \mathcal{F}_x(\xi,\eta) + \mathcal{F}_y(\xi,\eta) - \mathcal{F}_{xy}(\xi,\eta) \tag{4.26}$$

as illustrated in Fig. 4.6.

The generalization of this mapping technique to 3-dimensions is straightforward, and the resulting mapping is

$$\begin{aligned} \mathcal{F}_{3D}(\xi,\eta,\rho) \;=\; & \mathcal{F}_x(\xi,\eta,\rho) \;+\; \mathcal{F}_y(\xi,\eta,\rho) \;+\; \mathcal{F}_z(\xi,\eta,\rho) \\ & -\; \mathcal{F}_{xy}(\xi,\eta,\rho) \;-\; \mathcal{F}_{xz}(\xi,\eta,\rho) \;-\; \mathcal{F}_{yz}(\xi,\eta,\rho) \\ & +\; \mathcal{F}_{xyz}(\xi,\eta,\rho) \end{aligned} \tag{4.27}$$

This technique can be used for constructing $\mathcal{D}$-dimensional space domains. However, usually up to 3-dimensional deformed domains are of practical interest and easy to interpret physically. The dimension corresponding to time inside a given element is only affected by a linear transformation (stretched or compressed).

An example of a 3-dimensional domain representing the surroundings of a sphere is presented in Fig. 4.8. Note that the reconstructed region is not simply connected. Therefore it cannot be constructed out of a single element and must be divided into several sub-domains Ω^e. Each of these elements is then mapped with an independent mapping function $\mathcal{F}^e_{3D}$, analog to the 2D example in Fig. 4.7.

4.3 Chapter summary

This chapter introduced the fractional derivative operator from a numerical point of view and presented a review of the previous work on the subject. Three of the main concerns regarding fractional derivative implementation were addressed, namely

- high memory and storage requirements,
- singularity at one extreme of the problem domain,
- difficulties in the extension to multiple dimensions and irregular shapes.

The storage requirement issue is alleviated by recurring to high order element methods. In this way a reduced number of nodes is required in order to yield a representation accuracy similar to first order methods. The singular integral contained in the fractional derivative operator is elegantly evaluated by using Gauss-Jacobi quadratures. In order to simplify its practical application, the method for constructing the numerical operator is explained in detail. The chapter concludes by describing techniques for extending the implementation to arbitrarily shaped domains in multiple dimensions. These tools are of importance in Chapters 5 to 7.

Part III

Simulations and application to problems

Chapter 5

Cattaneo-Maxwell diffusion model

Fluidized bed reactors are widely used in gas processing facilities due to their superior heat and mass transfer characteristics. Reaction rates in these reactors depend on the diffusion of species into the catalytic particles. A more accurate description of diffusion than Fick's law provides is required for the optimization of the design of these reactors. This chapter describes how a Least Squares Spectral Element framework was implemented in order to solve the evolution of the concentration profile predicted by Cattaneo-Maxwell's law inside a catalytic pellet.

Section 5.1 introduces the physical context and motivation for this study. The Cattaneo-Maxwell model, also known as the hyperbolic mass diffusion equation, is presented in Section 5.2. Section 5.3 shows a comparison between time-slab and full-domain numerical approaches. The convenience of the latter is verified as it yields the same accuracy with lower computational cost. In Section 5.4 the models by Fick and Cattaneo-Maxwell are examined in contrast, yielding significantly different predictions for time scales similar to the relaxation time but converging asymptotically for larger time periods. Section 5.5 summarizes the main findings and conclusions of this chapter.

5.1 Introduction

Fluidized bed reactors (FBR) are a common processing choice in gas processing facilities and particularly in petrochemical industries. The strong points of the FBR are its outstanding heat and mass transfer characteristics, which make it a good choice for processing large volumes of gas. Many industrially produced polymers, such as rubber, vinyl chloride, polyethylene and styrene are made using FBR technology. In the FBR, the reaction rate depends on the rate at which gas diffuses into the catalyst active sites. Therefore, catalysts are shaped in the form of small porous particles in order to enhance the gas diffusion rate by increasing the gas-solid interfacial area. Hence, a better understanding and description of this transport process is required in order to improve the accuracy in the estimation of reactor dynamics.

Transient diffusion processes are usually modeled based on Fick's second law, a parabolic equation according to which the variance $\langle x^2 \rangle$ of a given concentration profile is expected to increase proportionally with time t, that is $\langle x^2 \rangle \approx t$. According to Fick's law, the information propagates at infinite velocity since a perturbation in any region of the domain is instantly detected everywhere. This inconsistence, denominated the *infinite propagation velocity paradox*, has been addressed in Section 2.1.1. As a result, even when the model is a good approximation for steady-state problems, it leads to erroneous results at short times in transient problems (Chen and Liu, 2003). In addition, the model is not suitable for describing processes at high frequencies, e.g. diffusion in polymer solutions (Depireux and Lebon, 2001).

Experimental results have verified that diffusion often proceeds faster or slower than predicted by Fick's law, and the variance of a given concentration profile evolves as $\langle x^2 \rangle \approx t^{\gamma}$, where γ is called the anomalous diffusion exponent (Ritchie et al., 2005). The cases with $\gamma < 1$ and $\gamma > 1$, not properly accounted by Fick's law, are designated as subdiffusion (Küntz and Lavallée, 2004) and superdiffusion (Küntz and Lavallée, 2001) respectively. An alternative model to deal with these problems that are inherent to Fick's law is Maxwell-Cattaneo's model. This model is the simplest generalization of Fick's law that allows a relaxation of the local equilibrium. It solves the infinite propagation velocity paradox and allows the modeling of different diffusion behaviors. It has been proven by Sharma in (Sharma, 2005) that this damped wave diffusion model can be deduced by allowing the depletion or accumulation of molecules near the diffusion plane. Besides having numerous applications in heat transfer processes (Compte and Metzler, 1997; Dorao, 2009), Cattaneo's law has been evaluated for diffusion modeling in binary fluid mixtures (Jou et al., 1991) and crystalline solids that can be considered to be far from their equilibrium point (Godoy and García-Colín, 1996; Buchbinder and Martaller, 2009).

Evidence of superdiffusion has been found observing water infiltration profiles in porous building materials (Küntz and Lavallée, 2001), and also subdiffusion has been observed in one-dimensional experimental setups in high concentration aqueous $CuSO_4$ solutions (Küntz and Lavallée, 2004). Extended versions of Cattaneo's equation including fractional derivatives are able to predict this behavior in a consistent way. However, more experimental effort is required for determining the parameters of these models. In particular, Cattaneo-Maxwell's model has been applied to pseudo-homogeneous modeling of reaction-diffusion inside a porous particle by a volume averaging procedure (Valdés-Parada et al., 2006). It was concluded that an effective diffusivity tensor can be computed as in the Fickian diffusion case for conditions found in practical applications.

According to Cattaneo's law, the concentration wave propagates at a speed $\sqrt{k_p/\tau}$, where k_p is the diffusion coefficient and τ is a parameter called relaxation time (Gómez-Díaz, 2006). The relaxation time is related to the molecular relaxation processes that take place in the microstructure of the material (Álvarez-

Ramírez et al., 2008). These processes involve a type of memory in particle collisions and imply that highly ordered microstructures such as crystals are expected to exhibit shorter relaxation times than disordered structures. This hyperbolic description has been proven valid for transient solute flows with small characteristic times (Auriault et al., 2007) and for transport of a passive scalar in a turbulent flow (Brandenburg et al., 2004). For certain parameter choices, the desorptive diffusive flux can persist after the diffussing species has been completely desorbed. However, such physically unrealistic behavior disappears when the values for parameters τ and k_p are constrained by relations that explicitly enforce the second law of thermodynamics. This is explained in detail in (Doghieri et al., 1993). In Sections 5.2 to 5.5, the Cattaneo-Maxwell model is discussed and a numerical solution is obtained using Least Squares Spectral Element Method.

5.2 The hyperbolic mass diffusion equation

The mass transfer in a one-dimensional system is governed by Eq. (2.14), known as the balance equation

$$\frac{\partial C\left(x,t\right)}{\partial t}+\frac{\partial J\left(x,t\right)}{\partial x}=0, \tag{2.14}$$

in combination with a constitutive equation. As an alternative to Fick's first law, the following equation is proposed by Cattaneo (Compte and Metzler, 1997)

$$J+\tau\frac{\partial J\left(x,t\right)}{\partial t}=-k_p\frac{\partial C\left(x,t\right)}{\partial x}. \tag{5.1}$$

In the equations above $C\left(x,t\right)$ represents the mass concentration, $J\left(x,t\right)$ is the mass flux, k_p is the diffusion coefficient, τ is the relaxation time and (x,t) represent the space and time coordinates. By combining Eqs. (2.14) and (5.1), Maxwell-Cattaneo model is obtained:

$$k_p\frac{\partial^2 C\left(x,t\right)}{\partial x^2}=\frac{\partial C\left(x,t\right)}{\partial t}+\tau\frac{\partial^2 C\left(x,t\right)}{\partial t^2} \tag{5.2}$$

Equation (5.2), known as Cattaneo-Maxwell's equation, is a damped-wave hyperbolic diffusion equation, which predicts that concentration waves propagate at a finite speed. This constitutive model yields the same results as Fick's law for steady-state cases, since the non-transient terms are the same. However, the results of both models are considerably different for time scales comparable to the relaxation time of the considered medium. It can be seen immediately that Cattaneo-Maxwell equation approaches Fick's law as $\tau\rightarrow 0$.

5.3 Numerical Solution

The objective of this chapter is to describe the solution of Eq. (5.2) by the Least Squares Spectral Element Method. By this procedure, a well-posed system of partial differential equations is transformed into a symmetric, positive definite system of algebraic equations (Gerritsma and De Maerschalck, 2010). These characteristics of the system enable the use of advantageous solving algorithms like the conjugate gradient method (Shewchuk, 2004).

As an alternative to Eq. (5.2), a second order differential equation, the first order system consisting of Eqs. (2.14) and (5.1) is solved. In a higher level of abstraction, the problem can be expressed as:

$$\mathcal{L}\mathbf{u} = \mathbf{g} \;\text{ in }\; \Omega \tag{3.1a}$$

$$\mathcal{B}\mathbf{u} = \mathbf{g}_\Gamma \;\text{ on }\; \Gamma \subseteq \partial\Omega \tag{3.1b}$$

where $\mathcal{L}$, $\mathbf{u}$ and $\mathbf{g}$ for this problem are defined as

$$\mathcal{L} = \begin{bmatrix} \dfrac{\partial \bullet}{\partial t} & \dfrac{\partial \bullet}{\partial x} \\ -k_p \dfrac{\partial \bullet}{\partial x} & \tau \dfrac{\partial \bullet}{\partial t} + \bullet \end{bmatrix} \;;\; \mathbf{u} = \begin{bmatrix} C \\ J \end{bmatrix} \;;\; \mathbf{g} = \begin{bmatrix} 0 \\ 0 \end{bmatrix} \tag{5.4}$$

Here $\mathbf{g}$ represents the source terms, $\mathcal{B}$ the boundary condition (trace) operator and $\mathbf{g}_\Gamma$ the solution at part of the domain boundaries.

The linear operator $\mathcal{L}$ defines the isomorphism $\mathcal{L} : X(\Omega) \longrightarrow Y(\Omega)$ for which two constants C_1 and C_2 exist that fulfill

$$C_1 \|\mathbf{u}\|_X \leq \|\mathcal{L}\mathbf{u}\|_Y \leq C_2 \|\mathbf{u}\|_X \;\; \forall \mathbf{u} \in X \tag{5.5}$$

As a consequence of this, the norms $\|\mathbf{u}\|_X$ and $\|\mathcal{L}\mathbf{u}\|_Y$ are equivalent, and so minimizing $\|\mathbf{u} - \mathbf{u}_{ex}\|_X$ is equivalent to minimizing $\|\mathcal{L}(\mathbf{u} - \mathbf{u}_{ex})\|_Y$ where $\mathbf{u}_{ex}$ is the exact solution.

To solve Eqs. (3.1a) and (3.1b), a norm-equivalent functional can be defined as

$$\mathcal{J}(\mathbf{u}) = \frac{1}{2}\|\mathcal{L}\mathbf{u} - \mathbf{g}\|^2_{Y(\Omega)} + \frac{1}{2}\|\mathcal{B}\mathbf{u} - \mathbf{g}_\Gamma\|^2_{Y(\Gamma)} \tag{3.2}$$

where the norm $\|\bullet\|^2_{Y(\Gamma)}$ is defined as

$$\|\bullet\|^2_{Y(\Gamma)} = \int_\Gamma \bullet \bullet \, d\Gamma \tag{3.2}$$

Solving the system for Eqs. (3.1a) and (3.1b) is equivalent to finding the function $\mathbf{u}$ that minimizes the functional Eq. (3.2). That is:

Find $\mathbf{u} \in X(\Omega)$ *such that:*

$$\mathbf{B}(\mathbf{u}, \mathbf{v}) = \mathbf{F}(\mathbf{v}) \;\; \forall \, \mathbf{v} \in X(\Omega) \tag{5.6}$$

with

$$\mathbf{B}(\mathbf{u},\mathbf{v}) = \langle \mathcal{L}\mathbf{u}, \mathcal{L}\mathbf{v}\rangle_{Y(\Omega)} + \langle \mathcal{B}\mathbf{u}, \mathcal{B}\mathbf{v}\rangle_{Y(\Gamma)} \tag{5.7}$$

$$\mathbf{F}(\mathbf{v}) = \langle \mathbf{g}, \mathcal{L}\mathbf{v}\rangle_{Y(\Omega)} + \langle \mathbf{u}, \mathcal{B}\mathbf{v}\rangle_{Y(\Gamma)} \tag{5.8}$$

where $\mathbf{B} : X \times X \longrightarrow \mathbb{R}$ is a symmetric continuous bilinear form, and $\mathbf{F} : X \longrightarrow \mathbb{R}$ a continuous linear form. The concepts introduced in Section 3.2 are in this way particularized to fit the actual problem by a proper choice of the operators and variables in Eq. (5.4).

As the boundary conditions are expressed in a weak form, functions that do not satisfy the boundary conditions can be included in the search space $X(\Omega)$. In order to perform the numerical calculations, this infinite search space is reduced to a finite search space $X_h(\Omega) \subset X(\Omega)$.

The computational domain Ω is divided into $N_e = N_{ex} \times N_{et}$ non-overlapping sub-domains or elements Ω_e, such that

$$\Omega = \bigcup_{e=1}^{N_e} \Omega_e \quad \Omega_e \cap \Omega_i = \emptyset \ \ \forall\ e \neq i \tag{5.9}$$

In each element, the unknown function $\mathbf{u}^e$ is approached by the set of all polynomials of degree up to O_x. The global approximation in Ω is constructed by attaching the local element approximations Ω_e. The solution is expanded in the base of Lagrange polynomials, as depicted in Fig. 5.1.

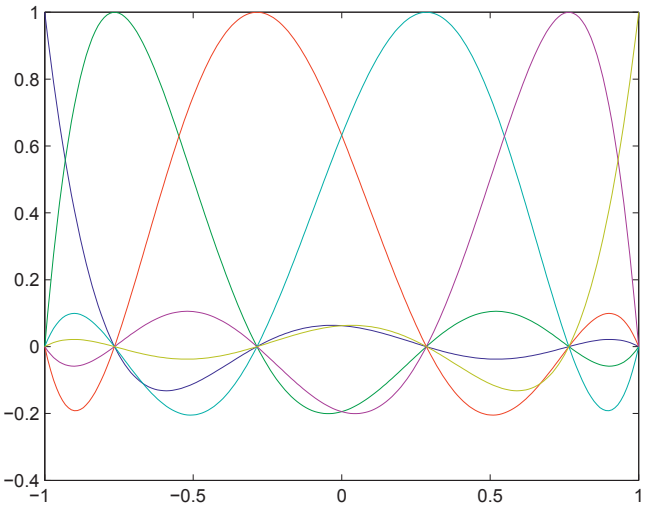

Figure 5.1: Lagrange polynomials of order $0 \leq O_e \leq 5$ for a reference domain

5.3.1 Time-space formulation

The problem was solved in a 2-dimensional domain, with x and t as the variables. Two numerical approaches were compared: a full domain approach consisting in the simultaneous solution of the complete 2-D domain in one hand, and on the other hand a time-slab approach, consisting in solving one slab at the time, using the solution of the previous slab as initial condition. Both solving schemes are presented in Fig. 5.2

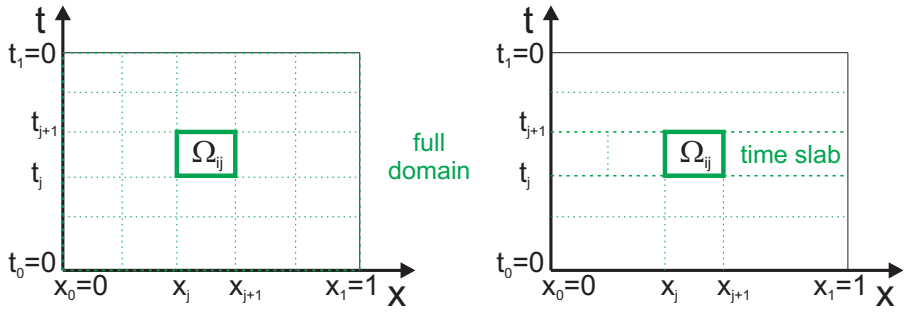

(a) Full-domain approach (b) Time-slab approach

Figure 5.2: Solving schemes for Cattaneo-Maxwell model: (a) full-domain simultaneous solution vs. (b) time-slab approach

The simultaneous solution of the full domain requires the solution of one linear equation system of large size, while the time-slab approach requires the solution of many linear equation systems of smaller size. In more concrete words, we compare solving of a system of size $\approx N_{ex}\ O_x \times N_{et}\ O_t$ against solving N_{et} systems of size $\approx N_{ex}\ O_x \times O_t$, where N_{ex}, N_{et}, O_x and O_t are the number of elements and the approximation order in x and t respectively.

The advantage of solving the problem with the time-slab approach becomes notorious as the size of the system increases. In this case, the computational cost is approximately proportional to the number of time slabs, while with the full domain solution, the computational cost grows faster than linearly.

5.4 Numerical examples

Simulations with different values of τ were performed in order to observe the effect of this parameter in the behavior of the normalized system coordinates x and t and variables C and J. The propagation of concentration waves in a slab as depicted in Fig. 5.3 was studied as a reference case. This can represent the evolution of the concentration profile inside a catalytic pellet submerged in a reactant medium. In order to illustrate the differences with Fick's law, the case with $\tau = 0$ is included in some figures.

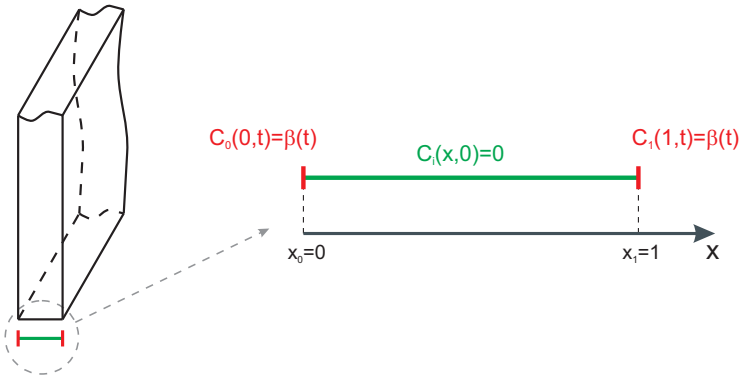

Figure 5.3: Physical interpretation of the 1-D numerical problem

5.4.1 Analysis of Cattaneo-Maxwell model

The most important conceptual difference between Fick's model and Cattaneo-Maxwell model is the finite propagation speed that arises as a relaxation term appears in the equation. The propagation velocity of the concentration wave is $v_c = \sqrt{\tau/k_p}$ (Gómez-Díaz, 2003).

Figure 5.4 shows the evolution of concentration in an initially depleted slab when a sudden change in concentration is applied on both boundaries at time $t = 0$. A comparison between the Fickian case ($\tau = 0$) and two different values of τ is presented in order to illustrate the effects generated by a finite propagation velocity. The smoothed shape of the wavefront and the lower boundary value of the solution for short times are due to the use of $\beta(t)$ functions instead of step functions as boundary conditions. This change was performed in order to avoid discontinuities that are difficult to treat numerically. Figures 5.4(a), 5.4(c) and 5.4(e) present the results in the complete simulation domain, while Figs. 5.4(b), 5.4(d) and 5.4(f) displays snapshots for different simulation times. In the Fickian case, Figs. 5.4(a) and 5.4(b), the concentration converges asymptotically to the boundary value, while two differences can be appreciated in the other plots:

- A propagation delay can be observed: the concentration in a given region of the domain does not start to increase until the propagation wave reaches that point. This is evident in Figs. 5.4(e) and 5.4(f).
- There is a concentration overshoot: since the information takes a finite time to propagate, constructive interference occurs between both counterdiffusing waves and uphill diffusion is observed.

Even when experimental evidence has been found on the existence of diffusion proceses that Fick's law cannot describe properly (Ritchie et al., 2005; Küntz and Lavallée, 2004; 2001), there are still no measurements that can conclusively

support Cattaneo-Maxwell model as accurate. This is partly due to the experimental difficulties associated with measuring concentration transients at a time scale similar to the relaxation time (Uemura and Macdonald, 1996; Nakawaga, 2003). Similar phenomena have been observed in heat transfer processes (Lane et al., 1947), suggesting that Cattaneo-Maxwell model could be appropriate.

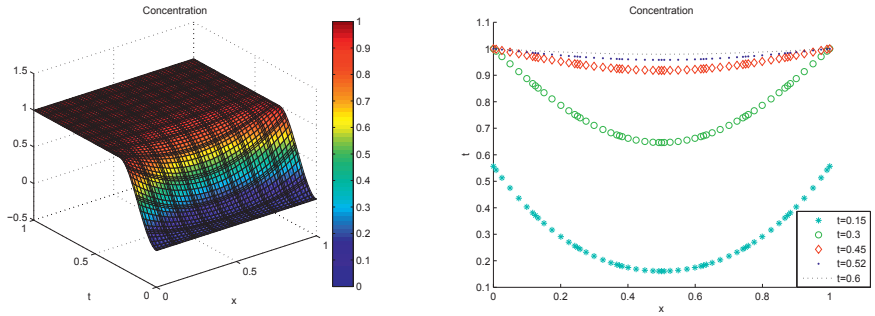

(a) Full solution for $\sqrt{k_p/\tau} = \infty$

(b) Profile snapshots for $\sqrt{k_p/\tau} = \infty$

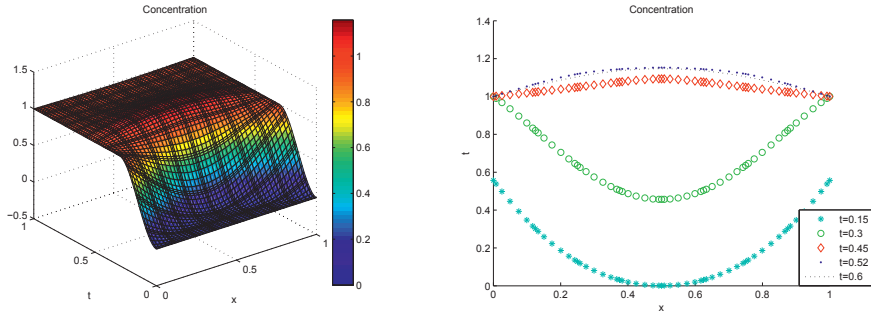

(c) Full solution for $\sqrt{k_p/\tau} = \sqrt{10}$

(d) Profile snapshots for $\sqrt{k_p/\tau} = \sqrt{10}$

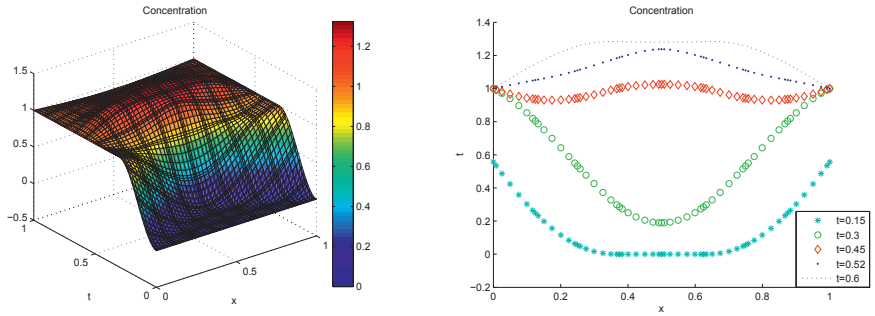

(e) Full solution for $\sqrt{k_p/\tau} = \sqrt{5}$

(f) Profile snapshots for $\sqrt{k_p/\tau} = \sqrt{5}$

Figure 5.4: Propagation of a concentration pulse for representative values of $\sqrt{k_p/\tau}$

5.4.2 Convergence study

In order to find guidelines for the optimal resolution (order and number of elements) to solve this problem, the residual and computing time were measured for the same problem with different resolutions. The results are shown in Fig. 5.5. The residual decreases as the order and number of elements is increased, which verifies that the problem is solved correctly. The oscillations evidenced in the decreasing tendency of the residual, specially in the red curves of Figs. 5.5(c) and 5.5(d), are due to the low resolution of the simulation. Being the number of points in the domain too low, the shape of the interpolating functions affects the quality of the approximation.

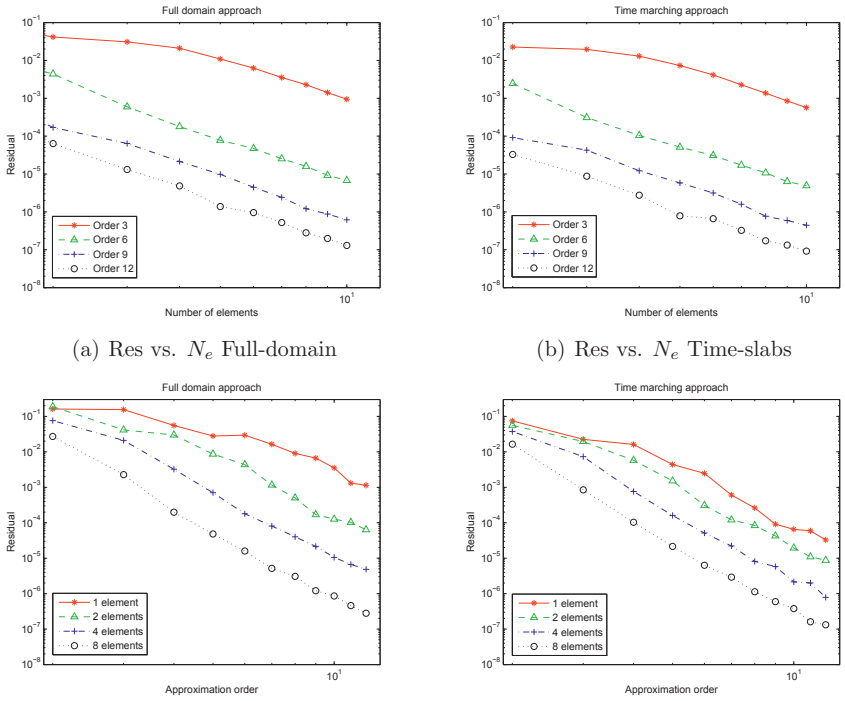

(a) Res vs. N_e Full-domain

(b) Res vs. N_e Time-slabs

(c) Res vs. O_x Full-domain

(d) Res vs. O_x Time-slabs

Figure 5.5: Convergence plots for full-domain and time-slab approaches

Figure 5.6 presents the residual against the computing time for both time-slab and full-domain approaches. The points in this plot were obtained from the solution of the same problem with different resolutions. All combinations of order O_x and element number N_{ex} were included in the plot, with $2 \leq O_x \leq 12$ and $1 \leq N_{ex} \leq 10$. The noise in the plot is attributed to the variation of O_x and N_{ex} at the same time.

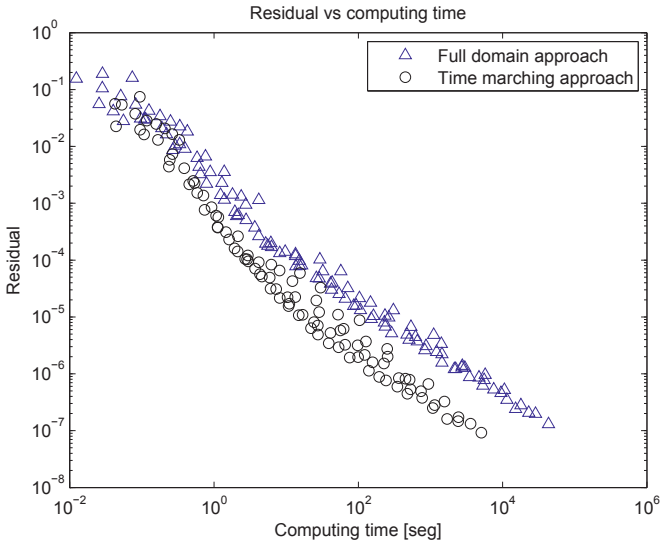

Figure 5.6: Residual vs. computing time for Full-domain and Time-slab approaches

The main fact to be observed from Fig. 5.6 is that the time-slab approach is more effective than the full-domain approach, producing better results with significantly less calculation time.

5.5 Chapter conclusions

A framework for Least Squares Spectral Element Method was implemented in order to solve the evolution of the concentration profile inside a catalytic pellet. A time-space formulation of Cattaneo-Maxwell equation was solved for different relaxation time values. This model approaches Fick's law for time scales well above the relaxation time. However, for time scales similar to the relaxation time, the finite propagation velocity proposed by Cattaneo-Maxwell model predicts the superimposition of two concentration waves that move towards each other. This can originate a transient uphill diffusion which is not predicted by Fick's law, but has been observed experimentally in (Baird et al., 1971; Vrentas et al., 1984). Two solution schemes were compared: a time-slab approach consisting in solving each time slab separately, and a full-domain approach consisting in solving the complete domain at once. The time-slab approach proved to be more efficient, allowing to achieve the same precision with less computing effort.

Chapter 6

Fractional diffusion models

Fractional derivatives provide a general approach for modeling transport phenomena occurring in diverse fields ranging from hydrology and viscoelasticity to electrochemistry, signal processing, magnetically confined plasmas and several anomalous diffusion cases. These models provide a general approach that can link Fick's law with hyperbolic diffusion theories and CTRW. Sub-diffusive and super-diffusive processes, not accounted for by traditional models, can be addressed by fractional diffusion equations. This chapter presents the most common fractional diffusion models and a selection of numerical solutions using the Least Squares Spectral Method.

Section 6.1 contains a brief review on applications of fractional diffusion and discusses the numerical difficulties in solving fractional differential equations. Section 6.2 introduces equations representing various relevant physical models. Guidelines to the Least Squares Spectral Method applied to this problem are provided in Section 6.3. Sample results and convergence analyses for validating the numerical tools are displayed in Section 6.4.

6.1 Introduction

Diffusion processes have traditionally been described using Fick's law, which gives sufficiently accurate results for many applications. However, as elaborated in Chapter 2, this model can be insufficient for some purposes and numerous approaches for deriving a more general formulation have been attempted.

Fractional differential equations constitute a generalization of differential equations which can account for any real value of the derivative exponent. These are employed as alternative models for describing many transport processes which cannot be accurately accounted for by Fick's law (Ercília and Sousa, 2009).

6.1.1 Fractional derivative applications

Fractional derivative formulations are attractive for describing diffusion phenomena since they provide a general approach that can link Fick's law with hyperbolic diffusion theories and CTRW (Compte and Metzler, 1997; Barkai, 2002; Hilfer and Anton, 1995; Luchko and Punzi, 2011). In addition, fractional differential equations are powerful tools for modeling phenomena occurring in diverse fields. Particular examples are found in hydrology (Benson et al., 2004; Berkowitz et al., 2006; Fomin et al., 2009; Gao et al., 2009; Küntz and Lavallée, 2001; 2004), electrochemistry (Oldham, 2010), viscoelasticity (Caputo and Mainardi, 1971; Rossikhin and Shitikova, 2011; 2006), magnetically confined plasmas (Lynch et al., 2003), signal processing (Mathieu et al., 2003; Chang, 2009) and anomalous diffusion (Lu and Hanyga, 2005; Giona and Roman, 1992; Hanert, 2011; Huang et al., 1995; Logvinova and Néel, 2004; Metzler et al., 1999) just to name a few. There are plenty of reviews on the vast range of applications of fractional derivatives, e.g. (Zhang et al., 2009; Conner and Wilson, 1994; Klages et al., 2008; Mainardi, 2010; Podlubny, 1999; Metzler and Klafter, 2000).

The transport of passive scalars by fluid flow in a porous medium is often modeled by a fractional derivative model (Meerschaert and Tadjeran, 2004; Huang et al., 2008). These models allow capturing experimentally observed super-diffusive and sub-diffusive behaviors in the fields mentioned above. Also memory effects and processes with long-range correlations can be represented by fractional models (Bagley and Torvik, 1983; Gorenflo et al., 2002; Metzler and Klafter, 2004).

A sound physical interpretation for the fractional derivative as a way of considering non-locality is given in (Molz et al., 2002). Following this concept, it is shown in (Hanneken et al., 2004) that fractional diffusion can be interpreted as the collective motion of separate ensembles of random walkers.

6.1.2 Numerical issues

The aforementioned facts make fractional derivatives a powerful model for studying anomalous diffusion cases. However, the solution of non-integer differential equations presents greater mathematical and computational challenges.

On the mathematical aspect, notwithstanding the wide application scope of fractional derivatives, simple cases with analytical solution and practical application are scarce. In addition, the physical meaning of fractional boundary conditions is still a matter of discussion (Podlubny, 2002; Deng, 2007; Rutman, 1995; Sabatier et al., 2010; Heymans and Podlubny, 2006; Malinowska and Torres, 2010; Zhang et al., 2007).

On the computational aspect, as discussed in Section 4.1, the singularity and non-locality of the fractional operator result in difficult numerical handling and high computational cost.

6.2 Physical models

This section introduces the multi-dimensional problems used for testing the performance of the LSSM applied to fractional differential equations, in addition to the *fractional advection-dispersion* and *fractional time diffusion* equations introduced in Section 2.4.2.

6.2.1 Time fractional diffusion equation (2D+Time)

The first problem considered in this section consists of a time fractional diffusion equation with order $0 < \beta \leq 1$, with given boundary conditions and evolving from a given initial condition:

$$\begin{cases} {}_0D_t^{\beta} C(x,y,t) &= \nabla^2 C(x,y,t) + s(x,y) & in\ \ \Omega = [-1,1]^2 \times [0,1] \\ C(x,y,0) &= C_0(x,y) & \\ C(x,y,t) &= g_D(x,y,t) & on\ \ \partial\Omega_D \\ \partial_n C(x,y,t) &= g_N(x,y,t) & on\ \ \partial\Omega_N \end{cases} \tag{6.1}$$

where $\partial_n C(\mathbf{x},t)$ is the normal derivative on the boundary and the vector $\mathbf{x}$ represents all the spatial coordinates $\mathbf{x} = [x,y]$. The boundary $\partial\Omega$ is subdivided into $\partial\Omega_D$ and $\partial\Omega_N$ where Dirichlet and Neumann boundary conditions are applied respectively. The subdivisions satisfy $\partial\Omega_D \cup \partial\Omega_N = \partial\Omega$ and $\partial\Omega_D \cap \partial\Omega_N = \emptyset$. Here ${}_0D_t^{\beta} C(x,y,t)$ represents the time fractional derivative operator defined in Eq. (2.10b). Note that Eq. (6.1) converges to Poisson's equation as $\beta \to 1$.

Analytical solution

The existence and uniqueness of this solution have been proven in (Li and Xu, 2010), and a finite difference solution is presented in (Brunner et al., 2010). In order to test the performance of the Least Squares Spectral Method, results and analysis are presented for the boundary conditions in Eq. (6.2).

$$\begin{cases} C_0(x,y) = \cos\left(\frac{\pi}{2}x\right)\cos\left(\frac{\pi}{2}y\right) \\ g_D(x,y,t) = 0 \\ \partial\Omega_D = \partial\Omega \\ \partial\Omega_N = \emptyset \end{cases} \tag{6.2}$$

The analytical solution to the system composed by Eqs. (6.1) and (6.2) is expressed as the product of separate functions for space and time variables (Brunner et al., 2010):

$$C(x,y,t) = E_{\beta}\left(-\tfrac{1}{2}\pi^2 t^{\beta}\right) C_0(x,y), \tag{6.3}$$

where $E_{\beta}(\xi)$ is the Mittag-Leffler function, defined as

$$E_{\beta}(\xi) = \sum_{k=0}^{\infty} \frac{\xi^k}{\Gamma(\beta k + 1)}. \tag{6.4}$$

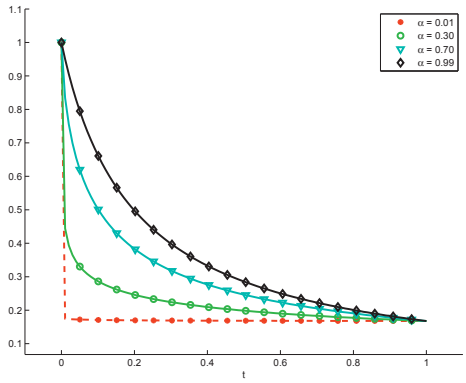

Figure 6.1: Plot of the temporal solution $E_\beta\left(-\frac{1}{2}\pi^2 t^\beta\right)$ in the interval $t \in [0,1]$

The initial condition $C_0(x,y)$ is in turn a product of separate functions in one variable. This characteristic is convenient for testing the convergence of the polynomial representation when increasing the polynomial degree (Jiang, 1998). The temporal dependence of the solution is given in the form of the Mittag-Leffler function which has the shape depicted in Fig. 6.1. The Mittag-Leffler function is steeper at the initial instants, and its steepness depends on the fractional derivative exponent β. This characteristic is useful in order to test the ability of polynomials to represent the solution as it approaches a singular function.

6.2.2 General fractional diffusion equation

The second problem introduced in this section is Eq. (6.5), which has been addressed as the general fractional diffusion equation in (Podlubny et al., 2009).

$$\begin{cases} {}_0D_t^{\beta_1} C(x,t) &= D_R^{\beta_3} C(x,t) + s(x,t) \quad in\ [x_0,x_1]\times[t_0,t_1] \\ C(x_0,t) &= 0 \\ C(x_1,t) &= 0 \\ C(x,t_0) &= 0 \\ s(x,t) &= 8 \end{cases} \tag{6.5}$$

Here $D_R^{\beta_3} C(x,t)$ denotes the Riesz fractional derivative, defined as

$$D_R^{\beta_3} C(x,t) = \frac{1}{2}\left({}_{x_0}D_x^{\beta_3} C(x,t) + {}_xD_{x_1}^{\beta_3} C(x,t)\right). \tag{6.6}$$

This case is a further extension of Poisson's equation in 1D, but fractional derivative exponents β_1 and β_3 are here considered in both space and time coordinates. Poisson's problem is again recovered for $\beta_1 = 1$ and $\beta_3 = 2$.

6.2.3 General fractional diffusion equation with delay

Equation (6.5) can even be generalized to include a delay δ into its formulation. This has the only purpose of testing the numerical framework since there is still no agreement on the physical meaning of this equation (Podlubny et al., 2009). The derivative exponent β_2 and the time delay δ are added, resulting in Eq. (6.7).

$$\begin{cases} \frac{1}{2}\left({}_0D_t^{\beta_1}C(x,t) + {}_0D_{t-\delta}^{\beta_2}C(x,t)\right) &= D_R^{\beta_3}C(x,t) + s(x,t) \quad in \ [x_0,x_1]\times[t_0,t_1] \\ C(x_0,t) &= 0 \\ C(x_1,t) &= 0 \\ C(x,t_0) &= 0 \\ s(x,t) &= 8 \end{cases} \tag{6.7}$$

6.3 Numerical solution

The problems introduced in the previous section: Eqs. (2.18), (2.19), (6.1), (6.5) and (6.7) are solved next by the Least Squares Spectral Method. The abstract formulation can be expressed as:

$$\mathcal{L}\mathbf{u} = \mathbf{g} \ \text{ in } \ \Omega \tag{3.1a}$$
$$\mathcal{B}\mathbf{u} = \mathbf{g}_\Gamma \ \text{ on } \ \Gamma \subseteq \partial\Omega \tag{3.1b}$$

where the operators $\mathcal{L}$, $\mathbf{u}$ and $\mathbf{g}$ are defined for Eq. (6.7) as

$$\begin{cases} \mathcal{L} = \frac{1}{2}\left({}_0D_t^{\beta_1}\bullet + {}_0D_{t-\delta}^{\beta_2}\bullet\right) - D_R^{\beta_3}\bullet \\ \mathcal{B} = \mathbb{I} \\ \mathbf{g} = s(x,t) \\ \mathbf{g}_\Gamma = 0 \\ \mathbf{u} = C \end{cases} \tag{6.9}$$

In order to solve the system of Eqs. (3.1) and (6.9), a norm-equivalent functional can be defined as

$$\mathcal{J}(\mathbf{u},\mathbf{g}) = \rho_{\mathcal{L}} \left\|\mathcal{L}\mathbf{u}-\mathbf{g}\right\|^2_{Y(\Omega)} + \rho_{\mathcal{B}} \left\|\mathcal{B}\mathbf{u}-\mathbf{g}_0\right\|^2_{Y(\Gamma)} \tag{3.2}$$

where the L_2 norm $\|\bullet\|^2_{Y(\Gamma)}$ is defined as

$$\|\bullet\|^2_{Y(\Gamma)} = \int_\Gamma \bullet\bullet \, d\Gamma \tag{3.4}$$

and the factors $\rho_{\mathcal{L}}$ and $\rho_{\mathcal{B}}$ in front of each term of the functional defined in Eq. (3.2) are found in practice as the combination that minimizes the numerical error. The

best performances in these simulations were found for $\rho_{\mathcal{B}}/\rho_{\mathcal{L}} > 1000$, which means assigning a greater weight to the boundary residual.

Solving the system for equation Eq. (3.1) is equivalent to finding the function $\mathbf{u}$ that minimizes the functional Eq. (3.2) by solving the weak form in Eq. (3.8) defined in Section 3.2.2.

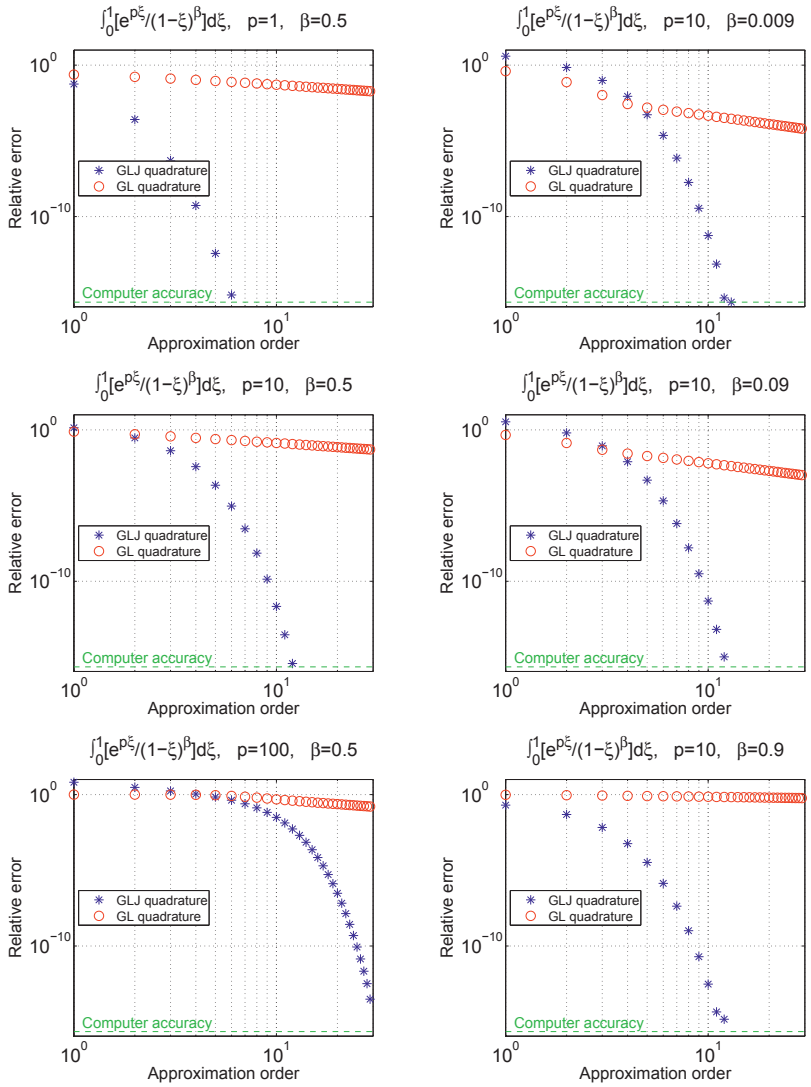

Figure 6.2: Convergence plots for integration: $g(\xi)$ with $\gamma_1(\xi) = e^{p\xi}$, with fixed $\beta = 0.5$ (left column) and with fixed coefficient $p = 10$ (right column)

6.4 Numerical verification

This section presents numerical examples used to validate the convergence of the numerical scheme. Validations for Gauss-Lobatto-Jacobi quadrature and the fractional derivative operator are presented in Sections 6.4.1 and 6.4.2 respectively. Sections 6.4.3 to 6.4.6 show numerical results for the models introduced in Section 6.3 and a comment about the convergence of the numerical scheme is included in Section 6.4.7.

6.4.1 Quadrature validation

The validation of GLJ quadrature was achieved by integrating two test functions of the form $g(\xi) = (1-\xi)^{-\beta}\gamma(\xi)$ over the domain $[0,1]$ for two representative choices of $\gamma(\xi)$.

The relative error in numerical integration is plotted in Fig. 6.2 as a function of the polynomial degree. The relative error is here defined as the absolute value of the difference between the exact integral and the quadrature approximation, divided by the absolute value of the exact integral

$$\text{err} = \frac{\left| \int_0^1 g(\xi)d\xi \; - \int_0^1 g_N(\xi)d\xi \right|}{\left| \int_0^1 g(\xi)d\xi \right|}.$$

Note that a Gauss-Lobatto quadrature of order N is equivalent to the exact integral of a polynomial approximation of order $2N-1$.

Case A The first choice of $\gamma(\xi)$ corresponds to the exponential function, i.e.

$$g(\xi) = \frac{\gamma_1(\xi)}{(1-\xi)^\beta}, \text{ with } \gamma_1(\xi) = e^{p\xi},$$

which is infinitely smooth for any value of p. As the function $g(\xi)$ cannot be exactly represented by a polynomial approximation with a finite number of terms, it is used to evaluate the relationship between the quadrature error and the number of quadrature points. The GLJ quadrature is therefore expected to converge exponentially to the integral as the number of quadrature points is increased (see Fig. 6.2). The convergence is always exponential and nearly independent of the derivative exponent β. A slower convergence is observed, as the coefficient p increases, due to the corresponding 'sharpening' of the integrand function $g(\xi)$. The results are compared with GL integration, which yields algebraic convergence.

Case B The second choice of $\gamma(\xi)$ corresponds to a polynomial, i.e.

$$g(\xi) = \frac{\gamma_2(\xi)}{(1-\xi)^\beta}, \text{ with } \gamma_2(\xi) = \xi^p.$$

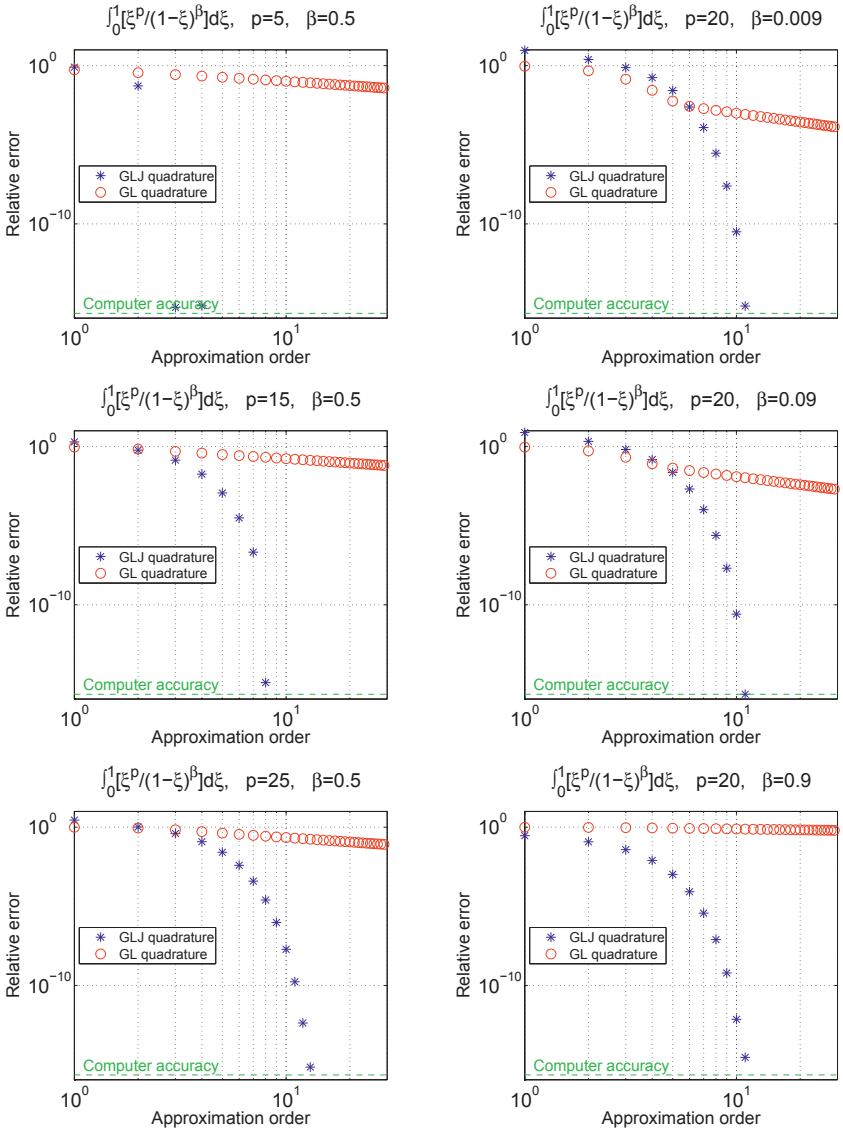

Figure 6.3: Convergence plots for numerical integration: $g(\xi)$ with $\gamma_2(\xi) = \xi^p$, with fixed $\beta = 0.5$ (left column) and with fixed coefficient $p = 20$ (right column)

Since the fractional derivative operator is intended to be applied to arbitrary functions which are approximated by polynomials, it is of interest to test its performance on polynomials.

The error in the numerical integration of $g(\xi)$ for different values of p and β is plotted in Fig. 6.3. Exponential and algebraic convergence is again obtained for GLJ and GL quadratures respectively. Cases A and B provide a validation of GLJ quadrature applied to functions of the form $g(\xi) = (1-\xi)^{-\beta}\gamma(\xi)$.

6.4.2 Validation of fractional derivative operators

The validation of the fractional derivative operators is performed by applying them to the function $\gamma(\xi) = \xi^p(1-\xi)^p$ in the domain $[0,1]$ as

$$D_q^\beta \gamma(\xi) = (1-q)\ {}_0D_\xi^\beta \gamma(\xi) + q\ {}_\xi D_1^\beta \gamma(\xi).$$

The reported measures for relative error are the L_2 and L_∞ norms of the difference between the numerical and analytical solutions normalized with the maximum absolute value of the analytical result as

$$err = \frac{\left\| D_q^\beta \gamma(\xi) - D_q^\beta \gamma_N(\xi) \right\|_{L_2,L_\infty}}{\left\| D_q^\beta \gamma(\xi) \right\|_{L_2,L_\infty}}.$$

The studied cases correspond to *Left*, *Right* and *Riesz* derivatives (i.e. $q = 0$, $q = 1$ and $q = 0.5$ respectively). Convergence results for the reference derivative exponent $\beta = 1/2$ are displayed in Fig. 6.4. For illustrative purposes, the analytical result and polynomial approximation of $D_q^\beta \gamma(\xi)$ are plotted in Fig. 6.5. It is not possible for the naked eye to distinguish the analytical and numerical solutions (order 19) in this figure. Note that for this particular choice of $\gamma(\xi)$ both Riemann-Liouville and Caputo definitions of fractional derivative are coincident.

6.4.3 Fractional advection-dispersion equation

The model given by Eq. (2.18) is solved for the following set of parameters: $q = 1/2$ (Riesz derivative), $\mu(x) = 1$, homogeneous initial and boundary conditions and with a source term $s(x,t) = 8$. The resulting system is

$$\begin{cases} \dfrac{\partial C(x,t)}{\partial t} - \dfrac{1}{2}\Big({}_0D_x^\beta C(x,t) + {}_xD_1^\beta C(x,t) \Big) = s(x,t), \qquad in\ \Omega = [0,1]\times[0,1] \\ C(0,t) = 0 \\ C(1,t) = 0 \\ C(x,0) = 0 \\ s(x,t) = 8 \end{cases} \tag{6.10}$$

where the fractional derivative operator has been defined according to the Caputo definition in Eq. (2.10b). The numerical solution of Eq. (6.10) is found by the LSSM described in Section 6.3. The finite difference result in (Podlubny et al.,

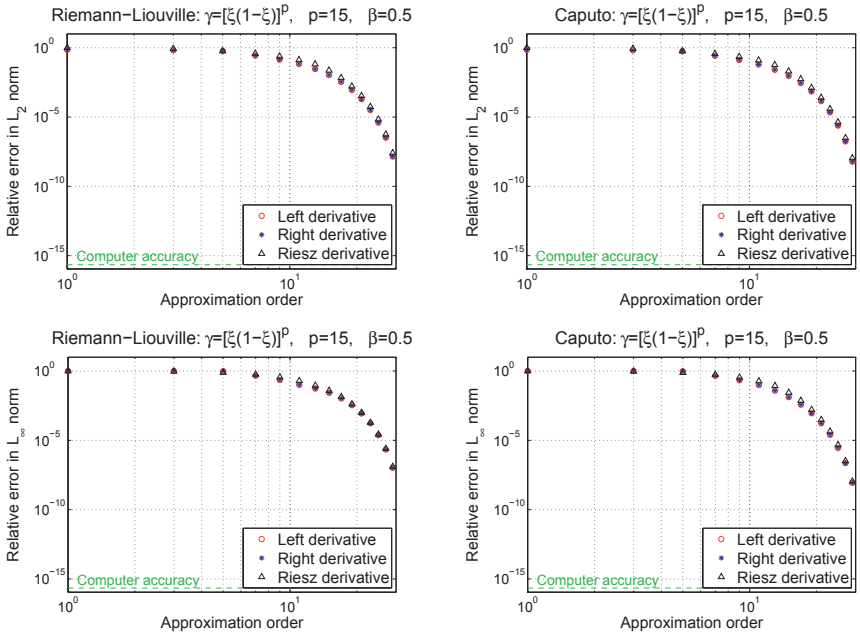

Figure 6.4: Convergence plots for Riemann-Liouville and Caputo fractional derivatives of the function $\gamma(\xi) = \xi^p(1-\xi)^p$ for $\beta = 0.5$

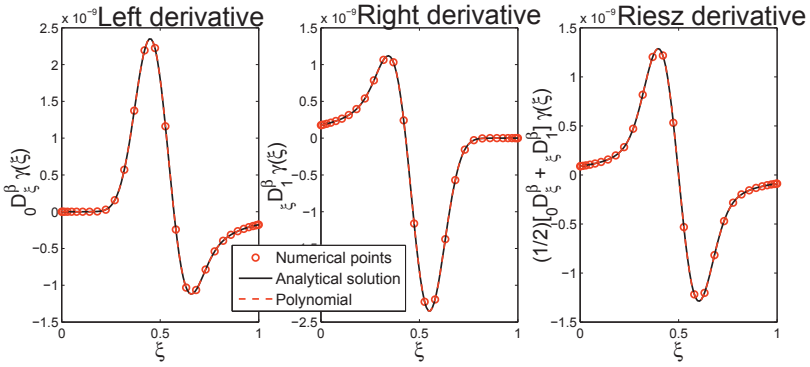

Figure 6.5: Analytical value and polynomial approximation (order 19) of ${}_aD_b^{\beta}\gamma(\xi)$

2009) is reproduced using a different approach, obtaining the solution presented in Fig. 6.6. A comparison of the $C(x,t)$ profiles predicted by each derivative exponent β for the final time is included in Fig. 6.6 in order to illustrate the qualitative differences in the predicted physical behavior. Note that $\beta = 2$ corresponds to Fick's law.

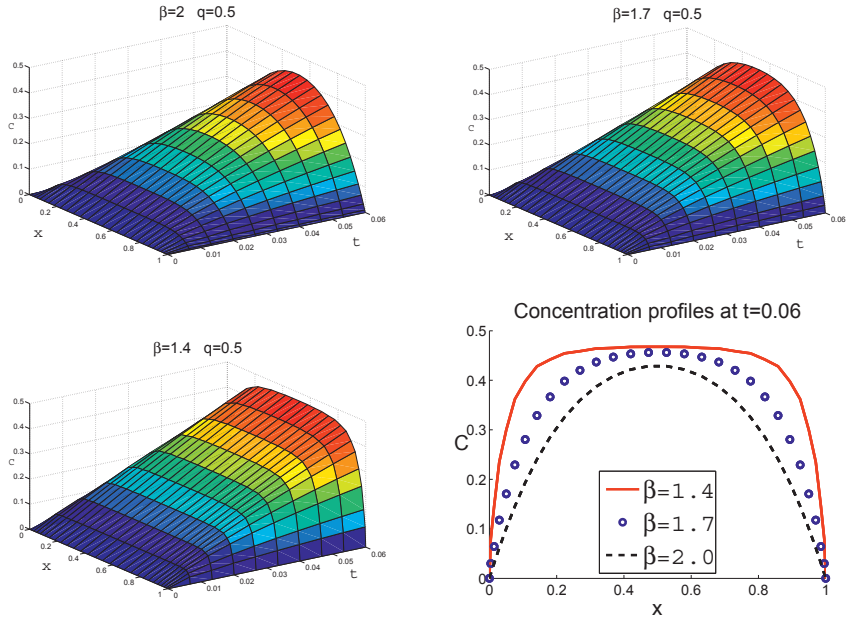

Figure 6.6: Obtained solutions for Eq. (6.10) with different derivative exponents β reproducing results in (Podlubny et al., 2009): spatial approximation of order 16

An important advantage of the LSSM as a solution method is its unconditional stability. This allows reducing considerably the number of nodes in the time discretization, depending on the smoothness of the solution. If the particular problem described in Eq. (6.10) is considered, its solution is linear in the variable t and can therefore be accurately resolved with just 2 nodes. This is a significant improvement over the 144 nodes used in (Podlubny et al., 2009). However, it is not possible to compare the performance of both methods in terms of accuracy and CPU time due to lack of information in the mentioned work.

The L^2 residual and condition number for this problem are plotted in Fig. 6.7 for approximation order up to 29 for both x and t coordinates. It can be seen in Fig. 6.7(a) that a refinement in the t coordinate does not improve the accuracy. This was the expected result since Eq. (6.10) is linear in that variable.

6.4.4 Time fractional diffusion equation (1D+Time)

The problem in Eq. (2.19) is solved in (Scherer et al., 2008) by a Grünwald-Letnikov approach and in (Podlubny et al., 2009) using finite differences with

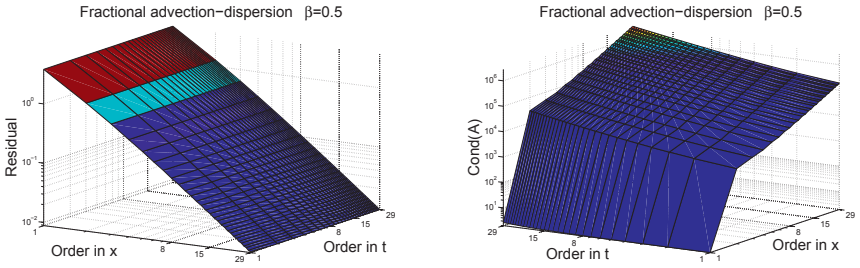

Figure 6.7: Plots corresponding to: (a) residual and (b) condition number of the problem matrix for different order approximations to Eq. (6.10)

fixed parameters $q = 1/2$ and $\mu(x) = 1$.

$$\begin{cases} \frac{1}{2}\left({}_0D_t^{\beta} C\left(x,t\right) + {}_t D_1^{\beta} C\left(x,t\right) \right) = \dfrac{\partial^2 C\left(x,t\right)}{\partial x^2}, \qquad in\ \ \Omega = [0,1]\times[0,1] \\ C(0,t) = 0 \\ C(1,t) = 0 \\ C(x,0) = 4x(1-x) \end{cases} \tag{6.11}$$

The same problem is solved here using LSSM. The results presented in Fig. 6.8 reproduce the calculations in (Podlubny et al., 2009) and (Scherer et al., 2008). Note however that the result presented in Fig. 6.8 was obtained using a polynomial of order 9 for the approximation in the time coordinate. The solution is therefore reconstructed using only 10 nodes, while results in the mentioned works required 150 and 6000 time steps respectively. Plots corresponding to L^2 residual and condition number are presented in Fig. 6.9 for approximation order up to 29 in both space and time. Again, it is not possible to compare the solution errors and CPU time of both methods due to lack of information.

A clarification should be made at this point regarding Figs. 6.6 and 6.8. As the calculated solution consists on the basis coefficients of a polynomial expansion, the numerical 'semi-analytical' solution is known over the complete domain and not only over the nodes used for the discretization. Therefore the meshes shown at these solution plots were chosen in order to improve the clarity of the figures, and are not related to the discretization.

6.4.5 Time fractional diffusion equation (2D+Time)

Snapshots of the solution of Eq. (6.1) using boundary and initial conditions from Eq. (6.2) are presented in Figs. 6.10 and 6.11 for fractional derivative exponents $\beta = 0.3$ and $\beta = 0.9$ respectively. A stronger superdiffusion is observed for the lower value of β. This is consistent with the expected evolution of the variance σ^2 in time ($\sigma^2 \propto t^{\beta}$) as explained in (Gorenflo et al., 2002).

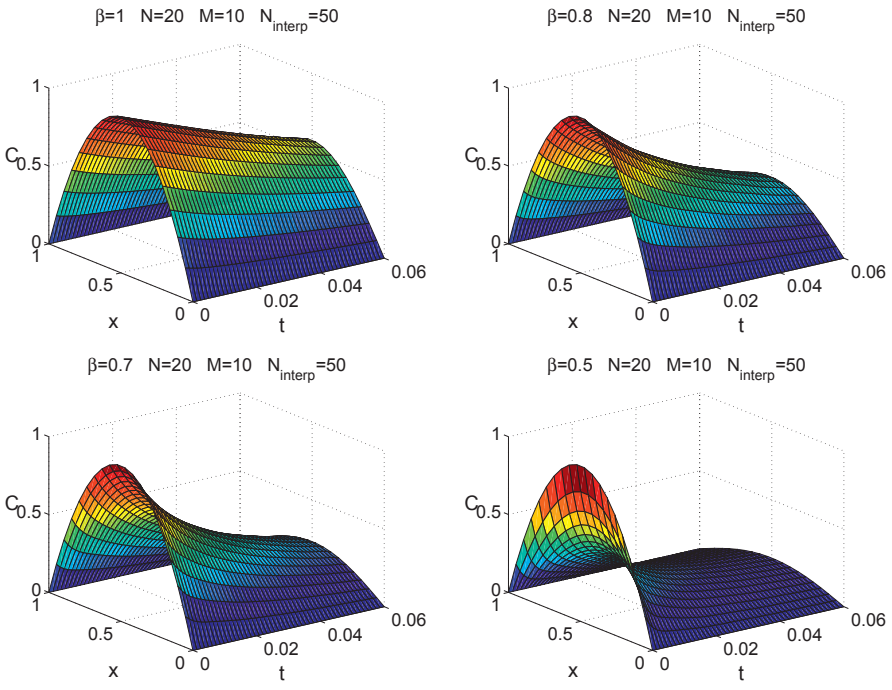

Figure 6.8: Solutions for Eq. (6.11) with different derivative exponents β, reproducing results in (Podlubny et al., 2009) and (Scherer et al., 2008) using $N = 20$ nodes and $M = 10$ nodes in spatial and temporal discretization

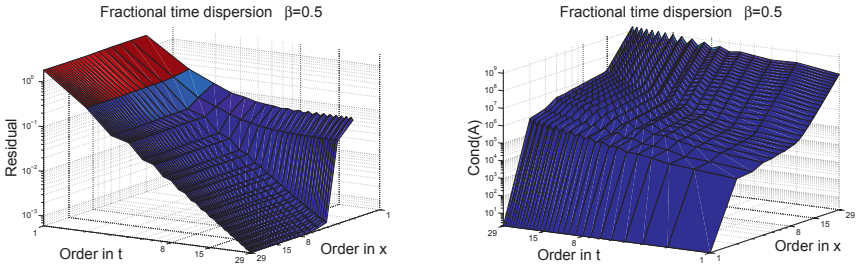

Figure 6.9: Plots corresponding to: (a) residual and (b) condition number of the problem matrix for different order approximations to Eq. (6.11)

As explained in Section 6.2.1, the analytical solution is formed as a product of decoupled space and time functions. The extremely high steepness of the time evolution for the case $\beta = 0.3$ (see Fig. 6.1) has important consequences on the

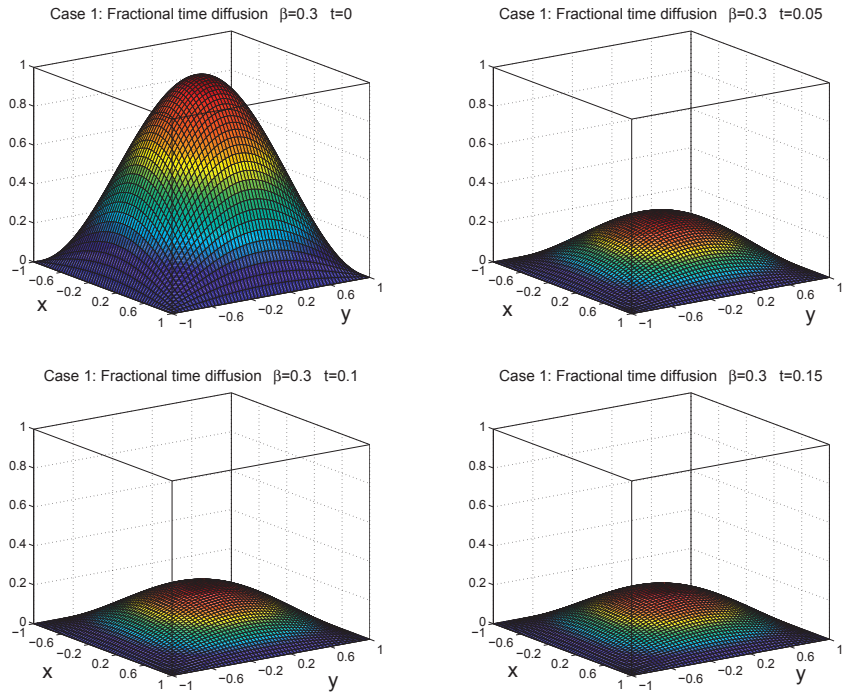

Figure 6.10: Numerical solution snapshots for Eq. (6.1) with $\beta = 0.3$ using BC and IC from Eq. (6.2). Decay is visibly faster than in Fig. 6.11.

quality of the numerical results obtained by the 3D+time LSSM scheme, as further elaborated in Section 6.4.7.

The results from Figs. 6.10 and 6.11 were calculated with a spectral discretization of order 16 in each direction. Note that the regular high resolution mesh used for the plots has been chosen for an optimal visualization and is not related to the problem discretization. This is possible as the numerical solution is a continuous polynomial in the coordinates x, y and t.

6.4.6 General fractional diffusion equation

Solutions to Eq. (6.5), the general fractional diffusion equation, are presented in Fig. 6.12. The simulation domain has been restricted to $[0, 1] \times [0, 0.06]$ and the space and time derivative exponents have been chosen respectively as $[\beta_1 = 0.7, \beta_3 = 1.4]$, $[\beta_1 = 0.7, \beta_3 = 1.7]$ and $[\beta_1 = 0.7, \beta_3 = 2.0]$ in order to reproduce the results obtained in (Podlubny et al., 2009) who used a finite difference approach.

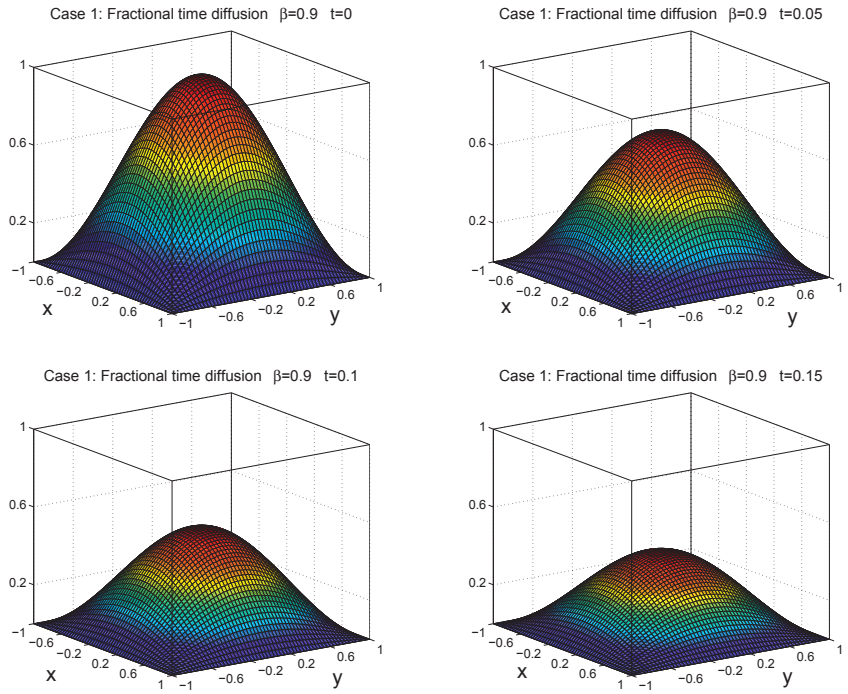

Figure 6.11: Numerical solution snapshots for Eq. (6.1) with $\beta = 0.9$ using BC and IC from Eq. (6.2). Decay is visibly slower than in Fig. 6.10.

An additional example with exponents $[\beta_1 = 0.7, \beta_3 = 2.2]$ is also included in order to show the consistency and generality of the scheme.

Numerical solutions for Eq. (6.7), the delayed form of the general fractional diffusion equation, are displayed in Fig. 6.13. The derivative exponents are chosen as $\beta_1 = 0.9$, $\beta_2 = 0.8$ and $\beta_3 = 1.9$ in all cases. The delay term δ is consecutively set to $\delta = 0.0025$, $\delta = 0.005$, $\delta = 0.01$ and $\delta = 0.015$ in order to compare the results with the ones presented in (Podlubny et al., 2009). An increase in the delay between the two advancing ridges proportional to δ is observed. The polynomial order in Fig. 6.13 has been set to 20 in order to accurately represent the non-smoothness in t.

It is important to note that the set of time values that the delay δ can take is limited if a finite difference approach is used. The delay parameter δ must coincide with exact multiples of the time step for any finite difference approach. The method presented in this thesis allows to account for *any real value of* δ without any restriction, which can be considered an advantage.

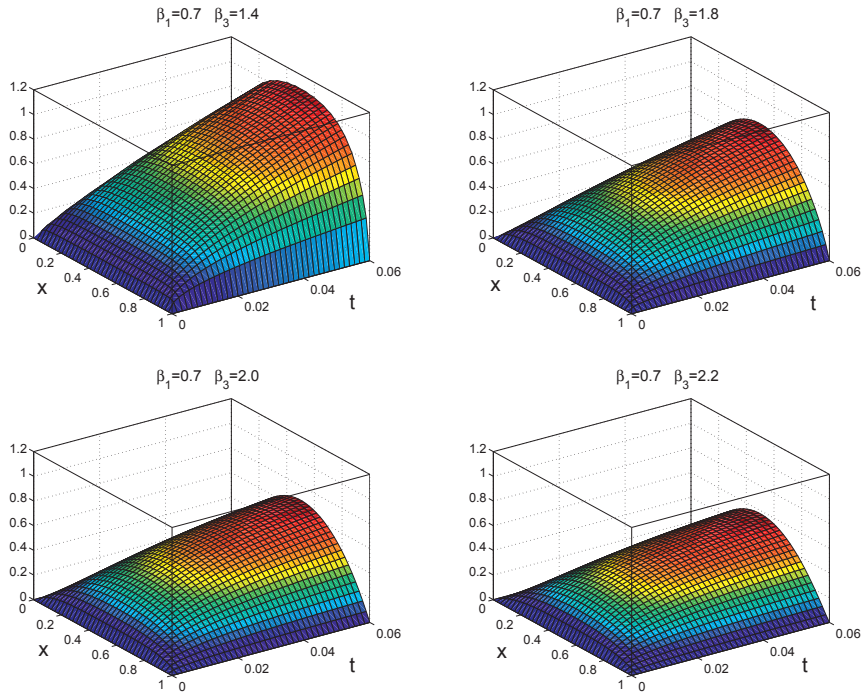

Figure 6.12: Numerical solutions to Eq. (6.5) for different choices of β_1 and β_3. The simulation domain has been chosen as to $[0,1] \times [0, 0.06]$ following (Podlubny et al., 2009).The space and time derivative exponents are indicated in the figure.

6.4.7 Convergence study of the numerical scheme

This section presents numerical convergence results used to test the applicability of the Least Squares Spectral Method for solving a time fractional differential equation. The system consisting in Eqs. (6.1) and (6.2) has been solved with growing approximation order in each coordinate ($O_x = O_y = O_t$) for three different values of the exponent β.

As already mentioned in Section 6.4.5, a polynomial may not be the best interpolant choice if functions as steep as Eq. (6.4) (see Fig. 6.1) need to be approximated. This function becomes steeper as the exponent β decreases, and this is evidenced in the tendency followed by convergence parameters as the approximation order increases. Figure 6.14 shows plots matching the approximation order with the following convergence parameters: (a) L_2 error norm, (b) L_∞ error norm, (c) residual, (d) condition number of the final linear system and (e) simulation time in seconds, as an estimator of computational cost.

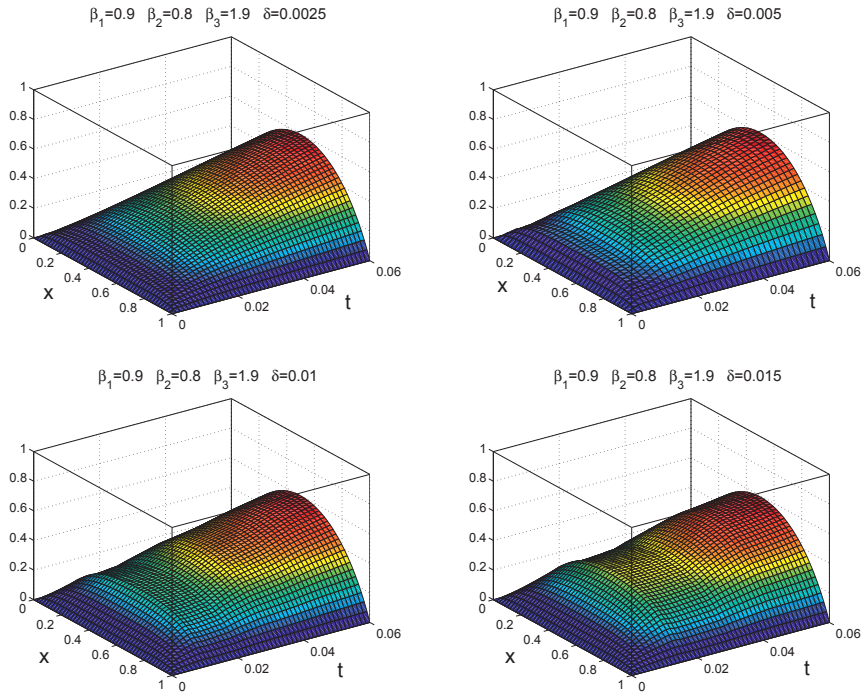

Figure 6.13: Numerical solutions to Eq. (6.7) for $\beta_1 = 0.9$, $\beta_2 = 0.8$ and $\beta_3 = 1.9$. The delay term δ is set to (a) $\delta = 0.0025$, (b) $\delta = 0.005$, (c) $\delta = 0.01$ and (d) $\delta = 0.015$ following (Podlubny et al., 2009).

The L_2 norm of the error decreases in all cases as the spectral order increases. It is evident though that the convergence improves as the derivative exponent β approaches unity. This is due to the reduction observed in the steepness of the solution. A similar situation is evidenced in the evolution of the L_∞ norm of the error, where a low value of β can hinder the convergence of the solution even up to the point of having a larger L_∞ error norm for higher approximation order. As β decreases, the solution becomes steeper and it is not possible to obtain an accurate representation without oscillations with a finite order continuous polynomial.

Another effect worth mentioning is that an increase in the approximation order results in an ill-conditioned linear system $A\mathbf{x} = b$ and higher computational costs (see Figs. 6.14(d) and 6.14(e)). This is not desirable as the condition number $\kappa(A)$ is a measure of the transfer of error from the matrix A and the vector b to the solution x. An accepted estimation is that at least $\log_{10}(\kappa(A))$ digits of precision are lost in solving the system $Ax = b$. The sensitiveness of the system to

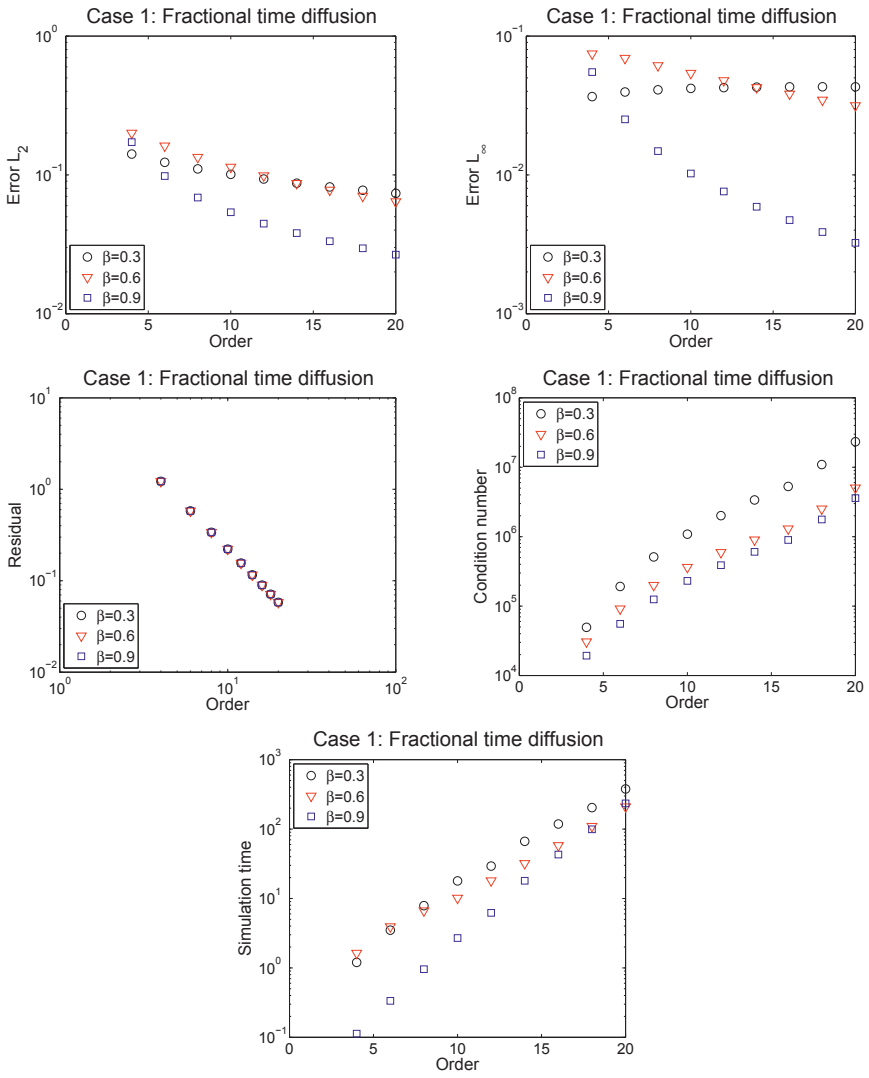

Figure 6.14: Convergence indicators for Eq. (6.1) with IC and BC from Eq. (6.2). Comparison of (a) error L_2, (b) error L_∞, (c) residual, (d) condition number and (e) simulation time in seconds for $\beta = 0.3$, $\beta = 0.6$ and $\beta = 0.9$.

perturbations A and b is reflected in A having a large condition number (Cheney and Kincaid, 2008, Chapter 8). In simple words, a high condition number $\kappa(A)$ translates into a penalty in the accuracy of the obtained results. Therefore, even

when a very high order approximation (Order $\to \infty$) would be able to reproduce any functional form, the resulting system would be so ill-conditioned that it would not be solvable in practice.

In order to increase the resolution of the numerical scheme and be able to deal with such steep solutions without incurring into an unmanageable condition number $\kappa(A)$, the extension of this method to elements is recommended. Work is currently being done at this front.

6.5 Chapter conclusions

This chapter introduced a multi-dimensional least-squares spectral technique for solving integro-differential and partial fractional differential equations. Five cases involving fractional differential operators were presented and analyzed.

The exponential convergence of the spectral fractional derivative operator was verified by comparison with analytical results. Numerical solutions were displayed and compared to either analytical solutions or results obtained by other numerical methods. A convergence study revealing strengths and weaknesses of the current implementation was exposed and discussed. In addition, references to other articles including theoretical considerations on spectral methods applied to fractional derivatives were provided.

It was concluded that the ability for accurately representing a solution with a reduced number of points makes LSSM a very suitable alternative for solving fractional differential problems given that solutions are sufficiently smooth. Work is currently being done on extending this implementation to a framework using multiple elements in each dimension.

Chapter 7

Coupling convection and diffusion

A good understanding of species transport in a fluid-particle system is a matter of importance in the design of packed bed chemical reactors. Diffusion plays an essential role in reaction dynamics, which in turn controls the conversion percentage and selectivity. This chapter presents simulations of a 2-Dimensional incompressible flow around a cylindrical particle coupled with two different anomalous diffusion models inside the particle: Cattaneo-Maxwell model and fractional time diffusion.

Section 7.1 introduces the concept and a multi-domain representation of a packed bed reactor. A physical model consisting in two domains with different constitutive laws is presented in Section 7.2. The numerical frameworks and sample results for the fluid and solid domains are presented in Sections 7.3 and 7.4 respectively. Section 7.5 summarizes the main findings of this chapter.

7.1 Introduction

Packed bed reactors are widely used in industry, ranging from petroleum and petrochemical applications (see Table 1.2) to environmental biotechnology (Doran, 2013; Dunn et al., 1983; Grace et al., 2005). Furthermore, most of commercial gas-phase catalytic processes are nowadays carried out in packed bed reactors.

Catalysts are often designed as porous support structures holding a dispersed active phase. As particles are made smaller in order to increase the solid-fluid interface area, the characteristic times become shorter. Therefore the transient diffusion period grows in importance and diffusion can no longer be regarded a steady-state process for calculation purposes. Under this conditions Fickian diffusion models, originally developed for addressing steady-state phenomena, become less appropriate as discussed in Chapter 2.

In catalytically enhanced chemical processes, the species concentration surrounding the catalyst determines the rate at which reactants can reach its active sites. This in turn limits the reaction rate, which is the main output of interest (Nagy, 2012, Chapter 4). One of the constraints currently limiting the optimization possibilities of these reactors is the inaccuracy in the predictions involving

diffusion into the catalysts.

Another important motive for attempting to achieve a better description of transport phenomena is the importance of predicting and controlling the temperature at the *hot spots*. These consist in regions of the chemical reactor where extremes temperatures are reached, particularly in exothermic processes. Temperatures higher than the allowable limits can unfavorably influence the equilibrium conversion, product selectivity or catalyst stability, resulting in extreme cases in unsafe operation (Jakobsen, 2008, Chapter 11).

This chapter presents a simple approach for studying the coupling of convective-diffusive flow of a component around a particle with anomalous transport models for that component inside the particle.

7.1.1 The problem scenario

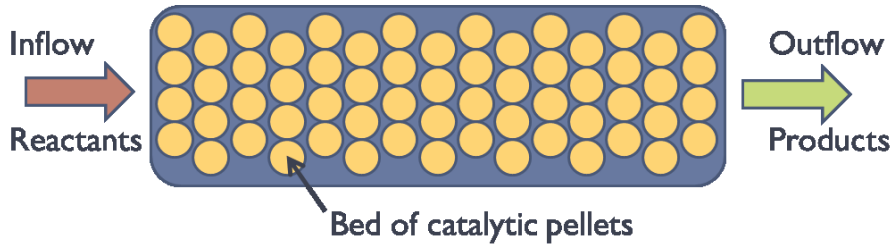

Figure 7.1: Simplified scheme of a packed bed reactor

A packed bed reactor consists in a stack of catalytic pellets through which the reactant is circulated, as illustrated in Fig. 7.1. Due to the complexity of the real system, a simpler case consisting in studying the flow around a single stationary particle is considered (see Fig. 7.2).

This is one of the simplest versions of the problem that still include two of the main implementing difficulties, namely

1. generation of deformed meshes,
2. coupling of non-overlapping domains with different constitutive laws.

7.2 The physical models

The problem in this chapter is the migration of one species into a particle immersed in a fluid flow. The simulation domain depicted in Fig. 7.2 is divided in two regions with different constitutive laws. The fluid in the region around the particle is modeled as an incompressible flow, while two different 'anomalous' models are tested for species diffusion.

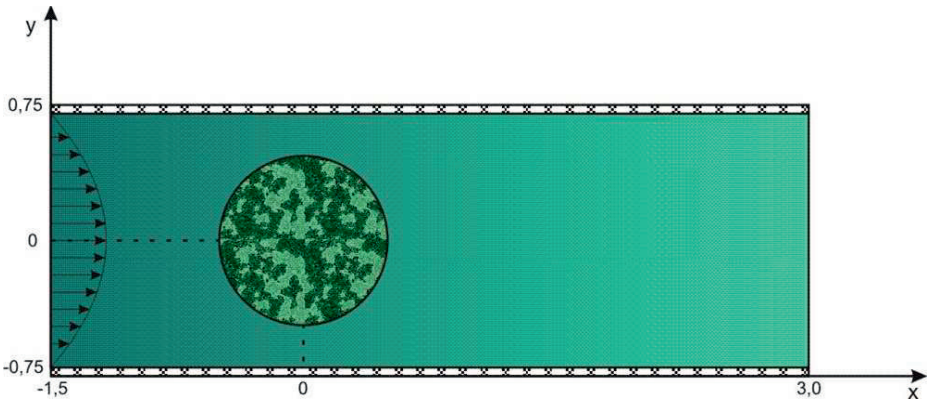

Figure 7.2: Sketch of the simulation domain: flow around a particle

7.2.1 The fluid model

The fluid flow around the particle is modeled by the incompressible Navier-Stokes equations without body forces in combination with the continuity equation

$$\rho\left(\frac{\partial \mathbf{v}}{\partial t} + \mathbf{v}\cdot\nabla\mathbf{v}\right) = -\nabla P + \mu\nabla^2\mathbf{v} \tag{7.1a}$$

$$\nabla\cdot\mathbf{v} = 0 \tag{7.1b}$$

where $\mathbf{v}$ represents the velocity vector, P the pressure field, ρ the density and μ the dynamic viscosity of the fluid. Equation (7.1a) enforces momentum conservation and Eq. (7.1b) enforces mass conservation.

The topology of the fluid domain is not equivalent to a single mapped element (i.e. the region is not simply connected). Therefore it becomes necessary to subdivide it into several simply connected elements, and the continuity of the interpolating basis across multiple elements becomes of importance. The Gauss-Lobatto-Legendre nodal basis used for reconstructing the solution yields C^0 continuity across elements. As described in (Jiang, 1998, Chapter 4), the global continuity requirement for a differential equation system whose residual is measured with the L_2 norm depends on its order. A first-order equation requires the interpolation to be continuous across the elements (C^0 continuity), while a second-order equation system like Eq. (7.1) requires also continuity in the derivatives between two elements (C^1 continuity). Briefly stated, the two simplest ways to satisfy the continuity requirements are either

1. transforming the second-order equation system into a first-order system, or

2. using base functions that yield C^1 continuity between adjacent elements.

These alternatives are compared and analyzed in (Sporleder et al., 2010). The first option is used here for tackling the current problem because of simplicity and generality, and also because of the usefulness of the new first-order variable (ω) defined in Eq. (7.2) in order to reduce the order of the system.

If the added variables were simply chosen to be the derivatives of the velocities in Eq. (7.1), the resulting system would consist of $(2\mathcal{D}+1)$ simultaneous first order equations and variables. A better strategy is using a vorticity formulation analog to the one presented in (Proot and Gerritsma, 2002), which reduces the problem to $(\mathcal{D}+2)$ equations, where $\mathcal{D}$) is the number of dimensions of the problem.

$$\nabla \cdot \mathbf{v} = 0 \tag{7.2a}$$

$$\frac{\partial \mathbf{v}}{\partial t} + \mathbf{v}\nabla\mathbf{v} + \nabla P + \frac{1}{Re}\nabla \times \omega = 0 \tag{7.2b}$$

$$\omega - \nabla \times \mathbf{v} = 0 \tag{7.2c}$$

where $\omega = \nabla \times \mathbf{v}$ represents the vorticity field and Re is the Reynolds number defined as $\rho u_m D/\mu$, with u_m the mean inlet velocity and D the particle diameter.

The species diffusion in the fluid is modeled by Eq. (7.3)

$$\frac{\partial C}{\partial t} + \nabla \cdot (\mathbf{v}C + \mathbf{J}) = 0 \tag{7.3a}$$

$$\mathbf{J} + k_f \nabla C = 0, \tag{7.3b}$$

where C represents the concentration field for the diffusing species, $\mathbf{J}$ the diffusive flux and k_f the diffusion coefficient. Equation (7.3a) enforces the mass conservation of the diffusing species, and Eq. (7.3b) is Fick's law for diffusion.

7.2.2 The solid diffusion models

Two models are tested for diffusion of species inside the (solid) particle domain: the Cattaneo-Maxwell model and the time fractional diffusion equation, presented in Chapters 5 and 6 respectively. A one-dimensional model assuming radial symmetry is used (variations in θ are not considered) since the fractional derivative operator is still in process of being implemented in a 2-dimensional deformed domain.

The radial Cattaneo-Maxwell model

The first of the tested models for diffusion inside the particle is the radial version of Cattaneo-Maxwell model. Here Eq. (7.4a) imposes the species conservation and Eq. (7.4b) is Cattaneo-Maxwell model for diffusion

$$\frac{\partial C}{\partial t} + \frac{1}{r}\frac{\partial}{\partial r}(r\mathbf{J}_r) = 0 \tag{7.4a}$$

$$\mathbf{J}_r + k_p \frac{\partial C}{\partial r} + \tau \frac{\partial \mathbf{J}_r}{\partial t} = 0. \tag{7.4b}$$

where r is the radial coordinate, $\mathbf{J}_r$ is the radial diffusive flux per unit area and k_p is the diffusive coefficient inside the particle. The parameter τ with time units is the *relaxation time*, already introduced in Section 5.2. The effect of the relaxation time in the diffusion model is to introduce a finite propagation velocity of the information v_D calculated as $v_D = \sqrt{k_p/\tau}$. This is only significant for the initial transient, since the term containing the relaxation time goes to zero for steady states (Gómez et al., 2010). Note that Eq. (7.4b) reduces to Fick's law for a cylindrical coordinate system with radial symmetry when $\tau = 0$.

The radial time fractional diffusion equation

The second tested model is the radial time-fractional diffusion equation, where radial symmetry in concentration is again assumed. The species transport inside the particle is modeled by Eq. (7.5).

$${}_0D_t^{\beta} C(r,t) = \frac{k_p}{r} \frac{\partial}{\partial r} \left(r \frac{\partial C(r,t)}{\partial r} \right) \tag{7.5}$$

where k_p is the diffusivity inside the particle and ${}_0D_t^{\beta} C$ is the time fractional derivative operator defined in Eq. (2.10) and β is the derivative exponent. Note that when β is equal to unity, Eq. (7.5) reduces to Fick's law for a cylindrical coordinate system with radial symmetry.

7.3 Numerical flow solution

In order to reduce the computational cost for the calculations at the first stage of testing, the solution to the incompressible flow system in Eq. (7.2) is found by using a mixed approach. Space discretization statement consists in searching the solution in a reduced spectral element subspace, and the time coordinate is approximated by a second order Crank-Nicolson finite difference scheme, as shown in (Jiang, 1998, Chapter 8).

The solution is calculated on successive time-space slab domains, with a time step defined as $\Delta t = t_{n-1} - t_n$. The initial condition for each space-time slab is the final solution for the previous slab and initial condition for the first slab is equal to the initial condition of the problem. The time step is chosen so that the largest CFL number ($|\mathbf{v}|\Delta t/h$) is close to unity. The system linearization is achieved by a Picard (fixed-point) iterative scheme, using the solution to the Stokes problem (nonlinear terms set to zero) as initial value. Iterations are stopped when the norm of the difference between two consecutive solutions is below a specified threshold.

Using the abstract formulation presented in Chapter 3, the problem can be expressed as

$$\mathcal{L}\mathbf{u} = \mathbf{g} \quad \text{in} \quad \Omega \tag{3.1a}$$
$$\mathcal{B}\mathbf{u} = \mathbf{g}_\Gamma \text{ on } \quad \Gamma \subseteq \partial\Omega \tag{3.1b}$$

with the operator $\mathcal{L}$, the source term $\mathbf{g}$ and the unknown vector $\mathbf{u}$ are defined as

$$\mathcal{L} = \begin{bmatrix} \dfrac{\partial \bullet}{\partial x} & \dfrac{\partial \bullet}{\partial y} & 0 & 0 \\ \bullet + \theta\Delta t \left[\mathbf{v}_x \dfrac{\partial \bullet}{\partial x} \mathbf{v}_y \dfrac{\partial \bullet}{\partial y} \right] & 0 & \Delta t \dfrac{\partial \bullet}{\partial x} & \dfrac{\theta\Delta t}{Re} \dfrac{\partial \bullet}{\partial y} \\ 0 & \bullet + \theta\Delta t \left[\mathbf{v}_x \dfrac{\partial \bullet}{\partial x} \mathbf{v}_y \dfrac{\partial \bullet}{\partial y} \right] & \Delta t \dfrac{\partial \bullet}{\partial y} & -\dfrac{\theta\Delta t}{Re} \dfrac{\partial \bullet}{\partial x} \\ \dfrac{\partial \bullet}{\partial y} & \dfrac{\partial \bullet}{\partial x} & 0 & \bullet \end{bmatrix} \tag{7.7a}$$

$$\mathbf{g} = \begin{bmatrix} 0 \\ \left(\bullet - (1-\theta)\,\Delta t \left(\mathbf{v}_x^{n-1} \dfrac{\partial}{\partial x} + \mathbf{v}_y^{n-1} \dfrac{\partial}{\partial y} \right) \right) \mathbf{v}_x^{n-1} + \dfrac{(1-\theta)\Delta t}{Re} \dfrac{\partial \omega^{n-1}}{\partial y} \\ \left(\bullet - (1-\theta)\,\Delta t \left(\mathbf{v}_x^{n-1} \dfrac{\partial}{\partial x} + \mathbf{v}_y^{n-1} \dfrac{\partial}{\partial y} \right) \right) \mathbf{v}_y^{n-1} + \dfrac{(1-\theta)\Delta t}{Re} \dfrac{\partial \omega^{n-1}}{\partial x} \\ 0 \end{bmatrix} \tag{7.7b}$$

$$\mathbf{u} = \begin{bmatrix} \mathbf{v}_x & \mathbf{v}_y & P & \omega \end{bmatrix}^T \tag{7.7c}$$

where $\theta = 0.5$ yields the Crank-Nicolson scheme. Implicit and explicit schemes are obtained for $\theta = 1$ and $\theta = 0$ respectively. Note that the finite difference scheme is implicit ($\theta = 1$) for P, in order to improve stability.

No-slip boundary conditions (i.e. $\mathbf{v} = 0$) are prescribed for the cylinder boundary. The prescribed velocity at the inlet as well as at the upper and lower borders of the domain is set to $(\mathbf{u}_x, \mathbf{u}_y) = (1, 0)$ for all cases. A point value is fixed for the pressure: $P(x_1, 0) = 0$.

Using an integral boundary condition for pressure is usually adviced when solving the Navier-Stokes system in order to stabilize the evolution of this variable (Isaev and Shapeev, 2010). However, calculating an integral over the problem domain prevents from using the highly efficient *Element by Element Conjugate Gradient* technique to solve the linear system that results from the discretization. As the accuracy in pressure estimation is not critical for this study, a point boundary condition is used in this work in order to reduce the computational effort.

Two example spatial meshes are depicted in Fig. 7.3, and the reproduction of a sample case (108 elements of order 4) is shown in Fig. 7.4. The problem domain

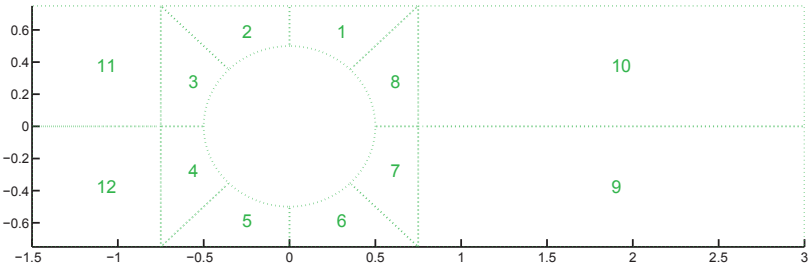

(a) Spatial discretization with 12 elements

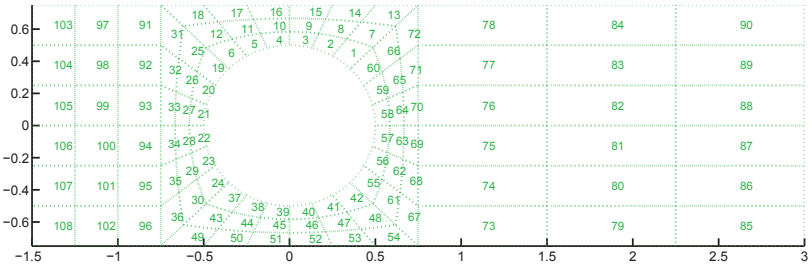

(b) Spatial discretization with 108 elements

Figure 7.3: Plot of the simulation domain for the fluid problem

is set to $(\Omega : -6 \leq x \leq 20, -6 \leq y \leq 6)$ and a circular cylinder with unit diameter is located at $(0, 0)$. The boundary conditions are specified as $\mathbf{v} = (\mathbf{v}_x, \mathbf{v}_y) = (0, 0)$ along the cylinder surface and $\mathbf{v} = (1, 0)$ on the top, bottom and inlet boundaries. A reference value for pressure ($P = 0$) is specified at the center of the right boundary. The initial condition corresponds to $\mathbf{v} = (1, 0)$ throughout the domain, as in (Jiang, 1998). Due to time constraints the simulation framework has still not been fully validated. This example is presented for illustrative purposes only.

The verification of the numerical solution is performed by running a convergence test where both the residual and the mass conservation are examined. Mass conservation for this incompressible problem is verified by calculating the divergence of the velocity field. Note that for this case the residual provides only a measure of the error in the spatial discretization. An excessively large time step would hinder the numerical accuracy without increasing the value of the residual.

Convergence plots showing the evolution of the residual and the divergence of the velocity field for $Re = 1$ are presented in Fig. 7.5. The velocity field corresponding to the verification case is displayed in Fig. 7.6, where the arrows represent the velocity vectors and the the colors correspond to the magnitude of the velocity in the x direction.

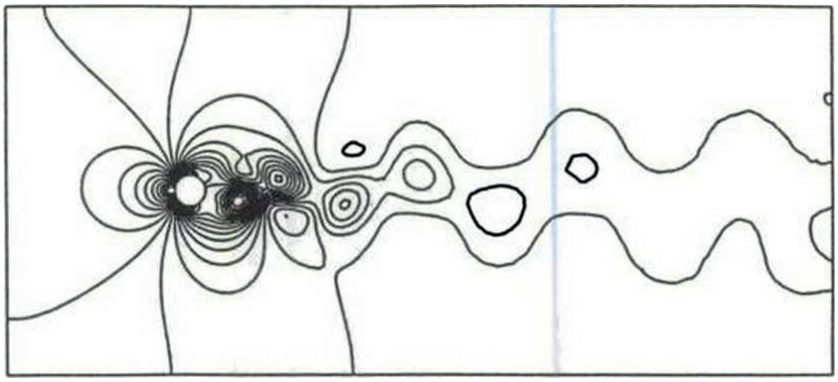

(a) Pressure contours

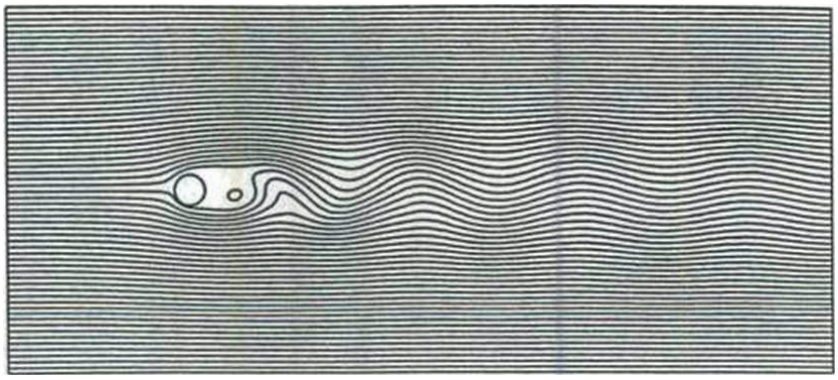

(b) Streamlines

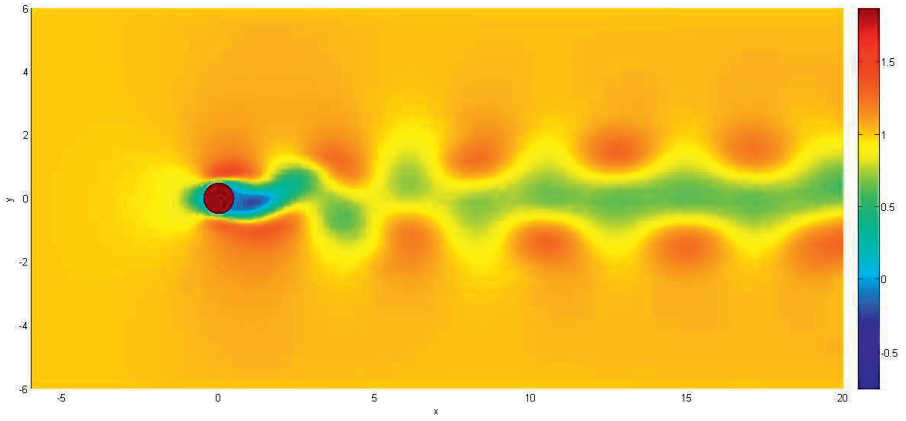

(c) Velocity component in the x direction

Figure 7.4: Vortex shedding by a circular cylinder at $Re = 200$ at $t = 150$: (a) Pressure contours and (b) Streamlines from (Jiang, 1998, p.174), (c) Velocity $\mathbf{v}_x$

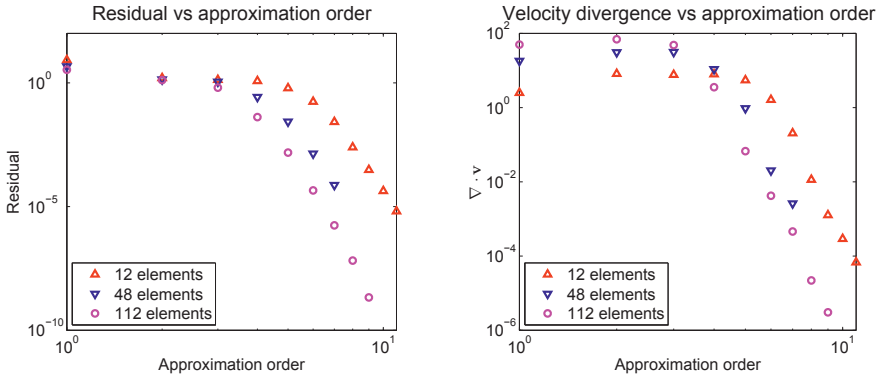

(a) 12 elements (b) 108 elements

Figure 7.5: Fluid problem convergence: (a) residual and (b) mass conservation

7.3.1 Species convection and diffusion

Using the calculated velocity field $\mathbf{v}$ as an input, the operators $\mathcal{L}$ and $\mathbf{g}$ and the unknown vector $\mathbf{u}$ for Eq. (7.3) can be written as

$$\mathcal{L} = \begin{bmatrix} \dfrac{\partial \bullet}{\partial t} & \dfrac{\partial \bullet}{\partial x} & \dfrac{\partial \bullet}{\partial y} \\ -\mathbf{v}_x \bullet + k_f \dfrac{\partial \bullet}{\partial x} & \bullet & 0 \\ -\mathbf{v}_y \bullet + k_f \dfrac{\partial \bullet}{\partial y} & 0 & \bullet \end{bmatrix} \tag{7.8a}$$

$$\mathbf{g} = \begin{bmatrix} 0 & 0 & 0 \end{bmatrix}^T \tag{7.8b}$$

$$\mathbf{u} = \begin{bmatrix} C & \mathbf{J}_x & \mathbf{J}_y \end{bmatrix}^T \tag{7.8c}$$

Note that, even when the output of interest is the concentration C, the definition of two auxiliary flux variables $\mathbf{J}_x$ and $\mathbf{J}_y$ is necessary for transforming Eq. (7.3) into a first order system, as discussed above.

The concentration for a sample case at different time instants is depicted in Fig. 7.7. The initial condition corresponds to $C = \text{erfc}(10(x - x_0))$, where $\text{erfc}(x)$ is the complimentary error function defined as

$$\text{erfc}(x) = 1 - \frac{2}{\sqrt{\pi}} \int_0^x e^{-x^2} dx.$$

The boundary conditions are

$$\begin{cases} C = 1 & \text{on } x = x_0 \\ \dfrac{\partial C}{\partial n} = 0 & \text{on } [x = x_1, y = y_0, y = y_1, \sqrt{x^2 + y^2} = 1] \end{cases}$$

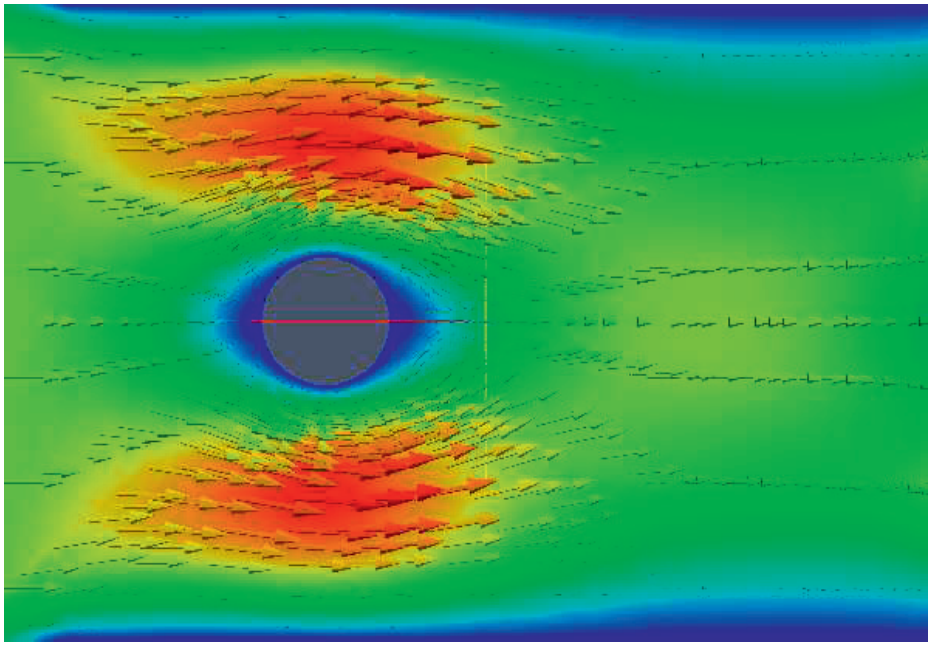

Figure 7.6: Velocity field around a circular cylinder at $Re = 1$

where the last condition assumes that the particle is not permeable to either the fluid or the diffusing species. The diffusion coefficient is set to $k_f = 10^{-2}$. The evolution of the average concentration around the particle during the first transient is shown in Fig. 7.8. The same discretization is used in Figs. 7.4, 7.6 and 7.8.

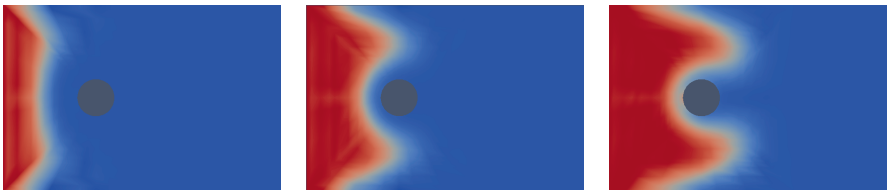

(a) $t = 1$s (b) $t = 2$s (c) $t = 3$s

Figure 7.7: Species concentration field for fluid region at different times

7.4 Diffusion in the particle

As a first attempt to coupling (convective and diffusive) species transport in the fluid flow with anomalous diffusion inside the particle, two different diffusion con-

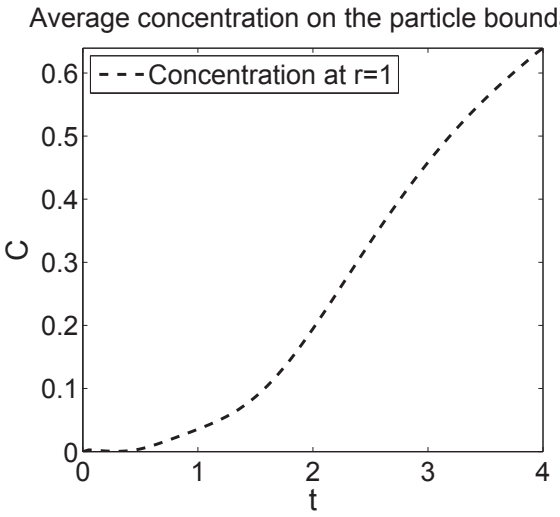

Figure 7.8: Time evolution of the average concentration on the particle boundary

stitutive laws are tested in a simplified geometry assuming radial symmetry.

The average concentration of species at the external boundary (Fig. 7.8), retrieved from the system made up by Eqs. (7.7) and (7.8), is used as a boundary condition for the test cases. The objective is to obtain a qualitative comparison between the models. Both radial models presented in Section 7.2.1 are solved in a single non-deformed spectral domain.

The operators $\mathcal{L}$ and $\mathbf{g}$ and the unknown vector $\mathbf{u}$ for Eq. (7.4) are

$$\mathcal{L} = \begin{bmatrix} \dfrac{\partial \bullet}{\partial t} & \dfrac{1}{r}\dfrac{\partial (r\bullet)}{\partial r} \\ k_p \dfrac{\partial \bullet}{\partial r} & \bullet + \tau \dfrac{\partial \bullet}{\partial t} \end{bmatrix} \tag{7.9a}$$

$$\mathbf{g} = \begin{bmatrix} 0 & 0 \end{bmatrix}^T \tag{7.9b}$$

$$\mathbf{u} = \begin{bmatrix} C & \mathbf{J}_r \end{bmatrix}^T \tag{7.9c}$$

and for Eq. (7.5) they turn into

$$\mathcal{L} = {}_0D_t^{\beta} \bullet - \frac{k_p}{r}\left(\frac{\partial \bullet}{\partial r} + r \frac{\partial^2 \bullet}{\partial r^2} \right) \tag{7.10a}$$

$$\mathbf{g} = 0 \tag{7.10b}$$

$$\mathbf{u} = C \tag{7.10c}$$

The results for the radial Cattaneo-Maxwell model in Eq. (7.4) and the radial time-fractional diffusion equation in Eq. (7.5) are presented in Figs. 7.9 to 7.12 for different values of the characteristic parameters τ and β. The initial condition for both models is $C(r,0) = 0$ throughout the particle. The case corresponding to Fick's law $\tau = 0$ and $\beta = 1$ is presented as a comparative reference at the top of each figure.

Figures 7.9 and 7.10 show a comparison between both models for a short initial transient ($0 \leq t \leq 2s$). In this scenario a variation of the derivative exponent β does not yield major differences in the observed concentration profiles. However, changes in the relaxation time τ affect the shape of the profiles and even *uphill diffusion* (against the concentration gradient) is observed, as exposed in Chapter 5. Note that the horizontal axis r has been inverted in the right half of Figs. 7.9 to 7.12 and the concentration flux goes from left ($r = 1$) to right ($r = 0$).

Figures 7.11 and 7.12 display a longer term evolution ($0 \leq t \leq 4s$) of the same cases. It can be seen here that the final profiles after the concentration information has propagated along the domain ($\sqrt{k_p/\tau} \gg r/t$) are practically independent of the relaxation time τ. On the other hand, the derivative exponent β affects the shape of the stationary concentration profiles, in accordance with the information presented in Chapter 6.

7.4.1 Anomalous diffusion in coupled phenomena

The presented alternative models converge to Fick's law when the extended model parameters τ and β approach the values $\tau \to 0$ and $\beta \to 1$ respectively. The profiles may be significantly different from Fick's law depending on the time scale of interest and the modeling parameters (τ) or the characteristic duration of the time transients of the problem (t_c).

For time scales close to the relaxation time ($t \approx \tau$), the Cattaneo-Maxwell model predicts concentration profiles that depart considerably from Fick's law. For longer time scales, Fick's law provides an excellent approximation to this model. Complementary, the fractional derivative model yields results that are significantly different for times longer than the characteristic transient time of the problem ($t \gg t_c$), while Fick's law is approached for shorter times.

These results are to be considered when coupling convection-diffusion phenomena (e.g. in chemical reactors). Whether significant deviations from Fick's law are to be expected or not depends on the model parameters and on the time scales involved in the problem. If no important deviations from Fick's law are expected, the extra numerical cost of considering either $\tau > 0$ or $\beta < 1$ is not justified and using Fick's law is the most computationally efficient alternative.

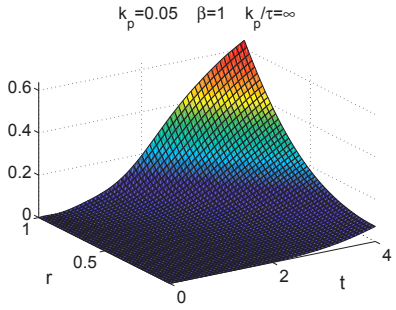

(a) Time-space solution, $\sqrt{k_p/\tau} = \sqrt{\infty}$

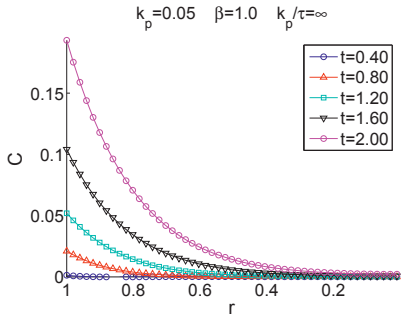

(b) Solution snapshots, $\sqrt{k_p/\tau} = \sqrt{\infty}$

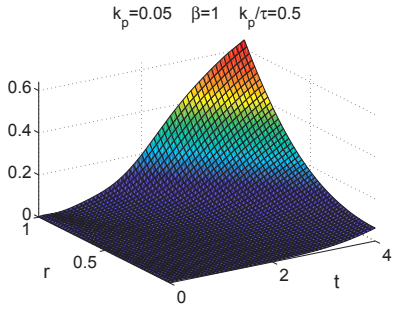

(c) Time-space solution, $\sqrt{k_p/\tau} = \sqrt{5}$

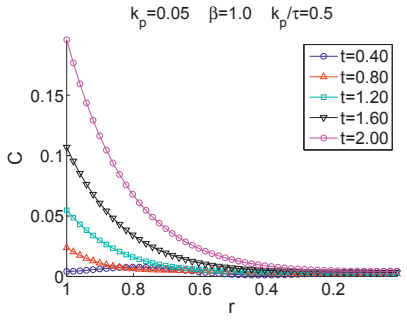

(d) Solution snapshots, $\sqrt{k_p/\tau} = \sqrt{5}$

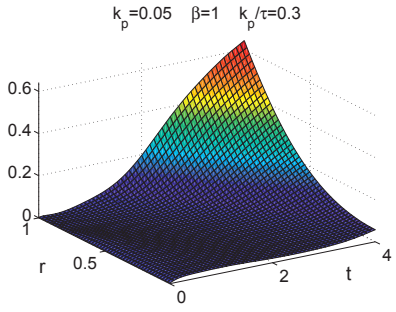

(e) Time-space solution, $\sqrt{k_p/\tau} = \sqrt{2}$

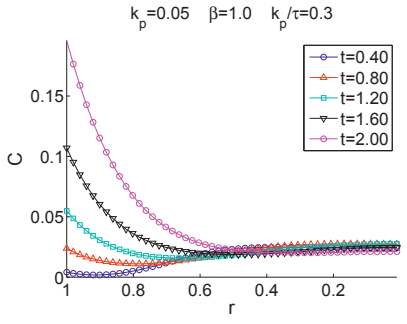

(f) Solution snapshots, $\sqrt{k_p/\tau} = \sqrt{2}$

Figure 7.9: Species concentration at short times (Cattaneo-Maxwell model)

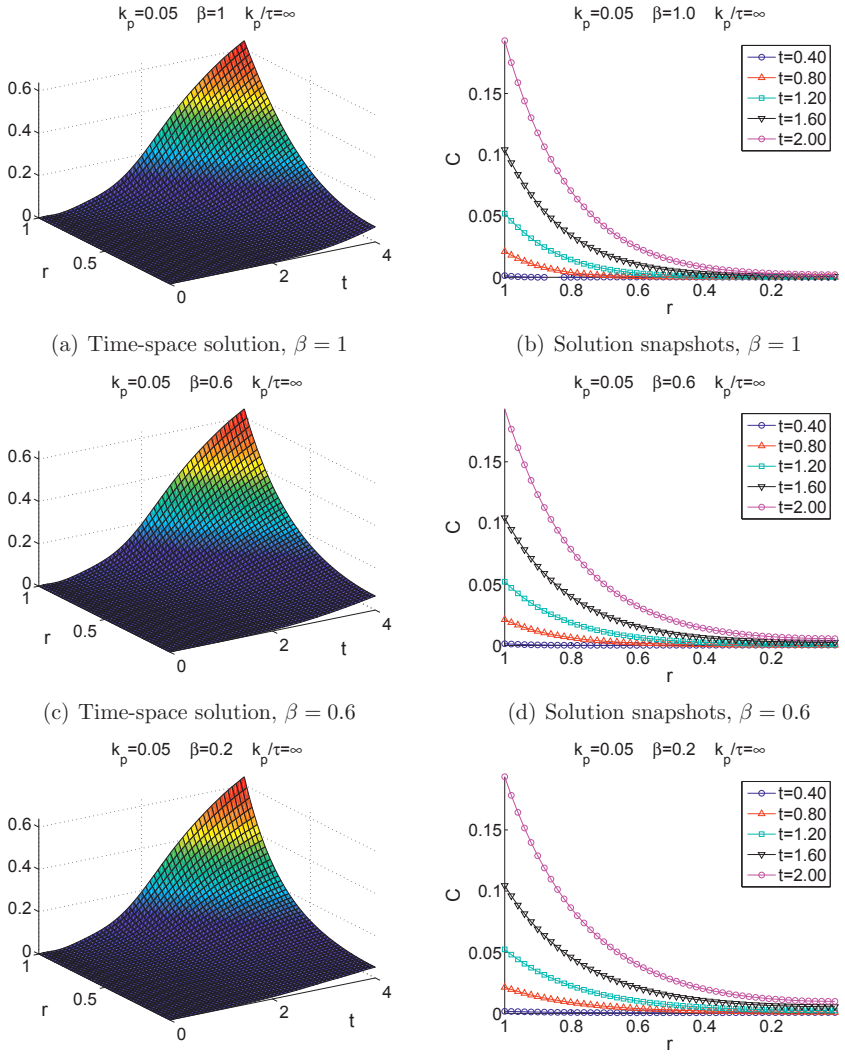

(a) Time-space solution, $\beta = 1$

(b) Solution snapshots, $\beta = 1$

(c) Time-space solution, $\beta = 0.6$

(d) Solution snapshots, $\beta = 0.6$

(e) Time-space solution, $\beta = 0.2$

(f) Solution snapshots, $\beta = 0.2$

Figure 7.10: Species concentration at short times (Fractional diffusion model)

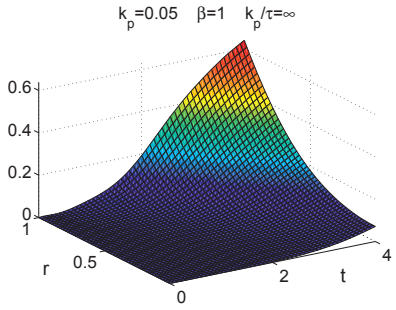

(a) Time-space solution, $\sqrt{k_p/\tau} = \sqrt{\infty}$

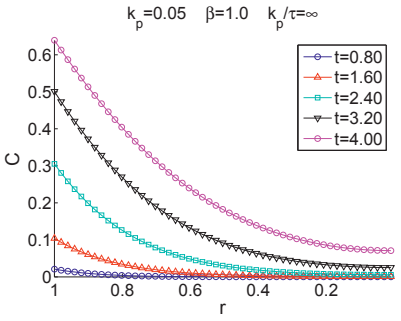

(b) Solution snapshots, $\sqrt{k_p/\tau} = \sqrt{\infty}$

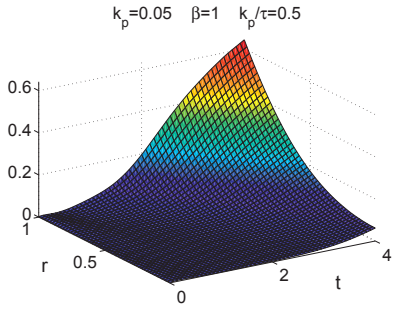

(c) Time-space solution, $\sqrt{k_p/\tau} = \sqrt{5}$

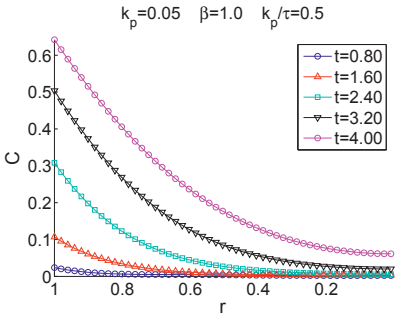

(d) Solution snapshots, $\sqrt{k_p/\tau} = \sqrt{5}$

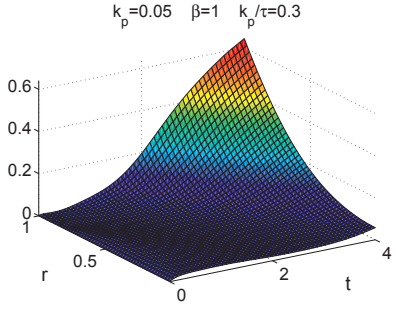

(e) Time-space solution, $\sqrt{k_p/\tau} = \sqrt{2}$

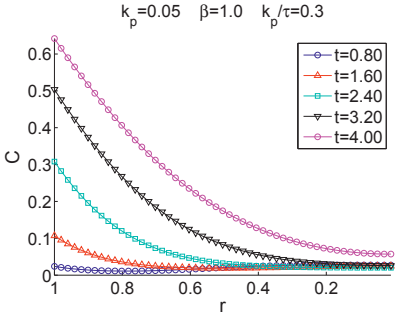

(f) Solution snapshots, $\sqrt{k_p/\tau} = \sqrt{2}$

Figure 7.11: Species concentration at long times (Cattaneo-Maxwell model)

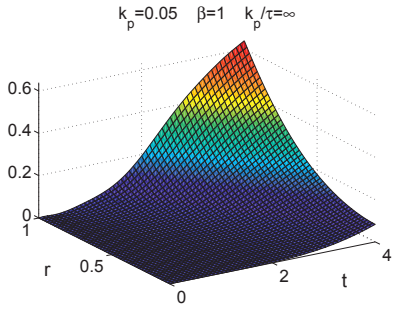

(a) Time-space solution, $\beta = 1$

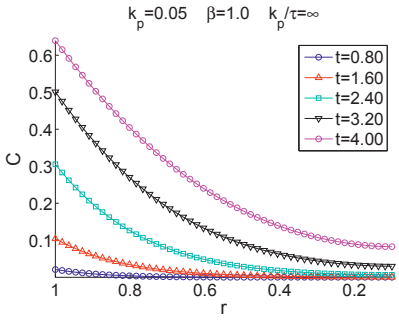

(b) Solution snapshots, $\beta = 1$

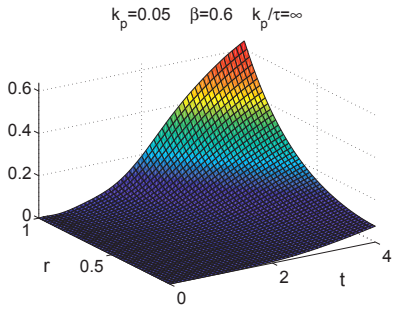

(c) Time-space solution, $\beta = 0.6$

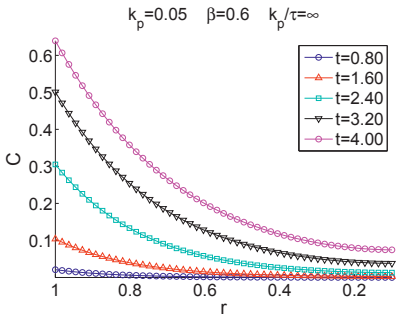

(d) Solution snapshots, $\beta = 0.6$

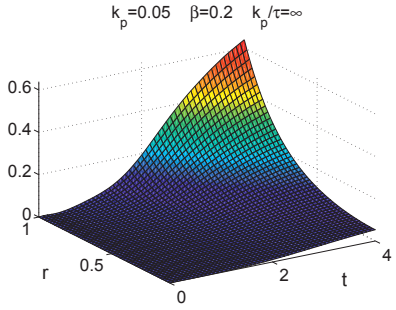

(e) Time-space solution, $\beta = 0.2$

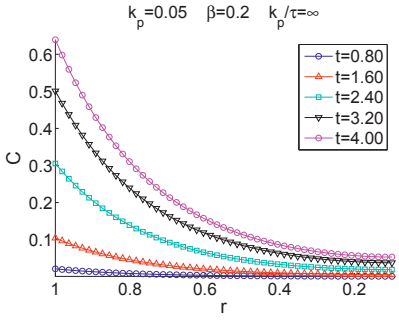

(f) Solution snapshots, $\beta = 0.2$

Figure 7.12: Species concentration at long times (Fractional diffusion model)

7.5 Chapter conclusions

This chapter presented a simulation framework for coupling convective flow around a particle with two different anomalous diffusion models inside the particle. The models were solved in two separate domains, and a one-way coupling was accomplished by neglecting the concentration changes in the fluid due to diffusion into the particle.

The implementation of convective flow was achieved by using the vorticity formulation of Navier Stokes equation in combination with Fick's law for diffusion in the fluid region. As a first approximation for obtaining qualitative results, the anomalous diffusion models were applied to a 1-dimensional geometry where radial symmetry was assumed. The concentration profiles inside the particle may yield very different results depending on which diffusion model is used.

Whether significant deviations from Fick's law are to be expected or not depends on the problem time scales and model parameters. This has implications for modeling coupling convection-diffusion phenomena (e.g. chemical reactors). If the problem is out of the range where important deviations from Fick's law are expected, the extra numerical cost of considering anomalous diffusion models is not justified and Fick's law is preferred.

Part IV

Final remarks

Chapter 8

Conclusions

The main purpose of this project has been developing tools for simulating anomalous diffusion phenomena related to solid particles inside a chemical reactor. This will in time allow for evaluating the convenience and applicability of different models and generating guidelines for their use. The long-term goal is improving the optimization possibilities for catalytic reactions applied to gas processes. This work succeeded in proposing anomalous transport models which were implemented and tested in order to extend the current modeling capabilities.

Various practical aspects regarding the use of least squares spectral element methods in the simulations were addressed along the thesis. Since the discussed concepts and obtained results are listed at the end of each chapter, the remarks presented here are just an overview featuring the most important conclusions.

Section 8.1 presents a short and concise reassessment of the original objectives. Section 8.2 contains a summary of the major contributions of this thesis, and Section 8.3 concludes with recommendations for further extending the scope of the current work.

8.1 Revisiting the objectives

In order to assess the outcome of the project, a review of the main objectives as postulated in Chapter 1 is presented next:

1. ***Developing an appropriate numerical technique for solving fractional differential equations.***
   Fractional differential models offer multiple possibilities for generalizing the scope covered by Fick's law in a consistent manner. However, their numerical implementation is challenging. The main concerns in this regard are their high computational requirements and mathematical complexity.

   A least squares spectral formulation was implemented for solving fractional differential equations. The proposed method was proven particularly well-suited for dealing with the numerical difficulties inherent to fractional dif-

ferential operators. The practical implementation details were explained thoroughly in order to enhance reproducibility, and guidelines were given for extending it to multiple dimensions and arbitrarily shaped domains.

2. ***Implementing models for anomalous diffusion in a particle.***
   Tools capable of reproducing and comparing different anomalous mass transport models are to be implemented. Three dimensional simulations may be required, but a two dimensional analysis is expected to suffice in accounting for the complete physics of the problem in many cases.

   A numerical framework for studying anomalous diffusion models in pellets was developed and validated by testing it against model problems. This simulation tool is capable of solving arbitrary integro-differential equations and can be effortlessly adapted to various problems in any number of dimensions.

3. ***Coupling solid diffusion and fluid flow.***
   The diffusion of species inside the particle is strongly coupled with the boundary conditions generated by the fluid flow around it. Therefore, modeling the flow is necessary in order to obtain accurate boundary conditions. A further step is coupling solid and fluid transport and studying their combined effect.

   Simulations of the flow around a particle were achieved by extending the functionality of the developed framework. A concept test case was analyzed coupling the boundary condition yielded by the fluid flow with the two main anomalous diffusion models studied in this work.

4. ***Identifying criteria for choosing a proper diffusion model.***
   A benchmark should be formulated that helps determining whether anomalous effects should be considered given a particular case. As anomalous transport models are computationally expensive, their use is advantageous only when a significant difference in the obtained predictions is expected.

   Qualitative guidelines based on the problem parameters and time-scales have been proposed which can be used to decide whether Cattaneo-Maxwell or fractional diffusion models will be satisfactorily approximated by Fick's law. If no deviations of practical significance are expected, the simpler Fick's model is preferred.

8.2 Contributions in this work

As a starting point for this thesis, a review of the most important evidence refuting the generality of Fick's law was carried out. The next step was trying to find an underlying structure among the numerous existing alternative diffusion models, all grouped under the common denomination *anomalous transport*.

Following guidelines from previous work, several anomalous transport models were categorized in a scale ranging from *simplicity* to *thoroughness* according to the

level of detail they accounted for. Of course, not all the models were simultaneously viable since it was necessary to achieve coherence between the different scales. This contributed to shorten the list of possibilities.

Of particular interest for this work were two macro-scale deterministic models: the *Cattaneo-Maxwell model*, also known as 'hyperbolic diffusion', and the *Fractional Diffusion model*. Both of them are consistent with their stochastic counterpart: the family of *Continuous Time Random Walk* (CTRW) models. This relation between a deterministic and a stochastic formulation is an extension of the analogy between Fick's law and the Random Walk model, which represents a particular case of these models.

The aforementioned context sets the stage for reviewing the most important contributions in this work. This section will present an overview of the main findings in the present study, and their application scope will be shortly discussed afterwards.

8.2.1 Contribution to knowledge

Fractional derivatives are non-local operators that allow generalizing the ordinary integrals and derivatives to intermediate orders. Applied to diffusion, this implies a capability to describe a wider scope of anomalous diffusive behaviors. The three main concerns regarding implementation of fractional differential operators were identified as *high storage requirements*, the inherent *singularity in their mathematical definition* and the consequent *difficulties in the extension to multiple dimensions and irregular shapes*.

The proposed least squares spectral formulation reduces the storage requirement by demanding a reduced number of nodes in order to yield a similar representation. The singular integral contained in the fractional derivative operator is elegantly evaluated by using Gauss-Jacobi quadratures. In addition, the implementation can be easily extended to arbitrarily shaped domains and multiple dimensions.

In order to simplify its practical application, the steps for implementing fractional derivative operators in a spectral framework were explained in detail. A procedure for mapping the operator into non-linear domains was described and example problems in multiple dimensions were presented and compared with results available in literature.

Numerical simulations in this work were based on least squares spectral element methods (LSSEM). Regardless of being considerably more complex than finite difference methods, LSSEMs provide advantages like generality, geometrical flexibility, numerical stability, a-posteriori error estimation and lower storage requirements. This last feature is crucial for fractional differential operators.

In order to facilitate the development process, the implementation of the numerical framework was carried out in two programming languages. On one hand

the meshing algorithm, involving higher complexity and short computing times, was coded in MATLAB®, a higher level language. On the other hand the solving algorithm was coded in C++, a more efficient lower level language. This coupling technique takes advantage of both ease of programming and computing efficiency, at the very low cost of requiring an interface to communicate both modules.

A numerical framework for studying anomalous diffusion models in pellets was developed and validated by testing it against example problems. The first test consisted in a comparison between Fick's law and its simplest hyperbolic generalization: Cattaneo-Maxwell's law. The physically relevant differences between both models were quantified in terms of the propagation velocity.

As a numerical experiment, a random walk simulation tool was developed and validated by comparing its results with the ones yielded by Fick's law. The simulations were later generalized to a Continuous Time Random Walk, allowing for greater flexibility. Coherence was verified between the latter and time fractional diffusion for an appropriate choice of parameters. This consistency contributed to clarify the physical interpretation of time fractional diffusion.

A simple problem was proposed for investigating the effect of coupling the fluid flow around a particle with two different anomalous diffusion models inside the particle: Cattaneo-Maxwell model and fractional time diffusion. The problems were solved in two separate domains, and a one-way coupling was accomplished by neglecting the concentration changes in the fluid due to diffusion into the particle. It was concluded that whether significant deviations from Fick's law are to be expected or not depends on the problem time scales and the model parameters. If the problem is out of the range where important deviations from Ficks law are expected, the additional complexity and numerical cost of considering anomalous diffusion models are not justified and Ficks law is preferred.

8.2.2 Application scope

As described in the introductory part, a better knowledge of the anomalous diffusion phenomena facilitated by the tools developed in this work will result in extended optimization possibilities for a wide variety of Oil & Gas related processes. The most relevant are summarized as:

1. **Catalytically enhanced processes.** Modern catalysts are usually designed as finely dispersed salts over an inert substrate acting as a mechanical support. Surface anomalous diffusion takes place when preferential interactions occur between some molecules and the catalyst surface.

    - Since efficiency and conversion rate depend on diffusion, a better knowledge of the dynamics of species transport will result in new guidelines for the design of catalytic particles.

2. **Transport of entrained particles.** Moving up to a larger scale, particles carried in a turbulent flow get periodically trapped in vortices that reduce the effective particle transport rate. This phenomenon is of special importance in fluidized bed reactors and can be studied using the models employed to describe anomalous diffusion.

    - An improved description of the migration of particles in the system will be translated into design and optimization criteria for fluidized bed reactors.

3. **Oil displacement in a reservoir.** The pressurizing water injected in an oil reservoir needs to diffuse into the oil-bearing substrate in order to displace the oil and allow its extraction. This process is tightly related to anomalous diffusion of water in porous rocks.

    - During the extraction procedure, a significant fraction of the oil is 'by-passed' and left in the less permeable substrate. A more suitable characterization of diffusion phenomena will allow to increase the final amount of extracted oil.

Many other applications for anomalous diffusion models have been included in Table 2.1, which provided a glimpse of the extension of this discipline. However, a full review has not been attempted due to the extraordinary vastness of the field.

8.3 Future work

Regarding the coupling between fluid transport and fluid in solid, only a concept proof was presented for a one-way coupling. Additional work should be directed to implementing a bidirectional coupling between the solid and fluid, accounting for the effect caused by the particle on its environment. This extension would result in larger computational costs occasioned by the need for solving larger systems, but its complexity is not substantially higher.

Additionally, two main directions for a further extension of the numerical framework are suggested.

- On one hand the present formulation could be extended from binary compositions to multicomponent mixtures. This would require the different mass transfer mechanism for each individual component to be considered.

- The effect of chemical reactions should be included in the dynamics of diffusion since the chemical reactive and diffusive processes are expected to be strongly interdependent, particularly in the field of gas processing.

Furthermore, a supplementary extension for including several particles, eventually subjected to relative movement, is to be considered. This would contribute

to determining the importance of the interference between particles, which is intimately related to the validation of the single-particle model as a representative sample of a complete reactor.

Regarding the modeling activity, an effort is constantly made to improve the accuracy in the description of diffusion in order to obtain more exact predictions for real systems. Since there is a lack of agreement between different diffusion theories, the most convenient validation method at this point seems to be comparing different simulations and experimental data. Simultaneously, the development of new measuring techniques is extending the availability of experimental results that in their turn promote the formulation and evaluation of new diffusion models.

References

[1] Abrell, J. (2010). Regulating CO2 emissions of transportation in Europe: A CGE-analysis using market-based instruments. *Transportation Research Part D: Transport and Environment 15*(4), 235 – 239. Cited on page 9.

[2] Álvarez-Ramírez, J., F. J. Valdés-Parada, and J. A. Ochoa-Tapia (2008). A Lattice-Boltzmann scheme for Cattaneo's diffusion equation. *Physica A: Statistical Mechanics and its Applications 387*(7), 1475 – 1484. Cited on page 68.

[3] Appl, M. (2000). *Ammonia*, pp. 155p. Wiley-VCH Verlag GmbH & Co. KGaA. Cited on page 11.

[4] Auriault, J., J. Lewandowska, and P. Royer (2007). About non-fickian hyperbolic diffusion. In *Congrès Français de Mécanique, 18ème, Grenoble, August 27-31, 2007*, pp. 6p. Cited on pages 21, 69.

[5] Bagley, R. L. and P. J. Torvik (1983). A theoretical basis for the application of fractional calculus to viscoelasticity. *Journal of Rheology 27*(3), 201–210. Cited on page 78.

[6] Baird, B. R., H. B. Hopfenberg, and V. T. Stannett (1971). The effect of molecular weight and orientation on the sorption of n-pentane by glassy polystyrene. *Polymer Engineering & Science 11*(4), 274–283. Cited on page 76.

[7] Balescu, R. (2005). *Aspects of Anomalous Transport in Plasmas*, Chapter 12, pp. 251–297. Series in Plasma Physics. Taylor & Francis. Cited on pages 22, 24.

[8] Balescu, R. (2007). V-Langevin equations, continuous time random walks and fractional diffusion. *Chaos, Solitons & Fractals 34*(1), 62 – 80. Cited on page 22.

[9] Barkai, E. (2002). CTRW pathways to the fractional diffusion equation. *Chemical Physics 284*(1-2), 13 – 27. Cited on page 78.

[10] Bendler, J. T., J. J. Fontanella, and M. F. Shlesinger (2007). Anomalous diffusion producing normal relaxation and transport. *Journal of Physics: Condensed Matter 19*(6), 065121. Cited on pages 20, 21, 25.

[11] Benson, D. A., C. Tadjeran, M. M. Meerschaert, I. Farnham, and G. Pohll (2004, 12). Radial fractional-order dispersion through fractured rock. *Water Resour. Res. 40*(12), 9pp. Cited on page 78.

[12] Berg, H. C. (1993). *Random Walks in Biology*. Princeton University Press. Cited on pages 22, 26.

[13] Berkowitz, B., A. Cortis, M. Dentz, and H. Scher (2006). Modeling non-fickian transport in geological formations as a continuous time random walk. *Rev. Geophys. 44*, 49 PP. Cited on pages 21, 22, 78.

[14] Beychok, M. R. (1975, May). Process and environmental technology for producing sng and liquid fuels. Consulting Report EPA-660/2-75-011, United States Environmental Protection Agency, Corvallis, Oregon 97330. Cited on page 8.

[15] Birk, C. and C. Song (2010). An improved non-classical method for the solution of fractional differential equations. *Computational Mechanics 46*, 721–734. Cited on page 51.

[16] Bossak, B. H. and M. R. Welford (2010). Spatio-temporal attributes of pandemic and epidemic diseases. *Geography Compass 4*(8), 1084–1096. Cited on page 25.

[17] Bottoms, R. R. (1930, December). Process for separating acidic gases. Cited on page 9.

[18] Bouchaud, J.-P. and A. Georges (1990). Anomalous diffusion in disordered media: Statistical mechanisms, models and physical applications. *Physics Reports 195*(4-5), 127 – 293. Cited on page 24.

[19] Brandenburg, A., P. Käpylä, and A. Mohammed (2004). Non-Fickian diffusion and tau approximation from numerical turbulence. *Physics of Fluids 16*(4), 1020–1027. Cited on page 69.

[20] Bright, T. J. (2009). Non-fourier heat equations in solids analyzed from phonon statistics. Master's thesis, Georgia Insitute of Technology. Cited on page 19.

[21] Brunner, H., L. Ling, and M. Yamamoto (2010). Numerical simulations of 2D fractional subdiffusion problems. *Journal of Computational Physics 229*(18), 6613 – 6622. Cited on pages 52, 53, 54, 79.

[22] Buchbinder, G. L. and P. Martaller (2009, Dec). Model for solute diffusion during rapid solidification of binary alloy in semi-infinite volume. Cited on page 68.

[23] Canuto, C., M. Hussaini, A. Quarteroni, and T. Zang (2006). *Spectral Methods*. Springer. Cited on pages 39, 52, 57.

[24] Caputo, M. (1967). Linear models of dissipation whose q is almost frequency independent-ii. *Geophysical Journal of the Royal Astronomical Society 13*(5), 529–539. Cited on page 31.

[25] Caputo, M. and F. Mainardi (1971). A new dissipation model based on memory mechanism. *Pure and Applied Geophysics 91*, 134–147. Cited on page 78.

[26] Carella, A. R. and C. A. Dorao (2012). Least-squares spectral method for the solution of a fractional advection-dispersion equation. *Journal of Computational Physics*. Article in Press. Cited on page 52.

[27] Casper, A. F., B. Dixon, E. T. Steimle, and M. L. Hall (2012). Scales of heterogeneity of water quality in rivers: Insights from high resolution maps based on integrated geospatial, sensor and rov technologies. *Applied Geography 32*(2), 455 – 464. Cited on pages 20, 21.

[28] Chang, W.-D. (2009). Two-dimensional fractional-order digital differentiator design by using differential evolution algorithm. *Digital Signal Processing 19*(4), 660 – 667. Cited on pages 53, 78.

[29] Chaves, A. S. (1998). A fractional diffusion equation to describe Lévy flights. *Physics Letters A 239*(1-2), 13 – 16. Cited on page 33.

[30] Chechkin, A. V., V. Y. Gonchar, and M. Szydlowski (2002). Fractional kinetics for relaxation and superdiffusion in a magnetic field. *9*(1), 78–88. Cited on page 25.

[31] Chen, H.-T. and K.-C. Liu (2003). Analysis of non-fickian diffusion problems in a composite medium. *Computer Physics Communications 150*(1), 31 – 42. Cited on page 68.

[32] Cheney, W. and D. Kincaid (2008). *Numerical Mathematics and Computing*. Brooks/Cole: Cengage Learning. Cited on page 94.

[33] Chenier, P. J. (2002). *Survey of industrial chemistry*. Plenum Publisher. Cited on page 11.

[34] Compte, A. and R. Metzler (1997). The generalized Cattaneo equation for the description of anomalous transport processes. *Journal of Physics A 30*, 7277–7289. Cited on pages 68, 69, 78.

[35] Conner, J. W. and H. R. Wilson (1994). Survey of theories of anomalous transport. *Plasma Physics and Controlled Fusion 36*(5), 719. Cited on page 78.

[36] Criminisi, A., I. Reid, and A. Zisserman (1999). A plane measuring device. *Image and Vision Computing 17*(8), 625 – 634. Cited on page 58.

[37] Cuevas, S., J. A. del Río, and M. López de Haro (1999). Consequences of a generalized ohm's law for magnetic transport in conducting media. *Journal of Physics D: Applied Physics 32*(6), 639. Cited on pages 19, 21.

[38] David, N. and T. Michel (Eds.) (2008). *Natural Gas Research Progress*. Nova Science Publishers Inc. Cited on page 3.

[39] De Maerschalck, B. (2003). Space-time least-squares spectral element method for unsteady flows-application and evaluation for linear and non-linear hyperbolic scalar equations. Master's thesis, Delft University of Technology, Department of Aerospace Engineering. Cited on page 43.

[40] Deng, W. (2007). Short memory principle and a predictor-corrector approach for fractional differential equations. *Journal of Computational and Applied Mathematics 206*(1), 174 – 188. Cited on pages 52, 78.

[41] Depireux, N. and G. Lebon (2001). An extended thermodynamics modeling of non-fickian diffusion. *Journal of Non-Newtonian Fluid Mechanics 96*(1-2), 105–117. Cited on page 68.

[42] Deville, M., P. Fischer, and E. Mund (2002). *High-Order Methods for Incompressible Fluid Flow*. Cambridge University Press. Cited on page 43.

[43] Devroye, L. (1986). *Non-Uniform Random Variate Generation*. Springer-Verlag. Cited on page 25.

[44] Diethelm, K. (2009). An improvement of a nonclassical numerical method for the computation of fractional derivatives. *Journal of Vibration and Acoustics 131*(1), 014502. Cited on page 51.

[45] Diethelm, K., J. M. Ford, N. J. Ford, and M. Weilbeer (2006). Pitfalls in fast numerical solvers for fractional differential equations. *Journal of Computational and Applied Mathematics 186*(2), 482 – 503. Cited on page 51.

[46] Doghieri, F., G. Camera-Roda, and G. Sarti (1993). Rate-type equations for the diffusion in polymers: Thermodynamic constraints. *AiChE Journal 39*(11), 1847–1858. Cited on page 69.

[47] Doran, P. M. (2013). Heterogeneous reactions. In *Bioprocess Engineering Principles (Second Edition)* (Second Edition ed.)., pp. 705 – 759. London: Academic Press. Cited on page 97.

[48] Dorao, C. A. (2009). Simulation of thermal disturbances with finite wave speeds using a high order method. *Journal of Computational and Applied Mathematics 231*(2), 637–647. Cited on page 68.

[49] Dorfman, J. R. (1999). *An introduction to Chaos in Nonequilibrium Statistical Mechanics*. Cambridge University Press. Cited on page 23.

[50] Dubrulle, B. and J.-P. Laval (1998). Truncated lvy laws and 2d turbulence. *The European Physical Journal B - Condensed Matter and Complex Systems 4*, 143–146. Cited on page 25.

[51] Dunn, I. J., H. Tanaka, S. Uzman, and M. Denac (1983). Biofilm fluidized-bed reactors and their application to waste water nitrification. *Annals of the New York Academy of Sciences 413*(1), 168–183. Cited on page 97.

[52] Dupuy, P. M. (2010). *Droplet Deposition in High-Pressure Natural-Gas Streams*. Ph. D. thesis, Norwegian University of Science and Technogy. Cited on page 9.

[53] Durr, C., D. Coyle, and S. Smith (2005). LNG Technology for the Commercially Minded. Gastech Conference, Bilbao, Spain. Cited on page 6.

[54] Economides, M. J. and D. A. Wood (2009). The state of natural gas. *Journal of Natural Gas Science and Engineering 1*(1-2), 1 – 13. Cited on pages 4, 7.

[55] Edino, M., G. Nsofor, and L. Bombom (2010). Perceptions and attitudes towards gas flaring in the niger delta, nigeria. *The Environmentalist 30*, 67–75. Cited on page 4.

[56] EIA (2003, December). The global liquefied natural gas market: Status & outlook. Gas market report DOE/EIA-0637 (2003), Energy Information Administration - U.S. Department of Energy, Washington, DC 20585. Cited on page 7.

[57] EIA (2012, February). Shortterm energy outlook. Gas market report, Energy Information Administration - U.S. Department of Energy, Washington, DC 20585. Cited on page 6.

[58] Ercília and Sousa (2009). Finite difference approximations for a fractional advection diffusion problem. *Journal of Computational Physics 228*(11), 4038 – 4054. Cited on page 77.

[59] E.S.A.A. (2000). Best available techniques for pollution prevention and control in the european sulphuric acid and fertilizer industries. Available online at http://www.efma.org/documents/file/bat/BATcid.pdf. Cited on page 11.

[60] Fitzgerald, A. and M. Taylor (2001, September). Offshore gas-to-solids technology. In *presented at the Offshore Europe Conference held in Aberdeen, UK, 4-7 September*. Cited on page 4.

[61] Fix, G. and J. Roop (2004). Least squares finite-element solution of a fractional order two-point boundary value problem. *Computers & Mathematics with Applications 48*(7-8), 1017 – 1033. Cited on pages 33, 51.

[62] Fomin, S., V. Chugunov, and T. Hashida (2009). Application of fractional differential equations for modeling the anomalous diffusion of contaminant from fracture into porous rock matrix with bordering alteration zone. *Transport in Porous Media 81*(2), 187–205. Cited on page 78.

[63] Gao, G., H. Zhan, S. Feng, G. Huang, and X. Mao (2009). Comparison of alternative models for simulating anomalous solute transport in a large heterogeneous soil column. *Journal of Hydrology 377*(3-4), 391 – 404. Cited on pages 19, 78.

[64] Gerritsma, M. and B. De Maerschalck (2010). Least-squares spectral element methods in computational fluid dynamics. *Lecture Notes in Electrical Engineering 71 LNCSE*, 179–227. Cited on pages 37, 38, 47, 70.

[65] Giona, M. and H. E. Roman (1992). Fractional diffusion equation for transport phenomena in random media. *Physica A: Statistical Mechanics and its Applications 185*(1-4), 87 – 97. Cited on page 78.

[66] Go, K. S., S. R. Son, S. D. Kim, K. S. Kang, and C. S. Park (2009). Hydrogen production from two-step steam methane reforming in a fluidized bed reactor. *International Journal of Hydrogen Energy 34*(3), 1301 – 1309. Cited on page 11.

[67] Godoy, S. and L. S. García-Colín (1996). From the quantum random walk to classical mesoscopic diffusion in crystalline solids. *Physical Review E 53*(6), 5779–5785. Cited on page 68.

[68] Gómez, H., I. Colominas, F. Navarrina, J. París, and M. Casteleiro (2010). A hyperbolic theory for advection-diffusion problems: Mathematical foundations and numerical modeling. *Archives of Computational Methods in Engineering 17*, 191–211. Cited on pages 20, 21, 101.

[69] Gómez-Díaz, H. (2003). Una nueva formulación para el problema del transporte por convección-difusión. In *Certamen universitario Arqumedes de introduccin a la generacin de conocimiento, Zaragoza, 2003*, pp. 27p. Cited on page 73.

[70] Gómez-Díaz, H. (2006). *Una formulación hiperbólica para el problema del transporte por convección-difusión en mecánica de fluidos computacional*. Ph. D. thesis, Universidade Da Coruña. Cited on pages 18, 68.

[71] Gordon, W. J. and C. A. Hall (1973). Construction of curvilinear co-ordinate systems and applications to mesh generation. *International Journal for Numerical Methods in Engineering 7*(4), 461–477. Cited on page 60.

[72] Gorenflo, R., F. Mainardi, D. Moretti, and P. Paradisi (2002). Time fractional diffusion: A discrete random walk approach. *Nonlinear Dynamics 29*, 129–143. Cited on pages 28, 78, 88.

[73] Gorenflo, R., F. Mainardi, E. Scalas, and M. Raberto (2001). Fractional calculus and continuous-time finance III: the diffusion limit. In *Mathematical Finance*, pp. 171–180. Birkhuser Basel. Cited on page 20.

[74] Grace, J. R., J. Chaouki, and T. Pugsley (2005). Fluidized bed reactor. *Encyclopedia of Chemical Processing* -, 1009 – 1020. Cited on page 97.

[75] Guo, B. and A. Ghalambor (2005). *Natural Gas Engineering Handbook*. Gulf Publishing Company. Cited on page 8.

[76] Gusev, A., R. Iskhakov, M. Zhidkov, and G. Komarova (2000). A system for preparing oil-associated gas for transportation by the use of a controlled three-flow vortex tube. *Chemical and Petroleum Engineering 36*, 414–417. Cited on page 4.

[77] Hall, K. R. (2005). A new gas to liquids (gtl) or gas to ethylene (gte) technology. *Catalysis Today 106*(1-4), 243 – 246. Cited on page 4.

[78] Hanert, E. (2011). On the numerical solution of space-time fractional diffusion models. *Computers & Fluids 46*(1), 33–39. Cited on pages 33, 78.

[79] Hanneken, J. W., B. N. N. Achar, D. M. Vaught, and K. L. Harrington (2004). A random walk simulation of fractional diffusion. *Journal of Molecular Liquids 114*(1-3), 153 – 157. Cited on page 78.

[80] Herwig, H. and K. Beckert (2000). Experimental evidence about the controversy concerning fourier or non-fourier heat conduction in materials with a nonhomogeneous inner structure. *Heat and Mass Transfer 36*, 387–392. Cited on page 17.

[81] Heymans, N. and I. Podlubny (2006). Physical interpretation of initial conditions for fractional differential equations with Riemann-Liouville fractional derivatives. *Rheologica Acta 45*, 765–771. Cited on page 78.

[82] Hilfer, R. (1996). Transport and relaxation phenomena in porous media. *Adv. Chem. Phys. XCII*, 299. Cited on pages 20, 21, 22.

[83] Hilfer, R. and L. Anton (1995, Feb). Fractional master equations and fractal time random walks. *Phys. Rev. E 51*, R848–R851. Cited on page 78.

[84] Huang, K., N. Toride, and M. T. V. Genuchten (1995). Experimental investigation of solute transport in large, homogeneous and heterogeneous, saturated soil columns. In *Transport in porous media*, pp. 283–302. Cited on page 78.

[85] Huang, Q., G. Huang, and H. Zhan (2008). A finite element solution for the fractional advection-dispersion equation. *Advances in Water Resources 31*(12), 1578 – 1589. Cited on page 78.

[86] Incropera, F. P. and D. P. DeWitt (2002). *Fundamentals of Heat and Mass Transfer* (5 ed.). Wiley - New York. Cited on page 18.

[87] Isaev, V. and V. Shapeev (2010). High-accuracy versions of the collocations and least squares method for the numerical solution of the navier-stokes equations. *Computational Mathematics and Mathematical Physics 50*, 1670–1681. Cited on page 102.

[88] Ishishone, M. (2004). Gas flaring in the niger delta: the potential benefits of its reduction on the local economy and environment. Available online at http://nature.berkeley.edu/classes/es196/projects/2004final/Ishone.pdf. Retrieved March 11, 2011. Cited on pages 3, 4.

[89] Islam, M. A. (2004). Fickian diffusion equationan unsolved problem. *Physica Scripta 70*(2-3), 114. Cited on pages 19, 21.

[90] Jahn, F., M. Cook, and M. Graham (2008). Reservoir dynamic behaviour. In F. Jahn, M. Cook, and M. Graham (Eds.), *Hydrocarbon Exploration & Production*, Volume 55 of *Developments in Petroleum Science*, Chapter 9, pp. 201 – 227. Elsevier. Cited on page 20.

[91] Jakobsen, H. A. (2008). *Packed Bed Reactors*. Springer Berlin Heidelberg. Cited on pages 6, 98.

[92] Jha, R., P. K. Kaw, D. R. Kulkarni, and J. C. Parikh (2003). Evidence of lvy stable process in tokamak edge turbulence. *10*(3), 699–704. Cited on page 25.

[93] Jiang, B.-n. (1998). *The Least-Squares Finite Element Method: Theory and Applications in Computational Fluid Dynamics and Electromagnetics*. Springer-Verlag Berlin / Heidelberg. Cited on pages 37, 38, 39, 42, 45, 47, 52, 57, 80, 99, 101, 103, 104.

[94] Jiang, W. and Y. Lin (2010). Approximate solution of the fractional advection-dispersion equation. *Computer Physics Communications 181*(3), 557 – 561. Cited on page 51.

[95] Joseph, D. D. and L. Preziosi (1989, Jan). Heat waves. *Rev. Mod. Phys. 61*, 41–73. Cited on page 19.

[96] Jou, D., J. Camacho, and M. Grmela (1991). On the nonequilibrium thermodynamics of non-fickian diffusion. *Macromolecules 24*, 3597–3602. Cited on page 68.

[97] Jumarie, G. (2009). Table of some basic fractional calculus formulae derived from a modified riemann-liouville derivative for non-differentiable functions. *Applied Mathematics Letters 22*(3), 378–385. Cited on page 31.

[98] Kaldany, R. (2006, December). Global gas flaring reduction: A time for action! In *Global Forum on Flaring and Gas Utilization*. World Bank. Cited on pages 3, 4.

[99] Kath, W. L. (1984). Waiting and propagating fronts in nonlinear diffusion. *Physica D: Nonlinear Phenomena 12*(13), 375 – 381. Cited on pages 19, 21.

[100] Kayser-Herold, O. and H. G. Matthies (2005). Least-squares fem literature review. Technical report, Institute of Scientific Computing, Technical University Braunschweig, Brunswick. Cited on page 38.

[101] Kenkre, V. M., E. W. Montroll, and M. F. Shlesinger (1973). Generalized master equations for continuous-time random walks. *Journal of Statistical Physics 9*, 45–50. Cited on page 24.

[102] Klafter, J. and I. Sokolov (2005). Anomalous diffusion spreads its wings. *Physics World 18*(8), 29–32. Cited on pages 19, 21, 32.

[103] Klages, R., G. Radons, and I. Sokolov (2008). *Anomalous Transport: Foundations and Applications*. Weinheim: Wiley-VCH Verlag GmbH & Co. KGaA. Cited on pages 19, 25, 28, 30, 78.

[104] Kleinz, M. and T. J. Osler (2000). A child's garden of fractional derivatives. *The College Mathematics Journal 31*(2), pp. 82–88. Cited on page 30.

[105] Kondepudi, D. and I. Prigogine (1998). *Modern Thermodynamics: From Heat Engines to Dissipative Structures*. Wiley and Sons, Chichester. Cited on page 21.

[106] Krommes, J. A. (2002). Fundamental statistical descriptions of plasma turbulence in magnetic fields. *Physics Reports 360*(1-4), 1 – 352. Cited on page 25.

[107] Küntz, M. and P. Lavallée (2001). Experimental evidence and theoretical analysis of anomalous diffusion during water infiltration in porous building materials. *Journal of Physics D 34*, 2547–2554. Cited on pages 18, 68, 73, 78.

[108] Küntz, M. and P. Lavallée (2004). Anomalous diffusion is the rule in concentration-dependent diffusion processes. *Journal of Physics D: Applied Physics 37*(1), L5. Cited on pages 18, 32, 68, 73, 78.

[109] Labeyrie, H. and A. Rocher (2010, April). Reducing flaring and improving energy efficiency: An operator's view. In *SPE International Conference on Health, Safety and Environment in Oil and Gas Exploration and Production*.

Society of Petroleum Engineers: Society of Petroleum Engineers. Cited on page 4.

[110] Landau, L. and E. Lifshitz (1959). *Fluid Mechanics*. Pergamon Press: Oxford. Cited on pages 19, 21.

[111] Lane, C., A. Fairbank, and W. Fairbank (1947). Second sound in liquid helium ii. *Physical Review 71*(9), 600–605. Cited on pages 22, 74.

[112] Langlands, T. and B. Henry (2005). The accuracy and stability of an implicit solution method for the fractional diffusion equation. *Journal of Computational Physics 205*(2), 719 – 736. Cited on page 53.

[113] Lee, C.-J. and C. Han (2009). Comparative economic analysis of gas-to-liquid processes for optimal product selection. In H. E. Alfadala, G. R. Reklaitis, and M. M. El-Halwagi (Eds.), *Proceedings of the 1st Annual Gas Processing Symposium*, pp. 354 – 361. Amsterdam: Elsevier. Cited on page 10.

[114] Leipertz, A. and A. P. Fröba (2005). Diffusion measurements in fluids by dynamic light scattering. In P. Heitjans and J. Kärger (Eds.), *Diffusion in Condensed Matter*, pp. 579–618. Springer Berlin Heidelberg. Cited on page 20.

[115] Li, C. and W. Deng (2007). Remarks on fractional derivatives. *Applied Mathematics and Computation 187*(2), 777 – 784. Cited on page 31.

[116] Li, J.-R. (2010). A fast time stepping method for evaluating fractional integrals. *SIAM Journal on Scientific Computing 31*(6), 4696–4714. Cited on page 51.

[117] Li, X. and C. Xu (2009). A space-time spectral method for the time fractional diffusion equation. *SIAM Journal on Numerical Analysis 47*(3), 2108–2131. Cited on page 52.

[118] Li, X. and C. Xu (2010, November). Existence and uniqueness of the weak solution of the space-time fractional diffusion equation and a spectral method approximation. *Commun. Comput. Phys. 8*(5), 1016–1051. Cited on pages 52, 79.

[119] Lin, Y. and C. Xu (2007). Finite difference/spectral approximations for the time-fractional diffusion equation. *Journal of Computational Physics 225*(2), 1533 – 1552. Cited on pages 51, 53.

[120] Liu, V. C. (1979). On the Instantaneous Propagation Paradox of Heat Conduction. *Journal of Non-Equilibrium Thermodynamics 4*, 143–148. Cited on page 18.

[121] Logvinova, K. and M.-C. Néel (2004). Fractional model for solute spreading in randomly heterogeneous porous media. In *XXI International Congress of Theoretical and Applied Mechanics, Warsaw, Poland, August 15-21, 2004*, pp. 2p. Cited on page 78.

[122] Loverro, A. (2004). Fractional calculus: History, definitions and applications for the engineer. Technical report, Department of Aerospace and Mechanical Engineering, University of Notre Dame. Cited on pages 31, 50.

[123] Lu, J.-F. and A. Hanyga (2005). Wave field simulation for heterogeneous porous media with singular memory drag force. *Journal of Computational Physics 208*(2), 651 – 674. Cited on pages 51, 52, 78.

[124] Luchko, Y. (2009). Maximum principle for the generalized time-fractional diffusion equation. *Journal of Mathematical Analysis and Applications 351*(1), 218 – 223. Cited on page 33.

[125] Luchko, Y. and A. Punzi (2011). Modeling anomalous heat transport in geothermal reservoirs via fractional diffusion equations. *GEM - International Journal on Geomathematics* -, 1–20. Cited on page 78.

[126] Lynch, V., B. Carreras, D. del Castillo-Negrete, K. Ferreira-Mejias, and H. Hicks (2003). Numerical methods for the solution of partial differential equations of fractional order. *Journal of Computational Physics 192*(2), 406 – 421. Cited on pages 28, 78.

[127] Maddox, R. N. and D. J. Morgan (1986, September). Select eor processes for co2. *Hydr. Proc. 65*(6), 59–63. Cited on page 9.

[128] Maddox, R. N. and D. J. Morgan (2008). *Gas conditioning and processing* (Fourth ed.), Volume 4. Campbell Petroleum Series. Cited on page 9.

[129] Mainardi, F. (2010, July). An historical perspective on fractional calculus in linear viscoelasticity. Available online at http://arxiv.org/abs/1007.2959. Cited on page 78.

[130] Mainardi, F., M. Raberto, R. Gorenflo, and E. Scalas (2000). Fractional calculus and continuous-time finance II: the waiting-time distribution. *Physica A: Statistical Mechanics and its Applications 287*(3-4), 468 – 481. Cited on page 20.

[131] Malinowska, A. B. and D. F. Torres (2010). Generalized natural boundary conditions for fractional variational problems in terms of the Caputo derivative. *Computers & Mathematics with Applications 59*(9), 3110 – 3116. Cited on page 78.

[132] Mathieu, B., P. Melchior, A. Oustaloup, and C. Ceyral (2003). Fractional differentiation for edge detection. *Signal Processing 83*(11), 2421 – 2432. Cited on page 78.

[133] Meerschaert, M. and C. Tadjeran (2004). Finite difference approximations for fractional advection-dispersion flow equations. *Journal of computational and Applied Mathematics 172*(1), 65–77. Cited on page 78.

[134] Meerschaert, M. M., D. A. Benson, and B. Bäumer (1999, May). Multidimensional advection and fractional dispersion. *Phys. Rev. E 59*(5), 5026–5028. Cited on page 33.

[135] Meerschaert, M. M., H.-P. Scheffler, and C. Tadjeran (2006). Finite difference methods for two-dimensional fractional dispersion equation. *Journal of Computational Physics 211*(1), 249 – 261. Cited on page 53.

[136] Meerschaert, M. M., Y. Zhang, and B. Baeumer (2010). Particle tracking for fractional diffusion with two time scales. *Computers & Mathematics with Applications 59*(3), 1078 – 1086. ¡ce:title¿Advance in Fractional Differential Equations¡/ce:title¿. Cited on page 23.

[137] Metzler, R., E. Barkai, and J. Klafter (1999). Anomalous transport in disordered systems under the influence of external fields. *Physica A: Statistical Mechanics and its Applications 266*(1-4), 343 – 350. Cited on page 78.

[138] Metzler, R. and J. Klafter (2000). The random walk's guide to anomalous diffusion: a fractional dynamics approach. *Physics Reports 339*(1), 1 – 77. Cited on pages 25, 78.

[139] Metzler, R. and J. Klafter (2004). The restaurant at the end of the random walk: recent developments in the description of anomalous transport by fractional dynamics. *Journal of Physics A: Mathematical and General 37*(31), R161. Cited on pages 25, 78.

[140] Mokhatab, S., W. A. Poe, and J. G. Speight (2006). *Handbook of Natural Gas Transmission and Processing*. Elsevier. Cited on page 8.

[141] Molz, F. J., G. J. Fix, and S. Lu (2002). A physical interpretation for the fractional derivative in Levy diffusion. *Applied Mathematics Letters 15*(7), 907 – 911. Cited on page 78.

[142] Montroll, E. W. and G. H. Weiss (1965). Random walks on lattices. ii. *6*(2), 167–181. Cited on page 24.

[143] Nagy, E. (2012). Diffusion accompanied by chemical reaction through a plane sheet. In *Basic Equations of the Mass Transport through a Membrane Layer*, pp. 81 – 120. Oxford: Elsevier. Cited on page 97.

[144] Nakawaga, K. (2003). Diffusion coefficient and relaxation time of aliphatic spin probes in a unique triglyceride membrane. *Langmuir 19*(12), 5078–5082. Cited on page 74.

[145] Nehb, W. and K. Vydra (2000). *Sulfur*, pp. 68p. Wiley-VCH Verlag GmbH & Co. KGaA. Cited on page 9.

[146] Odumugbo, C. A. (2010). Natural gas utilisation in nigeria: Challenges and opportunities. *Journal of Natural Gas Science and Engineering 2*(6), 310 – 316. Cited on page 3.

[147] Oldham, K. B. (2010). Fractional differential equations in electrochemistry. *Advances in Engineering Software 41*(1), 9 – 12. Cited on page 78.

[148] Pálfalvi, A. (2010). Efficient solution of a vibration equation involving fractional derivatives. *International Journal of Non-Linear Mechanics 45*(2), 169 – 175. Cited on page 51.

[149] Paradisi, P., R. Cesari, F. Mainardi, A. Maurizi, and F. Tampieri (2001). A generalized Fick's law to describe non-local transport effects. *Physics and Chemistry of the Earth, Part B: Hydrology, Oceans and Atmosphere 26*(4), 275 – 279. Cited on page 28.

[150] Podlubny, I. (1999). *Fractional Differential Equations*. 525B Street, Suite 1900, San Diego, California 92101-4495, USA: Academic Press. Cited on pages 30, 32, 50, 52, 53, 78.

[151] Podlubny, I. (2002). Geometric and physical interpretation of fractional integration and fractional differentiation. *Fractional Calculus and Applied Analysis 5*(4), 367–386. Cited on pages 31, 78.

[152] Podlubny, I., A. Chechkin, T. Skovranek, Y. Chen, and B. M. V. Jara (2009). Matrix approach to discrete fractional calculus II: Partial fractional differential equations. *Journal of Computational Physics 228*(8), 3137 – 3153. Cited on pages 80, 81, 85, 87, 88, 89, 90, 91, 92, 93.

[153] Press, W. H., S. A. Teukolsky, W. T. Vetterling, and B. P. Flannery (1993, January). *Numerical Recipes in C: The Art of Scientific Computing* (Second Edition ed.). Cambridge University Press. Cited on pages 44, 52.

[154] Proot, M. M. J. and M. I. Gerritsma (2002). Least-Squares Spectral Elements applied to the Stokes problem. *Journal of Computational Physics 181*(2), 454 – 477. Cited on pages 39, 47, 100.

[155] Rajnauth, J., K. Ayeni, and M. Barrufet (2008). Gas transportation: Present and future. In *CIPC/SPE Gas Technology Symposium 2008 Joint Conference*. Cited on page 9.

[156] Ramos-Fernndez, G., J. L. Mateos, O. Miramontes, G. Cocho, H. Larralde, and B. Ayala-Orozco (2004). Lévy walk patterns in the foraging movements of spider monkeys (ateles geoffroyi). *Behavioral Ecology and Sociobiology 55*, 223–230. Cited on page 25.

[157] Reynolds, A. M. and M. A. Frye (2007). Free-flight odor tracking in ¡italic¿drosophila¡/italic¿ is consistent with an optimal intermittent scale-free search. *PLoS ONE 2*(4), e354. Cited on page 25.

[158] Rieger, M. O. and M. Wang (2006). Cumulative prospect theory and the st. petersburg paradox. *Economic Theory 28*, 665–679. Cited on page 25.

[159] Ritchie, K., X.-Y. Shan, J. Kondo, K. Iwasawa, T. Fujiwara, and A. Kusumi (2005). Detection of non-brownian diffusion in the cell membrane in single molecule tracking. *Biophysical Journal 88*(3), 2266 – 2277. Cited on pages 68, 73.

[160] Roop, J. P. (2006). Computational aspects of FEM approximation of fractional advection dispersion equations on bounded domains in. *Journal of Computational and Applied Mathematics 193*(1), 243 – 268. Cited on page 51.

[161] Roop, J. P. (2008). Numerical approximation of a one-dimensional space fractional advection-dispersion equation with boundary layer. *Computers & Mathematics with Applications 56*(7), 1808 – 1819. Cited on page 51.

[162] Rossikhin, Y. A. and M. Shitikova (2006). Analysis of damped vibrations of linear viscoelastic plates with damping modeled with fractional derivatives. *Signal Processing 86*(10), 2703 – 2711. Cited on page 78.

[163] Rossikhin, Y. A. and M. V. Shitikova (2011). The analysis of the impact response of a thin plate via fractional derivative standard linear solid model. *Journal of Sound and Vibration 330*(9), 1985 – 2003. Cited on page 78.

[164] Rutman, R. S. (1995). On physical interpretations of fractional integration and differentiation. *Theoretical and Mathematical Physics 105*, 1509–1519. Cited on pages 31, 78.

[165] Sabatier, J., M. Merveillaut, R. Malti, and A. Oustaloup (2010). How to impose physically coherent initial conditions to a fractional system? *Communications in Nonlinear Science and Numerical Simulation 15*(5), 1318 – 1326. Cited on page 78.

[166] Sam and Holloway (1997). An overview of the underground disposal of carbon dioxide. *Energy Conversion and Management 38, Supplement*(0), S193 – S198. Cited on page 6.

[167] Scher, H. and E. W. Montroll (1975, Sep). Anomalous transit-time dispersion in amorphous solids. *Phys. Rev. B 12*, 2455–2477. Cited on pages 20, 21.

[168] Scherer, R., S. Kalla, L. Boyadjiev, and B. Al-Saqabi (2008). Numerical treatment of fractional heat equations. *Applied Numerical Mathematics 58*(8), 1212 – 1223. Cited on pages 87, 88, 89.

[169] Schindler, D. W. and R. E. Hecky (2009). Eutrophication: More Nitrogen Data Needed. *Science 324*(5928), 721–b–722. Cited on page 11.

[170] Schumer, R., D. A. Benson, M. M. Meerschaert, and S. W. Wheatcraft (2001). Eulerian derivation of the fractional advection-dispersion equation. *Journal of Contaminant Hydrology 48*(1-2), 69 – 88. Cited on page 33.

[171] Sharma, K. R. (2005). *Damped Wave Transport and Relaxation*. Radarweg 29, P.O.Box 211, 1000 AE Amsterdam, The Netherlands: Elsevier. Cited on page 68.

[172] Shewchuk, J. (2004). An introduction to the conjugate gradient method without the agonizing pain. In *School of Computer Science, Carnegie Mellon University, Pittsburgh, PA, 1994*, pp. 64p. Cited on page 70.

[173] Shlesinger, M. F., J. Klafter, and G. Zumofen (1999). Above, below and beyond brownian motion. *67*(12), 1253–1259. Cited on page 25.

[174] Sokolov, I. M. and J. Klafter (2005). From diffusion to anomalous diffusion: A century after einstein's brownian motion. *15*(2), 026103. Cited on page 19.

[175] Sporleder, F., C. A. Dorao, and H. A. Jakobsen (2010). Simulation of chemical reactors using the least-squares spectral element method. *Chemical Engineering Science 65*(18), 5146 – 5159. Cited on page 100.

[176] Stanley, I. O. (2009). Gas-to-liquid technology: Prospect for natural gas utilization in nigeria. *Journal of Natural Gas Science and Engineering 1*(6), 190 – 194. Cited on page 4.

[177] Stöcker, M. (2005). Gas phase catalysis by zeolites. *Microporous and Mesoporous Materials 82*(3), 257 – 292. Cited on page 22.

[178] Sugiura, H. and T. Hasegawa (2009). Quadrature rule for Abel's equations: Uniformly approximating fractional derivatives. *Journal of Computational and Applied Mathematics 223*(1), 459 – 468. Cited on page 51.

[179] Tadjeran, C. and M. M. Meerschaert (2007). A second-order accurate numerical method for the two-dimensional fractional diffusion equation. *Journal of Computational Physics 220*(2), 813 – 823. Cited on page 53.

[180] Tadjeran, C., M. M. Meerschaert, and H.-P. Scheffler (2006). A second-order accurate numerical approximation for the fractional diffusion equation. *Journal of Computational Physics 213*(1), 205 – 213. Cited on page 53.

[181] Tørå, G., T. Ramstad, and A. Hansen (2009). Anomalous diffusion on clusters in steady-state two-phase flow in porous media in two dimensions. *EPL (Europhysics Letters) 87*(5), 54002. Cited on pages 20, 21.

[182] Uemura, Y. and P. Macdonald (1996). Nmr diffusion and relaxation time studies of heur associating polymer binding to polystyrene latex. *Macromolecules 29*(1), 63–69. Cited on page 74.

[183] Uhde Engineering (2003, March). Methanol. Available online at http://www.uhde.eu/archive/upload/uhde_brochures_pdf_en_6.00.pdf. Cited on page 12.

[184] U.S. Energy (2008, November). Hydrogen production. Available online at www1.eere.energy.gov/hydrogenandfuelcells/pdfs/doe_h2_production.pdf. Cited on page 12.

[185] Valdés-Parada, F. J., J. A. Ochoa-Tapia, and J. Álvarez-Ramírez (2006). Effective medium equation for fractional cattaneo's diffusion and heterogeneous reaction in disordered porous media. *Physica A: Statistical Mechanics and its Applications 369*(2), 318 – 328. Cited on page 68.

[186] van Vliet, O. P., A. P. Faaij, and W. C. Turkenburg (2009). Fischertropsch diesel production in a well-to-wheel perspective: A carbon, energy flow and cost analysis. *Energy Conversion and Management 50*(4), 855 – 876. Cited on page 9.

[187] Vick, B. and M. N. Ozisik (1983). Growth and decay of a thermal pulse predicted by the hyperbolic heat conduction equation. *Journal of Heat Transfer 105*(4), 902–907. Cited on page 22.

[188] Visscher, P. B. (1984a, May). Analytic fixed points of discrete equations of motion: Universality in homogeneous diffusive systems. *Phys. Rev. B 29*, 5462–5471. Cited on page 17.

[189] Visscher, P. B. (1984b, May). Universality in disordered diffusive systems: Exact fixed points in one, two, and three dimensions. *Phys. Rev. B 29*, 5472–5485. Cited on page 17.

[190] Vrentas, J. S., J. L. Duda, and A.-C. Hou (1984). Anomalous sorption in poly(ethyl methacrylate). *Journal of Applied Polymer Science 29*(1), 399–406. Cited on page 76.

[191] Wesselingh, J. A. and R. Krishna (1990). *Mass Transfer*. Ellis Horwood. Cited on page 22.

[192] Wilhelm, D. J., D. R. Simbeck, A. D. Karp, and R. L. Dickenson (2001). Syngas production for gas-to-liquids applications: technologies, issues and outlook. *Fuel Processing Technology 71*(1-3), 139 – 148. Cited on pages 7, 11.

[193] World Bank (2009). World bank, ggfr partners unlock value of wasted gas. Available online at http://go.worldbank.org/ESORQZPSJ0. Cited on page 4.

[194] Yang, Q., F. Liu, and I. Turner (2010). Numerical methods for fractional partial differential equations with Riesz space fractional derivatives. *Applied Mathematical Modelling 34*(1), 200 – 218. Cited on page 51.

[195] Yuan, L. and O. P. Agrawal (2002). A numerical scheme for dynamic systems containing fractional derivatives. *Journal of Vibration and Acoustics 124*(2), 321–324. Cited on page 51.

[196] Yuste, S. B. (2006). Weighted average finite difference methods for fractional diffusion equations. *Journal of Computational Physics 216*(1), 264 – 274. Cited on page 53.

[197] Zhang, X., M. Lv, J. W. Crawford, and I. M. Young (2007). The impact of boundary on the fractional advection-dispersion equation for solute transport in soil: Defining the fractional dispersive flux with the caputo derivatives. *Advances in Water Resources 30*(5), 1205 – 1217. Cited on pages 20, 21, 78.

[198] Zhang, Y., D. A. Benson, and D. M. Reeves (2009). Time and space nonlocalities underlying fractional-derivative models: Distinction and literature review of field applications. *Advances in Water Resources 32*(4), 561 – 581. Cited on pages 20, 21, 78.

[199] Zhang, Y.-n. and Z.-z. Sun (2011). Alternating direction implicit schemes for the two-dimensional fractional sub-diffusion equation. *Journal of Computational Physics 230*(24), 8713 – 8728. Cited on page 53.

[200] Zhao, J. M. and L. H. Liu (2006). Least-squares spectral element method for radiative heat transfer in semitransparent media. *Numerical Heat Transfer, Part B: Fundamentals 50*(5), 473–489. Cited on page 47.

Appendix

Appendix A

Publications

This appendix comprises the following articles.

Article 1. Carella, A.R. and Dorao, C.A. (2010) *Solution of a Cattaneo-Maxwell diffusion model using a Spectral element least-squares method.* Journal of Natural Gas Science and Engineering **2**, pp. 253-258.
doi:10.1016/j.jngse.2010.08.001. ..... Page 147

Article 2. Carella, A.R., Dorao, C.A. (2011) *Migration of Species into a Particle Under Different Flow Conditions.* In Kuzmin, A. (Ed.): Computational Fluid Dynamics 2010, Proceedings of the Sixth International Conference on Computational Fluid Dynamics, ICCFD6, St. Petersburg, Russia, on July 12-16 2010. Springer-Verlag, Berlin Heidelberg. ISBN: 978-3-642-17883-2, pp. 869-871.
dx.doi.org/10.1007/978-3-642-17884-9_112 ..... Page 155

Article 3. Carella, A.R. and Dorao, C.A. (2011) *Least-Squares Spectral Method for the solution of a fractional advection-dispersion equation.* Journal of Computational Physics. Accepted for publication. Manuscript number JCOMP-D-11-00463R1.
dx.doi.org/10.1016/j.jcp.2012.04.050. ..... Page 161

Article 4. Carella, A.R. and Dorao, C.A. (2012) *Modeling of fractional diffusion on a catalytic particle under different flow conditions.* Defect and Diffusion Forum **323-325**(121), pp. 121-126.
dx.doi.org/10.4028/www.scientific.net/DDF.323-325.121 . Page 185

Article 5. Carella, A.R. and Dorao, C.A. (2012) *N-dimensional Least Squares Spectral Method formulation for the general Fractional Diffusion Equation.* Journal of Computational Physics - Under review. ..... Page 195

Article 1

Carella, A.R. and Dorao, C.A. (2010)

Solution of a Cattaneo-Maxwell diffusion model using a Spectral element least-squares method

Journal of Natural Gas Science and Engineering **2**, pp. 253-258.

Journal of Natural Gas Science and Engineering 2 (2010) 253–258

Contents lists available at ScienceDirect

Journal of Natural Gas Science and Engineering

journal homepage: www.elsevier.com/locate/jngse

Solution of a Cattaneo-Maxwell diffusion model using a Spectral element least-squares method

A.R. Carella*, C.A. Dorao

Dept. of Energy and Process Engineering, Norwegian University of Science and Technology, N-7491 Trondheim, Norway

ARTICLE INFO

Article history:
Received 25 March 2010
Received in revised form
31 May 2010
Accepted 4 August 2010
Available online 1 September 2010

Keywords:
Hyperbolic diffusion equation
Finite element
Cattaneo-Maxwell
Least squares method

ABSTRACT

Fluidized bed reactors are widely used in gas processing facilities due to their superior heat and mass transfer characteristics. Reaction rates in these reactors depend on the diffusion of species into the catalytic particles. A more accurate description of diffusion than Fick's law provides is required for the optimization of the design of these reactors. In this work, a Least Squares Finite Element framework was implemented in order to solve the evolution of the concentration profile predicted by Cattaneo-Maxwell's law inside a catalytic pellet. Fick's and Cattaneo-Maxwell's models were compared, being the obtained predictions significantly different for time scales similar to the relaxation time but converging asymptotically for larger time scales. Time-marching and full-domain numerical approaches were compared. The convenience of the time-marching approach was verified, since this approach yields the same accuracy with less computational cost.

1. Introduction

Fluidized bed reactors (FBR) are a common processing choice in gas processing facilities and particularly in petrochemical industries. The strong points of the FBR are its outstanding heat and mass transfer characteristics, which make it a good choice for processing large volumes of gas. Many industrially produced polymers, such as rubber, vinyl chloride, polyethylene and styrene are made using FBR technology. In the FBR, the reaction rate depends on the rate at which gas diffuses into the catalyst active sites. Therefore, catalysts are shaped in the form of small porous particles in order to enhance the gas diffusion rate by increasing the gas-solid interfacial area. Hence, a better understanding and description of this transport process is required to improve the estimation of reaction times.

Transient diffusion processes are usually modeled based on Fick's second law, a parabolic equation according to which the variance $\langle x^2 \rangle$ of a given concentration profile is expected to increase proportionally with time t, that is $\langle x^2 \rangle \approx t$. According to Fick's law, the information propagates at infinite velocity since a perturbation in any region of the domain is instantly detected everywhere. This inconsistence is referred to as the infinite propagation velocity paradox. As a result, even when the model is a good approximation for steady-state problems, it leads to erroneous results at short times in transient problems (Chen and Liu, 2003) and is not suitable for describing processes at high frequencies (e.g. Depireux and Lebon, 2001 diffusion in polymer solutions).

Experimental results (Ritchie, 2005) have verified that diffusion often proceeds faster or slower than predicted by Fick's law, so the variance of a given concentration profile evolves as $\langle x^2 \rangle \approx t^{\gamma}$, where γ is called the anomalous diffusion exponent. The cases with $\gamma < 1$ and $\gamma > 1$, which are not properly accounted by Fick's law, are termed subdiffusion (Küntz and Lavallée, 2004) and superdiffusion (Küntz and Lavallée, 2001) respectively. An alternative model to deal with these inherent problems of Fick's law is Maxwell-Cattaneo's model. This model is the simplest generalization of Fick's law that allows a relaxation of the local equilibrium. It solves the infinite propagation velocity paradox and allows the modeling of different diffusion behaviors. It has been proven by Sharma in (Kal Renganathan Sharma, 2005) that this damped-wave diffusion model can be deduced by allowing the depletion or accumulation of molecules near the diffusion plane. Besides having numerous applications in heat transfer processes (Compte and Metzler, 1997; Dorao, 2009), Cattaneo's law has been evaluated for diffusion modeling in binary fluid mixtures (Jou et al., 1991) and cristalline solids (Godoy and García-Colín, 1996; Buchbinder and Martaller, 2009) that can be considered far from their equilibrium point.

Evidence of superdiffusion has been found observing water infiltration profiles in porous building materials (Küntz and Lavallée, 2001) and also subdiffusion has been observed in one-dimensional diffusion in high concentration aqueous $CuSO_4$ solutions (Küntz and Lavallée, 2004). Extended versions of Cattaneo's equation including

* Corresponding author.
E-mail address: alfredo.carella@ntnu.no (A.R. Carella).

1875-5100/$ – see front matter © 2010 Elsevier B.V. All rights reserved.
doi:10.1016/j.jngse.2010.08.001

fractional derivatives are able to predict this behavior in a consistent way. However, more experimental effort is required for determining the parameters of this model. In particular, Cattaneo-Maxwell's model has been applied to pseudo-homogeneous modeling of reaction-diffusion inside a porous particle (Valdés-Parada et al., 2006) by a volume averaging procedure. It was concluded that an effective diffusivity tensor can be computed as in the Fickian diffusion case for conditions found in practical applications.

According to Cattaneo's law, the concentration wave propagates at a speed $\sqrt{D/\tau}$ (Gómez-Díaz, 2006), where D is the diffusion coefficient and τ is a parameter called relaxation time. The relaxation time is related to the molecular relaxation processes that take place in the microstructure of the material (Álvarez-Ramírez et al., 2008). These processes involve a type of memory in particle collisions and imply that highly ordered microstructures such as crystals are expected to exhibit shorter relaxation times than disordered structures. This hyperbolic description has been proven valid for transient solute flows with small characteristic times (Auriault et al., 2007) and for transport of a passive scalar in a turbulent flow (Brandenburg et al., 2004). For certain parameter choices, the desorptive diffusive flux can persist after the diffussing species has been completely desorbed. However, such physically unrealistic behavior disappears when the values for parameters τ and D are constrained by relations that explicitly enforce the second law of thermodynamics. This is explained in detail in (Doghieri et al., 1993). In this work, the Cattaneo-Maxwell's model is discussed and a numerical solution is obtained using Least Squares Finite Element method.

2. Cattaneo-Maxwell's hyperbolic mass diffusion equation

The mass transfer in a one-dimensional system is governed by the balance equation

$$\frac{\partial \rho(x,t)}{\partial t} + \frac{\partial J(x,t)}{\partial x} = 0 \tag{1}$$

in combination with a constitutive equation. As an alternative to Fick's first law, Cattaneo (Compte and Metzler, 1997) proposes the following constitutive equation

$$J + \tau \frac{\partial J(x,t)}{\partial t} = -D\frac{\partial \rho(x,t)}{\partial x} \tag{2}$$

In the equations above $\rho(x, t)$ represents the mass concentration, $J(x, t)$ is the mass flux, D is the diffusion coefficient, τ is the relaxation time, t is time and x is the space coordinate. By combining these equations, Maxwell-Cattaneo's model is obtained.

$$D\frac{\partial^2 \rho(x,t)}{\partial x^2} = \frac{\partial \rho(x,t)}{\partial t} + \tau \frac{\partial^2 \rho(x,t)}{\partial t^2} \tag{3}$$

Cattaneo-Maxwell's equation (3) is a damped-wave hyperbolic diffusion equation, which predicts that concentration waves propagate at a finite speed. This constitutive model yields the same results as Fick's law for steady-state cases. However, the results of both models are considerably different for time scales shorter than the relaxation time of the considered medium. It can be seen immediately that as the relaxation time τ approaches zero Cattaneo's equation approaches Fick's law.

3. Numerical solution

The objective of this work is to describe the solution of the stated problem by the Least Squares Finite Element Method. By this procedure, a well-posed system of partial differential equations (Gerritsma and De Maerschalck, 2010) is transformed into a symmetric, positive definite system of algebraic equations. These characteristics of the system enable the use of advantageous solving algorithms like the conjugate gradient method (Shewchuk, 2004).

Instead of solving the second order differential equation (3), the system composed by the two first order equations (1) and (2) is solved. The problem can be expressed as:

$$Lf - g = 0 \text{ in } \Omega \tag{4}$$

$$Bf - g_0 = 0 \text{ on } \Gamma \tag{5}$$

where L, f and g are defined as

$$L = \begin{bmatrix} \frac{\partial \bullet}{\partial t} & \frac{\partial \bullet}{\partial x} \\ -D\frac{\partial \bullet}{\partial x} & \tau\frac{\partial \bullet}{\partial t} + \bullet \end{bmatrix};\ f = \begin{bmatrix} C \\ J \end{bmatrix};\ g = \begin{bmatrix} 0 \\ 0 \end{bmatrix} \tag{6}$$

Here g represents the source terms, B the boundary condition (trace) operator and g_0 the solution at part of the domain boundaries.

The linear operator L defines the isomorphism $L : X(\Omega) \to Y(\Omega)$ for which two constants C_1 and C_2 exist that fulfill

$$C_1\|f\|_X \le \|Lf\|_Y \le C_2\|f\|_X \,\forall f \in X \tag{7}$$

As a consequence of this, the norms $\|f\|_X$ and $\|Lf\|_Y$ are equivalent, and so minimizing $\|f - f_{ex}\|_Y$is equivalent to minimizing $\|L(f - f_{ex})\|_Y$ where f_{ex} is the exact solution.

To solve Equations (4) and (5), a norm-equivalent functional can be defined as

$$J(f,g) = \frac{1}{2}\|Lf - g\|^2_{Y(\Omega)} + \frac{1}{2}\|Bf - g_0\|^2_{Y(\Gamma)} \tag{8}$$

where the norm $|\bullet|^2_{Y(\Gamma)}$ is defined as

$$\|\bullet\|^2_{Y(\Gamma)} = \int_\Gamma \bullet\bullet \mathrm{d}\Gamma \tag{9}$$

For simplicity, the L_2-norm is used in this work.

Solving the system for Equations (4) and (5) is equivalent to finding the function f that minimizes the functional (8). That is:

Find $f \in X(\Omega)$ such that

$$A(f,v) = F(v)\,\forall v \in X(\Omega) \tag{10}$$

with

$$A(f,v) = \langle Lf, Lv\rangle_{Y(\Omega)} + \langle Bf, Bv\rangle_{Y(\Gamma)} \tag{11}$$

$$F(v) = \langle g, Lv\rangle_{Y(\Omega)} + \langle f, Bv\rangle_{Y(\Gamma)} \tag{12}$$

where $A: X \times X \to \mathbb{R}$ is a symmetric continuous bilinear form, and $F: X \to \mathbb{R}$ a continuous linear form.

As the boundary conditions are expressed in a weak form, functions that do not satisfy the boundary conditions can be included in the search space $X(\Omega)$. In order to perform the numerical calculations, this infinite search space is reduced to a finite search space $X_h(\Omega) \subset X(\Omega)$.

The computational domain Ω is divided into $N_e = N_{ex} \times N_{et}$ non-overlapping sub-domains or elements Ω_e, such that

$$\Omega = \bigcup_{e=1}^{N_e} \Omega_e \quad \Omega_e \cap \Omega_i = \varnothing \ \forall \ e \neq i \tag{13}$$

In each element, the unknown function f^e is approached by the set of all polynomials of degree up to O_x. The global approximation in Ω is constructed by attaching the local element approximations Ω_e. The solution is expanded in the base of Lagrange polynomials (Fig. 1).

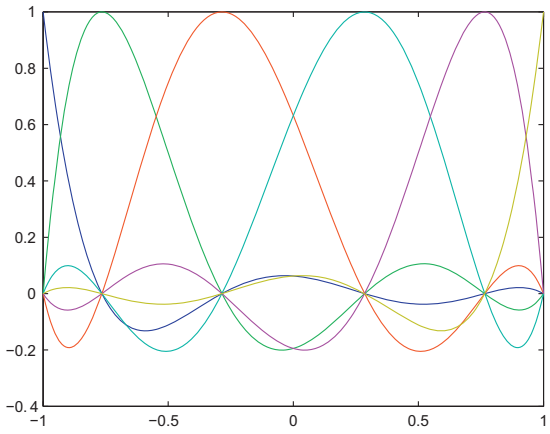

Fig. 1. Lagrange polynomials of order $0 \leq O_e \leq 5$ for a reference domain.

3.1. Time-space formulation

The problem was solved in a 2-dimensional domain, with x and t as the variables. Two numerical approaches were compared: a full domain approach consisting in the simultaneous solution of the complete 2-D domain in one hand, and on the other hand a time marching approach, consisting in solving one slab at the time, using the solution of the previous slab as initial condition. Both solving schemes are presented in Fig. 2.

The simultaneous solution of the full-domain requires the solution of one linear equation system of large size, while the time marching approach requires the solution of many linear equation systems of smaller size. In more concrete words, we compare solving of a system of size $\approx N_{ex}\, O_x \times N_{et}\, O_t$ against solving N_{et} systems of size $\approx N_{ex}\, O_x \times O_t$, where N_{ex}, N_{et}, O_x and O_t are the number of elements and the approximation order in x and t respectively.

The advantage of solving the problem with the time marching approach becomes more notorious as the size of the system increases. In this case, the computational cost is approximately proportional to the number of time slabs, while with the full domain solution, the computational cost grows faster than linearly.

4. Numerical examples

4.1. Analysis of Cattaneo-Maxwell's model

Simulations with different values of τ were performed in order to observe the effect of this parameter in the behavior of the normalized system coordinates x and t and variables T and J. The propagation of concentration waves in a slab was studied as a reference case. This can represent the evolution of the concentration profile inside a catalytic pellet submerged in a reactant medium (Fig. 3). In order to illustrate the differences with Fick's law, the case with $\tau = 0$ is included in some figures.

The most important conceptual difference between Fick's model and Cattaneo's model is the finite propagation speed that arises as a relaxation term appears in the equation. The propagation velocity of the concentration wave is $v_c = \sqrt{\tau/D}$ (Gómez-Díaz, 2003).

Fig. 4 shows the evolution of concentration in an initially depleted slab when a sudden change in concentration is applied on both boundaries at time $t = 0$. A comparison between the Fickian case ($\tau = 0$) and two different values of τ are plotted in order to illustrate the effects generated by a finite propagation velocity. The smoothed shape of the wave front and the lower boundary value of the solution for short times are due to the use of $\beta(t)$ functions instead of step functions as boundary conditions. This change was performed in order to avoid discontinuities that are difficult to treat numerically. The left half of Fig. 3 presents the results in the complete simulation domain, while its right half displays snapshots for different simulation times. In the Fickian case, Fig. 4(a) and 4(b), the concentration converges asymptotically to the boundary value, while two differences can be appreciated in the other plots:

- A propagation delay can be observed: the concentration in a given region of the domain does not start to increase until the propagation wave reaches that point. This is evident in Fig. 4(e) and (f).
- There is a concentration overshoot: since the information takes a finite time to propagate, constructive interference occurs between both counter diffusing waves and uphill diffusion is observed.

Even when experimental evidence has been found on the existence of diffusion processes that Fick's law cannot describe properly (Ritchie, 2005; Küntz and Lavallée, 2004, 2001), there are still no measurements that can conclusively support Cattaneo-Maxwell's model as accurate. This is partly due to the experimental difficulties associated with measuring concentration transients at a time scale similar to the relaxation time (Uemura and Macdonald, 1996; Nakawaga, 2003). However, similar phenomena has been observed and measured in heat transfer processes (Lane et al., 1947), which suggests that Cattaneo-Maxwell's model could be appropriate.

4.2. Convergence study

In order to find guidelines for the optimal resolution (order and number of elements) to solve this problem, the residual and computing time were measured for the same problem with different

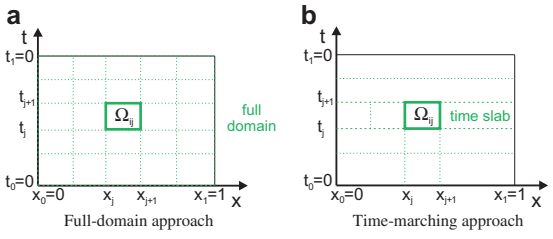

Fig. 2. Full domain simultaneous solution (a) vs one time slab at the time (b).

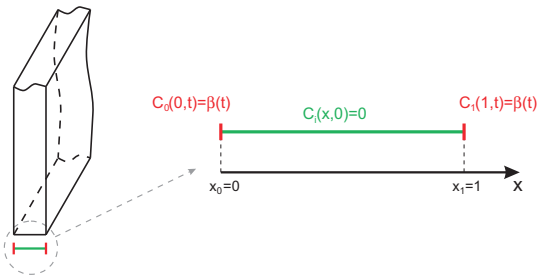

Fig. 3. Physical interpretation of the 1-D numerical problem.

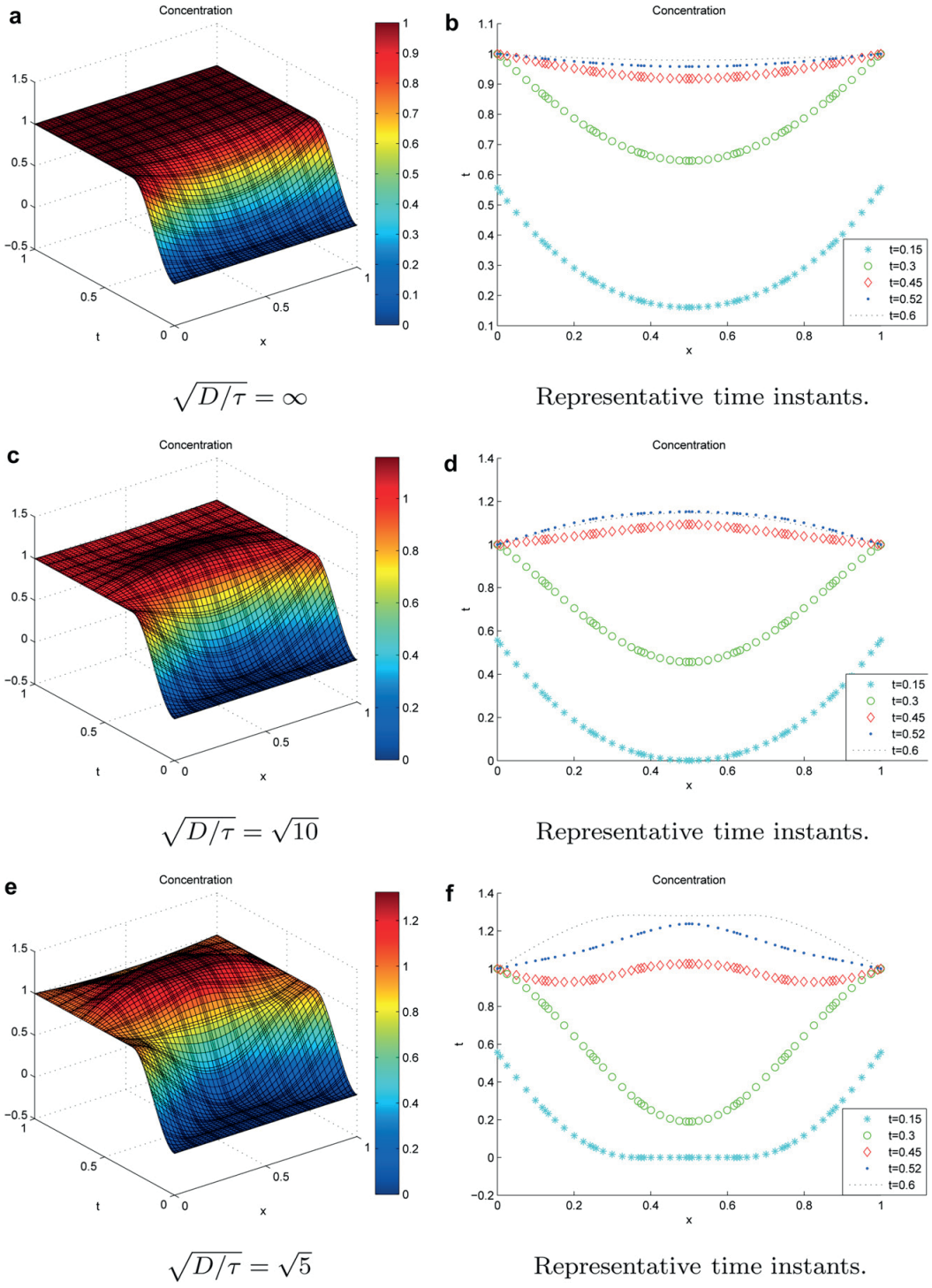

Fig. 4. Evolution of an unitary concentration pulse for different values of τ.

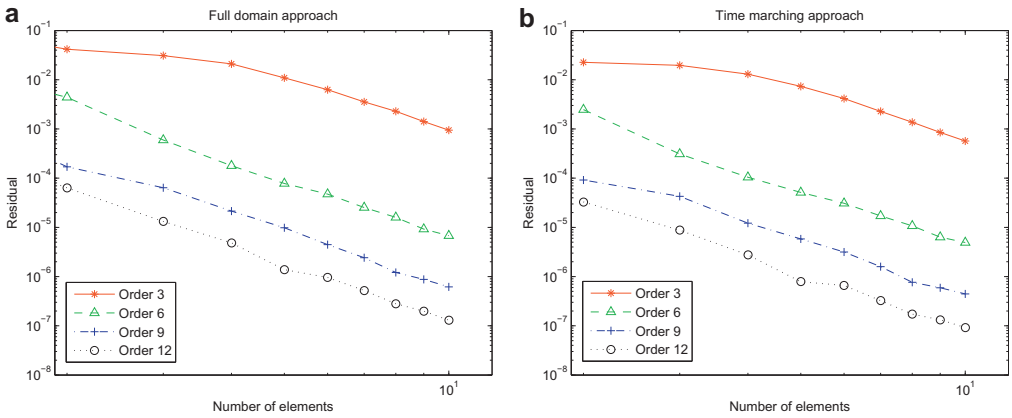

Res vs. N_e Full-domain. Res vs. N_e Time-marching.

Res vs. O_x Full-domain. Res vs. O_x Time-marching.

Fig. 5. Convergence plots for Full-domain and Time-marching approaches.

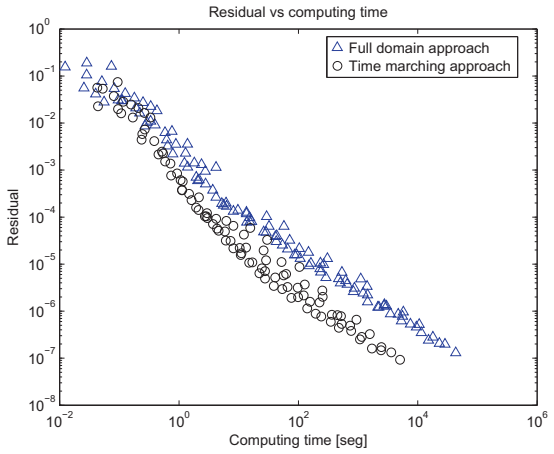

Fig. 6. Residual vs. computing time for Full-domain and Time-marching approaches.

resolutions. The results are shown in Fig. 5. The residual decreases logarithmically as the order and number of elements is increased, which verifies that the problem is solved correctly. The oscillations evidenced in the decreasing tendency of the residual, specially in the red curves of Fig. 5(c) and (d), are due to the low resolution of the simulation. Being the number of points in the domain too low, the shape of the interpolating functions affects the quality of the approximation.

Fig. 6 presents the residual against the computing time for both time-marching and full-domain approaches. The points in this plot were obtained from the solution of the same problem with different resolutions. All combinations of order O_x and element number N_{ex} were included in the plot, with $2 \leq O_x \leq 12$ and $1 \leq N_{ex} \leq 10$. The noise in the plot is probably due to the variation of O_x and N_{ex} at the same time.

The main fact to be observed from Fig. 5 is that the time-marching approach is more effective than the full-domain approach, producing better results with significantly less calculation time.

5. Conclusions

A Least Squares Finite Element framework was implemented in order to solve the evolution of the concentration profile inside

a catalytic pellet. A time-space formulation of Cattaneo-Maxwell's equation was solved for different relaxation time values. This model approaches Fick's law for large time scales. However, for time scales similar to the relaxation time, the finite propagation velocity proposed by Cattaneo-Maxwell's model predicts the superimposition of two concentration waves that move towards each other. This can originate a transient uphill diffusion which is not predicted by Fick's law, but has been observed experimentally in (Baird et al., 1971; Vrentas et al., 1984). Two solution schemes were compared: a time-marching approach consisting in solving each time slab separately, and a full-domain approach consisting in solving the complete domain at once. The time-marching approach proved to be more efficient, allowing to achieve greater precision with less computing time.

References

Álvarez-Ramírez, J., Valdés-Parada &, F.J., Ochoa-Tapia, J.A., 2008. A lattice-boltzmann scheme for cattaneo's diffusion equation. Physica A 387 (7), 1475–1484.

Auriault, J.L., Lewandowska, J., Royer, P. About non-fickian hyperbolic diffusion. In: Congrès Français de Mécanique, 18ème, Grenoble, August 27–31, 2007, 6p, 2007.

Baird, B.R., Hopfenberg, H.B., .Stannett, V.T., 1971. The effect of molecular weight and orientation on the sorption of n-pentane by glassy polystyrene. Polymer Engineering and Science 11 (4), 274–283.

Brandenburg, A., Käpylä, P.J., Mohammed, A., 2004. Non-fickian diffusion and tau approximation from numerical turbulence. Physics of Fluids 16 (4), 1020–1027.

Buchbinder, G.L., Martaller, P., Dec 2009. Model for solute diffusion during rapid solidification of binary alloy in semi-infinite volume. Electronic Publication.

Chen, H.T., Liu, K.C., 2003. Analysis of non-fickian diffusion problems in a composite medium. Computer Physics Communications 150, 31–42.

Compte, A., Metzler, R., 1997. The generalized cattaneo equation for the description of anomalous transport processes. Journal of Physics A 30, 7277–7289.

Depireux, N., Lebon, G., 2001. An extended thermodynamics modeling of non-fickian diffusion. Journal of Non-Newtonian Fluid Mechanics 96 (1–2), 105–117.

Doghieri, F., Camera-Roda, G., Sarti, G.C., 1993. Rate-type equations for the diffusion in polymers: thermodynamic constraints. AiChE Journal 39 (11), 1847–1858.

Dorao, C.A., 2009. Simulation of thermal disturbances with finite wave speeds using a high order method. Journal of Computational and Applied Mathematics 231 (2), 637–647.

Gerritsma, M., De Maerschalck, B., 2010. Least-squares Spectral Element Methods in Computational Fluid Dynamics. In: Advanced Computational Methods in Science and Engineering, vol. 71. Springer, Berlin Heidelberg. 179–227.

Godoy, S., García-Colín, L.S., 1996. From the quantum random walk to classical mesoscopic diffusion in crystalline solids. Physical Review E 53 (6), 5779–5785.

Héctor Gómez-Díaz. Una nueva formulación para el problema del transporte por convección-difusión. In: Certamen universitario Arquímedes de introducción a la generación de conocimiento, Zaragoza, 2003, 27p.

Héctor Gómez-Díaz. Una formulación hiperbólica para el problema del transporte por convección-difusión en mecánica de fluidos computacional. PhD thesis, Universidade Da Coruña, 2006.

Jou, D., Camacho, J., Grmela, M., 1991. On the nonequilibrium thermodynamics of non-fickian diffusion. Macromolecules 24, 3597–3602.

Kal Renganathan Sharma, 2005. Damped wave transport and relaxation. Elsevier, Radarweg 29, P.O.Box 211, 1000 AE Amsterdam, The Netherlands.

Küntz, M., Lavallée, P., 2001. Experimental evidence and theoretical analysis of anomalous diffusion during water infiltration in porous building materials. Journal of Physics D 34, 2547–2554.

Küntz, M., Lavallée, P., 2004. Anomalous diffusion is the rule in concentration-dependent diffusion processes. Journal of Physics D 37, L5–L8.

Lane, C.T., Fairbank, A., Fairbank, W.M., 1947. Second sound in liquid helium ii. Physical Review 71 (9), 600–605.

Nakawaga, K., 2003. Diffusion coefficient and relaxation time of aliphatic spin probes in a unique triglyceride membrane. Langmuir 19 (12), 5078–5082.

Ritchie, K., 2005. Detection of non-brownian diffusion in the cell membrane in single molecule tracking. Biophysical Journal 88 (3), 2266–2277.

Shewchuk, J.R. An introduction to the conjugate gradient method without the agonizing pain. In: School of Computer Science, Carnegie Mellon University, Pittsburgh, PA, 1994, page 64p, 2004.

Uemura, Y., Macdonald, P.M., 1996. Nmr diffusion and relaxation time studies of heur associating polymer binding to polystyrene latex. Macromolecules 29 (1), 63–69.

Valdés-Parada, F.J., Ochoa-Tapia &, J.A., Álvarez-Ramírez, J., 2006. Effective medium equation for fractional cattaneo's diffusion and heterogeneous reaction in disordered porous media. Physica A 369 (2), 318–328.

Vrentas, J.S., Duda, J.L., Hou, A.C., 1984. Anomalous sorption in poly(ethyl methacrylate). Journal of Applied Polymer Science 29, 399–406 (in V. McGahay. Inertial effects and diffusion. Journal of Non-Cristalline Solids, 349:234-241, 2004).

Article 2

Carella, A.R. and Dorao, C.A. (2011)

Migration of Species into a Particle Under Different Flow Conditions

In Kuzmin, A. (Ed.): Computational Fluid Dynamics 2010, Proceedings of the Sixth International Conference on Computational Fluid Dynamics, ICCFD6, St. Petersburg, Russia, on July 12-16 2010. Springer-Verlag, Berlin Heidelberg. ISBN: 978-3-642-17883-2, pp. 869-871.

Is not included due to copyright

Article 3

Carella, A.R. and Dorao, C.A. (2011)

LeastSquares Spectral Method for the solution of a fractional advection-dispersion equation

Journal of Computational Physics. Accepted for publication.
Manuscript number JCOMP-D-11-00463R1.

Least–Squares Spectral Method for the solution of a fractional advection-dispersion equation

Carella, A.R., Dorao, C.A.

Dept. of Energy and Process Engineering, Norwegian University of Science and Technology, N-7491 Trondheim, Norway

Abstract

Fractional derivatives provide a general approach for modeling transport phenomena occurring in diverse fields. This article describes a Least Squares Spectral Method for solving advection–dispersion equations using Caputo or Riemann–Liouville fractional derivatives.

A Gauss–Lobatto–Jacobi quadrature is implemented to approximate the singularities in the integrands arising from the fractional derivative definition. Exponential convergence rate of the operator is verified when increasing the order of the approximation.

Solutions are calculated for fractional–time and fractional–space differential equations. Comparisons with finite difference schemes are included. A significant reduction in storage space is achieved by lowering the resolution requirements in the time coordinate.

Keywords: Advection-dispersion; Caputo derivative; Riemann–Liouville derivative; Fractional derivative; Riesz derivative; Least-Squares; Spectral Method; Anomalous diffusion; Anomalous transport

1. Introduction

Diffusion processes have traditionally been described using Fick's law, which gives sufficiently accurate results for many applications. However, as has been stated many times and supported by new experimental evidence, this model can be insufficient in many cases [1, 2]. Numerous approaches for deriving a more general formulation have been attempted such as hyperbolic diffusion theories [3, 4, 5, 6] and Continuous Time Random Walks (CTRW) [7].

Fractional derivative formulations are attractive to describe diffusion phenomena since they provide a general approach with the possibility of linking hyperbolic diffusion theories [6] and CTRW [8, 9, 10]. In addition, fractional differential equations are powerful tools for modeling phenomena occurring in

Email address: alfredo.carella@ntnu.no (Carella, A.R.)

diverse fields. There are extended reviews on the vast range of applications of fractional derivatives e.g. [11, 12, 13, 14, 15, 16].

1.1. Fractional derivative applications

Numerous cases of fractional derivative models applied to physically relevant problems are found in the scientific literature. Fractional derivatives have been used to represent memory effects [17, 18]. In particular, fractional derivatives have been applied to electrochemistry [19], anomalous transport via coupling with CTRW [20, 9, 8], diffusion in porous media [21, 22] and general cases of anomalous transport [6, 10, 23, 24]. The transport of passive scalars by fluid flow in a porous medium is modeled by a fractional derivative model in [25, 7, 26]. These models allow capturing super–diffusive and sub–diffusive behaviors which are experimentally observed in groundwater hydrology [27, 1]. The applications of fractional derivatives extend also to the field of viscoelasticity. Examples can be found in [28, 29, 30]. It is interesting to note that notwithstanding the vast application scope of fractional derivatives some aspects related to boundary conditions and their interpretations are still under discussion [31, 32, 33, 34].

1.2. Numerical approaches to fractional derivatives

Different approaches have been used to calculate fractional derivatives during the last years and the common concern of integration over singularities has arisen in most of them. The quadrature problem for the fractional derivative operator has been addressed by [35, 36, 37]. Comparisons of different solution methods for problems with Dirichlet homogeneous conditions are presented in [38, 39, 40].

The Yuan–Agrawal method for calculating the time Caputo fractional derivative of a function ${}_0D_t^\beta f(t)$ is proposed in [41]. This method consists in solving an initial value problem in order to find an intermediate function $\Phi(w,t)$ where w is an auxiliary variable. This function is then integrated in w over the interval $[0,\infty)$ in order to calculate the fractional derivative. This method requires solving a stiff (as stated in [42]) first order equation for each quadrature point where $\Phi(w,t)$ is evaluated. Also several quadrature points are required for each operator evaluation, and thus the method becomes computationally expensive. In addition, the intermediate function $\Phi(w,t)$ has a singularity at $w=0$ and consequently the results of using Gauss–Laguerre quadrature yield a very slow convergence as discussed in [43, Section 3].

A modification to this method is presented in [42]. It consists in splitting the integration interval for the function $\Phi(w,t)$ in two domains $[0,c)$ and $[c,\infty)$ and then integrating the first part using Gauss–Jacobi quadrature. This notoriously improves the accuracy of the method, but requires solving a stiff differential equation for each quadrature point. A further modification consists in using Gauss–Jacobi quadrature [44].

J-R. Li presents a fast–time–stepping method for evaluating fractional derivatives [45]. A Gauss–Legendre quadrature is used in the smooth region of the operator integrand, obtaining good results. However, the model is restricted to what they call the region of analyticity, namely a region which is at least Δt

away from the singularity. In other words, the time history is only considered from $t \geq \Delta t$.

Due to the global time dependence, the fractional derivative operator may present high storage space requirements. An option for saving storage space and computing time is applying the so called short–memory principle as described in [46]. This approach capitalizes on the fact that the contribution of the function values to the temporal integral decays as we move away from the singularity region. Alternatively, Li and Xu [47, 48] present a space–time Galerkin spectral approach to fractional time derivatives. The spectral convergence of high order methods reduces considerably the amount of data that need to be stored in order to achieve good accuracy, and this fact is also exploited in the present work. It should be noted that the system of algebraic equations obtained by a Galerkin spectral method is not symmetric, positive-definite (non-SPD), and the boundary conditions are applied by restricting the set of base functions included in the search space.

Finite element approaches to the fractional derivative operator have been achieved by J. P. Roop in [49, 50]. A Least Squares Finite Element approach is presented by Fix and Roop in [51], where existence and uniqueness of the least squares approximation is proven. The singularity is avoided by applying the operator only to example functions that cancel it with zeros.

This article presents a Least Squares Spectral Method (LSSM) to solve a 1–dimensional fractional advection–dispersion equation (FADE). The main characteristic of this method consists in combining spectral convergence, the ability of dealing with the singular fractional derivative operator, the possibility of imposing boundary conditions in a weak form, yielding an SPD linear system and the existence of an a-posteriori error estimator [52].

The outline is as follows. Section 2 presents the physical model studied in this work. Section 3 summarizes the main features of the Least Squares Spectral Method used to solve the numerical model. Section 4 explains the use of Gauss–Lobatto–Jacobi quadrature for the evaluation of the fractional derivative operator. Section 5 describes in detail the construction of the fractional derivative operator for a high order polynomial discretization. Section 6 presents numerical results which validate the numerical framework developed here and a comparison with previous works. Section 7 contains a summary and the main conclusions of the work.

2. Physical model

Mass transfer in a one-dimensional system is governed by a transport equation in combination with a given constitutive equation. Equation (1) represents a transport equation without source terms. Here the variables $C(x,t)$ and $J(x,t)$ represent species concentration and species flux respectively.

$$\frac{\partial C(x,t)}{\partial t} + \frac{\partial J(x,t)}{\partial x} = 0 \tag{1}$$

The traditional constitutive equation used to model diffusion is Fick's first law (Eq. (2)) which is appropriate only in a very limited number of cases [1, 2]. Diffusive flux is then modeled as

$$J\left(x,t\right)=-\mu(x)\frac{\partial C\left(x,t\right)}{\partial x}, \tag{2}$$

where $\mu(x)$ is the diffusion coefficient.

When using a fractional advection–dispersion equation as a constitutive law the diffusive flux $J(x,t)$ results

$$J\left(x,t\right)=-\mu(x)\Bigg(\left(1-q\right)\ {}_0D_x^{\beta}C\left(x,t\right)+q\ {}_xD_1^{\beta}C\left(x,t\right)\Bigg),\qquad 0\leq\beta\leq 1, \tag{3}$$

where q is the relative contribution of the right derivative to the total derivative ($0\leq q\leq 1$). The cases $q=0$, $q=1$ and $q=0.5$ are called *left derivative*, *right derivative* and *Riesz derivative* respectively. The operator ${}_aD_b^{\beta}$ denotes either the Riemann–Liouville fractional derivative or the Caputo fractional derivative [15], defined respectively as

$$RL:\ {}_aD_b^{\beta}f\left(\xi\right)=\frac{1}{\Gamma(n-\beta)}\frac{d^n}{d\xi^n}\int_a^b\frac{f(\xi)d\xi}{(b-\xi)^{\beta+1-n}}, \tag{4a}$$

$$Ca:\ {}_aD_b^{\beta}f\left(\xi\right)=\frac{1}{\Gamma(n-\beta)}\int_a^b\frac{f^{(n)}(\xi)d\xi}{(b-\xi)^{\beta+1-n}}, \tag{4b}$$

where n is defined as the ceiling function of the derivative exponent β, that is the smallest integer that satisfies $\beta\leq n$.

Equation (3) has been proposed in [53, 54] as a generalization of integer order derivatives to describe diffusion processes in which Lévy flights occur. More on the interpretation of this equation can be found in [51, 55]. Note that if $\beta=1$, then Eq. (3) reduces to Eq. (2) which is the traditional Fick's law.

The formulation of a wide range of problems is achieved by combining Eq. (1) and Eq. (3) and adding Dirichlet boundary condition as shown in Eq. (5)

$$\begin{cases}\dfrac{\partial C\left(x,t\right)}{\partial t}=\mu(x)\Bigg(\left(1-q\right)\ {}_0D_x^{1+\beta}C\left(x,t\right)+q\ {}_xD_1^{1+\beta}C\left(x,t\right)\Bigg) & in\ \ \Omega=[0,1]\times[0,1]\\ C(0,t) = C_0\\ C(1,t) = C_1\\ C(x,0) = C_{IC}(x)\end{cases} \tag{5}$$

A further generalization of this model is presented in [56, 57]. In order to model superdiffusive systems, the fractional derivative is moved to the time

domain as presented in Eq. (6)

$$\begin{cases} (1-q)\ {}_0D_t^{\beta} C(x,t) + q\ {}_tD_1^{\beta} C(x,t) \ = \ \mu(x)\dfrac{\partial^2 C(x,t)}{\partial x^2}, & in\ \ \Omega = [0,1]\times[0,1] \\ C(0,t) \ = \ C_0 \\ C(1,t) \ = \ C_1 \\ C(x,0) \ = \ C_{IC}(x) \end{cases} \tag{6}$$

3. Numerical method

The goal of this work is to describe the solution of the problems stated in Eqs. (5) and (6) by the Least Squares Spectral Method. By this procedure, a well-posed system of partial differential equations (the system must be *bounded–below* as explained in [52]) is transformed into a SPD system of algebraic equations. The mentioned characteristics allow using highly efficient algorithms like the conjugate gradient method [58].

The problem can be expressed as:

$$\mathcal{L}f = G \ \ in \ \ \Omega \tag{7a}$$

$$\mathcal{B}f = G_0 \ on \ \ \Gamma \subset \partial\Omega \tag{7b}$$

where

$$\mathcal{L} = \begin{bmatrix} \frac{\partial \bullet}{\partial t} & \frac{\partial \bullet}{\partial x} \\ \mu\left[(1-q){}_0D_x^{\beta}\bullet + q\ {}_tD_1^{\beta}\bullet\right] & \bullet \end{bmatrix} \ ; \quad f = \begin{bmatrix} C \\ J \end{bmatrix} \ ; \quad G = \begin{bmatrix} 0 \\ 0 \end{bmatrix}$$

The linear operator $\mathcal{L}$ represents the isomorphism $\mathcal{L} : X(\Omega) \longrightarrow Y(\Omega)$ for which two non–negative constants C_1 and C_2 exist that satisfy

$$C_1 \left\|f\right\|_X \leq \left\|\mathcal{L}f\right\|_Y \leq C_2 \left\|f\right\|_X \ \ \forall f \in X, \tag{8}$$

the operator G represents the source terms, $\mathcal{B}$ is the boundary condition operator and G_0 the solution at part of the domain boundaries. As a consequence of Eq. (8), the norms $\left\|f\right\|_X$ and $\left\|\mathcal{L}f\right\|_Y$ are equivalent, and so minimizing $\left\|f - f_{ex}\right\|_X$ is equivalent to minimizing $\left\|\mathcal{L}f - \mathcal{L}f_{ex}\right\|_Y$ where f_{ex} is the exact solution [52].

In order to solve Eq. (7), a norm-equivalent functional can be defined as

$$\mathcal{J}(f,G) = \rho_{\mathcal{L}} \left\|\mathcal{L}f - G\right\|^2_{Y(\Omega)} + \rho_{\mathcal{B}} \left\|\mathcal{B}f - G_0\right\|^2_{Y(\Gamma)} \tag{9}$$

where the L_2 norm $\left\|\bullet\right\|^2_{Y(\Gamma)}$ is defined as

$$\left\|\bullet\right\|^2_{Y(\Gamma)} = \int_{\Gamma} \bullet \bullet \, d\Gamma \tag{10}$$

and the factors $\rho_{\mathcal{L}}$ and $\rho_{\mathcal{B}}$ in front of each term of the functional defined in Eq. (9) are found in practice as the combination that minimizes the numerical

error. The best performances in this work were found for $\rho_{\mathcal{B}}/\rho_{\mathcal{L}} > 1000$, which means assigning a greater weight to the boundary residual.

Solving the system for equation Eq. (7) is equivalent to finding the function f that minimizes the functional Eq. (9) by solving the weak form

Find $f \in X(\Omega)$ such that

$$A(f, v) = F(v) \;\; \forall \; v \in X(\Omega)$$

with the operators $A(f, v)$ and $F(v)$ defined as

$$A(f, v) = \langle \mathcal{L}f, \mathcal{L}v \rangle_{Y(\Omega)} + \langle \mathcal{B}f, \mathcal{B}v \rangle_{Y(\Gamma)} \tag{11}$$

$$F(v) = \langle G, \mathcal{L}v \rangle_{Y(\Omega)} + \langle f, \mathcal{B}v \rangle_{Y(\Gamma)} \tag{12}$$

where $A : X \times X \longrightarrow \mathbb{R}$ is a symmetric continuous bilinear form and the transformation $F : \; X \longrightarrow \mathbb{R}$ is a continuous linear form.

As the boundary conditions are expressed in a weak form, functions that do not satisfy the boundary conditions can be included in the search space $X(\Omega)$. In order to perform the numerical calculations, the infinite search space $X(\Omega)$ is reduced to a finite search space $X_h(\Omega) \subset X(\Omega)$ corresponding to a product of polynomials up to degree N in each dimension. The numerical solution is then expanded by Lagrangian interpolants $\phi_j(\xi)$ based on Gauss–Lobatto–Legendre points as

$$f_N(\xi) = \sum_{j=0}^{N} f(\xi_j)\phi_j(\xi), \tag{13}$$

where the interpolating polynomials $\phi_j(\xi)$ satisfy the property

$$\phi_j(\xi_i) = \delta_{i,j}$$

The integrals are approximated by quadratures as explained in Section 4. The conditioning arising from a high-order discretization is discussed in [59, Chapter 2.7].

4. Gauss–Lobatto–Jacobi quadrature

The integrals in Eqs. (4), (11) and (12) are not performed analytically but approximated by quadrature rules. More detail on high order polynomial approximations and quadratures can be found in [60, Chapter 2]. In the general case a quadrature can approximate the integral of the product of a given *integrand function* $f(\xi)$ times a *weight function* $W(\xi)$ over a one-dimensional *integration domain* Θ as a sum of the values of the integrand function evaluated in the *quadrature points* ξ_α multiplied by appropriate *quadrature weights* ω_α as

$$\int_{\Theta} W(\xi) f(\xi) \, d\xi \approx \sum_{\alpha=0}^{N} \omega_\alpha f(\xi_\alpha) \, . \tag{14}$$

GL quadrature. The quadratures of Gauss–Legendre (GL) type use the roots of the Legendre polynomial as quadrature points. The weight function is taken equal to unity. The GL quadrature is accurate and convenient as it has the property of yielding an exact integral exact when the integrand function is a polynomial of degree up to $2N + 1$.

GLL quadrature. An alternative to GL quadrature is Gauss–Lobatto–Legendre (GLL) quadrature, which forces the points at the extremes of the integration domain to coincide with the domain boundaries. Two degrees of freedom are therefore lost for choosing the location of the quadrature points and consequently the integration is exact for polynomials of degree up to $2N - 1$. However, including the boundary points results in greater simplicity regarding the imposition of boundary conditions and the implementation of a multi–domain approach.

GLJ quadrature. A further extension of GLL quadrature in order to include integration weights different from unity results in Gauss–Lobatto–Jacobi (GLJ) quadrature. Recalling Eq. (4) it can be observed that the evaluation of the fractional derivative operator requires the integration of a function $g(\xi)$ of the form

$$g\left(\xi\right) = \frac{f\left(\xi\right)}{\left(x-\xi\right)^{\beta}} \qquad 0 \leq \beta < 1 \tag{15}$$

over the interval $[a, x]$.

This integrand has a singularity at $\xi = x$. Therefore, the integration using GL quadrature yields highly inaccurate results. GLL quadrature is impracticable since the integrand would need to be evaluated at the singularity, which is not possible. A GL quadrature approximation would look like

$$\int_a^x g\left(\xi\right) d\xi = \int_a^x \frac{f\left(\xi\right)}{\left(x-\xi\right)^{\beta}} d\xi \approx \sum_{\alpha=0}^{N} \omega_{\alpha}^{GL} \frac{f\left(\xi_{\alpha}\right)}{\left(x-\xi_{\alpha}\right)^{\beta}} \tag{16}$$

becoming increasingly inaccurate as $\xi_{\alpha} \to x$. The singular integrand $g(\xi)$ from Eq. (15) can be integrated in a clever way by using the Gauss–Lobatto–Jacobi quadrature which takes the singularity into the integration weight function $W^{GLJ}(\xi) = (x-\xi)^{-\beta}$. In this way the quadrature approximation results

$$\int_a^x g\left(\xi\right) d\xi = \int_a^x \frac{f\left(\xi\right)}{\left(x-\xi\right)^{\beta}} d\xi = \int_a^x W^{GLJ}(\xi) f\left(\xi\right) d\xi \approx \sum_{\alpha=0}^{N} \omega_{\alpha}^{GLJ} f\left(\xi_{\alpha}\right) \tag{17}$$

Note that by using $\beta = 0$ the GLL quadrature rule is recovered.

5. Implementation of the fractional derivative operator

Using Eq. (17) to approximate the integral described in Eq. (15), approximations to the fractional derivative operators in Eqs. (4a) and (4b) can be expanded in a GLJ interpolant basis respectively as

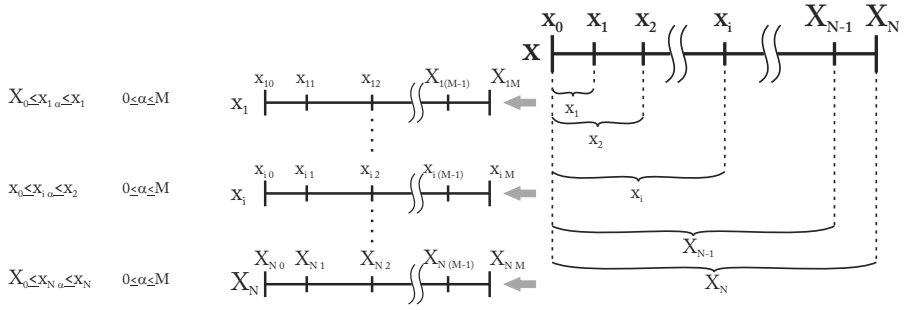

Figure 1: Scheme of integration domains to calculate the fractional derivative operator.

$$RL: \ {}_0D_x^{\beta} f(x) \approx \frac{1}{\Gamma(n-\beta)} \sum_{k=0}^{N} \phi_k^{(n)}(x_i) \left(\sum_{j=0}^{N} \Big(\sum_{\alpha=0}^{M} \omega_\alpha^k \phi_j(\xi_\alpha^k) \Big) f(x_j) \right) \tag{18a}$$

$$Ca: \ {}_0D_x^{\beta} f(x) \approx \frac{1}{\Gamma(n-\beta)} \sum_{j=0}^{N} \Big(\sum_{\alpha=0}^{M} \omega_\alpha^k \phi_j^{(n)}(\xi_\alpha^k) \Big) f(x_j). \tag{18b}$$

Note that the super-index GLJ over the variables ω_α^k and ξ_α^k has been omitted in order to simplify the notation. Here $\phi_k(x)$ represents the k-th GLL Lagrangian interpolant, ξ_α^k are the GLJ interpolant coordinates corresponding to the interval $[0 \leq \xi \leq x_j]$ and ω_α^k are the corresponding GLJ quadrature weights.

For the sake of clarity, a scheme of the domain is included in Fig. 1. The thick line marked as $\mathbf{x}$ represents the domain for the x variable, where x_0 and x_N are the domain boundaries and each x_i is one of the GLL quadrature points of order N. The fractional derivative at $x = x_0$ is trivially zero. For calculating the fractional derivative at the rest of the x_i points, N partially overlapping sub-domains $[x_0, x_i]$ are constructed ($1 \leq i \leq N$) and GLJ quadrature points of order M are generated on each of these sub-domains.

Equations (18a) and (18b) can be written in matrix form as

$$RL: \ {}_0D_x^{\beta} f(x) \approx \bar{\mathbf{D}}^n \cdot \ {}_{RL}\bar{\mathbf{In}} \cdot \mathbf{f} \tag{19a}$$

$$Ca: \ {}_0D_x^{\beta} f(x) \approx \ {}_{Ca}\bar{\mathbf{In}} \cdot \mathbf{f} \tag{19b}$$

where $\mathbf{f}$ and $\mathbf{f}^{(n)}$ denote respectively the function $f(x)$ and its n–th derivative evaluated at the GLL interpolation points x_j. The operators $\bar{\mathbf{D}}$, ${}_{RL}\bar{\mathbf{In}}$ and ${}_{Ca}\bar{\mathbf{In}}$

are defined as

$$\bar{\mathbf{D}}_{[ik]} = \left.\frac{d\phi_k(x)}{dx}\right|_{x_i}$$

$${}_{RL}\bar{\mathbf{In}}_{[kj]} = \frac{1}{\Gamma(n-\beta)}\sum_{\alpha=0}^{M}\omega_\alpha^k\phi_j(\xi_\alpha^k)$$

$${}_{Ca}\bar{\mathbf{In}}_{[kj]} = \frac{1}{\Gamma(n-\beta)}\sum_{\alpha=0}^{M}\omega_\alpha^k\phi_j^{(n)}(\xi_\alpha^k)$$

and the nodal interpolation property by which

$$\left(\bar{\mathbf{D}}^n\right)_{[ik]} = \phi_k^{(n)}(x_i) = \left.\frac{d^n\phi_k(x)}{dx^n}\right|_{x_i} = \overbrace{\left(\bar{\mathbf{D}}\cdot\bar{\mathbf{D}}\cdots\bar{\mathbf{D}}\right)}^{(n\ times)}{}_{[ik]} \tag{20}$$

has been used. Note that the operator construction method is general for any choice of the derivative exponent β and for both *left* and *right* derivative operators [23].

A crucial fact that should be highlighted is that the fractional derivative operators presented in Eq. (19) must be calculated only once, as long as the domain shape is preserved. The application of the operator to any vector is then achieved through a matrix-vector multiplication.

6. Numerical results

6.1. Quadrature validation

The validation of GLJ quadrature has been done through the integration of two test functions of the form $g(\xi) = (1-\xi)^{-\beta}\gamma(\xi)$ from Eq. (15) over the domain $[0,1]$ for two representative choices of $\gamma(\xi)$.

The absolute value of the relative error in numerical integration is plotted in Fig. 2 as a function of the polynomial degree. The relative error is here defined as the absolute value of the difference between the exact integral and the quadrature approximation, divided by the absolute value of the exact integral

$$\mathrm{err} = \frac{\left|\int_0^1 g(\xi) - \int_0^1 g_N(\xi)\right|}{\left|\int_0^1 g(\xi)\right|}.$$

Note that a quadrature of order N is equivalent to the exact integral of a polynomial approximation of order N.

Case A. The first choice of $\gamma(\xi)$ corresponds to the exponential function, i.e.

$$g(\xi) = \frac{\gamma_1(\xi)}{(1-\xi)^\beta},\ \text{with}\ \gamma_1(\xi) = e^{p\xi},$$

which is infinitely smooth for any value of p. As the function $g(\xi)$ cannot be exactly represented by a polynomial approximation with a finite number of terms, it is used to evaluate the relationship between the quadrature error and the number of quadrature points. The quadrature is therefore expected to converge exponentially to the integral as the number of quadrature points is increased (see Fig. 2). The convergence is always exponential and nearly independent of the derivative exponent β. A slower convergence is observed as the coefficient p increases which is due to the corresponding 'sharpening' of the integrand function $g(\xi)$. The results are compared with GL integration, which exhibits a poorer performance.

Since the fractional derivative operator is intended to be applied to arbitrary functions which are approximated with polynomials, it is of interest to test its performance on polynomials.

Case B. The second choice of $\gamma(\xi)$ corresponds to a polynomial, i.e.

$$g(\xi) = \frac{\gamma_2(\xi)}{(1-\xi)^\beta}, \text{ with } \gamma_2(\xi) = \xi^p.$$

The error in the numerical integration of $g(\xi)$ for different values of p and β is plotted in Fig. 3. The accuracy of results is similar to the previous case, and exponential convergence is again observed. Cases A and B provide a full validation of GLJ quadrature applied to functions of the form $g(\xi) = (1-\xi)^{-\beta}\gamma(\xi)$.

6.2. Validation of fractional derivative operators

The validation of the fractional derivative operators is performed by applying them to the function $\gamma(\xi) = \xi^p(1-\xi)^p$ in the domain $[0, 1]$ as

$$D_q^\beta \gamma(\xi) = (1-q)\ {}_0D_\xi^\beta \gamma(\xi) + q\ {}_\xi D_1^\beta \gamma(\xi).$$

The reported measures for relative error are the L_2 and L_∞ norms of the difference between the numerical and analytical solutions normalized with the maximum absolute value of the analytical result as

$$err = \frac{\left\| D_q^\beta \gamma(\xi) - D_q^\beta \gamma_N(\xi) \right\|_{L_2, L_\infty}}{\left\| D_q^\beta \gamma(\xi) \right\|_{L_\infty}}.$$

The studied cases correspond to *Left*, *Right* and *Riesz* derivatives (i.e. $q = 0$, $q = 1$ and $q = 0.5$ respectively). Convergence results for the reference derivative exponent $\beta = 1/2$ are displayed in Fig. 4. For illustrative purposes, the analytical result and polynomial approximation of $D_q^\beta \gamma(\xi)$ are plotted in Fig. 5. For order $N = 19$ (20 nodes) it is not possible for the naked eye to distinguish the analytical and numerical solutions in this figure. Note that for this particular choice of $\gamma(\xi)$ both Riemann–Liouville and Caputo definitions of fractional derivative are coincident.

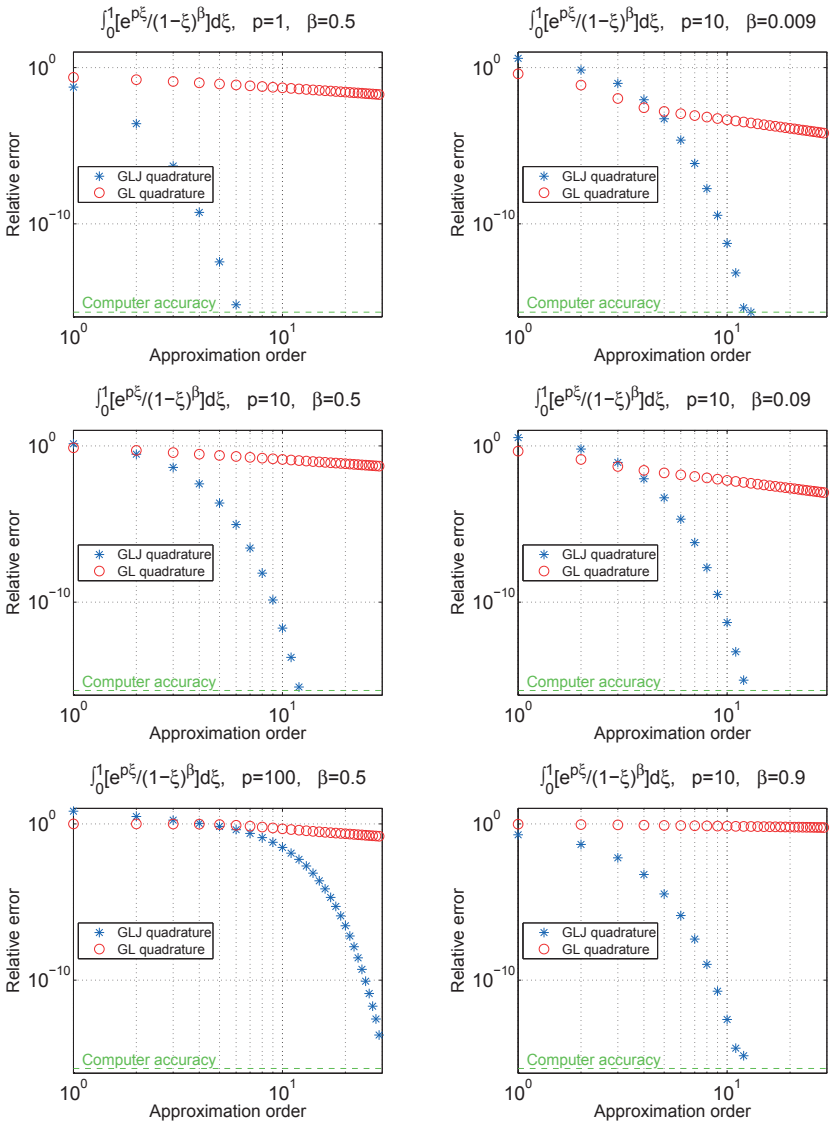

Figure 2: Convergence plots for integration: $\gamma_1(\xi) = e^{p\xi}$, with fixed $\beta = 0.5$ (left column) and with fixed coefficient $p = 10$ (right column).

6.3. Fractional advection–dispersion equation

The first proposed physical model (Eq. (5)) is solved for parameters $q = 1/2$ (Riesz derivative), $\mu(x) = 1$, homogeneous initial and boundary conditions and

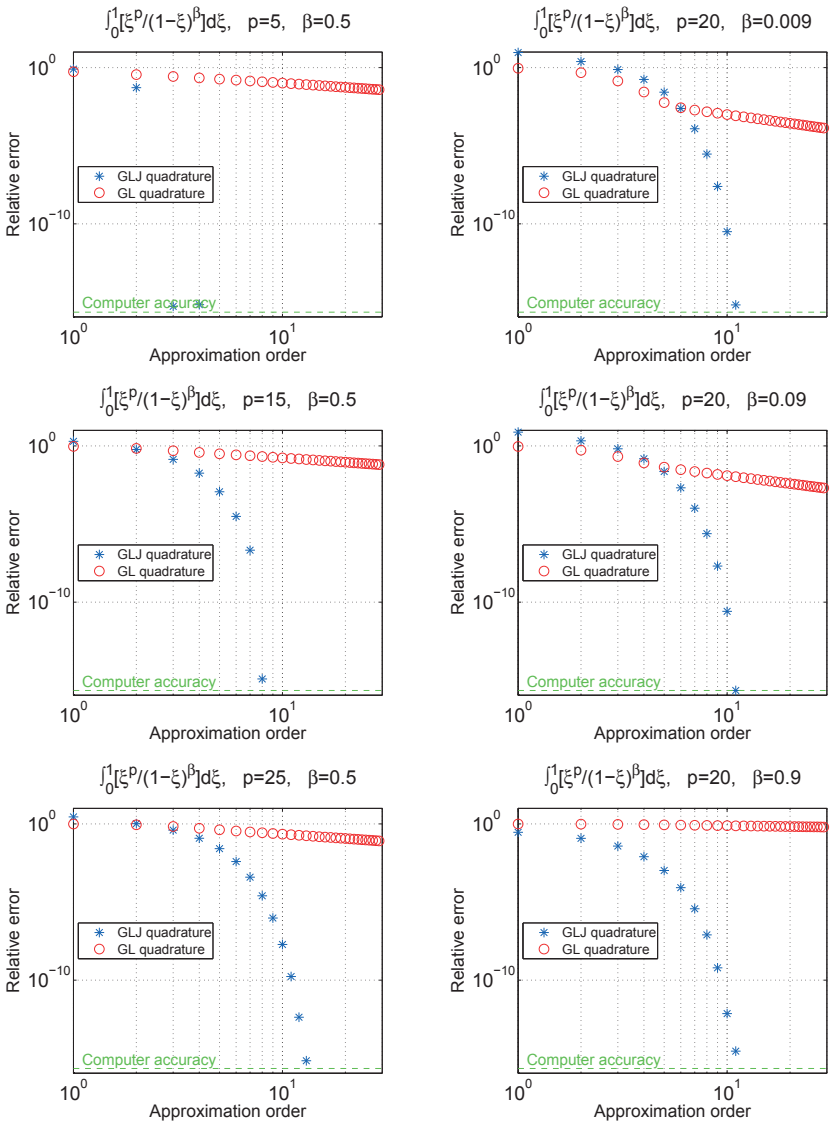

Figure 3: Convergence plots for integration: $\gamma_2(\xi) = \xi^p$, with fixed $\beta = 0.5$ (left column) and with fixed coefficient $p = 20$ (right column).

with a source term $s(x,t) = 8$. The resulting system is

$$\begin{cases} \dfrac{\partial C(x,t)}{\partial t} - \dfrac{1}{2}\Big({}_0D_x^{\beta} C(x,t) + {}_xD_1^{\beta} C(x,t) \Big) = s(x,t), \qquad in\ \Omega = [0,1]\times[0,1] \\ C(0,t) = 0 \\ C(1,t) = 0 \\ C(x,0) = 0 \\ s(x,t) = 8 \end{cases} \tag{21}$$

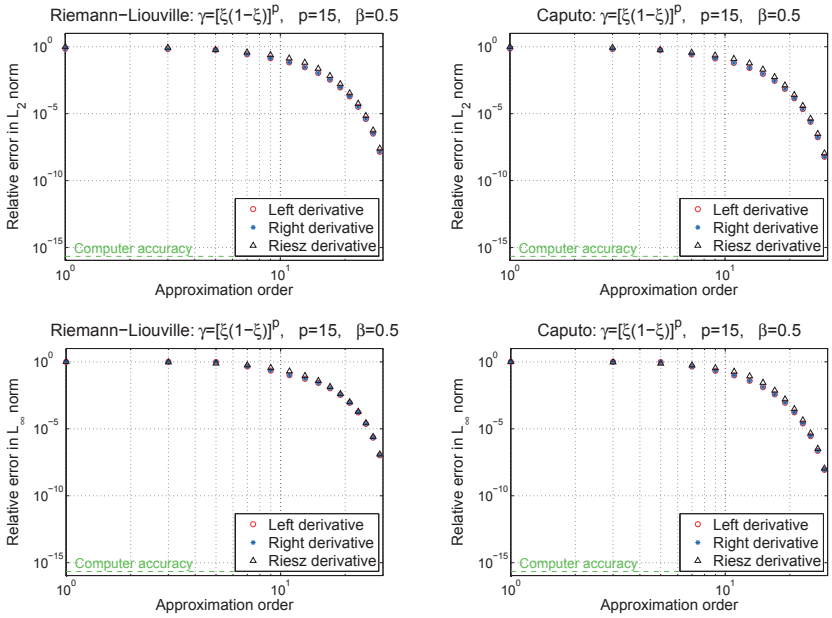

Figure 4: Convergence plots for Riemann-Liouville and Caputo fractional derivatives of the function $\gamma(\xi) = \xi^p(1-\xi)^p$ for derivative exponent $\beta = 0.5$. L_2 and L_∞ norms are presented.

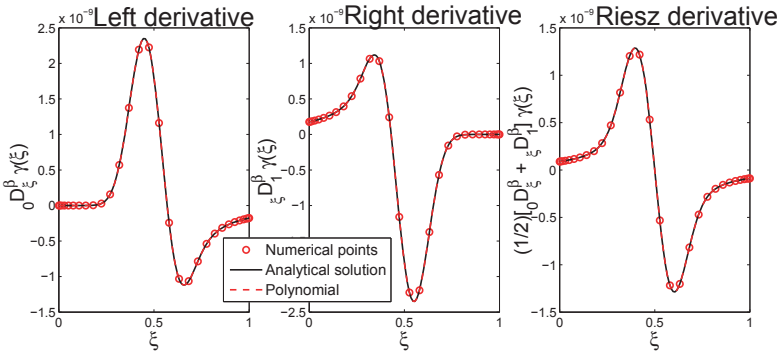

Figure 5: Analytical result and polynomial approximation (order 19) of ${}_aD_b^\beta\gamma(\xi)$

where the fractional derivative operator has been defined according to the Caputo definition in Eq. (4b). The numerical solution of Eq. (21) is found by the LSSM described in Section 3. It reproduces the finite difference result in [23] using a different approach, obtaining the solution presented in Fig. 6. A comparison of the profiles of $C(x,t)$ predicted by each derivative exponent β for the final time is included in Fig. 6(d) in order to illustrate the qualitative differences in the predicted physical behavior. Note that $\beta = 2$ corresponds to

Fick's law.

An important advantage of the LSSM as a solution method is its inconditional stability. This allows reducing considerably the number of nodes in the time discretization, depending on the smoothness of the solution. If the particular problem described in Eq. (21) is considered, its solution is linear in the variable t and can therefore be accurately resolved with few nodes. This is a considerable improvement over the 144 nodes used in [23]. However, it is not possible to compare the performance of both methods in terms of accuracy and CPU time due to lack of information.

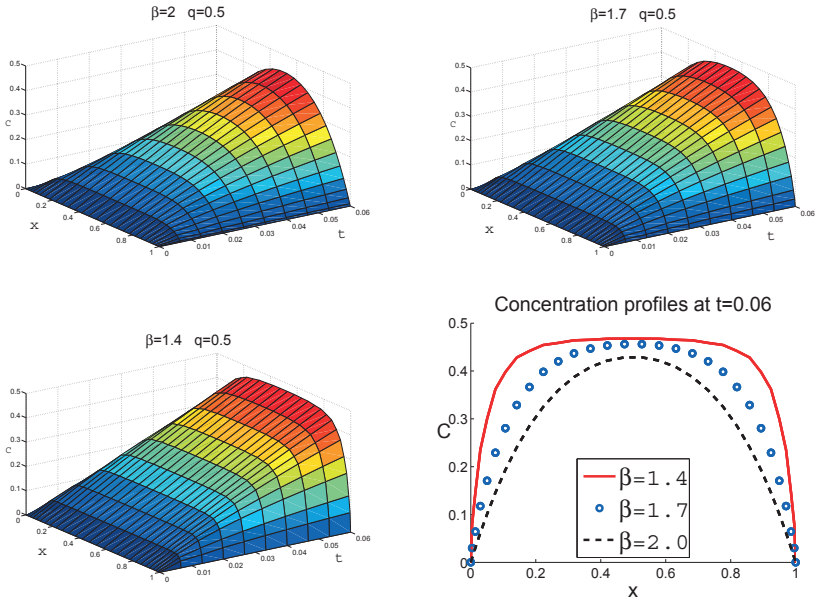

Figure 6: Obtained solutions for Eq. (21) with different derivative exponents β, reproducing results in [23]. A spatial approximation of order 16 is presented in this figure.

The residual and condition number for this problem are plotted in Fig. 7 for approximation order up to 29 for both x and t coordinates. It can be seen in Fig. 7(a) that a refinement in the t coordinate does not improve the accuracy. This was the expected result since Eq. (21) is linear in that variable.

6.4. Fractional time dispersion equation

The problem in Eq. (6) is solved in [61] (by a Grünwald–Letnikov approach) and [23] (using finite differences) with the fixed parameters $q = 1/2$

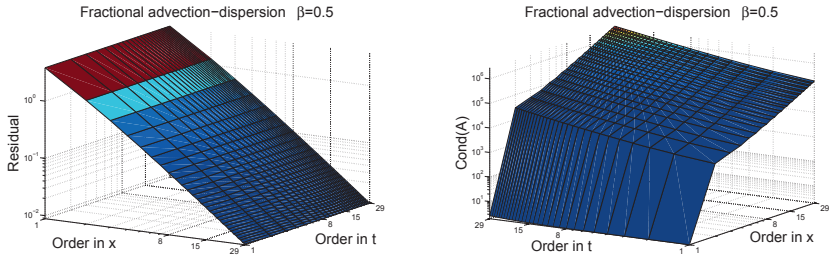

Figure 7: Plots corresponding to: (a) Residual and (b) Condition number of the problem matrix for different order approximations to Eq. (21).

and $\mu(x) = 1$.

$$\begin{cases} \frac{1}{2}\Big({}_0D_t^{\beta} C\left(x,t\right) + {}_t D_1^{\beta} C\left(x,t\right) \Big) = \dfrac{\partial^2 C\left(x,t\right)}{\partial x^2}, \qquad in\ \Omega = [0,1]\times[0,1] \\ C(0,t) \;=\; 0 \\ C(1,t) \;=\; 0 \\ C(x,0) \;=\; 4x(1-x) \end{cases} \tag{22}$$

The same problem is solved using LSSM. The results presented in Fig. 8 reproduce the calculations in [23] and [61]. Note however that the result presented in Fig. 8 was obtained using a polynomial of order 9 for the approximation in the time coordinate. The solution is therefore reconstructed using only 10 nodes, while results in the mentioned works required 150 and 6000 time steps respectively. Plots corresponding to residual and condition number are presented in Fig. 9 for approximation order up to 29 in both space and time. However, it is not possible to compare the solution errors and CPU time of both methods due to lack of information.

A clarification should be made at this point regarding Fig. 8. As the calculated solution consists on the basis coefficients of a polynomial expansion, the numerical 'semi–analytical' solution is known over the complete domain and not only over the nodes used for the discretization. Therefore the meshes shown at the solution plots in Figs. 6 and 8 were chosen in order to improve the clarity of the figures, and are not related to the discretization.

7. Conclusions

This article described a Least Squares Spectral Method for solving advection–dispersion equations using either Caputo or Riemann–Liouville fractional derivatives. The same approach is also valid for left and right derivatives. The described method required evaluating the function in a reduced number of points in order to obtain satisfactory results. Comparisons with finite difference results were included to provide support to this point.

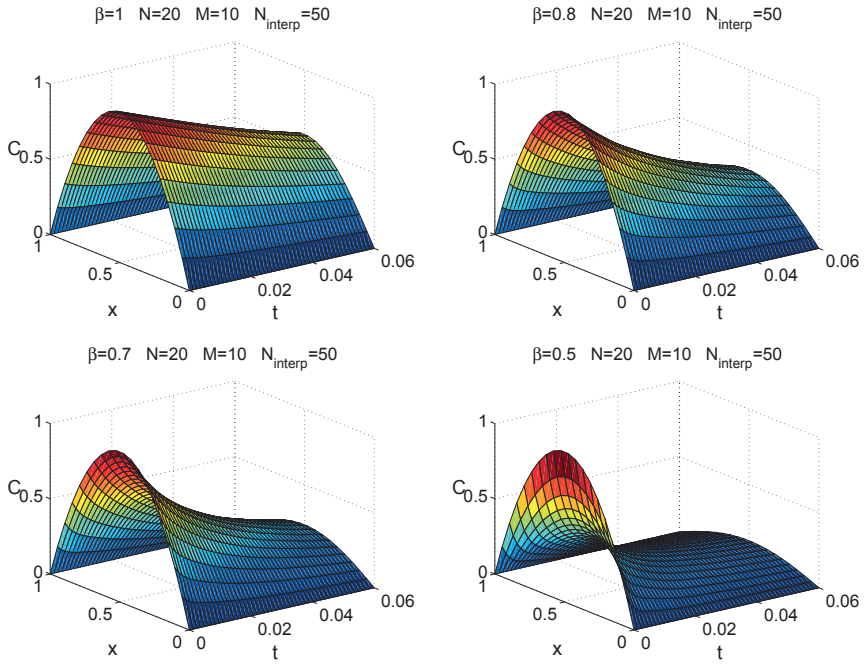

Figure 8: Solutions for Eq. (22) with different derivative exponents β, reproducing results in [23] and [61] using $N = 20$ nodes and $M = 10$ nodes in spatial and temporal discretization.

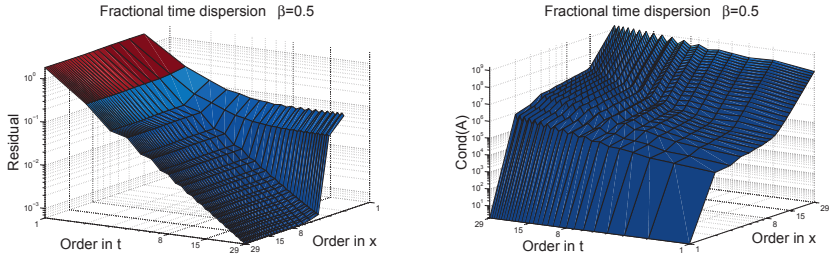

Figure 9: Plots corresponding to: (a) Residual and (b) Condition number of the problem matrix for different order approximations to Eq. (22).

As a necessary step for developing the LSSM framework, Gauss–Lobatto–Jacobi quadrature was implemented to approximate the singular integrands arising from the fractional derivative definition. The fractional derivative operator was applied to a test function and numerical and analytical results were compared. Exponential convergence was verified in this comparison. Convergence graphics were supplied to prove the suitability of this quadrature to this type of problem.

Work is currently being done on extending this implementation to multiple elements and dimensions.

8. Acknowledgements

The authors would like to thank Julio C. Pacio and Federico Sporleder for a critical review and fruitful discussions. This article would not have been possible without their encouragement and support.

References

[1] M. Küntz, P. Lavallée, Anomalous diffusion is the rule in concentration-dependent diffusion processes, Journal of Physics D: Applied Physics 37 (2004) L5.

[2] J. Klafter, I. Sokolov, Anomalous diffusion spreads its wings, Physics World 18 (2005) 29–32.

[3] H. Gomez, I. Colominas, F. Navarrina, J. París, M. Casteleiro, A hyperbolic theory for advection-diffusion problems: Mathematical foundations and numerical modeling, Archives of Computational Methods in Engineering 17 (2010) 191–211. 10.1007/s11831-010-9042-5.

[4] J. Álvarez-Ramírez, F. J. Valdés-Parada, J. A. Ochoa-Tapia, A lattice-boltzmann scheme for cattaneo's diffusion equation, Physica A: Statistical Mechanics and its Applications 387 (2008) 1475 – 1484.

[5] A. Carella, C. Dorao, Solution of a cattaneo-maxwell diffusion model using a spectral element least-squares method, Journal of Natural Gas Science and Engineering In Press, Corrected Proof (2010) –.

[6] A. Compte, R. Metzler, The generalized cattaneo equation for the description of anomalous transport processes, Journal of Physics A 30 (1997) 7277–7289.

[7] S. Fomin, V. Chugunov, T. Hashida, Application of fractional differential equations for modeling the anomalous diffusion of contaminant from fracture into porous rock matrix with bordering alteration zone, Transport in Porous Media 81 (2009) 187–205.

[8] E. Barkai, Ctrw pathways to the fractional diffusion equation, Chemical Physics 284 (2002) 13 – 27.

[9] R. Hilfer, L. Anton, Fractional master equations and fractal time random walks, Physical Review E 51 (1994) R848–R851.

[10] Y. Luchko, A. Punzi, Modeling anomalous heat transport in geothermal reservoirs via fractional diffusion equations, GEM - International Journal on Geomathematics - (2011) 1–20. 10.1007/s13137-010-0012-8.

[11] Y. Zhang, D. A. Benson, D. M. Reeves, Time and space nonlocalities underlying fractional-derivative models: Distinction and literature review of field applications, Advances in Water Resources 32 (2009) 561 – 581.

[12] J. W. Conner, H. R. Wilson, Survey of theories of anomalous transport, Plasma Physics and Controlled Fusion 36 (1994) 719.

[13] R. Klages, G. Radons, I. Sokolov, Anomalous Transport: Foundations and Applications, Wiley-VCH Verlag GmbH & Co. KGaA, Weinheim, 2008.

[14] F. Mainardi, An historical perspective on fractional calculus in linear viscoelasticity, 2010.

[15] I. Podlubny, Fractional Differential Equations, Academic Press, 525B Street, Suite 1900, San Diego, California 92101-4495, USA, 1999.

[16] R. Metzler, J. Klafter, The random walk's guide to anomalous diffusion: a fractional dynamics approach, Physics Reports 339 (2000) 1 – 77.

[17] R. L. Bagley, P. J. Torvik, A theoretical basis for the application of fractional calculus to viscoelasticity, Journal of Rheology 27 (1983) 201–210.

[18] R. Gorenflo, F. Mainardi, D. Moretti, P. Paradisi, Time fractional diffusion: A discrete random walk approach, Nonlinear Dynamics 29 (2002) 129–143. 10.1023/A:1016547232119.

[19] K. B. Oldham, Fractional differential equations in electrochemistry, Advances in Engineering Software 41 (2010) 9 – 12. Civil-Comp Special Issue.

[20] R. Metzler, E. Barkai, J. Klafter, Anomalous transport in disordered systems under the influence of external fields, Physica A: Statistical Mechanics and its Applications 266 (1999) 343 – 350.

[21] A. Chechkin, R. Gorenflo, I. Sokolov", Retarding subdiffusion and accelerating superdiffusion governed by distributed-order fractional diffusion equations, Physical Review E 66 (2002) 046129.

[22] K. Logvinova, M.-C. Néel, Fractional model for solute spreading in randomly heterogeneous porous media, in: XXI International Congress of Theoretical and Applied Mechanics, Warsaw, Poland, August 15-21, 2004, p. 2p.

[23] I. Podlubny, A. Chechkin, T. Skovranek, Y. Chen, B. M. V. Jara, Matrix approach to discrete fractional calculus ii: Partial fractional differential equations, Journal of Computational Physics 228 (2009) 3137 – 3153.

[24] Y. Zheng, C. Li, Z. Zhao, A note on the finite element method for the space-fractional advection diffusion equation, Computers & Mathematics with Applications 59 (2010) 1718 – 1726. Fractional Differentiation and Its Applications.

[25] M. Meerschaert, C. Tadjeran, Finite difference approximations for fractional advection-dispersion flow equations, Journal of computational and Applied Mathematics 172 (2004) 65–77.

[26] Q. Huang, G. Huang, H. Zhan, A finite element solution for the fractional advection-dispersion equation, Advances in Water Resources 31 (2008) 1578 – 1589.

[27] M. Küntz, P. Lavallée, Experimental evidence and theoretical analysis of anomalous diffusion during water infiltration in porous building materials, Journal of Physics D 34 (2001) 2547–2554.

[28] M. Caputo, F. Mainardi, A new dissipation model based on memory mechanism, Pure and Applied Geophysics 91 (1971) 134–147. 10.1007/BF00879562.

[29] Y. A. Rossikhin, M. V. Shitikova, The analysis of the impact response of a thin plate via fractional derivative standard linear solid model, Journal of Sound and Vibration 330 (2011) 1985 – 2003.

[30] Y. A. Rossikhin, M. Shitikova, Analysis of damped vibrations of linear viscoelastic plates with damping modeled with fractional derivatives, Signal Processing 86 (2006) 2703 – 2711. Special Section: Fractional Calculus Applications in Signals and Systems.

[31] N. Heymans, I. Podlubny, Physical interpretation of initial conditions for fractional differential equations with riemann-liouville fractional derivatives, Rheologica Acta 45 (2006) 765–771. 10.1007/s00397-005-0043-5.

[32] A. B. Malinowska, D. F. Torres, Generalized natural boundary conditions for fractional variational problems in terms of the caputo derivative, Computers & Mathematics with Applications 59 (2010) 3110 – 3116.

[33] J. Sabatier, M. Merveillaut, R. Malti, A. Oustaloup, How to impose physically coherent initial conditions to a fractional system?, Communications in Nonlinear Science and Numerical Simulation 15 (2010) 1318 – 1326.

[34] X. Zhang, M. Lv, J. W. Crawford, I. M. Young, The impact of boundary on the fractional advection-dispersion equation for solute transport in soil: Defining the fractional dispersive flux with the caputo derivatives, Advances in Water Resources 30 (2007) 1205 – 1217.

[35] H. Sugiura, T. Hasegawa, Quadrature rule for abel's equations: Uniformly approximating fractional derivatives, Journal of Computational and Applied Mathematics 223 (2009) 459 – 468.

[36] W. Jiang, Y. Lin, Approximate solution of the fractional advection-dispersion equation, Computer Physics Communications 181 (2010) 557 – 561.

[37] A. Pálfalvi, Efficient solution of a vibration equation involving fractional derivatives, International Journal of Non-Linear Mechanics 45 (2010) 169 – 175.

[38] Q. Yang, F. Liu, I. Turner, Numerical methods for fractional partial differential equations with riesz space fractional derivatives, Applied Mathematical Modelling 34 (2010) 200 – 218.

[39] K. Diethelm, J. M. Ford, N. J. Ford, M. Weilbeer, Pitfalls in fast numerical solvers for fractional differential equations, Journal of Computational and Applied Mathematics 186 (2006) 482 – 503.

[40] Y. Lin, C. Xu, Finite difference/spectral approximations for the time-fractional diffusion equation, Journal of Computational Physics 225 (2007) 1533 – 1552.

[41] L. Yuan, O. P. Agrawal, A numerical scheme for dynamic systems containing fractional derivatives, Journal of Vibration and Acoustics 124 (2002) 321–324.

[42] K. Diethelm, An improvement of a nonclassical numerical method for the computation of fractional derivatives, Journal of Vibration and Acoustics 131 (2009) 014502.

[43] J.-F. Lu, A. Hanyga, Wave field simulation for heterogeneous porous media with singular memory drag force, Journal of Computational Physics 208 (2005) 651 – 674.

[44] C. Birk, C. Song, An improved non-classical method for the solution of fractional differential equations, Computational Mechanics 46 (2010) 721–734. 10.1007/s00466-010-0510-4.

[45] J.-R. Li, A fast time stepping method for evaluating fractional integrals, SIAM Journal on Scientific Computing 31 (2010) 4696–4714.

[46] W. Deng, Short memory principle and a predictor-corrector approach for fractional differential equations, Journal of Computational and Applied Mathematics 206 (2007) 174 – 188.

[47] X. Li, C. Xu, A space-time spectral method for the time fractional diffusion equation, SIAM Journal on Numerical Analysis 47 (2009) 2108–2131.

[48] X. Li, C. Xu, Existence and uniqueness of the weak solution of the space-time fractional diffusion equation and a spectral method approximation, Commun. Comput. Phys. 8 (2010) 1016–1051.

[49] J. P. Roop, Computational aspects of fem approximation of fractional advection dispersion equations on bounded domains in, Journal of Computational and Applied Mathematics 193 (2006) 243 – 268.

[50] J. P. Roop, Numerical approximation of a one-dimensional space fractional advection-dispersion equation with boundary layer, Computers & Mathematics with Applications 56 (2008) 1808 – 1819.

[51] G. Fix, J. Roop, Least squares finite-element solution of a fractional order two-point boundary value problem, Computers & Mathematics with Applications 48 (2004) 1017 – 1033.

[52] B.-n. Jiang, The Least-Squares Finite Element Method: Theory and Applications in Computational Fluid Dynamics and Electromagnetics, Springer-Verlag Berlin / Heidelberg, 1998.

[53] A. S. Chaves, A fractional diffusion equation to describe lévy flights, Physics Letters A 239 (1998) 13 – 16.

[54] R. Schumer, D. A. Benson, M. M. Meerschaert, S. W. Wheatcraft, Eulerian derivation of the fractional advection-dispersion equation, Journal of Contaminant Hydrology 48 (2001) 69 – 88.

[55] M. M. Meerschaert, D. A. Benson, B. Bäumer, Multidimensional advection and fractional dispersion, Phys. Rev. E 59 (1999) 5026–5028.

[56] Y. Luchko, Maximum principle for the generalized time-fractional diffusion equation, Journal of Mathematical Analysis and Applications 351 (2009) 218 – 223.

[57] E. Hanert, On the numerical solution of space-time fractional diffusion models, Computers & Fluids In Press, Corrected Proof (2010) –.

[58] J. Shewchuk, An introduction to the conjugate gradient method without the agonizing pain, in: School of Computer Science, Carnegie Mellon University, Pittsburgh, PA, 1994, p. 64p.

[59] M. Deville, P. Fischer, E. Mund, High-Order Methods for Incompressible Fluid Flow, Cambridge University Press, 2002.

[60] C. Canuto, M. Hussaini, A. Quarteroni, T. Zang, Spectral Methods, Springer, 2006.

[61] R. Scherer, S. Kalla, L. Boyadjiev, B. Al-Saqabi, Numerical treatment of fractional heat equations, Applied Numerical Mathematics 58 (2008) 1212 – 1223.

Article 4

Carella, A.R. and Dorao, C.A. (2012)

Modeling of fractional diffusion on a catalytic particle under different flow conditions

Defect and Diffusion Forum **323-325**(121), pp. 121-126.

Is not included due to copyright

Diffusion in Materials - DIMAT 2011
10.4028/www.scientific.net/DDF.323-325

Modeling of Fractional Diffusion on a Catalytic Particle under Different Flow Conditions

10.4028/www.scientific.net/DDF.323-325.121

Article 5

Carella, A.R. and Dorao, C.A. (2012)

N-dimensional Least Squares Spectral Method formulation for the general Fractional Diffusion Equation

Journal of Computational Physics - Under review.

Is not included due to copyright